Members of the jury

Prof. Dr. S. Hendrix, Universiteit Hasselt, Diepenbeek, Belgium, Chairman.

Prof. Dr. I. Lambrichts, Universiteit Hasselt, Diepenbeek, Belgium, Promoter.

Dr. E. Wolfs, Universiteit Hasselt, Belgium, Diepenbeek, Co-promoter.

Prof. Dr. C. Politis, Katholieke Universiteit Leuven, Leuven and Universiteit Hasselt, Diepenbeek, Belgium.

Prof. Dr. B. Brône, Universiteit Hasselt, Diepenbeek, Belgium.

Prof. Dr. A. Bronckaers, Universiteit Hasselt, Diepenbeek, Belgium.

Prof. Dr. C. Chaussain, Université Paris 5 René Descartes, Paris, France

Prof. Dr. P. Ponsaerts, Universiteit Antwerpen, Wilrijk, Belgium

Research is what I am doing when I do not know what I am doing

Table of Contents

Chapter 3 : Neurogenic maturation of human dental pulp stem cells following neurosphere generation induces morphological and electrophysiological characteristics of functional neurons...................61

Chapter 5 : The neuroprotective and neuroregenerative potential of human dental pulp stem cells on primary cortical neurons and neural stem cells is not enhanced by Leukocyte- and Platelet-Rich Fibrin priming **119**

List of Figures

List of Tables

List of Abbreviations

ALP	Alkaline phosphatase
MTT	3-(4,5-Dimethylthiazol-2-yl)-2,5-diphenyltetrazolium bromide
DAPI	4,6-diamidino-2-phenylindole
ASCs	Adipose tissue-derived mesenchymal stem cells
α-MEM	Alpha-modification of minimum essential medium
ABMSCs	Alveolar bone-derived mesenchymal stem cells
Tm	Annealing temperatures
bFGF	Basic fibroblast growth factor
BLI	Bioluminescence imaging
BOLD fMRI	Blood oxygenation level-dependent functional MRI
BBB	Blood-brain barrier
BMMNC	Bone marrow mononuclear cells
BMSC	Bone marrow-derived mesenchymal stem cell
BLBP	Brain lipid-binding protein
BDNF	Brain-derived neurotrophic factor
BrdU	Bromodeoxyuridine
CNS	Central nervous system
CPC	Cetylpyridinium chloride
CFU	Colony Forming Unit
CCA	Common carotid artery
CM-hDPSC	Conditioned medium of human dental pulp stem cells
prCM-hDPSC	Conditioned medium of L-PRF primed hDPSCs
CXCR4	C-X-C chemokine receptor type 4
cAMP	Cyclic adenosine monophosphate
DFPC	Dental follicle precursor cells
DG	Dentate Gyrus
DAB	Diaminobenzidine
dbcAMP	Dibutyryl cyclic adenosine monophosphate
DTI	Diffuse tensor imaging
DMSO	Dimethylsulfoxide
DAG	Donkey anti-goat
DAM	Donkey anti-mouse

List of Abbreviations

DAR	Donkey anti-rabbit
DP	Donkey polyclonal
D-MEM/F12	Dulbecco's modified Eagle's medium and F12 medium
EM	Electron microscopy
ESC	Embryonal stem cell
EGF	Epidermal growth factor
ECA	External carotid artery
FABP-4	Fatty acid binding protein 4
FBS	Fetal bovine serum
fluc	*Firefly luciferase*
fluc-hDPSCs	*Firefly luciferase*-transduced hDPSCs
FITC	Fluorescein isothiocyanate
GMSCs	Gingival mesenchymal stem cells
GFAP	Glial fibrillary acidic protein
GDNF	Glial-derived neurotrophic factor
GAM	Goat anti-mouse
GP	Goat polyclonal
GFP	Green fluorescent protein
GAP.43	Growth associated protein 43
HSC	Hematopoietic stem cell
HRP	Horse-radish peroxidase
hDPSC	Human dental pulp stem cell
hDPSC-EZ	Human dental pulp stem cell isolated by enzymatic digestion
hDPSC-OG	Human dental pulp stem cell isolated by the outgrowth method
ICC	Immunocytochemistry
IGF-1	Insulin-like growth factor-1
IHC	Immunohistochemistry
IL-1ß	Interleukin 1 beta
IL-6	Interleukin 6
iPSCs	Induced pluripotent stem cells
ITS	Insulin Transferrin Selenite
ICA	Internal carotid artery
IA	Intra-arterial
IV	Intravenous

L-PRF	Leukocyte- and platelet-rich fibrin
CM L-PRF	L-PRF derived conditioned medium
EX L-PRF	L-PRF derived exudate
MRI	Magnetic resonance imaging
MMP	Matrix metalloprotease
MSC	Mesenchymal stem cell
MAP-2	Microtubule associated protein 2
MCA	Middle cerebral artery
mNSS	Modified neurological severity score
MCP-1	Monocyte chemotactic protein-1
MM	Mouse monoclonal
NGF	Nerve growth factor
NGFR	Nerve growth factor receptor
NCAM	Neural cell adhesion molecule
NSC	Neural stem cell
d-hDPSCs	Neurogenic differentiated human dental pulp stem cells
NeuN	Neuronal nuclei
NT-3	Neurotrophin-3
OGD	Oxygen and glucose deprivation
PFA	Paraformaldehyde
PDGF	Platelet-derived growth factor
PDLSC	periodontal ligament stem cells
PNS	Peripheral nervous system
PBS	Phosphate buffered saline
PE	Phycoerythrin
PDGF	Platelet-derived growth factor
PET	Positron emission tomography
pCN	Primary cortical neurons
PI	Propidium iodide
RP	Rabbit polyclonal
ROS	Reactive oxygen species
RGC	Retinal ganglion cells
RA	Retinoic acid
RER	Rough endoplasmic reticulum

SPECT	Single-photon emission computed tomography
SHEDs	Stem cells from exfoliated deciduous teeth
SCAP	Stem cells from the apical papilla
SCU	Stroke care unit
SDF-1	Stromal derived factor-1
SVZ	Subventricular Zone
SPIO	Superparamagnetic iron oxide
TEA	Tetraethyl ammonium
TEM	Transmission electron microscopy
TGF-ß1	Transforming growth factor beta 1
TGF-β3	Transforming growth factor beta 3
TGPCs	Tooth germ progenitor cells
tMCAO	Transient middle cerebral artery occlusion
TNF-α	Tumour necrosis factor alpha
tPA	Tissue plasminogen activator
TTC	Triphenyl tetrazolium chloride
TTX	Tetrodotoxin
UCMSCs	Umbilical cord matrix stem cells
VEGF	Vascular endothial growth factor
ZOL	Ziekenhuis Oost-Limburg

Chapter 1 : Introduction and Aims

Parts of this chapter are based on

Gervois, P., E. Wolfs, J. Ratajczak, Y. Dillen, T. Vangansewinkel, P. Hilkens, A. Bronckaers, I. Lambrichts, and T. Struys, Stem Cell-Based Therapies for Ischemic Stroke: Preclinical Results and the Potential of Imaging-Assisted Evaluation of Donor Cell Fate and Mechanisms of Brain Regeneration. Med Res Rev, 2016. 36(6): p. 1080-1126.

1.1 Ischemic Stroke

Worldwide, stroke is the second single most common cause of death, accounting for 10-15% of deaths each year [1-3]. Moreover, stroke is an important cause of adult disability as 90% of patients that survive from a stroke are left with a residual deficit [4, 5]. Therefore, it is clear that stroke-related public and insurance costs constitute a major burden on healthcare systems worldwide [1, 2]. Combining the expectation that the amount of people over the age of 65 will double by 2030, and that the risk of suffering a stroke doubles for each decade over the age of 55, will even lead to a further increase in patient numbers with permanent disabilities and socioeconomic burden [2, 5-7].

Despite this increased incidence, current available therapies are unable to sufficiently ameliorate the disease outcome or are even not applicable for subgroups of patients due to many contraindications as will be discussed below. Therefore, new therapeutic strategies are needed for treating and preventing stroke that can be applied to patients with distinct risk profiles and in a broader time frame, as time plays a crucial role in the treatment of acute ischemic stroke. In addition to clinical advances in stroke management, cell-based therapies have emerged as a potential candidate to promote functional recovery in patients suffering from stroke [8].

1.1.1 Pathophysiology of Stroke

The pathophysiology of stroke can be defined as a neurologic dysfunction of vascular origin with the sudden or rapid occurrence of symptoms and signs corresponding to the involvement of focal areas in the brain [9]. Two different types of stroke can occur: ischemic stroke (80%-85%) and haemorrhagic stroke (15%-20%). Ischemic stroke is most frequently caused by thromboembolisms while haemorrhagic stroke most often results from vessel wall pathology associated with hypertension and micro aneurysms [10]. This Chapter will only focus on ischemic stroke as the main pathology.

In ischemic stroke, the blood supply to certain brain areas is compromised due to vascular occlusion thereby causing several changes at the (sub)cellular level and ultimately tissue damage. These cellular and molecular processes start with energy depletion followed by glutamate release leading to glutamate-induced

excitotoxicity, ion channel dysfunction and free radical production. These processes in turn disrupt the cellular membrane, damage mitochondria and DNA, generate an immune response and trigger necrotic and apoptotic cell death (Fig. 1.1) [11]. In the ischemic core, these cellular changes are irreversible [12]. However, the tissue surrounding the core, also termed as the ischemic penumbra, is functionally impaired but still viable [13]. This area 'at risk' is therefore considered as the main target for therapeutic interventions that are believed to exert a neuroprotective effect in intervening with the cellular processes discussed above [14, 15]. Using non-invasive imaging methods, the ischemic penumbra has been divided in additional border zones characterised by different grades of hypoperfusion and varying risk of progressing towards lost infarcted tissue if a proper treatment is not initiated (Fig. 1.1) [16, 17].

When considering therapies that are aimed to salvage the ischemic penumbra by restoring perfusion, it is also important to take into account that restoring the blood flow in ischemic tissue by thrombolytic treatment can lead to secondary damage by reperfusion injury. This reperfusion injury is mediated by leukocyte infiltration through local disruption of the blood-brain barrier (BBB) and accompanying matrix metalloprotease (MMP) production in addition to stimulation of reactive oxygen species (ROS) production, thereby damaging the reperfused environment [11, 12, 18-20]. In turn, the reperfused ischemic stroke lesion can transform into a petechial haemorrhage that does not influence the prognosis or it can transform into an intracerebral hematoma which is associated with a poor outcome [20-22].

Due to the complexity of the molecular processes that are involved in the onset of stroke, but also in ischemic reperfusion injury, multiple strategies are considered for treating stroke. These strategies include both acute and long-term approaches. Acute therapies aim to salvage the ischemic penumbra and limit reperfusion injury, while long-term therapeutic strategies aim to reconstitute the lost tissue from the ischemic core.
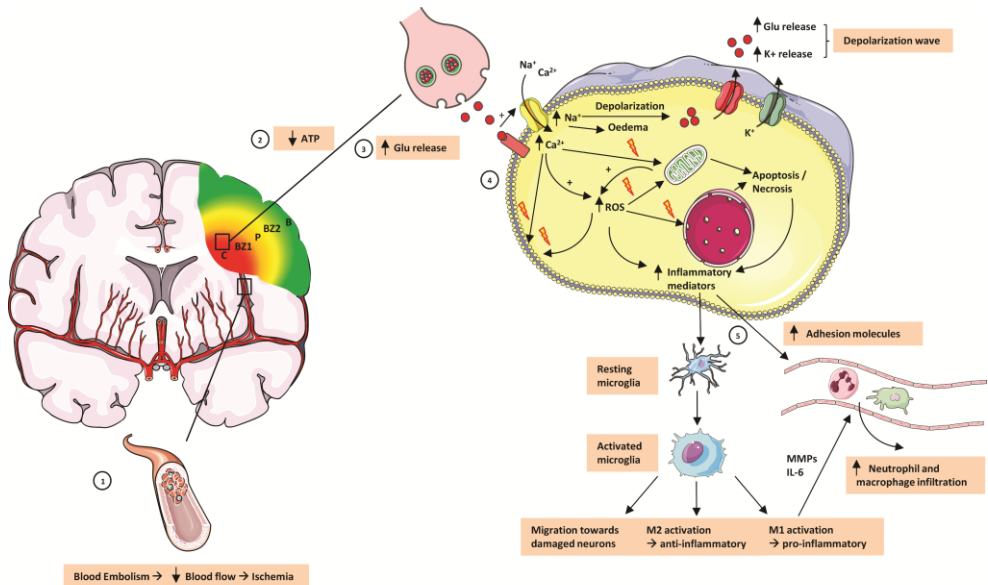
Figure 1.1: Areas at risk and pathophysiology of ischemic stroke. (1) Blood flow to focal areas of the brain is diminished by vascular occlusion by for example an embolism. The affected ischemic tissue can be divided into the ischemic core (C) where tissue damage is irreversible, the salvageable ischemic penumbra (P) and a zone of benign oligemia (B) where blood supply can be obtained by leptomeningeal collaterals. Additional border zones with different grades of hypoperfusion and varying risk of progressing towards unsalvageable tissue if a treatment is not initiated were identified with perfusion-weighted MRI. These areas are the core-penumbra border zone (BZ1) and the penumbra-benign oligemia zone (BZ2). (2) The cellular changes ultimately leading to cell death initiate with ATP depletion due to ischemia, followed by depolarization of the affected neurons which triggers (3) glutamate release. (4) Glutamate-induced excitotoxicity is mediated by an elevated sodium and calcium influx which causes cell-swelling, a depolarization wave that will lead to damage in neighbouring cells, activation of a cascade of enzymatic reactions ultimately leading to membrane- and mitochondrial damage and ROS production which will additionally damage mitochondria and DNA ultimately leading to cell death. (5) Necrotic/apoptotic neurons secrete inflammatory mediators which activate resting microglia and enhance neutrophil and macrophage infiltration. The effects of activated microglia vary and include migration towards- and phagocytosis of damaged neurons and depending on the M1/M2 activation state of activated microglia, pro- and/ or anti-inflammatory mediators are released. Image was created using Servier Medical Art

1.1.2 Limitations and potential improvements of available therapies for ischemic stroke

Current therapies or approaches that have been proven to be effective in reducing the mortality rate and improving the functional outcome of acute ischemic stroke include the establishment of a specialized stroke care unit (SCU) [23], thrombolysis with a tissue plasminogen activator (tPA) such as alteplase or desmoteplase, a next generation tPA with less side-effects [24-26], aspirin administration [27] and decompressive surgery following ischemic stroke [28]. The most remarkable advance in stroke management that reduced the mortality and disability rate, has been the establishment of a SCU, which is a separate physical space in general medical wards with specialized and specifically dedicated trained staff [23]. Despite these advances in stroke management, they can only be applied in a short therapeutic window. The FDA-approved standard treatment for stroke, thrombolysis with tPA, is only applicable to less than 10% of stroke patients and ideally needs to be initiated within 3 hours after the onset of ischemia. This time window can be extended to 4.5 hours if low-risk patients are selected together with providing extensive care due to the higher risk of secondary damage and increased mortality due to reperfusion injury [29, 30]. Other approaches such as decompressive surgery and aspirin administration need to be started within 48 hours after the onset of stroke. Moreover, the benefits of aspirin administration are small while decompressive surgery is only applicable for patients whose stroke-associated infarct region is caused by middle cerebral artery-related pathology, combined with malignant space-occupying brain oedema [31].

Various interventions are currently under investigation, which include extending the time window for thrombolysis with desmoteplase or alteplase [26, 32], ultrasound-enhanced thrombolysis [33], the creation of new thrombectomy devices [34] and neuroprotective drugs [15]. However, the ischemic brain still needs to be protected from reperfusion injury. Approaches to reduce reperfusion injury aim at reducing the local production of ROS and BBB-damaging MMPs, or mediating the local immune response that would otherwise lead to secondary damage [35-38]. One of these approaches is therapeutic hypothermia [39]

which has been shown to decrease ischemic and reperfusion injury by influencing local excitotoxicity, neuroinflammation and ROS production [40].

While these therapies and novel interventions aim at mitigating the disease outcome, they can only be applied in the first few hours or days after the onset of ischemic stroke. Patients surviving stroke and not treated properly within this narrow time window are therefore often left with permanent disabilities, associated with the focal areas of the brain that are affected. In these patients, a therapy that can be applied weeks to months after stroke onset can be beneficial. These therapies aim at restoring the lost neural tissue or stimulating neuroplasticity to improve the functional outcome. Stem cell-based therapies have been shown to be a promising approach in achieving such results [41].

1.2 Stem cell sources and mechanisms of action for cell-based therapies

One of the greatest medical breakthroughs of the twentieth century was the discovery of stem cells. These are defined as clonogenic cells with the ability to self-renew and the potency to differentiate into different cell types. Three types of stem cells have been defined, based on their capacity to differentiate into different cell types or -lineages. Totipotent stem cells have the ability to develop into an entire organism, including all extraembryonic tissue. In animals, totipotent stem cells can be isolated from the zygote and the morula. Pluripotent stem cells are capable of developing into all types of cells and tissues that arise from the three germ layers: ectoderm, endoderm and mesoderm. However, these cells cannot develop into an entire organism by itself due to the inability to differentiate into extraembryonic tissue. Pluripotent stem cells can be found in the inner cell mass of the blastocyst. The third type of stem cell is the multipotent stem cell. These cells include postnatal or adult stem cells with the capability of multilineage differentiation, generally committed to one germ layer. Multipotent stem cells can be subdivided into three major classes: neural stem cells (NSC), hematopoietic stem cells (HSC), and mesenchymal stem cells (MSC) [42, 43]. In addition to these endogenous stem cell types, induced pluripotent stem cells (iPSCs) were discovered by Takahashi and Yamanaka in 2006 by transforming fibroblasts to pluripotent stem cells by retroviral transduction with the transcription factors Oct3/4, Sox2, Klf4 and c-Myc, the so-called 'Yamanaka factors'. These iPSCs were shown to be able to differentiate into all three germ

layers *in vitro* and *in vivo*, confirming their pluripotency and opening numerous possibilities for regenerative medicine [44, 45]. The ability of iPSCs to differentiate into tissues of all three germ layers offers numerous potential therapeutic approaches. However, the main drawback in using iPSCs for transplantational studies is that these cells, like human ESCs, form teratomas when injected in an undifferentiated pluripotent state [46].

When considering stem cells sources for a cell-based therapy in ischemic stroke, *ex vivo* expanded and manipulated NSCs or neural precursor cells (NPCs) would be the ideal candidates to stimulate repair in the central nervous system (CNS) due to their neurogenic differentiation potential and predisposition [47-50]. Promising results have already been achieved with human NSCs in animal models of neurological disorders, including stroke [8, 51]. However, there is a need for alternative stem cell sources with neuroregenerative potential due to ethical considerations with regard to the isolation of NSCs from embryonic or fetal tissue together with isolation and culturing complications of adult NSCs [52, 53]. These alternative stem cells need to be able to reconstitute the lost tissue or stimulate endogenous repair. The most promising alternatives for NSC that are of non-embryonic or -fetal origin are MSCs, induced pluripotent stem cells (iPSCs) and bone marrow mononuclear cells (BMMNCs). These stem cell sources have shown to possess regenerative effects on the brain and allogeneic transplantation potential (i.e. [54-60]). Moreover, both iPSCs and MSCs can be obtained by means of minimal invasive procedures thereby reducing donor site morbidity during isolation. Although it remains a topic of debate whether MSCs possess NPC properties, several studies have reported the ability of subtypes of MSCs to acquire neuronal features following exposure to the proper environmental stimuli [61-63]. In addition to the discussion of which stem cell source is most suitable for stroke research, different animal models such as the middle cerebral artery occlusion (MCAO) model or photothrombotic stroke model are available to induce stroke in an experimental setting, each with their own strengths and weaknesses [64-66].

Multiple mechanisms have been proposed for stem cell-mediated therapies, including neuroprotection, cell replacement, immunomodulation and promoting both neuroplasticity and angiogenesis in damaged brain regions (Fig. 1.2) [41].

Interestingly, these mechanisms are mainly thought to be mediated by the effect of the stem cell-secretome on endogenous stem cells and on the host microenvironment instead of directly replacing the lost cells although encouraging results have also been achieved with cell-replacement studies. Therefore, the transplanted cells can be seen as a vehicle for sustained growth factor delivery at the stroke lesion which can also respond dynamically to changes in the local microenvironment as will be discussed next and into more detail in the following sections.

Paracrine-mediated neuroprotective effects have been observed in *in vitro* and *in vivo* models of neurological disorders [67-69]. In addition, interventions aiming at the directed recruitment and differentiation of NSCs to the site of injury are considered as it is known that NSCs are present in the subventricular zone (SVZ) and dentate gyrus (DG) of the hippocampus in the adult brain [50, 70, 71]. Moreover, following ischemic stroke, endogenous NSCs differentiate into neurons and migrate towards the site of stroke injury and contribute to brain repair [72, 73]. Unfortunately, the endogenous repair by NSCs is insufficient to completely replace the lost tissue. Therefore, novel cell-based therapies are focusing on improving the recruitment of- and repair by endogenous NSCs. Direct cell replacement by the stem cells themselves is also a route that is being considered although it is uncertain whether the transplanted stem cells are able to survive and adequately integrate into the host brain [54, 56]. Another theory in which cell-based therapies are believed to improve the functional outcome in stroke, is by directly inducing neuronal plasticity after the ischemic insult. Although studies report the functionality of transplanted cells in the endogenous neuronal circuitry, these effects are thought to be mainly mediated by promoting the formation of new synapses between existing neuronal cells and not by functionally integrating into the host neuronal network [54, 55, 74, 75].

A key concept in the regeneration of lost tissue, is establishing adequate blood supply to the regenerating tissue. Without proper vascularization which provides oxygen and nutrients the newly formed neuronal tissue will be unable to survive. Previously, it has been shown that stem cells can form vascular structures *in vitro* and secrete pro-angiogenic factors that can positively influence the growth of blood vessels *in vitro* and *in vivo* [76-78]. Therefore, stimulating angiogenesis

is another mechanism by which cell-based therapies can influence stroke outcome.

In addition to protecting damaged neurons, restoring the lost neuronal circuitry and blood supply, stem cells have been shown to be able to mediate the immune response [79, 80]. The mechanisms of these immunomodulating properties include influencing the activation state of monocytes, natural killer cells, B-cells, T-cells and neutrophils. Stem cells were also shown to mediate immunoglobulin release from plasma cells and to upregulate the amount of regulatory T cells [80, 81]. However, it is important to take into account that in ischemic stroke, one of the most common causes of stroke-related morbidity is severe systemic immunosuppression, making patients susceptible to infections [35]. Therefore, additional systemic immunosuppression by cell-based therapies could worsen stroke outcome. Fortunately, no adverse effects on systemic cytokine levels were observed following stem cell transplantation in a rat model of stroke [81].
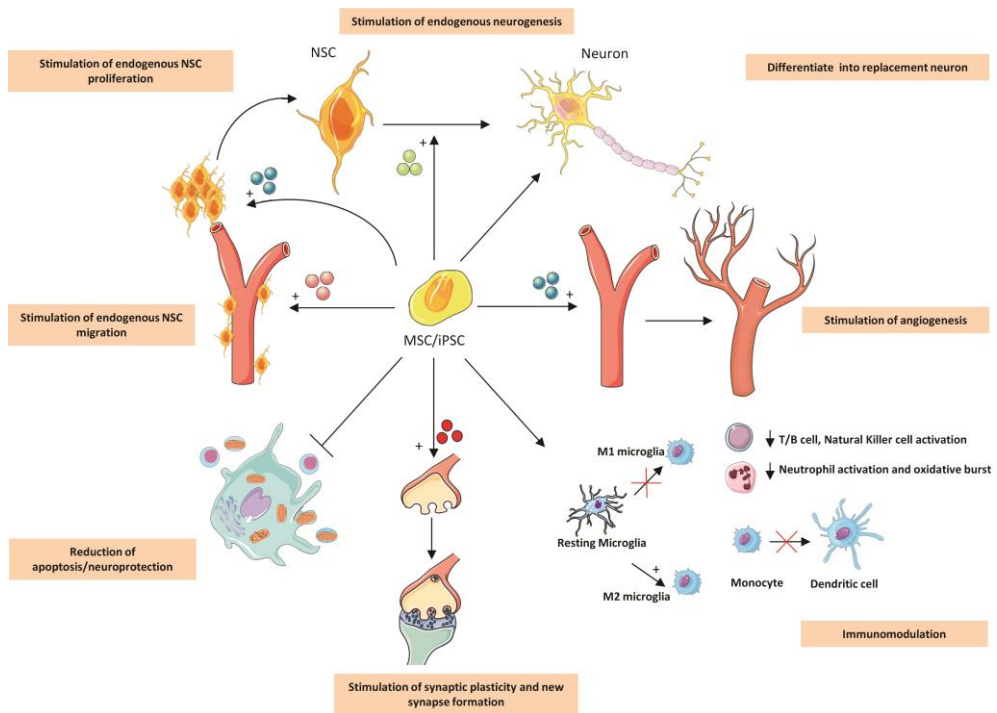
Figure 1.2: Mechanisms of action of cell-based therapies in ischemic stroke. The post-stroke microenvironment can be modulated by exogenously delivered stem cells by multiple mechanisms to trigger tissue repair. Stem cells can contribute to post-stroke recovery by stimulating the migration of endogenous NSCs towards the stroke lesion, where proliferation and differentiation towards replacement neurons can be triggered. In addition, transplanted stem cells are thought to be able to replace the lost neurons themselves in addition to stimulating host NSCs. Moreover, the formation and attraction of new blood vessels towards the ischemic lesion and the stimulation of synaptogenesis and synaptoplasticity contributes to host repair. In addition to directly stimulating the formation of new brain tissue, the degradation of existing cells in for example the ischemic penumbra is inhibited by neuroprotective mechanisms such as ROS scavenging by the transplanted cells. Immunomodulatory effects are also observed and include the inhibition of neutrophil activation and migration, effector T and B cells inhibition, reducing the activation and attraction of peripheral dendritic cells and stimulating the M2 microglial phenotype. These effects are predominantly caused by the soluble factors released by the stem cells, but also cell-cell interactions appear to play a role. Image was created using Servier Medical Art

1.3 Mesenchymal Stem Cells

MSCs, initially discovered in the bone marrow, termed bone marrow-derived MSCs (BMSCs) by Friedenstein *et al.* in the late 1960s [82] were later found to be able to differentiate towards cells producing mesenchymal tissues including bone-forming osteoblasts, cartilage-producing chondroblasts and adipocytes [83]. In addition to bone marrow, MSCs have been isolated from a varying range of other tissues including but not limited to adipose tissue (ASCs), Wharton's Jelly in the umbilical cord (UMSCs); umbilical cord blood (UCBC), and dental tissues [84-88]. Additional research into the differentiation capacity of MSCs suggested that these cells were able to differentiate towards hepatocytes [89], cardiomyocytes [90] and neuron-like cells [91]. The presence of MSCs in various easily accessible and available donor tissues such as the dental pulp and adipose tissue makes MSCs a promising cell type for stem cell based therapies. However, the main problem in the extensive research with MSCs, is the difficulty to compare study outcomes between different research groups. Research groups often have their own methods of isolating, expanding and characterizing the cells, leading to diverging criteria to define MSCs [84-86, 92, 93]. MSCs are a heterogeneous population that generally express the surface markers, CD29, CD44, CD90, CD117 and CD146 while they do not express CD34 and CD45 although subpopulations of CD45- and CD34-expressing MSCs were identified [94].

1.3.1 *In vitro* evidence for the neuroregenerative and neuroprotective potential of MSCs in stroke

Despite interlaboratory differences in defining and culturing MSCs, researchers agreed on the multilineage differentiation potential (i.e. [83, 84, 95]) of these stem cells and subsequently investigated the ability of these cells to transdifferentiate into neuronal or neural-like cells in order to obtain a cell source to replace the lost tissue after ischemic stroke. Early studies that investigated the neurogenic differentiation potential of MSCs were performed using BMSCs, but also hASCs and dental tissue- and umbilical cord- derived stem cells were successfully differentiated to cells with a neuronal immunophenotype [63, 91, 96, 97]. Although a consensus was not found between the differentiation protocols, epidermal growth factor (EGF) and basic

fibroblast growth factor (bFGF) are thought to play an important role in inducing MSCs towards a neuronal cell lineage. Subsequent maturation of the induced cells was based on increasing intracellular cyclic adenosine monophosphate and protein kinase C signalling or by specific growth factor administration [63, 91, 96-98]. However, few studies performed electrophysiological measurements on the differentiated cells but were able to report both voltage-gated Na^+ and K^+ currents that could be reversibly blocked by tetrodotoxin (TTX) and tetraethylammonium (TEA) respectively [63, 91, 96, 98]. Of these studies, only the studies by Wislet-Gendebien *et al.* and Gervois *et al.* could demonstrate the ability of the differentiated cells to generate a single action potential in neuronally differentiated BMSCs and human dental pulp stem cells (hDPSCs; see Chapter 3) respectively, demonstrating only incomplete neuronal differentiation.

In addition to the neuronal differentiation capacity of MSCs, researchers also investigated the neuroprotective and regenerative potential of the MSC-secretome. Hypoxia- and glutamate-induced excitotoxicity assays were used as *in vitro* models for ischemic stroke. It was shown that the MSC protect SH-SY5Y neuroblastoma cells against hypoxia- and glutamate-induced excitotoxicity both in co-culture assays and assays using conditioned medium of MSCs, suggesting paracrine effects [67, 69, 99, 100]. Although the influence of the MSC secretome on NSC survival and/or differentiation is not evaluated *in vitro*, the MSC secretome has been shown to stimulate neurite outgrowth in dorsal root ganglia (DRG) [101, 102] and axotomized retinal ganglion cells (RGCs) [68], and been shown to enhance survival of these axotomized RGCs [68] and of primary cortical [103] and dopaminergic neurons [104]. Neurotrophins/growth factors that are secreted by MSCs include glial-derived neurotrophic factor (GDNF), neurotrophin-3 (NT-3), nerve growth factor (NGF) and brain derived neurotrophic factor (BDNF) [68, 101-106].

As mentioned previously, another key concept in promoting neuroregeneration after ischemic stroke is stimulating revascularization of the regenerating tissue. Therefore, the influence of the MSCs was not only investigated in neuroprotective or neurite outgrowth assays, but also the ability of the MSCs to stimulate angiogenesis was evaluated. These studies showed that MSCs are able to stimulate tube formation and endothelial cell migration, enhance wound

healing and improve blood vessel formation in the chorioallantoic membrane essay (reviewed in [76], [107, 108]). These pro-angiogenic properties of MSCs were attributed to the soluble factors that are secreted by the cells (Table 1 in [76], [77]). Furthermore, it was shown that MSCs protect endothelial cells against hypoxia-induced cell death [109]. Several studies also suggest that MSCs not only promote angiogenesis by paracrine effects, but that these cells are also able to differentiate into endothelial cells (Table 2 in [76]).

Although neurogenic differentiated MSCs express neuronal markers, differentiation of these cells towards mature neurons appears limited, as only immature electrophysiological profiles can be generated from these cells. Nonetheless, MSCs show great promise *in vitro* as shown by the neuroprotective and pro-angiogenic effects of the MSC secretome. Therefore, several studies have transplanted MSCs into animal models of ischemic stroke and evaluated the outcome, as will be discussed below.

1.3.2 MSCs as a therapy for stroke *in vivo*

Due to the encouraging *in vitro* results of MSCs in protecting damaged neurons and stimulating revascularization in addition to secreting multiple soluble factors, the potential of different subtypes of MSCs to ameliorate stroke outcome after transplantation was evaluated *in vivo* (Table 1.1). These studies evaluated the functional outcome after transplantation with a variety of behavioural tests. These tests include global neurological assessments to evaluate the disease severity such as the Bederson test and the modified neurological severity score (mNSS) which evaluates sensory, motor and cognitive impairments. Specific motor tests include the cylinder test, staircase test, grid walking test, the ledged tapered-beam test and the reaching chamber. Other tests not only aim to evaluate motor function, but also take sensory function into account. These sensorimotor tests include the adhesive removal test, accelerated rotarod, stepping test, corridor test, and the corner test. Specific assessments to evaluate cognitive impairment are the Morris water maze and the radial arm maze. For additional information on behavioural tests in animal models of stroke, see Schaar et al and balkaya *et al.* [110, 111]. Taken together, the studies that report an improvement in general neurological-, sensorimotor-, motor- or cognitive function are described in Table 1.1. Studies that compared

different routes and timing of cell administration, or that compared different stem cell sources are marked with an asterisk.

The proposed underlying mechanisms responsible for the improvement in stroke outcome suggested by the studies listed in Table I are diverse. One of the possibilities was that the transplanted cells migrated towards the stroke lesion and differentiated locally towards neurons, establishing new connections with the host environment (i.e. [112]) although the majority of the *in vivo* studies using MSCs as a therapy for stroke support paracrine mediated brain regeneration (i.e.[56, 113, 114]). Regardless of the administration route, the fate of the transplanted cells could be tracked using markers such as DiI [57, 115-118] for fluorescence imaging of the target cells or by iron particle [57, 119] or radionuclide labelling [120, 121]. *Ex vivo*, antibodies directed against human mitochondria or human nuclei when human MSCs were grafted in a rodent stroke model [113, 122-124] could be used. While the listed studies in Table 1.1 could observe improvement of stroke outcome after transplantation, the amount of engrafted cells that was present in the stroke lesion was limited. Pioneered by Zhao *et al.*, intracranial transplantation of MSCs showed that MSCs migrated towards the brain infarct region and were able to survive in the host brain and promote functional recovery [125]. Additional studies showed that although they were present only in low numbers [56, 115, 122, 126, 127], the transplanted cells locally differentiated towards neural cells with a predisposition towards astroglial cells in preference to neurons [56, 115, 126]. Despite the local delivery of the transplanted cells in the stroke lesion, functional integration and replacement of the lost neural circuitry does not appear to be the mechanism of action of intracerebral transplanted MSCs to improve stroke outcome. The results of these studies suggest that the soluble factors secreted by the MSCs are the main actors in improving the functional outcome[56, 115, 125, 126]. After cerebral transplantation of the MSCs, improved angiogenesis [115, 122, 127], increased neuronal activity [122], reduced loss of peri-infarct cells [126] and immunomodulatory effects [128] were observed. After transplantation, the local levels of soluble factors such as BDNF, vascular endothelial growth factor (VEGF), bFGF and angiopoetin-2 were elevated [115, 122]. In order to increase the regenerative potential of intracerebral administered MSCs, several alternative research approaches were investigated.

These include culture of stem cells in preconditioned medium, or under hypoxic conditions [122, 129] with a different outcome on functional recover, favouring hypoxic preconditioning.

Intracerebral administration of MSCs is an invasive procedure and can lead to iatrogenic damage. Therefore, systemic administration of the transplanted cells via the arterial or venous route was considered. Intra-arterial administration (IA) of MSCs in stroke has shown beneficial effects in animal stroke models. Interestingly, IA-transplanted cells are able to cross the BBB after ischemic stroke and migrate towards the stroke lesion. Even though MSCs were found in the core and peri-infarct zone and expressed both astrocyte and neuronal markers [113, 116, 130], paracrine mechanisms of action of IA-delivered MSCs are thought to be responsible for the enhanced stroke outcome although integration into the host brain was observed but not functionally confirmed [112]. At the ischemic boundary zone, MSCs are only present in low numbers but were found to enhance axonal sprouting and remyelination [131], angiogenesis and BDNF production while decreasing MMP-9 levels and suppressing microglial activity [113]. Furthermore, BMSC-administration into aged rats showed a sustained effect and donor cell survival up to one year after transplantation [130].

Another route of MSC transplantation is via the venous system. Remarkably, MSCs that were intravenously (IV) delivered, improved the functional outcome after stroke without MSCs being observed in the ischemic brain or in lower numbers than in IA or intracerebral transplantation [57, 123, 124, 132, 133]. Despite being almost absent in the ischemic brain, IV transplantation of MSC induced an increase in peri-infarct zone microvasculature density and the expression of pro-angiogenic factors [57, 123, 132, 133] and improved oligodendrogenesis and synaptogenesis [57, 123, 134]. Remarkably, when BMSCs were transplanted IV in a chronic stroke model 60 days after surgery, the beneficial effects of the graft were attributed to their immunomodulatory effects on the stroke lesion and on the spleen where the cells preferentially homed towards [135]. Another successfully applied therapeutic approach was to transduce BMSCs with viral vectors to upregulate platelet-derived growth factor (PDGF) or CXCR4 [136, 137] which further improved the functional outcome

after stroke. The SDF-1/CXCR4 (Stromal derived factor-1; C-X-C chemokine receptor type 4) interaction in chemotaxis was found to be stimulated after intravenous administration of MSCs and plays an important role in MSC-homing towards the stroke lesion [118, 137, 138]. In accordance with the other routes of administration, the paracrine effects of the transplanted cells appear to be responsible for the post-transplantation effects on stroke outcome. This was supported by a recent study by Doeppner *et al.*, who showed that repeated IV administration of extracellular vesicles produced by BMSC, led to a similar improvement as injecting the stem cells themselves [114]. Moreover, this study also showed reduced post-stroke immunosuppression after EV transplantation.

This overview shows a variety of studies that were performed, using subtypes of MSCs and different administration routes. Although similar results were achieved with different subtypes of MSC, it remains debatable which is the most suitable source for MSC. Moreover, MSCs showed great promise in replacing the neuronal tissue after transplantation due to their –limited- *in vitro* neurogenic differentiation potential. However, cell replacement could not be proven *in vivo* and it is assumed that paracrine factors are responsible for the beneficial effects after MSC injection which mainly stimulate angiogenesis and protect the host environment against additional damage without adequately stimulating endogenous neurogenesis or replacing lost neurons.

Table 1.1: Overview of preclinical stroke studies using MSCs. IGF-1= Insulin-like growth factor 1; HGF= hepatocyte growth factor; SHR= spontaneous hypertensive rats; SHR-SP= stroke-prone SHR; 99mTc-HMPAO = 99-technetium bound to hexamethylpropylene amine oxine; hUTCs= Human Umbilical tissue derived cells; EV= extracellular vesicles; MCP-1 = monocyte chemotactic protein-1; TNF-α = tumour necrosis factor alpha. prefix h= human; m= mouse; r= rat. *= comparative studies for timing, cell numbers, administration route and/or stem cell-source

Stem Cell Type	(Pre)differentiation and/or treatment	Species	Occlusion time	Time of Transplantation	Dose and Location of Transplantation	Cell Fate	Outcome	Ref
h-DPSCs	no	Sprague-Dawley Rats	2h	24h post-surgery	3×10^5 intrastriatal; 3×10^5 intracortical	2,3% migrates towards the stroke lesion. differentiation towards astrocytes in preference to neurons	Improvement in forelimb sensorimotor function at 4 weeks post-treatment, mediated by paracrine effects	[56]
h-UMSCs	hUMSCs, hUMSCs cultured in neuronal conditioned medium	Sprague-Dawley Rats	90 min	24h post-surgery	2.5×10^5 intracortical in 2 sites	36d survival, not quantified	Significant improvements in motor function, greater metabolic activity of cortical neurons, and better revascularization in the infarct cortex due to paracrine effects.	[122]
h-UMSCs	no	Wistar rats	2h	24h post-surgery	2×10^5 intracortical	5 week survival, <3% expressing neural markers	hUMSC accelerate neurologic recovery after stroke by promoting angiogenesis	[115]

h-BMSCs	no	SHR rats	permanent	1 week post-surgery	7.5×10^4 in 3 different cortical sites	6 weeks after grafting, donor cells expressed astrocyte, oligodendroglial and neuronal markers. Functional integration was unlikely	Improved functional outcome, mediated by paracrine factors that are produced by the surviving donor cells	[125]
r-BMSC and h-BMSCs	Notch-induced BMSCs	Sprague-Dawley Rats	1h	4-6 weeks post-surgery	6×10^4 intrastriatal in 3 sites	r-BMSCs show higher survival (15% vs 7%) and differentiation than h-BMSCs	Improvement in locomotor and neurological function. Reduced loss of striatal peri-infarct cells.	[126]*
h-ASCs	no	C57BL/6J mice	1,5h	1 week post-surgery	5×10^6 in the stroke lesion	Large percentage hASCs express MAP2. Low percentage of GFAP expression	Cognitive recovery and decrease in infarct size. Immunomodulation by decreasing the presence of Iba-1+ microglia and GFAP+ astrocytes.	[128]
m-ASCs	no	C57BL/6J mice	permanent	24h post-surgery	1.8×10^4 above the corpus callosum	Migration after 1 week, towards vessels, 5% survival after 4 weeks	Ischemia induces ASC-survival, migration towards the lesion and microvessels, differentiation into smooth muscle cells	[127]

r-BMSC	Hypoxic pre-treatment (HP)	C57BL/6J mice	permanent	24h post-surgery	1.0×10^6 intranasal	1.5h after administration, donor cells were observed in the ischemic cortex. No long-term follow up was performed	HP of BMSCs induced a higher expression of migration-associated and significantly reduced infarct size and improved sensorimotor function compared to non-HP BMSCs	[129]
r-BMSCs	no	Wistar rats	90 min	1h, 6h, 24h or 48h post-surgery	1×10^6 into the carotid artery	q-dot nanocrystal marked BMSCs could be detected 7d post-stroke.	Injecting BMSCs 24h after stroke had the most significant effect on graft survival/integration, infarct size reduction and improvement of neurological function. SDF-1 and bFGF were upregulated.	[112]*
r-BMSCs	no	Wistar rats	2h	24h post-surgery	2×10^6 into the carotid artery	n/a	BMSCs facilitate axonal sprouting and remyelination in the cortical ischemic boundary zone and corpus callosum	[131]
r-BMSCs	no	Wistar rats	2h	30 min after reperfusion	1×10^6 into internal carotid artery	Magnetically labelled BMSCs could be detected with MRI	Magnetically labelled IA delivered BMSCs could be detected with MRI and high cerebral engraftment rates are associated with impeded cerebral blood flow after injection	[119]

h-BMSCs	no	Wistar rats	90min	24h post-surgery	1.1×10^6 or 0.5×10^6 into the external carotid artery	Transient localization of engrafted cells in the host brain	localization of BMSCs in the brain but relocated to other organs 24h later. Increased radioactivity counts in the ipsilateral stroke hemisphere	[120]*
h-BMSCs	no	Sprague-Dawley Rats	75 min	24h, 4d and 7d post-surgery	1×10^6 into the carotid artery	Low survival, no expression of neuronal markers. Migration towards the lesion and secretion of BDNF	Time dependent functional recovery and cell distribution around the lesion. Mechanisms of action: neuroprotection, angiogenesis and enhancing reactive astrocytes, downregulation of MMP9	[113]*
Autologous r-ASCs	no	Sprague-Dawley Rats	90 min	3d post-surgery	2×10^6 into the carotid artery	1,5% of surviving cells expressed NeuN. 1% survival of transplanted cells	Improvement of neurological deficits, migration of donor cells to lesion. Attenuation of astroglial activity, inhibition of apoptosis and promotion of cellular proliferation	[116]

r-BMSCs	no	Aged Wistar rats	2h	24h post-surgery	2×10^6 into the carotid artery	Donor cells survive up to 1 year and preferentially differentiate towards astrocytes	The beneficial effects of cell transplantation persisted for at least 1 year. Donor cells survived, differentiated towards astrocytes or neurons or colocalized with microglia and endothelial cells. Reduction of axonal loss and glial scar thickness	[130]
h-ASCs and r-ASCs	no	Sprague-Dawley Rats	permanent	30 min post-surgery	2×10^6 h-ASCs or r-ASCs	No migration/implantation of donor cells was observed	Improved functional outcome, reduction in neuronal cell death. No reduction in lesion size. VEGF and synaptofysin was upregulated and GFAP was downregulated in the treated groups. No difference was observed between the h-ASC and r-ASC treated groups.	[139]*
h-BMSCs	Immortalized cells	Wistar rats	1h	24h post-surgery	3×10^6 into the jugular vein	After 7 days no donor cells were detected	IV- transplanted human MSCs induced functional improvement, reduced infarct volume, and neuroprotection by providing IGF-1 and inducing neurotrophin expression in host brain	[132]

h-BMSCs and h-BMSC -EVs	no	C57BL/6J mice	30 min	24h post-surgery. Repeated after 3 and 5 days for hBMSC-EVs	1×10^6 BMSCs or EVs from 2×10^6 BMSC in the femoral vein	n/a	Mice receiving EVs showed improved neurological function and long-term survival associated with improved angio- and neurogenesis. which resembled BMSC responses.	[114]*
r-BMSCs	no	Wistar rats	2h	30 min after reperfusion	1×10^6 into the femoral vein	Magnetically labeled IV delivered BMSCs could not be detected	Magnetically labeled IV delivered BMSCs could not be detected	[119]
h-BMSCs	BMSCs, PDGF Gene-Transfected MSCs	Sprague-Dawley Rats	permanent	6h post-surgery	1×10^7 intravenously	LacZ-expressing PDGF-hBMSCs were found primarily in the penumbra and express NeuN (+/-10%) and GFAP (<17,23%)	hBMSCs and PDGF-transfected BMSCs improved angiogenesis, reduced the lesion size and elicited functional improvement, the effect was more pronounced in PDGF-transduced BMSCs	[136]
r-BMSCs	BMSCs, CXCR4 Gene-Transfected BMSCs and siRNA-CXCR4 transfected BMSCs	Sprague-Dawley Rats	2h	24h post-surgery	2×10^6 into the femoral vein	Increase in CXCR4-BMSCs surrounding the infarct compared to non-transfected and siRNA-CXCR4 transfected BMSCs	CXCR4-transfected BMSCs increased the peri-infarct capillary bed, reduced the infarct size and improved the functional outcome compared to non-transfected and siRNA-CXCR4 transfected BMSCs	[137]

r-ASCs	no	Sprague-Dawley Rats	3h	0h, 12h and 24h after stroke onset	2×10^6 intravenously	Migration towards the lesion, questionable differentiation towards endothelial cells	Reduction of infarct region. Improvement in sensorimotor function, upregulation of CXCR4 and SDF-1. Decreased apoptosis in infarct region.	[117]*
r-BMCS and r-ASCs	no	Sprague-Dawley Rats	60 min	30 min after reperfusion	2×10^6 into the femoral vein	Migration of transplanted cells towards the lesion was not observed	BMSC and ASC administration improves functional recovery independent of reducing the infarct volume and cell migration. Treated groups show higher cell proliferation, oligodendrogenesis, synaptogenesis and angiogenesis markers	[57]*
m-BMSCs and m-ASCs	no	C57BL/6J mice	90 min	Immediately after reperfusion	1×10^5 ASCs or BMSCs into the tail vein	n/a	ASC administration attenuated ischemic damage. Incomplete ASC incorporation in the brain. HGF and angiopoietin-1 expression was significantly increased in ASC-treated mice compared with the BMSC group.	[133]*

h-BMSCs	no	Sprague-Dawley rats	90 min	7d post-surgery	$3.4 +/- 1.2 \times 10^6$ into the saphenous vein	Donor cells accumulate in the ischemic hemisphere, but also in the spleen and lungs	IV-injected 99mTc-HMPAO labelled MSCs home to the ischemic lesion but also accumulate in the lungs and the spleen	[121]
h-BMSCs	no	Sprague-Dawley rats	Hours, no details	60d post-surgery	4×10^6 in the jugular vein	Donor cells preferentially migrate to the spleen, up to 12 days post-injection.	Significant reduction in striatal and peri-infarct area. Reduced loss of hippocampal neurons, significant reduction in MHC-II activated inflammatory cells in grey and white matter. TNF-α expression in the spleen was decreased.	[135]
r-BMSCs	no	Sprague Dawley rats	90 min	1d, 4d or 7d post-surgery	3×10^6 intravenously	Cells transplanted 1d after stroke migrated towards the cortex, cells transplanted after 4d or 7d migrated to the striatum	Functional recovery (mNSS score) was highest when cells were transplanted 1d after surgery. This was correlated with a time dependent expression of SDF-1 and MCP-1 between ischemic regions.	[118]*

r-BMSCs	no	Aged Wistar rats	2h	1 month after surgery	3×10^6 intravenously	Preferential differentiation towards astrocytes (13%) over neurons (6%). Survival of donor cells was not quantified	Significant sensorimotor and general neurological recovery after cell compared with control animals. BMSC treatment reduced scar thickness, increased the number of proliferating cells and oligodendrocyte precursors. SDF-1 is upregulated in the ischemic boundary zone after stroke. BMSCs express CXCR4	[138]
r-BMSCs from SHR-SP rats	no	Aged SHR-SP rats	permanent	30 days before stroke onset	5×10^5 into the tail vein	No direct transplantation, injected donor cells prior to MCAO	SHR-SP BMSCs transplantation increased microvasculature density in the peri-infarct zone, reduced ischemic brain damage and improved neurologic function. Rejuvenation of bone marrow from aged rats with young cells enhanced the ischemic response at the level of endothelial/vascular activation	[134]

h-UTCs	no	Aged Wistar rats	permanent	24h post-surgery	1×10^7 cells/kg into the tail vein	Very few donor cells present at lesion site, no reactivity for MAP2 or GFAP	IV administration of hUTC improved neurological functional recovery without reducing infarct size, increased progenitor cell proliferation and vessel density in the ischemic boundary zone and enhanced synaptogenesis	[123]
r-BMSCs, h-BMSC	no	Aged Sprague-Dawley Rats	3h	6h post-surgery	1×10^6 cells/kg into the tail vein	1% migrates towards the lesion	Daily treatment with G-CSF improved neurological function. G-CSF + BMSC transplantation stimulated angiogenesis in the infarct core but did not further improve neurological function or infarct volume size	[124]*

1.4 Dental pulp stem cells: MSCs from the human dental pulp with neuroregenerative potential

As mentioned previously, MSCs are found to be present in the stroma of almost every adult organ in the human body. The presence of MSCs in various easily accessible organs makes this type of stem cell a promising cell type for stem cell based therapies. However, despite the encouraging results described in section 1.3, it remains undecided which is the most suitable source of MSCs for the treatment of neurodegenerative disorders such as stroke. Within the human tooth and its environment, several subpopulations of MSCs can be distinguished. The tooth-associated populations comprise dental pulp stem cells (DPSCs) [85], stem cells from the apical papilla (SCAPs) [140], periodontal ligament stem cells (PDLSCs) [141], dental follicle precursor cells (DFPCs) [142] and tooth germ progenitor cells (TGPCs) [143]. The periodontal ligament is believed to contain another dental stem cell-source residing in the epithelial cell rests of Malassez which are present in the periodontal ligament matrix [144]. Therefore, Full-grown or developing teeth are therefore a valuable resource for MSC-subtypes. Moreover, the gingiva surrounding the tooth is postulated to contain gingival MSCs (GMSCs) [145] and the alveolar bone contains alveolar bone-derived MSC (ABMSCs) [146]. In addition, several studies reported that deciduous teeth can be utilized to isolate stem cells from the pulp of human exfoliated deciduous teeth (SHEDs) [88] and deciduous periodontal ligament (DePDL) [147]. Figure 1.3 provides a schematic overview of the location of these subpopulations of MSCs associated with dental tissue. While these MSC subpopulations hold great promise for regenerative medicine, the work described in this dissertation will focus on hDPSCs.

Figure 1.3: Sources of dental tissue-associated MSCs. Multiple subpopulations of MSCs can be isolated from the tooth and tooth-associated tissues. These include the stem cells from human exfoliated deciduous teeth (SHEDs). Tooth germ progenitor cells (TGPCs) and dental follicle precursor cells (DFPCs) from the developing tooth. Alveolar bone-derived MSCs (ABMSCs) and gingival MSCs (GMSCs) from the tooth-surrounding tissues and in and around the tooth itself periodontal ligaments stem cells (PDLSCs), stem cells from the apical papilla (SCAPs) and DPSCs can be isolated. Image adapted from Liu *et al.* [148].

After the discovery of MSCs in human dental pulp, various applications of these cells came into mind. In the adult teeth, hDPSCs are activated after severe injury caused by mechanical trauma and dentinal degradation by bacteria. Severe damage to the tooth requires reparative dentinogenesis in which new dentin-secreting odontoblasts are formed out of hDPSCS [149]. A study by Gronthos *et al.* showed that hDPSCs were able to form dentin both *in vitro* and following transplantation into immunocompromised mice. Therefore, hDPSCs were firstly isolated and expanded, considering possible applications in tooth engineering. Subsequent studies compared hDPSCs with BMSCs, the most extensively studied MSC. Immunophenotypical analysis of hDPSCs and BMSCs showed a comparable set of surface markers. Furthermore, it was shown that hDPSCs were plastic adherent under standard culture conditions and were able to differentiate into classical mesodermal cell lineages, forming adipocytes, chondroblasts and osteoblasts *in vitro* [83, 85, 150]. In addition, hDPSCs showed a higher proliferative rate than BMSCs. Comparing hDPSCs and BMSCs by cDNA microarray analysis aimed to provide additional information of both cell types. Over 4000 known human genes were found to have a similar expression level in both human hDPSCs and BMSCs [151]. Another argument that favours

hDPSCs as a suitable alternative for BMSCs, is the ease in which they can be harvested. hDPSCs can be isolated from dental pulp from extracted teeth, mainly third molars which are removed for orthodontic reasons, whilst BMSCs need to be isolated from bone marrow aspirates with a higher chance of donor site morbidity.

In addition to trilineage differentiation, several studies focussed on the plasticity of DPSCs to transdifferentiate to neural-like cells. A study by Sasaki *et al.* described the ability of rat DPSCs to undergo transdifferentiation and generate neurospheres *in vitro*, while a study by Stevens *et al.* describes sphere forming abilities of human DPSC [152, 153] which is a feature of NSC/NPCs [50]. This indicates that DPSCs maintain some form of plasticity, being potentially able to differentiate into neural tissue which is derived from the ectoderm. During embryogenesis, cells migrate from the neural crest to the region of the mesenchyme that will later contribute to the development of the head and the neck. In this region, tooth germs are formed which will later differentiate into dental structures, including the dental pulp. As a result, dental tissue is composed of both neural crest-derived mesoderm (ectomesenchym) and other mesenchymal components [154]. Supportive of neuronal differentiation, a study by Arthur *et al.* showed that hDPSCs can differentiate towards functionally active neurons producing a sodium current when cultured in appropriate neuronal inductive growth media [155]. Subsequently, Kiràly *et al.* showed the presence of both voltage gated sodium and potassium currents that could be blocked by TTX and TEA respectively. However, no action potentials were generated by the differentiated hDPSCs. As mentioned previously, the therapeutic effect of transplanted hDPSCs for stroke is most likely to be attributed to the plethora of growth factor secreted by these cells. Nosrat *et al.* already showed in 2001 that rat DPSCs promote neurite outgrowth and cell survival in trigeminal neurons and motor neurons by paracrine mediated effects [156] and afterwards showed that also hDPSCs secreted these neurotrophins [104]. Another study has shown that in *in vitro* models of Alzheimer's and Parkinson's disease, rat DPSCs have a neuroprotective effect in primary neurons [157]. DPSCs obtained from rhesus monkeys were engrafted into the hippocampus of immunosuppressed mice by Huang *et al.* This resulted in the proliferation of endogenous neural cells and the

recruitment of pre-existing neural progenitor cells and mature neurons to the site of engraftment. The graft promoted growth factor signalling, increasing the expression of ciliary neurotrophic factor, VEGF and FGF [158]. In addition, Mead *et al.* showed the importance of the hDPSC-derived growth factors in neurite outgrowth and survival of axotomized RGCs and demonstrated a superior growth factor secretion profile of hDPSCs over BMSCs and ASCs [68]. Together, these results suggest that DPSCs can promote the survival of different subsets of neurons, promote proliferation and maturation of endogenous progenitor- and stem cells. Furthermore, DPSCs can adapt a neural-like morphology and phenotype in culture.

The rationale behind using hDPSCs as a potential stem cell source in treating disorders of the nervous system and more particularly stroke, is therefore two-fold. On the one hand, there are indications that (differentiated) DPSCs have a neurotrophic effect by the release of neurotrophic factors. On the other hand, tissue repair by engrafting functionally active neurons is another approach for DPSC transplantation in neurodegenerative disorders. To date, only one study has been performed that evaluates the use of hDPSCs in *in vivo* models for ischemic stroke [56] after transcranial transplantation into the rat brain. Moreover, the underlying mechanisms of action of hDPSCs-based therapies remain elusive as the *in vitro* effect of hDPSCs on NSC/NPCs or primary (striato)cortical neurons has not been evaluated. Nonetheless, hDPSCs remain an attractive alternative stem cell source for NSCs due to their ease of isolation and encouraging preclinical results.

1.4.1 Enhancing the (neuro)regenerative effect of hDPSCs by *in vitro* pre-treatment

It is important to take into account the hypoxic and inflammatory stroke microenvironment in which the transplanted cells are to exert their therapeutic effect, which can influence the secretome content and survival rate of the engrafted cells [159]. Therefore, efforts are being made to prepare or 'prime' stem cells for the microenvironment they are to be transplanted in, prior to transplantation. A hypoxic preparation condition can consist of priming the cells with hypoxia-mimetic pharmacological agents such as deferoxamine to enhance their neuroregenerative effects [160] or hypoxia itself. Priming cells with

30

hypoxia or hypoxia-mimetics mainly had an influence on the angiogenic properties of the primed cells. Hypoxic preconditioning did not influence hDPSC-proliferation and enhanced VEGF expression. Moreover, the secretome of hypoxic preconditioned hDPSCs increased human microvascular endothelial cell proliferation and sprouting compared to non-preconditioned DPSCs [161]. In addition, it was shown by Ahmed *et al.* that the growth, stem cell properties and secretome trophic effect on fibroblasts and SH-SY5Y neuroblastoma cells was enhanced by culturing hDPSCs in 5% O_2 [162]. Hypoxic mimetic agents have also been used to precondition hDPSCs. Prolyl-hydroxylase inhibitors such as cobalt chloride, L-mimosine and dimethyloxalglycine have been shown to increase VEGF secretion and hypoxia induced factor 1 alpha (HIF-1α) expression in DPSCs [163]. Similar to the prolyl hydroxylase inhibitors, the iron chelator hinokitiol has been shown to upregulate HIF-1α expression and VEGF secretion in hDPSCs. Moreover, the conditioned medium of these hinokitiol-exposed hDPSCs enhanced angiogenesis *in vitro* and *in vivo* [164].

Another approach in priming hDPSCs is by exposing these cells to blood components which play a role in the inflammatory response after stroke. To this extent, Leukocyte and Platelet Rich Fibrin (L-PRF) can be used to mimic an inflammatory microenvironment *in vitro* in order to enhance the neuroregenerative characteristics of hDPSCs. L-PRF is an autologous blood-derived biomaterial that is already being successfully applied clinically with beneficial results [165]. L-PRF contains leukocytes and platelets concentrated in a flexible fibrin matrix which has been shown to spectacularly enhance wound- and bone healing. The accelerated restorative effects of L-PRF have been attributed to the amount of growth factors and extracellular matrix that are slowly released over time *in vitro* [166, 167]. It has been demonstrated that L-PRF secretes transforming growth factor beta 1, platelet-derived growth factors A and B, VEGF and insulin growth factor 1 in addition to extracellular matrix proteins. The mechanisms of action of L-PRF on the site of injury are unknown but it is postulated that the leukocyte and platelet content of the L-PRF creates a local inflammatory milieu that favours regeneration and that recruits and activates wound repairing cells and stem cells. Whereas Ehrenfest *et al.* only concentrated on the L-PRF-secretome [166], Schär *et al.* showed that L-PRF attracts human MSCs and endothelial cells, which potentially favours

revascularization and repair at the site of injury [167]. No previous studies have been performed to evaluate the of use of L-PRF for other applications. Thinking of L-PRF as a 'tissue in a dish' that can provide a suitable inflammatory microenvironment to prime hDPSCs prior to transplantation is an novel application that could potentially enhance the neuroregenerative properties of hDPSCs.

1.5 Aims of this Study

Given the encouraging results of MSCs in preclinical research and experimental evidence supporting the therapeutic potential of MSCs in stroke, this study was devoted to improve and unravel several aspects regarding MSC-based therapies for ischemic stroke. hDPSCs are a relatively low studied MSC source in the field of neuroregeneration. Nonetheless, they possess similar and even superior properties to BMSCs and can be acquired with less invasive surgical procedures and donor site morbidity. However, there is ongoing discussion on the preferred isolation method of hDPSCs as they can be acquired by two often-used methods: the explant method and enzymatic digestion method. The explant method is based on the plastic adherence of MSCs and outgrowth of cells out of tissue fragments that adhered to plastic [95]. The enzymatic digestion method on the other hand, is based on exposing tissue fragments to collagenase I and dispase to digest the pulp tissue after which a single-cell suspension is acquired [168]. Therefore, **the first aim of this study was to compare the stem cell properties and multilineage differentiation potential of hDPSCs isolated by the explant- and enzymatic digestion method**. The results of this comparison can be found in Chapter 2.

As mentioned previously, the rationale behind using MSCs (and hDPSCs) in stroke and other neurodegenerative diseases is two-fold: neural differentiation and cell replacement on the hand and paracrine-mediated stimulation of endogenous neuronal repair on the other hand. Neuronal differentiation of hDPSCs has thus far been encouraging but also limited as no action potential generation could be observed in the differentiated cells. **The second part of this study aimed to improve the neuronal differentiation protocol of hDPSCs** by implying a two-step protocol based on neuronal induction by neurosphere formation and subsequent neuronal maturation by providing the

proper environmental cues, as discussed in Chapter 3. In order to investigate the paracrine mediated effects of hDPSCs on NSCs and/or NPCs, we first needed to optimize a proper *in vitro* model to study the effect of the factors produced by hDPSCs. Therefore, in first instance, human SH-SY5Y neuroblastoma cells were used to assess the effect of the hDPSC-secretome on cells with neuronal characteristics. In the **third part of the study, the effect of the hDPSC-secretome on neuronal differentiation, migration and neuritogenesis of SH-SY5Y cells was evaluated** and is described in Chapter 4. In the **fourth part of this study**, the models that were introduced in Chapter 3 were used to determine **the paracrine-mediated neuroprotective and neuroregenerative potential of human dental pulp stem cells on primary cortical neurons and neural stem cells**. Moreover, the potential of L-PRF priming to enhance these features of the hDPSC-secretome was evaluated. In addition to the effect of L-PRF on hDPSCs, the effect of L-PRF itself as a biomaterial on neuronal cells was also evaluated as it currently is unclear what causes the beneficial clinical effect of L-PRF. These results are described in Chapter 5.

In order to evaluate the therapeutic potential of hDPSCs in stroke, an adequate and physiologically relevant animal model should be established. Whereas different animal models exist to induce stroke in an experimental setting, we opted to introduce, optimize and use the transient middle cerebral artery mouse stroke model in our lab. **The final part of this study (Chapter 6) was to introduce and optimize the stroke model** regarding occlusion time which is correlated with lesion size and stroke severity. Additionally, several behavioural tests were introduced in order to assess motor- and sensorimotor function. Finally, **a proof-of-principle study** was performed in which firefly luciferase-transfected hDPSCs were transplanted I.V. 24h after stroke onset after which the cell fate was tracked with bioluminescence imaging (BLI). Moreover, behavioural testing was performed every 2-3 days and lesion size was evaluated by means of MRI.

Chapter 2 : Effect of isolation methodology on the stem cell properties and multilineage differentiation potential of human dental pulp stem cells

Based on:

*:Equally contributing authors

2.1 Abstract

Human dental pulp stem cells (hDPSCs) are an attractive alternative mesenchymal stem cell (MSC) source due to their isolation simplicity compared to the more invasive methods associated with harvesting other MSC sources. However, there is ongoing discussion about which isolation method is to be favored in obtaining hDPSC cultures. This study compares the stem cell properties and multilineage differentiation potential of hDPSCs that were obtained using the two most widely adapted isolation procedures. hDPSCs were either isolated by enzymatic digestion of the pulp tissue (hDPSC-EZ) or by the explant method (hDPSC-OG), while keeping the culture media constant throughout all experiments and both isolation methods. Assessment of the stem cell properties of hDPSC-EZ and hDPSC-OG showed no significant differences between both groups with regard to proliferation rate and colony formation. Phenotype analysis indicated that hDPSC-EZ as well as hDPSC-OG were positive for CD29, CD44, CD90, CD105, CD117 and CD146 expression without any significant differences. The multilineage differentiation potential of both stem cell types was confirmed using standard immuno(histo/cyto)chemical stainings together with an in-depth ultrastructural analysis by means of transmission electron microscopy. Our results indicate that both hDPSC-EZ and hDPSC-OG could be successfully differentiated into adipogenic, chrondrogenic and osteogenic cells, although the adipogenic differentiation of both cell populations appeared limited. These data indicate that both the enzymatic digestion and outgrowth method could be applied to obtain a suitable autologous dental pulp stem cell resource for tissue replacement therapies of both bone and cartilage.

2.2 Introduction

Since the discovery of bone marrow as a source of mesenchymal stem cells (BM-MSC), additional stem cell niches have been identified in a variety of tissues including the umbilical cord, adipose tissue and skeletal muscle. More recently, the dental pulp was also found to contain a stem cell niche [85, 87, 169-171]. As was shown by a number of studies, human dental pulp stem cells (hDPSCs) originate from the neural crest [172, 173]. However, recent investigations of Feng *et al.* on mouse incisors, suggested the contribution of pericyte-derived MSCs to odontoblast differentiation in case of tissue damage, next to the migration of cells from the MSC-niche within the tooth which supports tooth growth by continuous cell supply [174]. hDPSCs can be characterised as mesenchymal-like stem cells; based on their plastic adherence and the expression of stem cell markers such as CD29, CD90, CD44 and Stro-1. In addition, it has been shown that these stem cells are capable of differentiating into adipocytes, chondroblasts and osteoblasts *in vitro* [83, 85, 95, 150, 151]. Furthermore, studies have indicated that hDPSCs are not only capable of differentiating into odontoblasts *in vitro*, but that they are also able to form an organized dentin-pulp-like complex lined with odontoblast-like cells when seeded onto a scaffold and transplanted into immunocompromised mice [85, 175]. These observations suggest the potential role of hDPSCs in the repair of diseased and damaged dental tissues. Besides applications in tooth regeneration and repair, hDPSCs could also be clinically applied in other domains since they are capable of differentiating into several other lineages, such as muscle cells [176], endothelial cells[176, 177] and functional neurogenic cells showing electrophysiological currents and the expression of neuron-related surface markers [98, 155]. Furthermore, since hDPSCs are isolated relatively easy from extracted third molars without any risk to the donor, have a higher proliferative and immunomodulatory capacity than BM-MSC and retain their multilineage differentiation capacity after cryopreservation, these stem cells display several advantages over BM-MSC with regard to future *in vivo* use and clinical applications [178-180].

However, there is ongoing discussion about which isolation method is to be favoured when obtaining hDPSCs. The two most widely applied isolation

methods to harvest the stem cells are enzymatic digestion of the tissue and the explant method. While the explant method is based upon the plastic adherence of MSC and subsequent outgrowth of cells out of tissue fragments, enzymatic digestion applies collagenase I and dispase in order to digest pulp tissue to acquire single cell suspensions [168]. Both techniques have been used successfully with hDPSCs, umbilical cord matrix stem cells and adipose tissue derived MSC [85, 95, 168, 170, 171, 181-183]. Research regarding the preferred isolation method of hDPSCs focused on the differentiation into a specific cell type, mainly odontoblasts, and their application in tooth engineering [168, 184]. These studies only included a comparison on the osteogenic differentiation potential and did not focus on differentiation capacity into chondrocytes and adipocytes and other stem cell properties of the hDPSCs obtained by these two isolation methods. Furthermore, in most studies the DPSC-OG and DPSC-EZ were not cultured in the same culture media. Therefore, our study aims to compare hDPSCs isolated by means of enzymatic digestion (hDPSC-EZ) with hDPSCs isolated using the explant method (hDPSC-OG), with regard to their stem cell properties and multilineage differentiation potential. In terms of stem cell properties, the proliferation rate, colony formation and immunophenotype of hDPSC-EZ and hDPSC-OG were compared. In addition, the stem cell morphology was assessed at the ultrastructural level. The multilineage differentiation potential into osteogenic, chondrogenic and adipogenic lineages of both stem cell types was confirmed by means of different immunostainings and a detailed ultrastructural analysis.

2.3 Materials and methods

2.3.1 Materials

Alpha-modification of minimum essential medium (α-MEM) and 1:1 ratio of Dulbecco's modified Eagle's medium and F12 medium (D-MEM/F12), fetal bovine serum (FBS, Biochrom AG, Berlin, Germany), penicillin and streptomycin were obtained from Invitrogen (Carlsbad, CA, USA). For the enzymatic digestion, following enzymes were bought from Sigma (Sigma-Aldrich, St-Louis, MO, USA): Collagenase (Catalog number C2674, enzymatic activity 387.1 U/mg) and Dispase II (Catalog number D4693, enzymatic activity: 0.70 U/mg). Phycoerythrin (PE)-conjugated anti-human CD34 and PE-conjugated anti-

human CD44 (Immunotools, Friesoythe, Germany). PE-conjugated anti-human CD45, Fluorescein isothiocyanate (FITC)-conjugated anti-human CD90 and PE-conjugated anti-human CD105 (eBioscience, Vienna, Austria). PE-conjugated anti-human NGFR p75 (Biolegend, San Diego, CA, USA), PE-conjugated anti-human Stro-1 (Santa Cruz Biotechnology, Santa Cruz, CA, USA) and mouse anti-alkaline phosphatase (R&D systems, Minneapolis, MN, USA). Mouse anti-human CD29, rabbit anti-human CD29 and rabbit anti-human CD146 (Abcam, Cambridge, UK), rabbit anti-human CD117/c-kit (Santa Cruz Biotechnology), Alexa Fluor 555-conjugated donkey anti-mouse IgG and Alexa Fluor 488-conjugated donkey anti-rabbit IgG (Invitrogen).

To induce differentiation of hDPSCs to osteogenic, chondrogenic and adipogenic cell-lineages, the Human Mesenchymal Stem Cell Identification Kit was used from R&D systems (Minneapolis, MN, USA). This kit also included goat anti-mouse fatty acid binding protein 4 (FABP-4) and goat anti-human aggrecan antibodies.

2.3.2 Cell culture

Human dental pulp tissue was obtained with informed consent from patients (15 - 20 years of age) undergoing extraction of third molars for orthodontic reasons at the Department of Maxillofacial Surgery, Ziekenhuis Maas en Kempen, Belgium. After disinfection of the tooth surface, the teeth were mechanically fractured and the dental pulp was gently isolated with forceps, without any drilling, as this can have detrimental effects on the viability of hDPSCs. The pulp tissue was rinsed in αMEM supplemented with 2 mM L-Glutamine, 100 U/ml penicillin, 100 μg/ml streptomycin and 10% FBS (which will be referred to as standard DPSC culture medium), after which it was minced into fragments of 1-2 mm³. hDPSCs were then isolated according to two different methods, namely enzymatic digestion and the explant method (see Fig. 2.1). With regard to the explant method (DPSC-OG), a subset of tissue fragments was cultured in 6-well plates in standard DPSC culture medium [95, 185, 186]. The other subset of pulp fragments (DPSC-EZ) was incubated for 60 min at 37°C with a solution containing 3 mg/ml collagenase type I and 4 mg/ml dispase. After centrifugation at 300 g, cell suspensions were obtained by passing the resuspended digested tissue fragments through a 70 μm cell strainer. The cells were cultured in 6-well

plates in standard DPSC culture medium. All cell cultures were maintained at 37°C in a humidified atmosphere containing 5% CO_2. The culture medium was changed every 2-3 days and the cell cultures were monitored regularly with an inverted phase-contrast microscope (Nikon, Eclipse TS100, Nikon co., Japan). When reaching 70-80% confluence, cells were harvested using 0.05% Trypsin/EDTA (Sigma) and sub-cultured for further experiments. All differentiation protocols, expansion assays and immunophenotyping tests were conducted in parallel for the two isolation methods. Cells between passage 2 and 4 were used. For each assay, stem cells of at least 4 different donors were used.
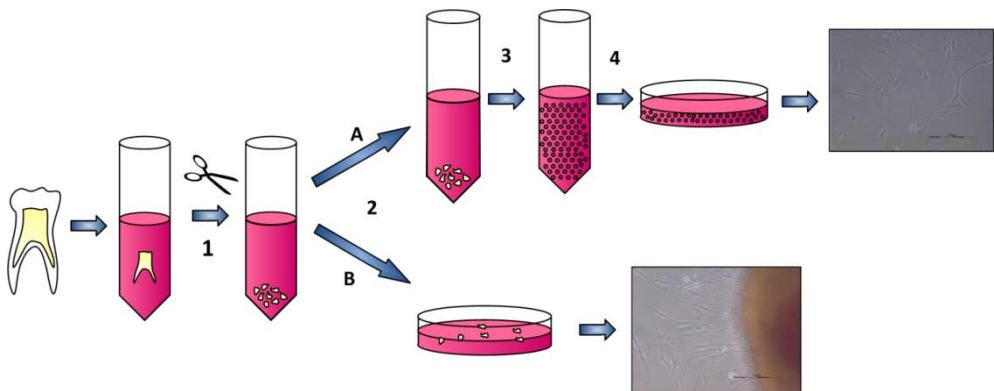
Figure 2.1: Isolation methods of hDPSCs. Pulp tissue was removed from the pulp cavity, rinsed with culture medium and cut into pieces of 1 mm3 (1). Next (2), half of the tissue fragments were processed for enzymatic digestion (A), whereas the other half were cultured by the explant method (B). In the enzymatic digestion method (A), tissue fragments were incubated with a collagenase/dispase solution for 1 h at 37 °C (3). This solution was centrifuged at 300g and passed through a cell strainer and the obtained single-cell suspension was divided among 6-well plates (4). For the explant method (B), tissue fragments were also divided among 6-well plates. After 48–72 h, tissue fragments had adhered onto the plastic surface and stem cells were able to grow out

2.3.3 Colony Forming Unit assay

The colony forming properties of both populations of hDPSCs were evaluated by means of a Colony Forming Unit (CFU) assay. Cells were seeded at 52.6 cells/cm² or 210.5 cells/cm², in a 6-well plate in standard hDPSCs culturing

medium. Each condition was performed in duplicate. After 10 days of culturing, hDPSCs were fixed in 4% paraformaldehyde (PFA) in PBS and colonies were visualized with a Toluidine Blue staining (Merck). Pictures were taken with a high resolution digital camera and macroscopic colonies (>50 cells) were quantified by three independent individuals with Image J cell counter Software.

2.3.4 Cell proliferation assay

In order to determine the proliferation rate of hDPSCs in culture, a 3-(4,5-Dimethylthiazol-2-yl)-2,5-diphenyltetrazolium bromide (MTT) assay was performed. Cells were seeded at 6.25×10^3 cells/cm² in a 96-well plate in standard DPSC culturing medium. All conditions were performed in triplicate. After 24h, 48h, 72h and 96h of culturing, the culture medium was replaced with 500 µg/ml MTT in standard DPSC culturing medium containing 0.1% FBS. After 4h of incubation, the MTT solution was removed and a mixture of 0.01 M glycine in dimethylsulfoxide (DMSO) was added to allow reduction to formazan. The absorbance was measured at a wavelength of 570 nm with a Benchmark microplate reader (Biorad Laboratories).

2.3.5 Fluorescence-activated cell sorting analysis

hDPSCs of both isolation methods were seeded in 25 cm² culture flasks and were harvested by trypsinisation after 7 days. Then, for each staining, 0.5×10^5 cells were washed once with PBS containing 2% FBS and were incubated for 30 min at room temperature in PBS with 2% FBS to allow re-expression of receptor proteins at the cell surface. Then, the cells were incubated for 45 min at room temperature with primary antibody (see Table 2.1). As a negative control for non-specific background staining, appropriate isotype controls were also included. Thereafter, cells were washed three times with PBS and analysed on a FACScalibur™ flow cytometer equipped with CellQuest Pro™ Software (BD Biosciences, Franklin Lakes, NJ).

Table 2.1: Primary antibodies and isotype controls for flow cytometry. M= mouse.

Marker	Species	Isotype	Cat. nr	Dilution	Label	Company
Primary Antibodies						
CD34	M	IgG1	21270344	1/100	PE	Immunotools
CD44	M	IgG2b	21270444	1/100	PE	Immunotools
CD45	M	IgG1,k	12-0459-41	1/100	PE	eBioscience
CD90	M	IgG1,k	11-0909-42	1/100	FITC	eBioscience
CD105	M	IgG1,k	12-1057-41	1/100	PE	eBioscience
NGFR (p75)	M	IgG1,k	345106	1/100	PE	Biolegend
Stro-1	M	IgM	sc47733	1/20	PE	Santa Cruz
Isotype controls						
IgG1,k	M	IgG1,k	11-4714-42	1/100	FITC	eBioscience
IgG1,k	M	IgG1,k	12-4714-42	1/100	PE	eBioscience
IgM	M	IgM	sc2870	1/20	PE	Santa Cruz
IgG2b	M	IgG2b,k	12-4732-42	1/100	PE	eBioscience

2.3.6 Trilineage differentiation of hDPSC-EZ and hDPSC-OG

Adipogenic differentiation was induced as instructed by the manufacturer (R&D systems). hDPSC-EZ and hDPSC-OG were seeded at a density of 2.1×10^4 cells/cm² on glass coverslips for light microscopy or on plastic coverslips (Thermanox®, Electron Microscopy Sciences, Hatfield, PA) for Electron Microscopy (EM). When the cells reached 70-80% confluence, cells were incubated with adipogenic differentiation medium consisting of α-MEM supplemented with 10% FBS and 1% adipogenic supplement (R&D systems). This supplement contains dexamethasone, ascorbate-phosphate, and β-glycerolphosphate to induce differentiation. The differentiation medium was changed every 3-4 days. After 3 weeks of differentiation, adipogenic differentiated hDPSC-EZ and hDPSC-OG seeded on glass coverslips were washed with PBS and fixed with 4% PFA for 20 min at room temperature. Fixed cells were subjected to an Oil red O staining to detected lipid droplet accumulation and an immunocytochemistry (ICC) for FABP-4 was also performed. Adipogenic

differentiated stem cells seeded on plastic coverslips were fixed with 2% glutaraldehyde in 0.05M cacodylate buffer (pH 7.3) at 4°C for EM processing.

Differentiation of hDPSC-EZ and hDPSC-OG to chondrogenic cells was initiated according to the guidelines delivered by the manufacturer (R&D systems). A pellet containing 2.5×10^5 cells in a 15 ml conical tube was subjected to the chondrogenic differentiation medium consisting of D-MEM/F12 supplemented with 1% Insulin Transferrin Selenite (ITS) (Sigma) and 1% chondrogenic supplement (R&D systems). This supplement contains dexamethasone, ascorbate-phosphate, proline, pyruvate and TGF-β3. Every 3-4 days, this differentiation medium was changed. After hDPSC-EZ and hDPSC-OG were able to differentiate for 21 days, the pellets were either fixed with 4% PFA for IHC analysis or with 2% glutaraldehyde in 0.05 M cacodylate buffer (pH 7.3) at 4°C for EM processing. For IHC analysis, chondrogenic pellets were embedded in paraffin and sections of 7 µm were made. On these sections, a Trichrome of Masson staining was performed to assess the presence of connective tissue (such as collagen II in case of chondrogenic differentiation) and also IHC against aggrecan, a protein typical for cartilaginous tissue was done.

Osteogenic differentiation was induced as instructed by the manufacturer (R&D systems). Briefly, coverslips were coated with 1 µg/ml Fibronectin (R&D systems) overnight, prior to seeding hDPSC-EZ and hDPSC-OG at a density of 4.2×10^3 cells/cm² on glass coverslips for IHC or on plastic coverslips for EM. After reaching 50-70% confluence, seeded cells were subjected to the osteogenic differentiation medium consisting of α-MEM supplemented with 10% FBS and 5% osteogenic supplement (R&D systems). The osteogenic supplement contains dexamethasone, ascorbate-phosphate and β-glycerolphosphate in concentrations determined by the manufacture. The differentiation medium was changed twice per week. After 2-3 weeks of differentiation, cells were fixed for LM and EM processing. Calcium deposits were detected by a 40 mM Alizarin Red S staining. In addition, a quantitative analysis of the Alizarin Red S uptake was performed with a Cetylpyridinium Chloride (CPC, Sigma-Aldrich) assay as previously described [187]. Briefly, after staining the differentiated cells with 40 mM Alizarin Red S for 10 min at room temperature the cells were washed thoroughly with distilled water to remove excess Alizarin Red S. Subsequently, a

10% CPC solution in 10 mM sodium phosphate was added to the samples for 15 min at room temperature. The samples were collected and absorption was measured at 550 nm. Alkaline Phosphatase (ALP) immunoreactivity was also assessed.

2.3.7 Immunocytochemistry

Cells were seeded at 2.5 x 10³ cells/cm² on glass coverslips in standard hDPSC culture medium (unless mentioned otherwise). When 80-90% confluence was reached, the cells were fixed in 4% PFA and immunostainings were performed according to a standardized protocol. Briefly, in case of an intracellular epitope, cells were permeabilised with 0.05% Triton X-100 in PBS for 30 min at 4°C. 10% donkey serum was used to block aspecific binding sites. For immunofluorescence, the cells were incubated overnight at 4°C with the primary antibodies listed in Table 2.2. Negative controls were included and were performed by omitting the primary antibody. After thoroughly rinsing with PBS, the wells were incubated for 30 min. with one of the secondary antibodies listed in Table 2.2. After counterstaining of the cellular nuclei with 4,6-diamidino-2-Phenylindole (DAPI), the coverslips were mounted with anti-fade mounting medium (Dako, Glostrup, Denmark) on glass slides. Non-fluorescent immunostainings were performed using a DAB EnVision™ System kit (Dako). Briefly, aspecific binding sites were blocked with 10% normal goat serum after which the cells were incubated for one hour at room temperature with the primary antibodies listed in Table 2.2. Depending on the primary antibody, the cells were incubated with the appropriate secondary antibody. The staining was visualized by means of a 3,3' diaminobenzidine (DAB) chromogen solution according to the manufacturer's instructions. After counterstaining with Mayer's hematoxylin, the coverslips were mounted on glass slides using Aquatex® (Merck, Darmstadt, Germany). Pictures were taken with a Nikon Eclipse 80i Fluorescence Microscope equipped with a 2MBWc digital sight camera or a Nikon Eclipse 80i Microscope equipped with a DS-5M digital camera.

2.3.8 Transmission electron microscopy

Samples cultured on plastic Thermanox® coverslips were fixed with 2% glutaraldehyde in 0.05M sodium cacodylate buffer (pH=7.3) at 4°C and processed as previously described [95]. Postfixation was achieved by treating the samples with 2% osmiumtetroxide in 0.05 M sodium cacodylate buffer (pH=7.3) for 1 h at 4°C after which the samples were stained with 2% uranyl acetate in 10% acetone for 20 min. Dehydration of the cell-seeded coverslips was performed by exposing them to ascending concentrations of aceton. The dehydrated samples were impregnated overnight in a 1:1 mixture of aceton and araldite epoxy resin at room temperature. After impregnation, samples were embedded in araldite epoxy resin at 60°C using the pop-off method [188]. The embedded samples were cut in slices of 40-60 nm, making use of a Leica EM UC6 microtome (Leica, Wetzal, Germany) and were then transferred to 0.7% formvar coated copper grids (Aurion, Wageningen, The Netherlands). The samples were contrasted using a Leica EM AC20 (Leica) with 0.5% uranyl acetate and a stabilized solution of lead citrate. TEM analysis was performed with a Philips EM208 S electron microscope (Philips, Eindhoven, The Netherlands). Digital images were obtained with a Morada Soft Imaging System camera with corresponding iTEM-FEI software (Olympus SIS, Münster, Germany).

2.3.9 Statistical analysis

Statistical analysis was performed using Graphpad Prism 4 software (Graphpad, San Diego, CA). After testing for normality by means of a D'Agostino & Pearson omnibus normality test, experimental groups were compared by means of a (non)parametric t-test. Differences were considered statistically significant at P-values ≤ 0.05. All data were expressed as mean ± standard deviation (S.D.).

Table 2.2: Primary and secondary antibodies for immunocytochemistry. (FABP-4= fatty-acid-binding protein 4, ALP= Alkaline Phosphatase; HRP= horseradish peroxidase, MM= mouse monoclonal; RP= Rabbit polyclonal; GP= Goat Polyclonal; DP = Donkey Polyclonal; DAM= Donkey anti-mouse; DAR= Donkey anti-rabbit; GAM= Goat anti-mouse; DAG= Donkey anti-goat)

Marker	Type	Clone/ Cat. nr	Dilution	Label	Company
Primary Antibodies					
CD29	MM	4B7R; ab3167	1/50		Abcam
CD117	RP	Sc-168	1/100		Santa Cruz Biotechnology
CD146	RP	epr3208; ab75769	1/100		Abcam
Aggrecan	GP	962644	1µg/100ml		R&D Systems
ALP	MM	B4-78	1/50		R&D Systems
FABP-4	GP	/	1µg/100ml		R&D Systems
Secondary Antibodies					
DAM	DP IgG	A31570	1/500	Alexa Fluor 555	Invitrogen
DAR	DP IgG	A21206	1/500	Alexa Fluor 488	Invitrogen
GAM	GP IgG	/	RTU	HRP	Dako
DAG	DP IgG	705-035-003	1/500	HRP	Jackson Immunoresearch Laboratories

2.4 Results

2.4.1 Morphology and immunophenotype of DPSC-EZ and DPSC-OG

After isolating the stem cells according to the described methods, regular monitoring with a phase-contrast microscope showed that the enzymatic digestion method gave rise to adherent cells overnight, while the cells yielded from the explants started to adhere and proliferate after 2-4 days. After approximately one week, hDPSC-EZ reached 80-90% confluence. In contrast, hDPSC-OG were found confluent after ten to fourteen days. In terms of cellular morphology, phase-contrast pictures showed the appearance of elongated fibroblast-like cells (e, Fig. 2.2A) in both EZ- as OG-cultures. Enzymatic digestion, however, gave rise to a more heterogeneous cell culture in comparison to the outgrowth method, given the presence of polygonal cells with multiple processes (p, Fig. 2.2A). At the ultrastructural level, both hDPSC-EZ and hDPSC-OG were characterised by an elongated cellular appearance with a perinuclear organelle-rich zone (p, Fig. 2.2C, D), containing rough endoplasmic reticulum cisternae (r, Fig. 2.2E, F) and mitochondria (m, Fig. 2E, F), which could clearly be distinguished from an electron-lucent organelle-poor peripheral zone (o, Fig. 2.2C, D). Large euchromatic nuclei with one or more nucleoli (n, Fig. 2.2C, D) were also visible. Although no significant morphological differences between cells from both isolation methods were observed, hDPSC-EZ showed extensive vacuolization throughout the entire cytoplasm (v, Fig. 2.2E) while this was not the case for hDPSC-OG.
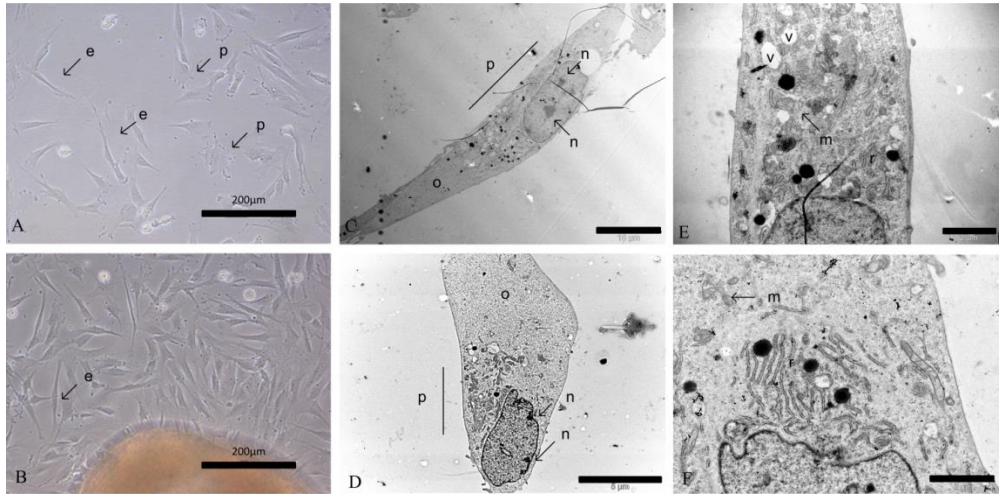
Figure 2.2: Morphology of hDPSC-EZ and hDPSC-OG at light microscopic and ultrastructural level. hDPSC- EZ cultures consisted of a heterogeneous cell population (A, C E) while hDPSC-OG cultures mainly displayed elongated fibroblast-like cells (B, D, F). Abbreviations: (e: elongated, p: polyclonal, m: mitochondria; n: nucleolus; o: organelle-poor region; p: perinuclear region; r: endoplasmic reticulum; v: vesicles) Scale bars: A, B =200 μm; C = 10 μm; D= 5 μm; E, F = 2 μm. Data courtesy of dr. Petra Hilkens.

The immunophenotype of hDPSC-EZ and hDPSC-OG was evaluated by means of immunocytochemistry and flow cytometry. Immunofluorescence showed a uniform expression of CD29 by both groups of hDPSCs (Fig. 2.3A-D), while CD117 showed interdonor variability (Fig. 2.3A-D). hDPSCs were also positive for endothelial marker CD146 (Fig. 2.3E,F) With regard to the expression of stem cell markers CD90 and CD44, flow cytometry showed high levels of expression for DPSC-EZ as well as DPSC-OG. However, no significant difference could be observed. Furthermore, both experimental groups were also strongly positive for CD105, although there was no significant difference between the two isolation methods (Fig. 2.3H). Expression analysis also indicated that hDPSCs were not only negative for CD34 and CD45, but also showed no expression of NGFR (p75) and Stro-1 (Fig. 2.3G).
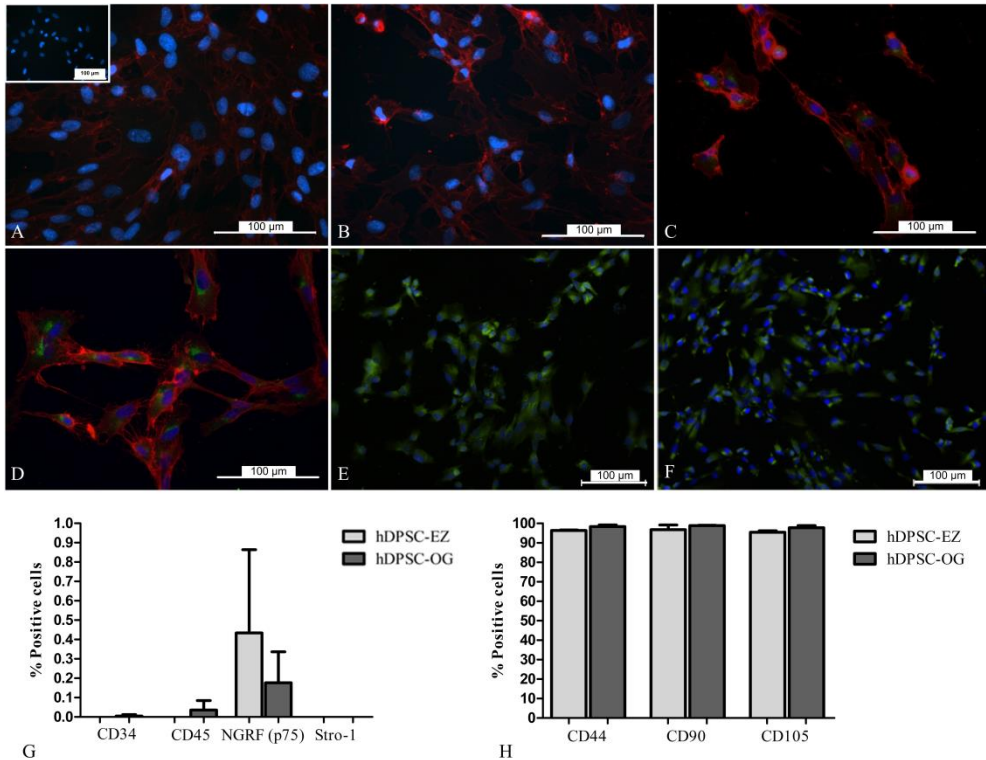
Figure 2.3: Immunophenotype of hDPSC-EZ and hDPSC-OG. (A-F) Representative immunofluorescent staining against CD29 (red); CD117 (green) and CD146 (green). (A) hDPSC-EZ CD29^{+} CD117^{-}. (B) hDPSC-OG CD29^{+} CD117^{-}. (C) hDPSC-EZ CD29^{+} CD117^{+}. (D) hDPSC-OG CD29^{+}CD117^{+}. (E) hDPSC-EZ CD146^{+}. (F) hDPSC-OG CD146^{+}. Scale bars = 100 μm. (G, H) Flow cytometry conducted in parallel on 3 different donors in 3 independent assays. (G) DPSCs of both isolation methods were negative for CD34, CD45, NGFR p75 and Stro-1 with no significant differences between both groups. (H) hDPSC-EZ and hDPSC-OG were strongly positive for CD44, CD90 and CD105 with no significant differences between both groups Data are represented as mean ± S.D. Data courtesy of dr. Petra Hilkens.

2.4.2 Proliferation rate and colony formation

In order to assess potential differences in proliferation rate between hDPSC-EZ and hDPSC-OG, an MTT assay was performed on six donors samples. Analysis showed a gradual increase of proliferation during 72h followed by the onset of stabilization for both hDPSC-EZ and hDPSC-OG. During the observed time frame

there was only a significant difference in proliferation rate in favour of hDPSC-EZ after 24h (Fig. 2.4A). With regard to colony forming properties, hDPSC-EZ as well as hDPSC-OG were able to form numerous colonies during 10 days of culturing. However, independent quantification of four different donor samples indicated no significant differences between both isolation methods (Fig. 2.4B).
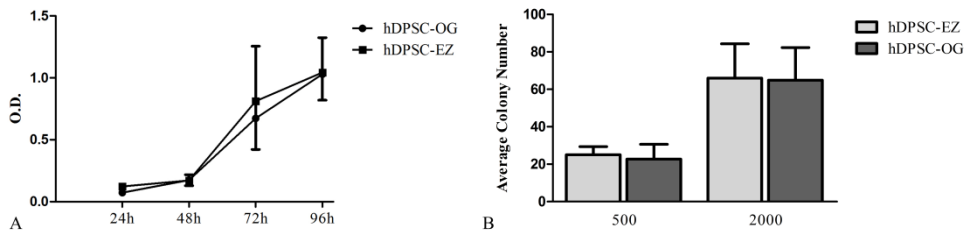
Figure 2.4: Proliferation rate and colony forming properties of hDPSC-EZ and hDPSC-OG. (A) MTT analysis of hDPSC-EZ and hDPSC-OG showed that there was no significant difference between both isolation methods with regard to proliferation rate. Results were obtained in parallel for EZ-OG on 6 different donors in 3 independent assays. Data are expressed as mean ± S.D. (B) CFU analysis of hDPSC-EZ and hDPSC-OG showed that the average number of colonies did not differ significantly between both isolation methods. Assay was conducted independently on 4 different donors. O.D.= optical density. Data are represented as mean ± S.D. Data courtesy of dr. Petra Hilkens.

2.4.3 Trilineage differentiation potential of differentially isolated human dental pulp stem cells

Maintaining hDPSC-OG and hDPSC-EZ in adipogenic differentiation medium for 3 weeks induced strong FABP-4 expression in a subset of cells (Fig. 2.5A, B). These cells also displayed big transparent droplets in their cytoplasm which are lipid-containing vacuoles. Quantification indicated that adipogenic differentiation appeared to be more successful in hDPSC-OG cells (12.35 % for hDPSC-OG versus 9.5% for hDPSC-EZ), but this difference was not found to be significantly different (Fig. 2.5E). In both cell cultures, Oil red O staining demonstrated the presence of intracellular lipid droplets (Fig. 2.5C, D) in a subset of cells.

On the ultrastructural level, adipogenic differentiated hDPSC-OG and hDPSC-EZ were both characterised by a globular appearance, with cytoplasm containing a

dilated rough endoplasmic reticulum (RER) and numerous small transparent vesicles (Fig. 2.5F). Typically, these intracellular organelles were spread uniformly throughout the cell cytoplasm and not only in the perinuclear area, as was the case in undifferentiated cells. A subset of cells also contained small electron-dense lipid droplets, confirming the results of the FABP-4 and Oil red O staining (Fig. 2.5G, H). A dilated RER and branched mitochondria were also present in the cytoplasm. No morphological difference between adipogenic differentiated hDPSC-OG or hDPSC-EZ was observed. Also, the ultrastructural analysis revealed that not all cells became adipocytes, but that only a subset of cells showed dense lipid droplets.
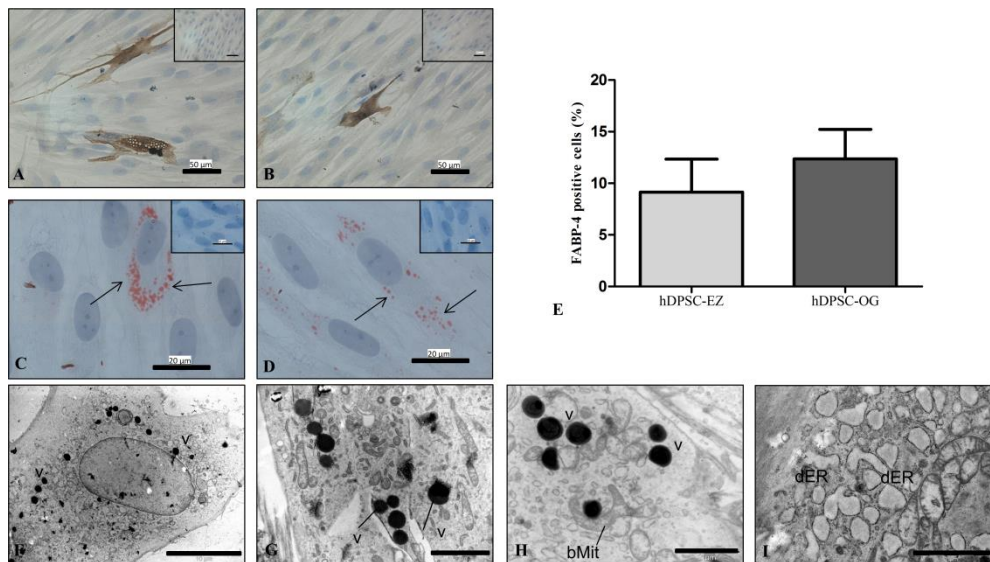
Figure 2.5: Adipogenic differentiation. Adipogenic differentiation of hDPSC-EZ (A, C) and hDPSC-OG (B, D). FABP-4 expression (A, B) and lipid droplet accumulation (C, D) was observed following 3 weeks of incubation in adipogenic differentiation medium (A, B). Inserts of these pictures show undifferentiated hDPSC-EZ (A,C) or hDPSC-OG (B ,D). Quantification indicated that there was no difference in immunopositive FABP-4 cells between both isolation methods (E) (n=4, data are represented as mean ± S.D). Ultrastructurally, adipogenic differentiated cells are globularly shaped (F) with a cytoplasm filled with electron-dense vesicles (v in figure G and H), branched mitochondria (H, bMit) and dilated rough endoplasmic reticulum (I, dER). Scale bars: A, B= 50 μm; C, D = 20 μm; F= 10μm; G, H, I = 2 μm.

Subjecting hDPSC-OG and hDPSC-EZ to osteogenic differentiation for 2-3 weeks induced ALP synthesis (Fig. 2.6A, B) compared to controls (inserts). Alizarin Red S staining of osteogenic differentiated hDPSC-OG and hDPSC-EZ showed the formation of calcified nodules (Fig. 2.6C, D). These nodules were susceptible to inter-donor variability in size and number in both experimental subgroups and were not observed in control samples. Subsequent analysis with CPC (Fig. 2.6E) indicated that osteogenic differentiation induced a significant increase in calcium deposition in both hDPSC-EZ and DPSC-OG compared to controls. However, no significant difference in calcium deposition was detected between both osteogenic differentiated hDPSC-EZ and hDPSC-OG.

Ultrastructurally, both osteogenic induced hDPSC-EZ and hDPSC-OG were characterised by an osteoblast-like morphology with an eccentric nucleus and a cytoplasm containing multiple lamellar and dark matrix-producing vesicles (Fig. 2.6F, I). Primary cilia were detected in both hDPSC-EZ and hDPSC-OG (Fig. 2.6G, I). Numerous globular mineralized nodules consisting of hydroxyapatite needles (Fig. 2.6J) were observed in the extracellular space in addition to striated collagen fibres (Fig. 2.6K) in both experimental conditions. Large mineralized fragments and fused mineralized nodules both interacted with surrounding collagen fibres.
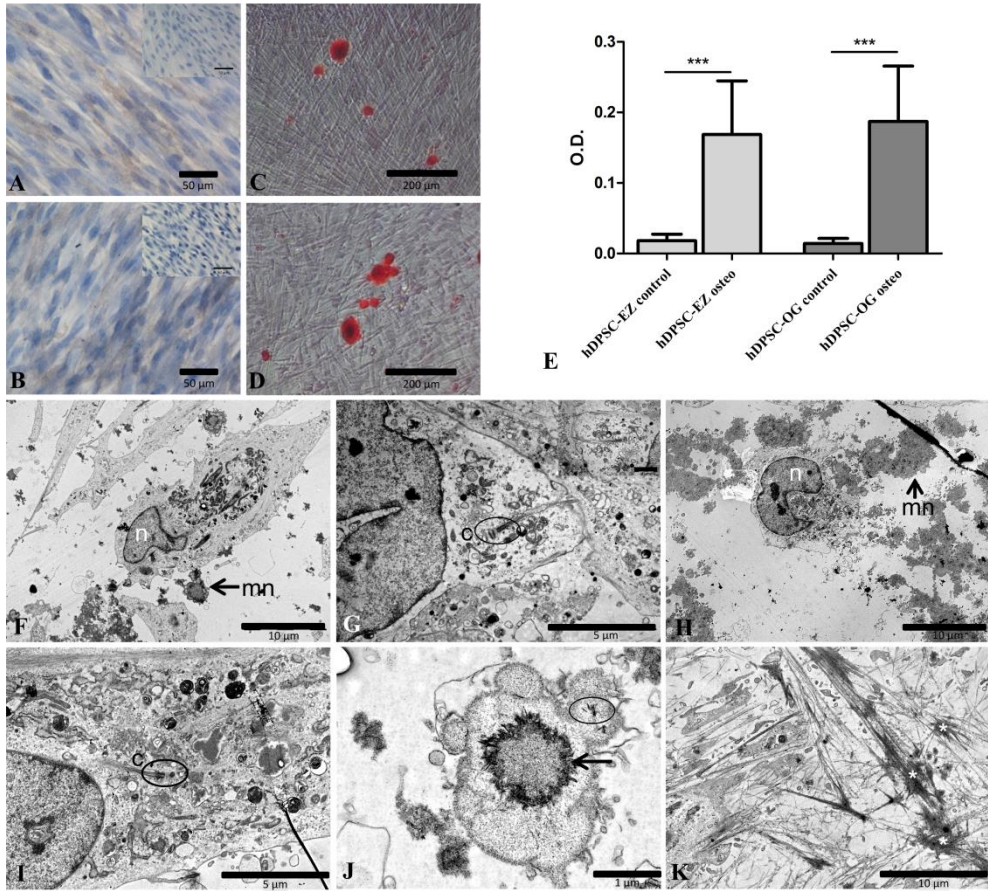
Figure 2.6: Osteogenic differentiation. Osteogenic differentiated hDPSC-OG (A) and hDPSC-EZ (B) expressed ALP. Calcium deposits were detected by Alizarin Red S staining in both hDPSC-OG (c) and hDPSC-EZ (d). (E) Quantification of calcium deposits with CPC showed a significant difference between controls and osteogenic differentiated hDPSCs, both in the OG and EZ group. No significant difference was found between osteogenic differentiated hDPSC-EZ and hDPSC-OG. (n= 8; ***= P-value < 0.001; data is represented as mean ± S.D.). Ultrastructural analysis of osteogenic differentiated hDPSC-EZ (F, G) and hDPSC-OG (H-K). Figures F and H are representative for the extracellular space of both cell types. Differentiated hDPSC-EZ and hDPSC-OG are characterised by an osteoblast-like morphology, displaying an eccentric nucleus (n) and the accumulation of lamellar- and matrix-containing vesicles in the cytoplasm (F-I). Primary cilia (c) were observed in both differentiated DPSC subgroups (g, i) with perpendicular basal bodies present at the base of the cilia (encircled; G, I). In the extracellular space, mineralized nodules (mn, arrow) consisting of hydroxyapatite needles were present (F, H). A detailed analysis of one of these nodules (J) shows that individual hydroxyapatite needles in

vesicles (encircled) are appositionally added to the core of these nodules (arrow). Large mineralized structures were found to interact with the surrounding striated collagen fibres (K). (Scale bars: A, B= 50µm; C, D= 200µm; F, H= 10 µm; G, I, K= 5 µm; J= 1 µm)

Following three weeks of chondrogenic differentiation, both hDPSC-OG and hDPSC-EZ formed 3D cell spheres. Aggrecan staining of these spheres showed immune-reactivity in both hDPSC-OG and hDPSC-EZ (Fig. 2.7A, B and C, D respectively). Masson's trichrome revealed the presence of collagen formation (blue) in the extracellular matrix surrounding the differentiated stem cells of both isolation methods (Fig. 2.7E, H). In addition, cartilage fragments (arrows, Fig. 2.7H) were visible in a subset of 3D spheres. TEM analysis of both chondrogenic differentiated hDPSC-EZ (Fig. 2.7I) and hDPSC-OG (Fig. 2.7L) showed that chondrogenic differentiated hDPSC were characterised by an elongated cell morphology with a cytoplasm enriched with ribosomes and numerous electron dense (grey) intracellular matrix vesicles (mv, Fig.7m,k), probably containing glycosaminoglycans. At higher magnifications, numerous striated collagen fibres were visible in the ECM (Fig. 2.7J). Cartilage fragments (ca) were present in the ECM of both experimental conditions and were closely interacting with the surrounding cellular and ECM compounds (Fig. 2.7K, N).
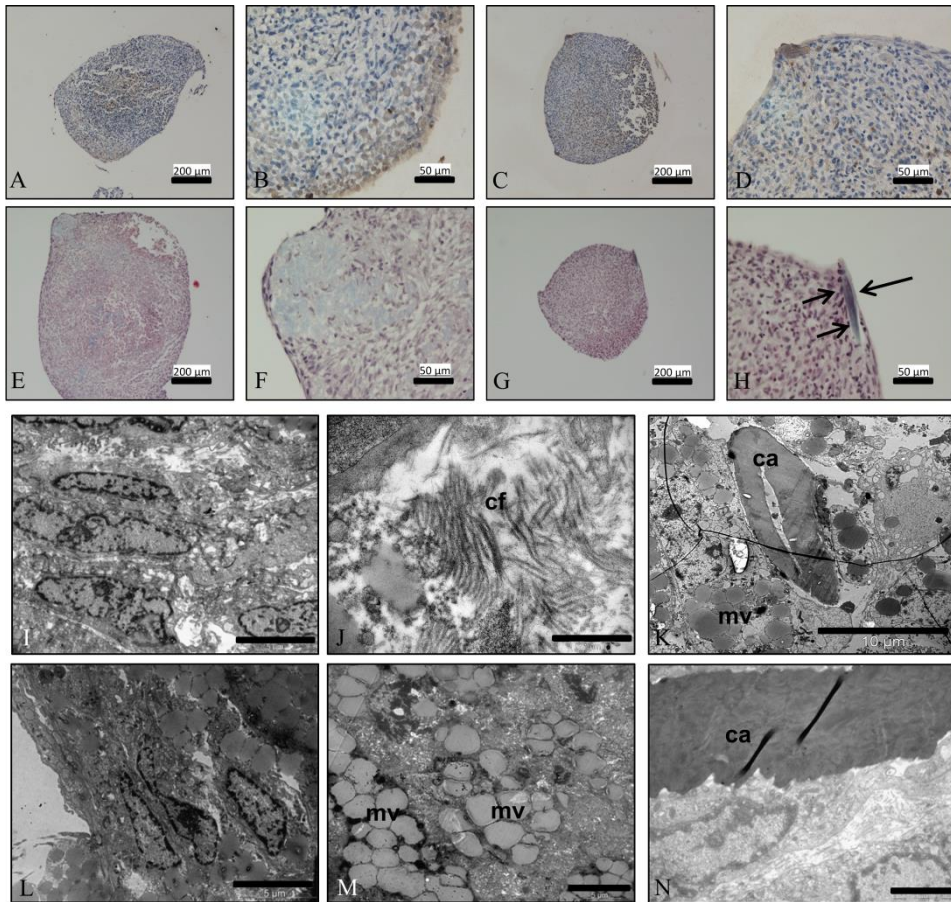
Figure 2.7: Chondrogenic differentiation. (A-D) Immunohistochemical staining against aggrecan of chondrogenic differentiated hDPSC-EZ (A, B) and hDPSC-OG (C, D). After differentiation, aggrecan was present in ECM of both stem cell types. (E-H) Masson's trichrome staining of chondrogenic differentiated hDPSC-EZ (E, F) and hDPSC-OG (G, H). After 3 weeks of differentiation, this staining on paraffin-embedded sections of 3D-chondrogenic spheres revealed the presence of collagen (blue) in stem cells of both isolation methods. Also, in some pellets cartilage fragments (arrows, H) were visible. (I-N) TEM analysis of 3D-chondrogenic differentiated DPSCs. Chondrogenic differentiated hDPSC-EZ (I) and hDPSC-OG (L) both displayed an elongated cell phenotype with a cytoplasm containing numerous ribosomes and electron-dense intracellular matrix vesicles (K, M, mv). Striated collagen fibres (cf) are abundant in the ECM (J). Cartilage fragments (ca) are present in the ECM of both cell types and are closely interacting with the surrounding hDPSCs and ECM (K, N). (Scale bars: a,c= 200 μm; b,d= 50 μm; e,g= 200 μm; f,h= 50 μm; i,l,m = 5 μm; j= 1 μm; k= 10 μm; n= 2 μm). TEM data courtesy of prof. dr. Annelies Bronckaers.

2.5 Discussion

In order for hDPSCs to be used as a MSC source in stem cell based research in regenerative medicine and tissue engineering, a consensus needs to be established on how these cells are preferably isolated. Therefore, this study evaluated the influence of isolation methodology on the stem cell properties and multilineage differentiation potential of DPSC-EZ and DPSC-OG. This study is the first to compare the effect of isolation methodology on stem cell properties and multilineage differentiation potential of hDPSCs while keeping all conditions constant throughout the performed experiments. In our study, the two most applied isolation methods for hDPSCs are compared, namely (1) the enzymatic digestion method, by which the dental pulp is subjected to a cocktail of dispase and collagenase to obtain a single cell suspension, and (2) the so-called 'outgrowth or explant method', by which the stem cells are allowed to grow out of small pieces of dental pulp tissue. Gronthos *et al.,* who were the first to describe the hDPSCs and their differentiation capacities, applied the enzymatic digestion method [85, 150], while many other research groups that mainly investigated various aspects of pulp cell physiology and differentiation into odontoblasts or mineral-forming cells *in vitro,* utilized the outgrowth method [95, 168, 183, 185, 186, 189, 190]. Already in 2006, Huang *et al.* compared these two isolation methods [168]. However, the culture conditions between both cell isolation methods were not the same: their hDPSC-EZ were cultured in α-MEM with 20% FBS, while hDPSC-OG were kept in D-MEM with 10% FBS. It cannot be excluded that the variances they observed between the different isolation methods could be caused by the use of different culture media. Also Bakopoulou *et al.* compared both isolation methods for dental stem cells of deciduous teeth and in that study also the culture medium differed between EZ and OG cells [184]. A previous report by Spath *et al.* [191] also compared enzymatic digestion versus the outgrowth method, but the outgrowth method described in our study (which is also widely used by other research groups) [95, 168, 183, 185, 189, 190] is slightly different from theirs. Spath *et al.* first digest the pulp tissue for 5 min. with trypsin, discarding all obtained cells, before the remaining tissue is transferred to a Petri dish and the stem cells are allowed to grow out of this tissue. In contrast, in most studies including ours, pulp tissue is not treated with any enzymes before it is placed into culture. In that study it

also remains unclear whether the origin of all their stem cells is of the same donors and all the cells are cultured in the same medium [191], while in our study both hDPSC-EZ and hDPSC-OG are isolated from the same donors and kept in the same growth medium. Finally, we also included the analysis of the adipogenic and chondrogenic differentiation potential of EZ and OG derived stem cells. Furthermore, cell morphology and differentiation success of both stem cell populations are compared at the ultrastructural level.

In terms of cellular morphology, elongated fibroblast-like cells were observed in hDPSC-EZ as well as in hDPSC-OG cultures. However, enzymatic digestion seemed to give rise to a more heterogeneous cell culture, given the presence of some cuboidal and polygonal cells. These observations were also made earlier by Bakopoulou *et al.* regarding dental pulp stem cells derived from human deciduous teeth [184]. These findings support earlier reports which state that enzymatic digestion not only allows the isolation of fibroblast-like (stem) cells but also the release of endothelial cells and pericytes, while the outgrowth method yields a more uniform population of fibroblast-like cells which migrate out of various tissue fragments, leaving non-migrating cells to disintegrate within the tissue [85, 150, 168, 192]. Despite the presence of vacuolization in DPSC-EZ, no apparent differences between both cultures were observed at the ultrastructural level. In spite of the aforementioned morphological discrepancies, no general significant difference could be observed in the proliferation rate of DPSC-EZ and DPSC-OG, except for an increased proliferation of DPSC-EZ after 24h. A similar proliferation rate was also the case for dental pulp stem cells derived from human deciduous teeth, while other studies suggest an increased proliferation rate either in favour of hDPSC-EZ or hDPSC-OG [168, 184, 191], although these discrepancies can be explained by the different isolation methods and culture conditions as described above. Colony forming assays also showed no significant differences between DPSC-EZ and DPSC-OG, both methods gave rise to pulp cells capable of forming an average amount of 66 colonies (when seeded at 210.5 cells/cm²) after 10 days. During this time frame, Huang *et al.* also observed similar colony formation for DPSC-EZ as well as DPSC-OG [168]. With regard to the immunophenotype, both isolation methods yielded hDPSCs which were strongly positive for CD44, CD90, CD105 and CD146 with no significant differences between both methods. The same immunophenotype was

recently observed by Karamzadeh *et al.*, although they indicated a significantly higher expression of CD105 and CD146 by DPSC-OG [193]. In fact, the expression of the perivascular cell marker CD146 supports the localization of hDPSCs in a perivascular niche of the dental pulp, as demonstrated earlier by Shi and Gronthos [172]. In contrast to earlier reports but in agreement with the aforementioned study of Karamzadeh *et al.*, hDPSC-EZ as well as hDPSC-OG were negative for Stro-1 expression [85, 150, 184, 193]. Both groups of hDPSCs were also negative for p75 expression, despite earlier reports of our group and others indicating a p75-positive subset of hDPSCs [185, 194]. Although Patel *et al.* indicated that continued passaging of dental pulp cells leads to the selection of more differentiated cells, which is reflected in a decreased expression of stem cell markers, the absence of Stro-1 and p75 could not be explained by this phenomenon since hDPSCs of early passage were used in all experiments [195]. Other potential explanations could be differences in cell cultivation methods or inter-donor variability due to age, dental health and the amount of exerted orthodontic force, factors which all have their impact on cellular homeostasis and marker expression. Inter-donor variability was also observed with regard to the expression of CD117; only subpopulations of certain hDPSC-EZ and hDPSC-OG samples showed reactivity for this marker. These findings confirm earlier reports on different hDPSC subpopulations [196, 197]. Finally, in agreement with previous studies and the general definition of MSC, both hDPSC-EZ as well as hDPSC-OG were negative for hematopoietic markers CD34 and CD45 [191, 193, 198, 199]. More recently, different studies oppose the observation that DPSCs are CD34$^-$ and have even used FACS to identify more potent subtypes of hDPSCs with regard to CD34 expression and targeted differentiation. Laino *et al.* described c-kit$^+$/CD34$^+$/CD45$^-$ DPSCs to be a potent subtype of hDPSCs for applications in bone-tissue engineering as they showed the *in vitro* formation of living autologous fibrous bone tissue by this cell type [197, 200]. In the present study, we have chosen not to use a specific subtype of DPSCs. The aim of this study was to compare the effects of the two mostly used isolation methodologies of hDPSCs without a cell sorting procedure. In that way, a heterogeneous population of DPSCs was obtained and the effect of preselecting hDPSCs for lineage-specific differentiation was excluded. Furthermore, depending on the clinical situation, a different approach of cell-based therapies can be applied.

When using a cell-based therapy in clinical relevant situations, a heterogeneous group of cells might be preferred as these can cope with the various environmental cues that are present within the tissue of interest. However, in other cases, preselected or pre-differentiated engrafted cells can have a beneficial effect compared to heterogeneous stem cells. For example, Iohara *et al.* showed that local transplantation of porcine CD31$^-$/CD146$^-$ DPSCs leads to an better increase in functional blood vessel formation compared to CD31$^+$/CD146$^-$ DPSCs in a murine ischemic hind limb model [201].

Subjecting hDPSC-EZ and hDPSC-OG to adipogenic differentiation showed the presence of intracellular accumulation of lipid droplets and the induced expression of FABP-4, both distinctive for adipocytes. No significant difference in differentiation potential between both cell types was observed. However, in both isolation methods, only a subpopulation of the hDPSCs was able to differentiate into adipocytes, indicating that further optimization of the differentiation protocol is needed and that hDPSCs may not be the ideal stem cell source for the replacement of fatty tissue.

Inducing osteogenic differentiation in hDPSC-EZ and hDPSC-OG had a comparable outcome in both cell types. Osteogenic differentiation induced ALP expression and the production of calcified nodules, although no significant difference between both isolation methods was observed. In contrast, the research report of Bakopoulou *et al.* regarding pulp stem cells from deciduous teeth revealed that the EZ method yielded stem cells with a higher mineralization rate [184]. However, this report did not keep all experimental conditions constant for both isolation methods. The ultrastructural evaluation of osteogenic differentiated hDPSC-EZ and hDPSC-OG confirms the results of the immuno(cyto/histo)chemical stainings as calcified nodules and an osteoid-like extracellular matrix containing striated collagen fibres were observed. These results are consistent with the requirement that cells showing hard-tissue engineering potential must be able to produce both the organic and inorganic bone matrix components [85, 197, 200]. In addition, primary cilia were observed in both osteogenic differentiated hDPSCs, suggesting that these cells can translate extracellular chemical and mechanical stimuli into cellular responses [202].

Chondrogenic differentiated hDPSC-EZ and hDPSC-OG were both characterised by similar morphological features and no differences between both populations could be noted. The cytoplasm was characterised by the presence of numerous intracellular vesicles and the ECM matrix was comprised of this ground substance, together with collagen fibres (collagen type II) and as an indisputable proof of chondrogenic differentiation, cartilage fragments.

Taken together, the ultrastructural evaluation of multilineage differentiated hDPSC-EZ and hDPSC-OG demonstrated that both cell types show trilineage differentiation potential. The in-depth ultrastructural analysis presented in this study provides a valuable addition to the performed ICC and IHC stainings in punctuating the differentiation potential of hDPSCs. In most studies, the differentiation success is measured by IHC, histological stainings, RT-PCR or Western blot analysis. However, these methods are merely based on intracellular molecular alterations and ECM deposits and do not take into account the real morphological changes that occur within the cell or in the ECM following differentiation inducing conditions. Upregulation of several markers does not necessarily mean that the stem cells are differentiated into a specific cell type. It can therefore be considered that an ultrastructural analysis of differentiated hDPSCs is mandatory to strengthen *in vitro* differentiation of hDPSCs and stem cells in general.

Conclusion

This study revealed that there is no difference in cellular morphology, proliferation rate, stem cell marker expression and mesenchymal differentiation potential between hDPSCs, isolated by means of the enzymatic digestion or the outgrowth method, when these cells are kept in the same culture conditions and are derived from the same donors. Both isolation methods yielded stem cell populations that are particularly capable of differentiation into osteoblasts and chondroblasts, leading to the conclusion that these stem cells provide a promising strategy for the treatment of bone and cartilage injuries.

Chapter 3 : Neurogenic maturation of human dental pulp stem cells following neurosphere generation induces morphological and electrophysiological characteristics of functional neurons

Based on:

Gervois, P., T. Struys, P. Hilkens, A. Bronckaers, J. Ratajczak, C. Politis, B. Brone, I. Lambrichts, and W. Martens, Neurogenic maturation of human dental pulp stem cells following neurosphere generation induces morphological and electrophysiological characteristics of functional neurons. Stem Cells Dev, 2015. **24**(3): p. 296-311

3.1 Abstract

Cell-based therapies are emerging as an alternative treatment option to promote functional recovery in patients suffering from neurological disorders, which are a major cause of death and permanent disability. The present study aimed to differentiate human dental pulp stem cells (hDPSCs) towards functionally active neuronal cells *in vitro*. hDPSCs were subjected to a two-step protocol. First, neuronal induction was acquired through the formation of neurospheres, followed by neuronal maturation, based on cAMP and NT-3 signalling. At the ultrastructural level, it was shown that the intra-spheral microenvironment promoted intercellular communication. hDPSCs grew out of the neurospheres *in vitro* and established a neurogenic differentiated hDPSC culture (d-hDPSCs) upon cAMP and NT-3 signalling. d-hDPSCs were characterised by the increased expression of neuronal markers such as NeuN, MAP-2, NCAM, GAP.43, Synapsin I and Synaptophysin compared to non-differentiated hDPSCs. ELISA demonstrated that the secretion of BDNF, VEGF and NGF differed between d-hDPSCs and hDPSCs. d-hDPSCs acquired neuronal features including multiple intercommunicating cytoplasmic extensions and increased vesicular transport as shown by electron microscopic observation. Patch clamp analysis demonstrated the functional activity of d-hDPSCs by the presence of TTX- and TEA-sensitive voltage-gated sodium and potassium channels respectively. A subset of d-hDPSCs was able to fire a single action potential. The results reported in this study demonstrate that hDPSCs are capable of neuronal commitment following neurosphere formation, characterised by distinct morphological and electrophysiological properties of functional neuronal cells.

3.2 Introduction

Neurological disorders of the central nervous system (CNS) account for more than 10% of deaths and new cases of permanent disability [5]. Of these neurological disorders, Alzheimer's disease and cerebrovascular diseases such as stroke are the most important contributors [5]. Moreover, current therapies are only applicable within a small therapeutic window, or are unable to cure the disease or sufficiently ameliorate the disease outcome [30, 203, 204]. As these disorders predominantly affect the elderly and it is expected that the amount of people over the age of 60 will triple by 2050, new strategies and therapies are required for the treatment and prevention of neurological disorders in addition to therapies that can improve the quality of life of people with disabilities [6]. Cell-based therapies emerged as a potential candidate to promote functional recovery in patients suffering from neurological disorders [8].

Following CNS damage, endogenous repair of the affected tissue by neural stem cells (NSCs) is limited [70, 72]. The ideal candidates for stimulating repair in CNS injuries are *ex vivo* expanded and manipulated NSCs, due to their neurogenic predisposition [47-50]. Indeed, promising results have been achieved with human NSCs in animal models of neurological disorders including multiple sclerosis, spinal cord injury, ischaemic stroke, Parkinson's- and Alzheimer's disease (reviewed in [8]). However, there are arguments that human NSCs might not be as suitable for stem cell-based therapies in neurological disorders, contrary to what was originally thought. Firstly, there are ethical considerations with regard to the invasive isolation of human NSCs, derived from embryonic and fetal stem cells [52]. Secondly, researchers experienced difficulties in isolating and culturing NSCs in addition to the low number of cells that can be isolated from the adult human brain [53]. Therefore, there is need for an easy-accessible alternative stem cell-source with a neurogenic differentiation potential that is able to reconstitute the lost neural tissue or with the capacity to stimulate endogenous repair by host NSCs.

Human dental pulp stem cells (hDPSCs) can be cultured under neural stem cell conditions in order to produce cells with a neurogenic phenotype and to offer a potential alternative source of stem cells which can be used to produce functional neurons *ex vivo*. hDPSCs, firstly described by Gronthos *et al.* in 2000, can be isolated from extracted third molars and are believed to originate from

migrating neural crest cells [85, 205]. Furthermore, hDPSCs have been shown to possess Mesenchymal Stem Cell (MSC) characteristics, similar as bone marrow-derived stem cells (BMSCs), and can be isolated with less donor site morbidity [85, 172]. hDPSCs, like BMSCs, are able to differentiate *in vitro* into the classical mesodermal cell-lineages, forming bone, cartilage and fat-producing cells. However, the adipogenic differentiation potential of hDPSCs appears to be less achievable [92, 95]. The presence of specific MSC surface markers, CD29, CD44, CD90, CD117 and CD146, can also be used to characterise cultured hDPSCs. In addition, like cultured BMSCs, hDPSCs are negative for CD34 and CD45. However, subsets of CD34^{+} hDPSCs and MSC were identified by other studies, suggesting that hDPSCs and MSC cultures are a heterogeneous cell population [92, 93, 153]. Similar to BMSCs, hDPSCs are also thought to possess immunomodulating properties [79] making them good candidates for transplantation studies and/or cell-based therapies.

More recently, researchers gained more interest in the neurogenic properties of hDPSCs due to their neuroectodermal origin. It was shown that hDPSCs are characterised by the basal expression of neurogenic markers [61]. In addition, hDPSCs secrete growth/neurotrophic factors including brain-derived neurotrophic factor (BDNF), nerve growth factor (NGF) and glial cell-derived neurotrophic factor (GDNF) [104, 156]. Vascular endothelial growth factor (VEGF) and other pro-angiogenic growth factors were also found to be present in the hDPSCs secretome [108]. These findings suggest that hDPSCs can provide trophic support to neuronal cells. Not only do hDPSCs show promising results *in vitro*, also in various *in vivo* models, encouraging effects have been observed following transplantation of hDPSCs. The proposed mechanisms of action of disease amelioration by the transplanted cells included integration of the transplanted cells in the host brain and/or stimulating the proliferation and differentiation of endogenous NSCs [56, 104, 156, 201, 206-208].

In our study, we hypothesized that hDPSCs could be more successfully differentiated to neuronal cells *in vitro* when neurosphere formation precedes neuronal maturation. Neurosphere formation is considered to be a standard cell culture procedure in which NSCs are propagated and is used to investigate neural precursor characteristics [50]. Furthermore, it is assumed that neurospheres create a suitable microenvironment in which the intra-

neurospheral cells differentiate towards neuronal and/or glial precursors [209]. Neurosphere formation is highly dependent on EGF and bFGF signalling. Moreover, it is necessary to carefully monitor the size of the neurospheres as this influences cell-viability and the differentiation capacity of the intra-neurospheral cells [50, 210-212]. After neurosphere formation, the neurospheres are collected and reseeded on an adherent surface allowing attachment of the neurospheres and outgrowth of the cells in serum-free differentiation promoting conditions [213].

Although, (h)DPSCs –and other dental tissue-derived stromal cells- were shown to be able to form neurosphere-like structures *in vitro,* the full neurogenic maturation potential of these sphere-derived cells was not further elucidated [152, 153, 214-216]. Therefore, we established a neurosphere-culture by adding trophic support of EGF and bFGF. Subsequent neurogenic maturation was based on cAMP and neurotrophin-3 (NT-3) signalling [98, 152, 153, 155, 216, 217]. By means of transmission electron microscopy (TEM), the ultrastructural characteristics of intra-neurospheral hDPSCs and their microenvironment were determined. Neurogenic maturated hDPSCs were subjected to immunocytochemical (ICC), PCR, ultrastructural and electrophysiological analysis. In addition, an Enzyme-Linked Immunosorbent Assay (ELISA) was performed for VEGF, NGF, BDNF and GDNF in order to evaluate a differential growth factor secretion profile of hDPSCs before and after neurogenic differentiation.

3.3 Materials and Methods

3.3.1 Cell Culture Media and Chemicals

α-MEM, 1:1 ratio of Dulbecco's modified Eagle's medium and F12 medium (D-MEM/F12), Neurobasal medium, penicillin, streptomycin, L-Glutamine, N2 and B27 supplement were obtained from Thermo Fisher Scientific Inc (Waltham, MA, USA). Fetal bovine serum (FBS) was purchased from Biochrom AG (Berlin, Germany). EGF, bFGF, BDNF and NT-3 were acquired from Immunotools (Friesoythe, Germany). All other chemicals were bought from Sigma-Aldrich (St. Louis, Mo., USA).

3.3.2 Isolation and Cell Culture of hDPSCs

Human dental pulps were obtained from both male and female patients from 15 - 25 years of age (n=9; average age = 18y and 5 months) undergoing routine extraction of third molars for orthodontic reasons at the Department of Maxillofacial Surgery, Ziekenhuis Oost-Limburg, Genk, Belgium with informed consent of the patient or via their legal guardians in the case of under aged patients (< 18 years of age). This study was approved by the medical ethical committee of Hasselt University (13/0104u). Obtaining the pulp tissue and subsequent isolation and culture of the hDPSCs was performed using the explant method as described previously in Chapter 2 [95]. All experiments were conducted with hDPSCs between passage two and seven.

3.3.3 Neurosphere Generation and Neurogenic Differentiation of hDPSCs

Neurospheres were generated by seeding hDPSCs (n= 9 different cell donors) at a density of 7.5 x 10^3 cells/cm² in Hydrocell® 6 cm Ø Petri dishes (Thermo Scientific) in DMEM/F12 supplemented with 100 U/ml penicillin, 100 µg/ml streptomycin, 2% B27 supplement, 20 ng/ml EGF and 20 ng/ml bFGF. Medium was changed every 3-4 days. Floating neurospheres were kept in culture for 6-8 days, while carefully monitoring that the diameter of the spheres did not exceed 250 µm as this is crucial for neurosphere viability [212]. Free-floating neurospheres were collected and fixed in 2% glutaraldehyde for TEM analysis or rinsed with PBS and resuspended in neurogenic maturation medium. Subsequently, the collected neurospheres were seeded on glass- or plastic (Thermanox®, Electron Microscopy Sciences, Hatfield, Pa., USA) coverslips, Petri dishes or in culture plates which were previously coated with 15 µg/ml Poly-L-Ornithine (PLO) and 2 µg/ml Laminin, allowing outgrowth of neurosphere-cells. Neurogenic maturation was induced via the addition of Neurobasal medium supplemented with 100 U/ml penicillin, 100 µg/ml streptomycin, 2 mM L-glutamine, 2% B27, 1% N2, 1 mM dbcAMP and 30 ng/ml NT-3. This maturation medium was changed every 2-3 days and the cells were kept under maturation-promoting conditions for four weeks. Neurogenic differentiated hDPSCs (d-hDPSCs), grown on glass coverslips, were fixed with 4% paraformaldehyde (PFA) for ICC analysis while cells grown on Thermanox® coverslips were fixed with 2% glutaraldehyde for TEM analysis. d-hDPSCs grown on Petri dishes were

used for patch-clamp recordings. The culture medium of d-hDPSCs, was collected 48h after the final medium change (referred to as conditioned medium) and used for ELISA. Subsequently, the remaining d-hDPSCs were collected, counted and immediately processed for RNA isolation with an Arcturus® PicoPure® RNA Isolation Kit (Applied Biosystems; Foster City; CA; USA).

3.3.4 Control Samples

Control samples (n= 9) were obtained by seeding hDPSCs in standard culture medium at the following densities: 1×10^4 cells/cm² on glass and Thermanox® coverslips for ICC and TEM analysis; 5×10^3 cells/cm² in Petri dishes for electrophysiological recordings and 2×10^4 cells/cm² for ELISA and RNA isolation. All cell culture material was pre-coated with 15 µg/ml Poly-L-Ornithine (PLO) and 2 µg/ml Laminin. After 24h, the culture medium was changed to Neurobasal medium supplemented with 100 U/ml penicillin, 100 µg/ml streptomycin, 2 mM L-glutamine, 2% B27 and 1% N2. After 48h, the conditioned medium was collected and cells were either fixed with 4% PFA or 2% glutaraldehyde for ICC or TEM analysis respectively, subjected to electrophysiological recordings or processed for RNA isolation. As a positive control for RT-PCR reactions, neurogenic differentiated SH-SY5Y neuroblastoma cells (Sigma-Aldrich) were used. These cells were differentiated according to a BDNF-based protocol and were previously found to express neuron-associated genes [218-221].

3.3.5 Transmission Electron Microscopy

Preparation of Free-floating neurospheres cultures and samples on plastic Thermanox® coverslips and TEM analysis was performed as described in Chapter 2.

3.3.6 Immunocytochemistry

Cells seeded on PLO/laminin coated glass coverslips were fixed in 4% PFA and immunostainings were performed according to a standardized protocol described in Chapter 2. The primary and secondary antibodies that were used in this study are listed in Table 3.1. Nuclei were counterstained with DAPI and coverslips were mounted with anti-fade mounting medium (Dako, Glostrup, Denmark) on glass slides. Negative controls were included in each staining in which the staining

procedure was performed in parallel with the other samples but with omission of the primary antibody. Micrographs were taken with a Nikon Eclipse 80i Fluorescence Microscope equipped with a 2MBWc digital sight camera and NIS-elements software. Mean fluorescence intensity (MFI) was quantified by measuring the total fluorescent area divided by the total number of cells on the micrographs. Threshold levels for the fluorescent signal were kept constant throughout all quantifications. For each marker, representative images from five different patient samples were used and at least 300 cells were counted per sample.

Table 3.1: Primary and secondary antibodies for immunocytochemical analysis.
MM= Mouse Monoclonal antibody; RP= Rabbit Polyclonal antibody; DAR= Donkey anti-rabbit; DAM= Donkey anti-mouse; DP= Donkey Polyclonal

Marker	Species	Clone	Dilution	Label	Company
Primary Antibodies					
A2B5	MM	Clone A2B5-105	1/200		Millipore Billerica, MA, USA
CD29	MM	ab3167 4B7R	1/200		Abcam, Cambridge, UK
CD44	MM	ab34485 NKI-P2	1/200		Abcam
GAP.43	RM	ab75810 Clone EP890Y	1/500		Abcam
GFAP	MM	Clone G-A-5	1/400		Sigma-Aldrich, St-Louis, MO, USA
MAP-2	MM	ab11267 HM-2	1/500		Abcam
NCAM	MM	sc-7326 123C3	1/250		Santa Cruz Biotechnology, Santa Cruz, CA, USA
Nestin	MM	mAb5326 Clone 10C2	1/400		Millipore
NeuN	MM	mAb377 Clone A60	1/100		Millipore
Stro-1	MM	Mab1038 Clone STRO-1	1/50		R&D Systems, Minneapolis, MN, USA
Synapsin I	RP	ab64581	1/100		Abcam,
Synaptophysin	MM	Clone SY38	1/20		DakoCytomation, Glostrup, Denmark
Secondary Antibodies					
DAR	DP IgG	A31570	1/500	Alexa Fluor 555	Invitrogen, Carlsbad, CA, USA
DAM	DP IgG	A21206	1/500	Alexa Fluor 488	Invitrogen

3.3.7 Enzyme-Linked Immunosorbent Assay

ELISAs were performed for BDNF, NGF, VEGF and GDNF (Raybiotech[®]; Norcross, GA, USA). Conditioned medium of d-hDPSCs and hDPSCs was collected as described previously and was centrifuged at 300g to exclude the uptake of cellular material before aliquoting. Subsequently, samples were stored at -80°C until needed. ELISAs were performed according to the guidelines of the manufacturer (available online at http://www.raybiotech.com, representative methods are presented in [222]). The absorbance of the end product was measured at a wavelength of 450 nm with a iMark microplate reader (Bio-Rad Laboratories, Hercules, CA, USA). The concentrations of the growth factors of interest were determined using a standard curve and were adjusted to 1×10^5 cells per ml of conditioned medium.

3.3.8 Reverse-Transcriptase PCR

Whole RNA was isolated with an Arcturus[®] PicoPure[®] RNA isolation kit (Thermo Fisher Scientific) according to the instructions of the manufacturer (available online at http://www.lifetechnologies.com, [223]). The concentration of RNA was determined with a Nanodrop 2000 spectrophotometer (Thermo Fisher Scientific), measuring the absorbance of RNA at 260 nm. cDNA was synthesized from 700 ng RNA per sample using random primers in a total volume of 20 μl with a Reverse Transcription System (Promega, Madison, WI, USA). Subsequently, cDNA was amplified by PCR with specific oligonucleotide primers and a Taq DNA polymerase dNTPack (Roche Diagnostics, Indianapolis, IN, USA). After optimization of the PCR reaction with the gradient PCR method, the cDNA samples were amplified with the primers and annealing temperatures (Tm) listed in Table 3.2. Primers for NCAM and MAP-2 were adopted from Nourbakhsh *et al.* [224]. PCR reactions were performed with a MyCycler thermal cycler (Bio-Rad Laboratories). The PCR products were analysed by gel electrophoresis on a 1.2% agarose gel and stained with ethidiumbromide (2.5 μM, Merck, Darmstadt, Germany). A UV transilluminator (Bio-Rad Laboratories) was used to visualize and photograph the amplicons.

Table 3.2: Primers and reaction conditions for reverse transcriptase–polymerase chain reaction. B2M= ß-2 Microglobulin

Name	Sense Primer (5' - 3')	Anti-sense Primer (5' - 3')	Accession No.	Length (bp)	Tm (°C)
NCAM	TGGCAGGAGATGCCAAAGAT	CTCGGCCTTTGTGTTTCCAG	NM_000615	342	61
MAP-2	CTGGGTCTACTGCCATCACTC	CCCCTTTAGGCTGGTATTTGA	NM_002374.3	282	60
Mash-1	CCCCCAACTACTCCAACGAC	TTGTGCGATCACCCTGCTTC	NM_004316.3	191	61
SCG10	ACGTCTGCAGGAAAAGGAGAG	TGAAGAGCGATTTCACGGCT	NM_007029.3	841	61
B2M	CTCACGTCATCCAGCAGAGA	CGGCAGGCATACTCATCTTT	NM_004048.2	213	60

3.3.9 Patch-clamp Recordings and Electrophysiological Measurements

Voltage clamp recordings were performed using the whole cell configuration of the patch-clamp technique [225]. For electrophysiological recordings, the growth medium was replaced with a bath solution containing 145 mM NaCl, 1.5 mM KCl, 2 mM $CaCl_2$, 2 mM $MgCl_2$, 10 mM HEPES and 10 mM glucose which was adjusted to pH 7.4 with NaOH (~307 mOsm/kg). When appropriate, this extracellular solution was supplemented with tetrodotoxin (1 µM, TTX; Alomone Labs, Jerusalem, Israel) or tetraethyl ammonium (35 mM, TEA). These chemicals were applied using a fast perfusion system (SF-77B, Warner Instruments, Holliston, MA, USA) by rapidly moving the solution interface across the cell surface. Micropipettes (2-5 MΩ resistance) were fabricated from 1.5 mm (o.d.) borosilicate glass capillary tubes (Hilgenberg, Malsfeld, Germany). The pipette solution contained 125 mM KCl, 1 mM $CaCl_2$, 2 mM $MgCl_2$, 2 mM Mg-ATP, 2 mM Na_2ATP, 10 mM HEPES, 10 mM EGTA and was adjusted to pH 7.2 with KOH, (~283 mOsm/kg). All recordings were carried out at room temperature using a computer-controlled patch-clamp amplifier (EPC-10; HEKA Electonics, Lambrecht, Germany) and Patchmaster software (HEKA Electronics). Residual capacitances and leak currents were eliminated by means of a P/6 protocol. Currents were filtered at 2.9 kHz, sampled at 10 kHz and stored on a computer hard disk for later analysis. Cells were clamped at a holding potential of -70 mV during 100 ms. Current patterns were obtained by depolarizing the cell membrane from the holding potential to voltages between -80 mV and +60 mV

at intervals of 10 mV. Pulse duration was 50 ms. Na^+ and K^+ current amplitudes were measured respectively at the peak inward and outward value. The changes in current amplitudes were expressed as changes in current densities to correct for cell size (pA/pF). Action potentials were recorded under current clamp conditions in which the cells were stimulated with 50 – 300 pA current injection during 2000ms. Data were analysed off-line with Fitmaster v2x69 software (HEKA Electronics).

3.3.10 Statistical Analysis

Statistical analysis was performed using Graphpad Prism 5 software (Graphpad, San Diego, CA, USA). Experimental groups were compared by means of a non-parametric Mann-Whitney U test. Patch clamp data were assumed to be normally distributed and were analysed with a two-tailed unpaired t-test or repeated measures ANOVA followed by a Bonferroni post-test. Differences were considered statistically significant at p-values ≤ 0.05. Data were expressed as mean ± standard error of the mean (S.E.M) except for the electrophysiological recordings which were expressed as mean ± standard error (S.E.).

3.4 Results

3.4.1 hDPSCs Acquire a Neuronal Morphology During the Differentiation Process

Throughout the two-step differentiation process, hDPSCs underwent multiple morphological adaptations ranging from the formation of neurospheres to establishing a culture of neuron-like cells with a large perikaryon and intercommunicating cytoplasmic extensions (Fig. 3.1). In the first step, explant-derived hDPSCs grown as a monolayer were transformed to free floating neurospheres in low-attachment Petri dishes (Fig. 3.1A, B). hDPSCs formed neurospheres after 24-48 hours in culture and after 6-8 days, the obtained neurospheres were transferred to a pre-coated surface, allowing outgrowth of neurosphere-cells (Fig. 3.1C). After 4 weeks in maturation-promoting conditions, hDPSCs acquired morphological characteristics of neuronal cells, characterised by large, round perikarya with a peripheral halo (Fig. 3.1D, encircled) and

multiple cytoplasmic extensions that formed an intercellular network (Fig. 3.1D, arrowheads).
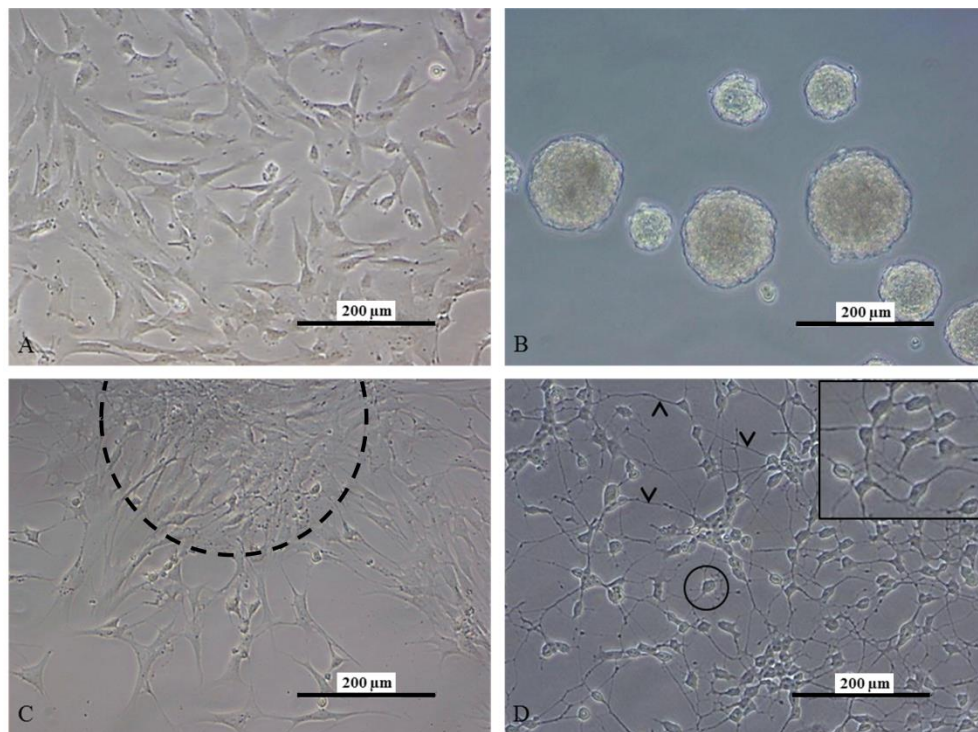
Figure 3.1: hDPSCs acquired a neuronal morphology during the differentiation process. Explant-derived hDPSCs were cultured as a monolayer (A). In the first part of the neurogenic differentiation process, these cells were transformed into free-floating neurospheres (B). Subsequently, the neurospheres were transferred to a PLO-laminin coated surface after which the cells grow out of the neurospheres (C, dashed line). After 4 weeks of neurogenic maturation (D), d-hDPSCs were characterised by multiple cytoplasmic extensions (arrowheads) that contributed to an intercellular network and large perikarya with a peripheral halo (circle and insert) Scale bars A-D: 200 µm

3.4.2 Ultrastructural Characteristics of Intra-Neurospheral hDPSCs

To gain insight into the intercellular interactions that take place within the neurospheres, these spheres were subjected to TEM analysis (Fig. 3.2). Intra-neurospheral hDPSCs appeared as elongated cells with prominent nucleoli (Fig. 2A, asterisk), a prominent Golgi apparatus and a dilated rough endoplasmic

reticulum (RER) (Fig. 3.2B, black arrow and asterisk respectively), suggesting an increased metabolic activity within neurospheres *in vitro*. These features were more prominent in the cells at the center of the neurosphere. However, areas of intracellular vacuolization and loss of cell integrity were observed in a subset of intra-neurospheral hDPSCs (Fig. 3.2A, arrowheads). This loss of cell integrity was reflected in a decrease in cell viability of approximately 45.74% (s.d. = 7.56%; n = 6 individual neurosphere generation experiments) as quantified by neurosphere dissociation with accutase and subsequent cell-number determination with trypan blue exclusion (data not shown).

In addition to the increased metabolic activity of intra-neurospheral hDPSCs, intercellular communication also seemed to be stimulated. Vesicular transport was observed at cell-cell contact zones as demonstrated by the presence of coated pits and vesicles suggesting signs of endo- or exocytosis (Fig. 3.2C, arrowhead and circle). Intra-neurospheral hDPSCs produced electron-dense vesicles containing an unknown substance and ECM deposits were observed between adjacent cells (Fig. 3.2D, asterisk and arrowhead respectively).
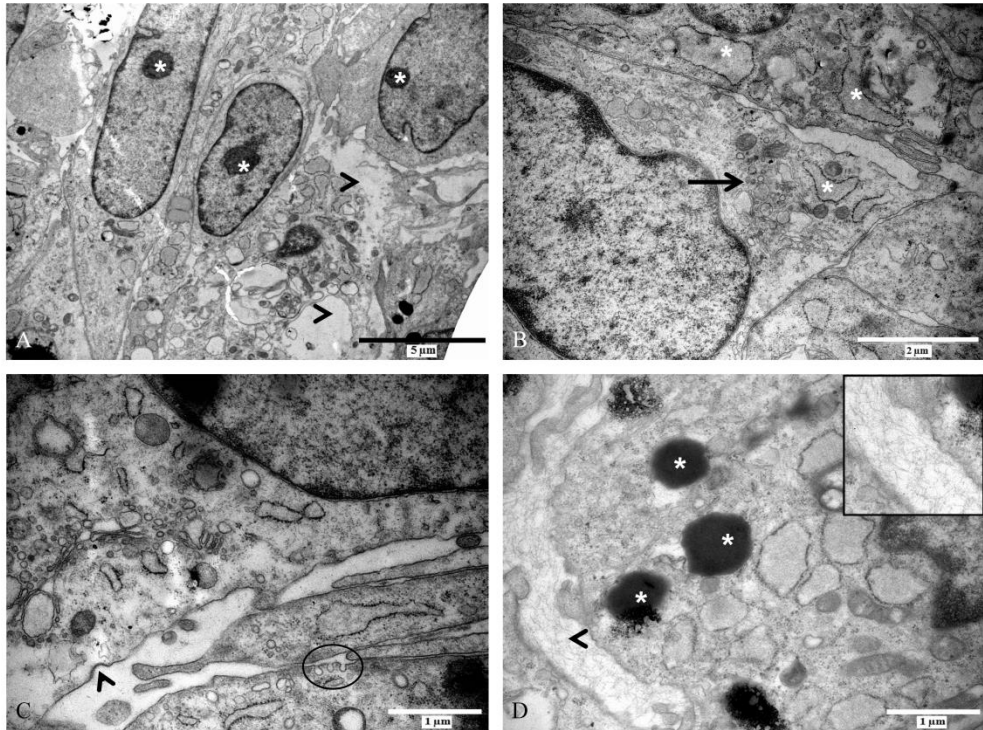
Figure 3.2: Intra-neurospheral hDPSCs are characterised by an increased metabolic activity and intercellular communication. Intra-neurospheral hDPSCs were characterised by a prominent nucleolus (A, asterisk), RER (B, asterisk) and Golgi apparatus (B, arrow) indicating an increased metabolic activity. Cell integrity was lost in a subset of neurospheral cells (A, arrowheads). Intercellular communication was increased, as shown by coated pits and vesicle uptake (C, arrowhead and circle) in addition to the presence of electron-dense vesicles in the cytoplasm of intra-neurospheral cells (D, asterisk). ECM deposition was observed between cells (D, arrowhead, detail in insert). Scale bars: A = 5 µm; B = 2µm; C, D = 1 µm.

3.4.3 Immunocytochemical, PCR and Secretome Analysis of d-hDPSCs

After the four-week neuronal maturation period, the neurogenic differentiated hDPSCs showed immune-reactivity for neuron-related markers (Fig. 3.3A-F). A quantitative analysis for the level of immune-reactivity was performed for both the number of immune-reactive cells as for the MFI per cell. The data demonstrated an increase in Neuronal Nuclei (NeuN; Fig. 3.3A, B), Microtubule-Associated Protein 2 (MAP-2; Fig. 3.3C, D), Neural Cell Adhesion Molecule

(NCAM; Fig. 3.3E, F), Growth-Associated Protein 43 (GAP.43; Fig. 3.3G, H), Synaptophysin (Fig. 3.3I, J), Synapsin I (Fig. 3.3K, L) and Glial Fibrillary Acid Protein (GFAP, Fig. 3.3M, N) immune-reactivity in d-hDPSCs compared to hDPSCs. A2B5 (Fig. 3.3O, P) expression was observed in < 2% of d-hDPSCs. Nestin expression was decreased in d-hDPSCs compared to controls (Fig. 3.3Q, R). No fluorescent signal was detected in the negative controls. The differential expression of neuron-related markers in d-hDPSCs and hDPSCs was also demonstrated by measuring the MFI per cell (Fig. 3.3T). A significant difference (p-value ≤ 0.05) between NeuN-, MAP-2-, NCAM-, Synaptophysin-, Synapsin I-, GFAP- and Nestin expression was observed between hDPSCs and d-hDPSCS (n= 5). Similarly, the percentage of cells that were immune-reactive for these markers also increased significantly in d-hDPSCs compared to hDPSCs (Fig. 3.3S). In addition to evaluating the expression of neuronal markers in d-hDPSCs compared to controls, the percentage and MFI per cell of the stem cell markers CD29, CD44 and Stro-1 were also evaluated. No significant difference in the percentage of immune-positive cells and MFI per cell was detected between d-hDPSCs and hDPSCs (Fig. 3.4). A detailed statistical analysis of the percentage of immune-reactive cells and the MFI per cell can be found in Table 3.3. The differential expression of MAP-2 and NCAM was confirmed by RT-PCR (Fig. 3.3U). However, the expression of the neuron-specific genes Mash-1 and SCG10 could not be observed in both hDPSCs and d-hDPSCs (n= 4).

The secretome of hDPSCs was compared with that of d-hDPSCs in order to investigate if neurogenic differentiation of hDPSCs altered the secretome of these cells (Fig. 3.3J-M). ELISA of conditioned medium of hDPSCs and d-hDPSCs demonstrated a significant increase in VEGF (n= 6; p-value = 0.0022) and NGF (n= 5; p-value= 0.0159) secretion by d-hDPSCs compared to hDPSCs (Fig. 3.3V, W). BDNF (n=6; p-value= 0.0022) secretion was significantly decreased after neurogenic maturation (Fig. 3.3X). Differential secretion of GDNF (n= 6; p-value= 1.00) by hDPSCs and d-hDPSCs could not be observed (Fig. 3.3Y).
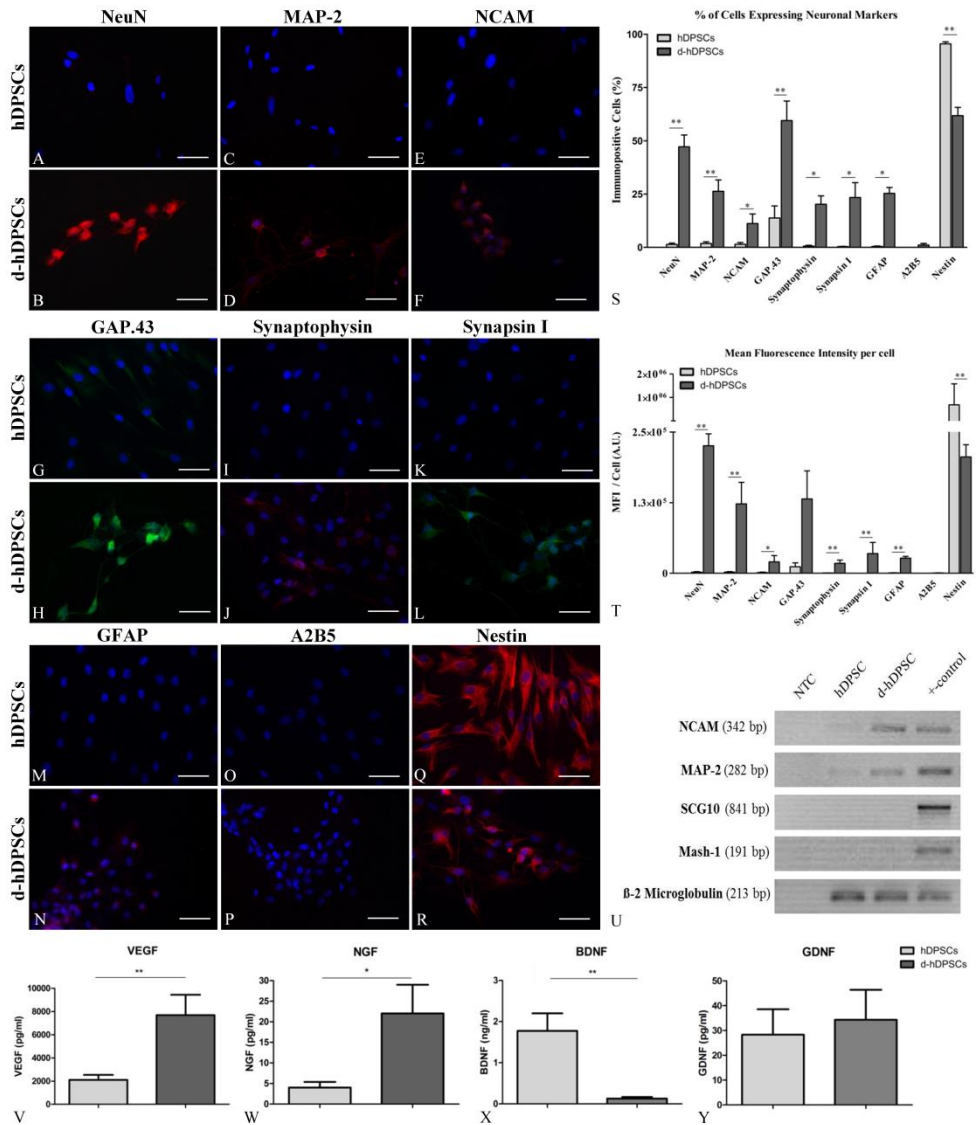
Figure 3.3: d-hDPSCs acquired immune-reactivity for neuron-related markers and showed an increased expression of neuronal genes in addition to an altered secretome. Compared to controls, neurogenic maturation induced the expression of NeuN (A, B) , MAP-2 (C, D), NCAM (E, F), GAP.43 (G, H), Synaptophysin (I, J), Synapsin I (K, L) and GFAP (M, N). A2B5 expression was low (<2%) in both hDPSCs and d-hDPSCs (O, P). Nestin expression was decreased in d-hDPSCs compared to controls (Q, R). The presented images in B, D, F, H, J, L, N and R are representative for the immune-positive cells in d-hDPSC-cultures (n= 5). Quantitatively, both the MFI per cell and the percentage of cells expressing neuronal markers were significantly increased in d-hDPSCs, except for nestin

which was significantly decreased following neurogenic differentiation (S, T). No significant difference in the MFI per cell was detected for GAP.43. RT-PCR analysis confirmed the upregulation of MAP-2 and NCAM on the gene expression level (n= 4). The expression of the neuron-related genes Mash-1 and SCG10 was not observed (U). ß-2 Microglobulin was used as an endogenous control. VEGF (n= 6) and NGF (n= 5) secretion was significantly increased in d-hDPSCs compared to hDPSCs (V, W). BDNF (n= 6) secretion was significantly decreased after neurogenic maturation (X). Differential secretion of GDNF (n= 5) between hDPSCs and d-hDPSCs could not be observed (Y). A.U.= Arbitrary Units; NTC = Non Template Control; Scale bars A-R = 50 µm; * = p-value ≤ 0.05; ** = p-value ≤ 0.01; data are represented as mean ± S.E.M.
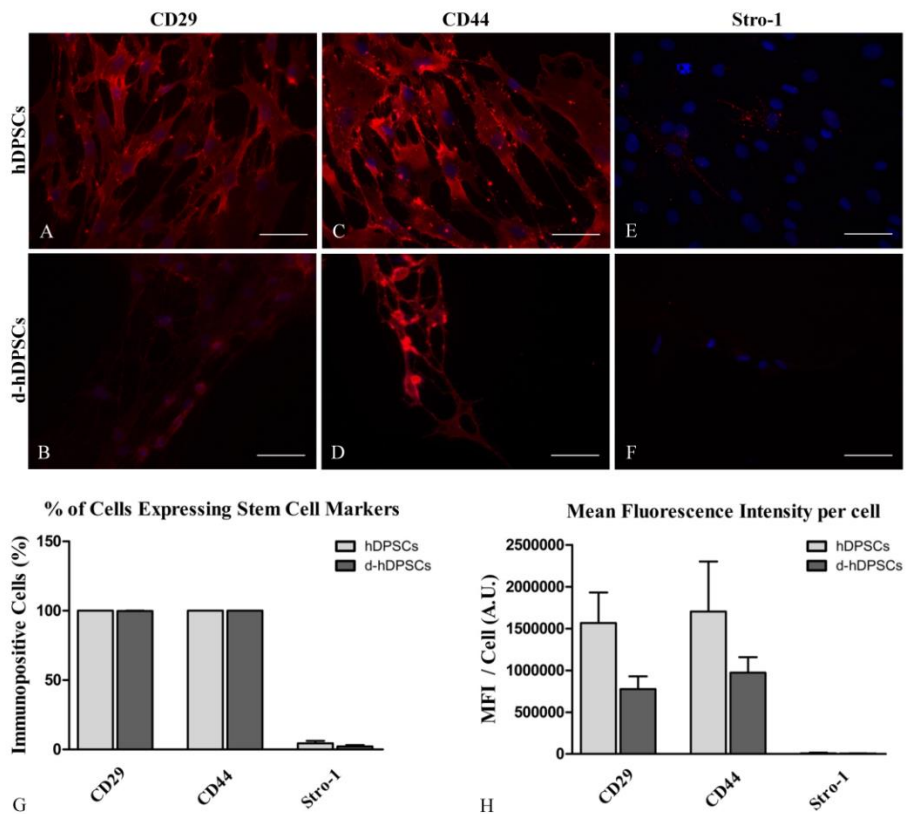
Figure 3.4: The expression of stem cells markers is preserved following neurogenic differentiation of hDPSCs. Similar to controls, d-hDPSCs express CD29 (A, B), CD44 (C, D) and Stro-1 (E, F) (n= 5). Quantitatively, no significant difference in both the MFI per cell and the percentage of cells expressing stem cells markers was observed (G, H). A.U.= Arbitrary Units. Data are represented as mean ± S.E.M. Scale bars A-F = 50 µm.

Table 3.3: Statistical overview of the percentage of immune-positive cells and the MFI per cell for neuron associated and stem cell markers following neurogenic differentiation

	% of Immune-positive cells			MFI per cell (A.U)			
	hDPSCs	d-hDPSCs	p-value	hDPSCs	d-hDPSCs	p-value	fold-change
Neuron-Associated markers							
NeuN	1.38 ± 0.6	47.18 ± 5.54	0.0079	1980.48 ± 981.4	225702,5 ± 21223	0.0079	x 113.96
MAP-2	1.82 ± 0.78	26.34 ± 5.29	0.0079	2079.64 ± 897.3	122848.7 ± 38205	0.0079	x 59.07
NCAM	1.43 ± 0.86	11.19 ± 4.46	0.0212	1218.28 ± 796.8	20103.65 ± 11192	0.0159	x 16.5
GAP.43	13.8 ± 5.64	59.47 ± 9.16	0.0079	11434.77 ± 6997	131726.57 ± 49650	0.0556	x 11.52
Synaptophysin	0.59 ± 0.37	20.23 ± 3.94	0.0119	356.49 ± 296.4	17506.82 ± 5724	0.0079	x 49.1
Synapsin I	0.33 ± 0.15	23.39 ± 7.0	0.0119	34.97 ± 13.46	34882.33 ± 19724	0.0079	x 997.6
GFAP	0.44 ± 0.21	25.33 ± 2.774	0.0119	550.1 ± 314.5	26737 ± 3209	0.0079	x 48.6
A2B5	0.0 ± 0.0	1.092 ± 0.78	0.5	82.03 ± 78.83	388.3 ± 289.4	0.31	x 4.73
Nestin	95.5 ± 0.95	61.8 ± 3.97	0.0079	1171230.14 ± 223859	205946 ± 21593	0.0079	: 5.89
Stem Cell Markers							
CD29	100.00 ± 0.00	99.97 ± 0.13	1.0	1566291.14 ± 364243	776937.8 ± 150651	0.1508	: 2.01
CD44	100.00 ± 0.00	100.00 ± 0.00	1.0	1703892.3 ± 597539	971027.81 ± 185351	0.5476	: 1.75
Stro-1	4.43 ± 1.76	2.13 ± 1.11	0.4206	8194 ± 7458	4561 ± 3338	0.6905	: 1.79

3.4.4 Ultrastructural Characteristics of d–hDPSCs

d-hDPSCs were subjected to an ultrastructural analysis using TEM (Fig. 3.5). The perikaryon of d-hDPSCs was characterised by a large central nucleus with a prominent nucleolus (Fig. 3.5A, asterisk). Abundant organelles associated with metabolic activity and protein synthesis were present in the cytoplasm of d-hDPSCs (Fig. 3.5B). These organelles included an extended Golgi apparatus and RER (Fig.3.5B, bracket and white arrows), indicating increased packing of proteins in membrane bound vesicles. In addition, d-hDPSCs developed multiple cytoplasmic extensions containing longitudinal aligned cytoskeletal elements and varicosities along their length (Fig. 3.5C, between arrowheads, Fig. 3.5D, arrowheads). Interestingly, intercellular contact sites containing mitochondria were observed at these varicosities (Fig. 3.5D, circle). A detailed analysis of intercellular contact zones showed the presence of electron-dense vesicles (Fig. 3.5E, asterisk) at the distal fraction of the cytoplasmic extension. Moreover, multiple small vesicles (Fig. 3.5E, bracket) and granular material were present in the intercellular cleft and the internalization of membrane bound vesicles by receptor-mediated mechanisms was observed (Fig. 3.5E, arrowheads). Multi-vesicular bodies (Fig. 3.5F, MVB) were found in the vicinity of the coated pits (Fig. 3.5F, arrowheads) at the distal parts of the cytoplasmic extensions.
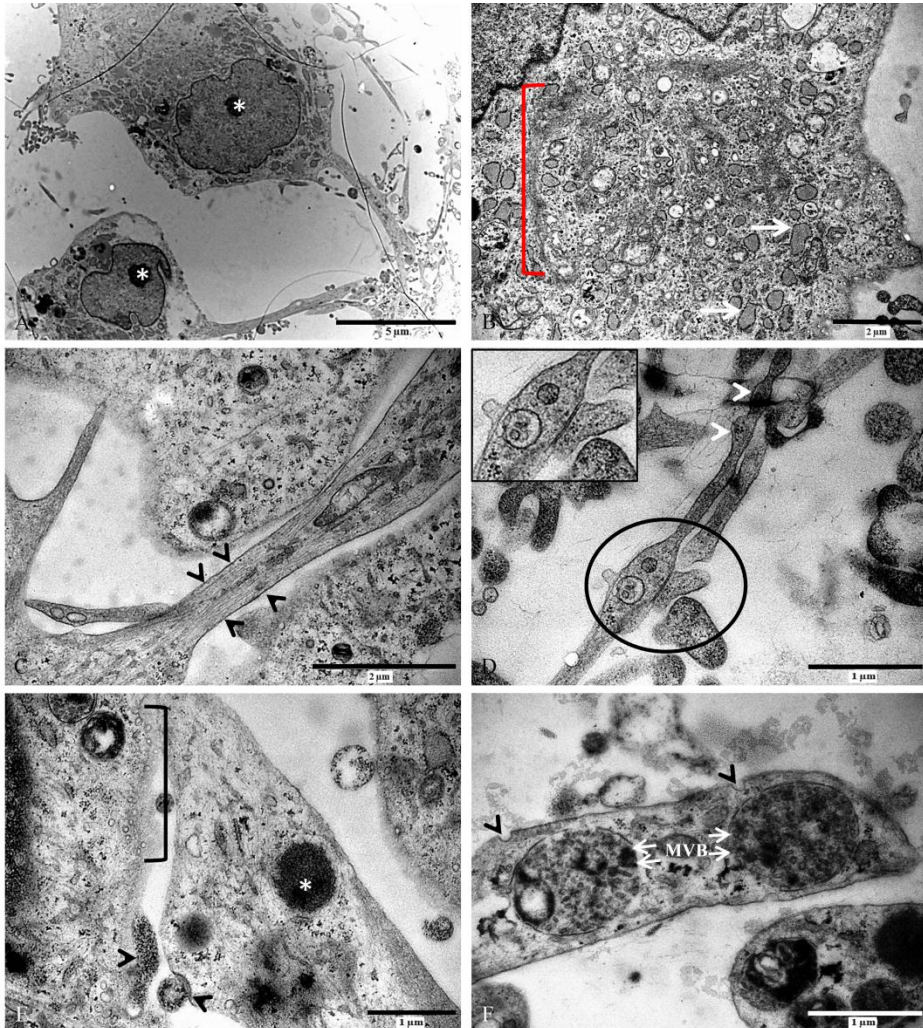
Figure 3.5: d-hDPSCs developed ultrastructural features of neuronal cells. The perikaryon of d-hDPSCs was characterised by a large central nucleus with a prominent nucleolus (A, asterisk) and the cytoplasm showed abundant organelles associated with metabolic activity and protein synthesis (B). d-hDPSCs developed multiple cytoplasmic extensions in which the cytoskeletal elements were visible (C, between arrowheads). These cytoplasmic extensions showed varicosities along their course (D, white arrowheads) with cell-cell contact sites (D, circle and insert). At the intercellular contact zones, electron-dense vesicles (E, asterisk) were observed. In the intercellular cleft, multiple small vesicles (E, bracket) were present in addition to granular material being secreted and internalized (E, arrowheads). Multivesicular bodies (F, MVB) were found in the vicinity of coated pits (E, arrowheads) at the distal parts of cytoplasmic extensions. Scale bars: A = 5 μm; B, C = 2 μm; D, E, F = 1 μm

3.4.5 Electrophysiological Properties of d-hDPSC

In order to evaluate the functional maturation of d-hDPSCs, whole-cell patch-clamp recordings were performed on three parallel differentiated d-hDPSCs- and control hDPSCs cultures (Fig. 3.6). The I–V relationship of voltage-dependent potassium and sodium currents was recorded on both d-hDPSCs (n= 10) and hDPSCs (n= 12) (Fig. 3.6A, B). Voltage-dependent potassium currents were present in d-hDPSCs, but not in hDPSCs (Fig. 3.6A). These currents were activated at membrane potential more positive than -10 mV and showed a typical delayed rectifier I-V profile. A statistically significant increase in outward currents was reached at +20 mV (p-value = 0.0408) and more positive membrane potentials. A peak value of 35.65 ± 15.6 pA/pF was measured at + 60 mV. Furthermore, these outward potassium currents could be completely and reversibly blocked by 35 mM TEA (Fig. 3.6B) (n= 6). Similarly, the I-V relationship of voltage-dependent sodium currents recorded on both experimental conditions showed the presence of these currents in d-hDPSCs but not in hDPSCs (Fig. 3.6C). These inward sodium currents were activated at a threshold between -40 mV and -30 mV and statistically significant currents were observed from -20 mV to + 60 mV (p-value at -20 mV = 0.0136). A peak (negative) value of -25.9 ± 11.4 pA/pF was reached at a membrane potential of 0 mV. These voltage-dependent sodium currents could be reversibly blocked by 1 µM TTX (Fig. 3.6D) (n= 6). A significant decrease in voltage-dependent sodium currents by applying TTX was observed at a membrane potential of -10 mV (p-value = 0.0289) and more positive membrane potentials. Consequently, after washing out TTX, the voltage-dependent sodium currents were restored. No significant difference in the amplitude of voltage-dependent sodium currents was observed between control traces and after washout of TTX. Representative traces of sodium- (Fig. 3.6E) and potassium currents (Fig. 3.6F) recorded in d-hDPSCs under non-blocking (black trace), blocking (red trace) and washout (green trace) conditions, confirmed the reversible blocking of voltage-gated sodium channels by TTX and voltage-gated potassium channels by TEA. Finally, upon current stimulation (50-300 pA), a single action potential was observed in a subset of d-hDPSCs (n= 3) (Fig. 3.6G). This action potential was characterised by an initial depolarization of the membrane potential in d-hDPSCs followed by

incomplete repolarization of the membrane potential. Repetitive action potential firing was not observed.
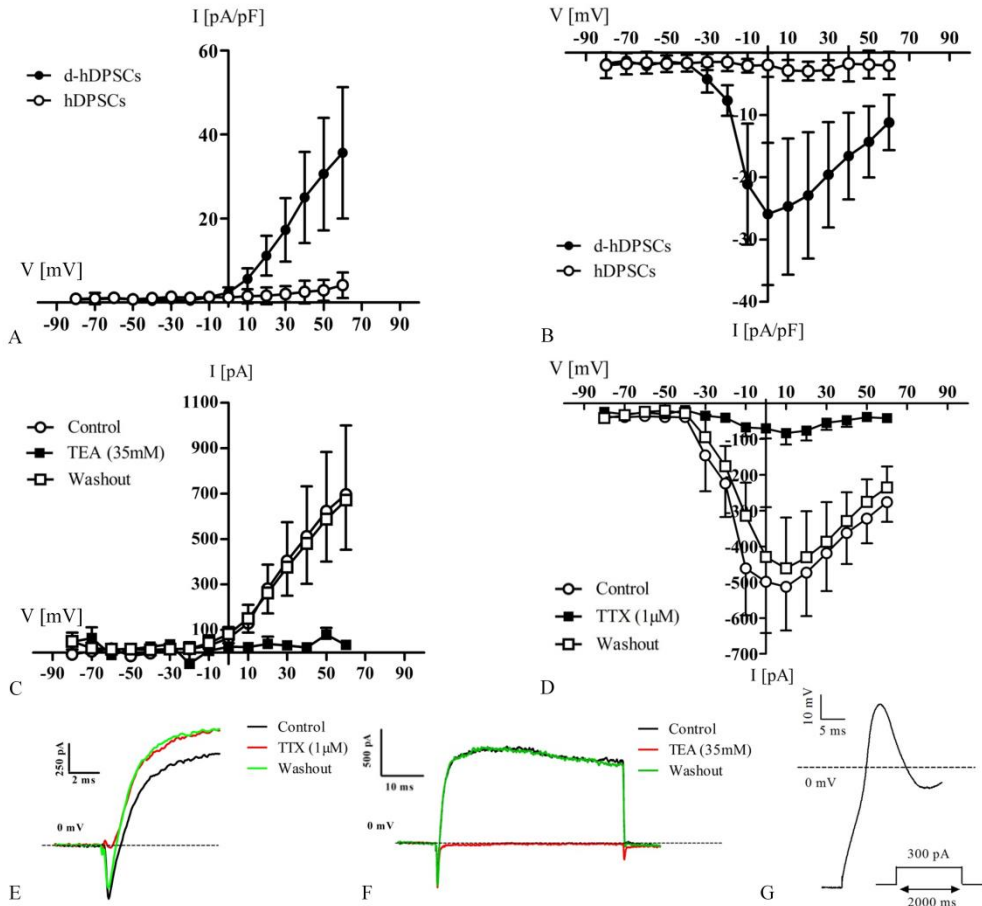
Figure 3.6: Voltage dependent sodium and potassium channels in d-hDPSCs could be selectively blocked by respectively TTX and TEA. The I–V relationship of voltage-dependent potassium and sodium currents was recorded on both d-hDPSCs (n= 10) and hDPSCs (n= 12) (A, B respectively). Voltage-dependent potassium currents were present in d-hDPSCs, but not in hDPSCs (A). These voltage-dependent potassium currents could be reversibly blocked by 35 mM TEA (C) (n= 6). Similarly, the I-V relationship of voltage dependent sodium currents recorded on both experimental conditions showed the presence of these currents in d-hDPSCs (n= 10), but not in hDPSCs (n= 12) (B). Moreover, these voltage-dependent sodium currents could be reversibly blocked by 1 µM TTX (n= 6) (D). Washing out TTX restored these voltage-dependent sodium currents. No difference in the amplitude of voltage-dependent sodium currents was observed between

control traces and after washout of TTX. Representative traces of sodium currents recorded in d-hDPSCs under normal (non-blocking) conditions, after administration of 1 µM TTX and after washout of the sodium channel blocker (E). Traces of potassium currents recorded in control, blocking and washout conditions (F). Upon current stimulation, a subset of d-hDPSCs (n= 3) generated a single action potential with a depolarization phase followed by incomplete repolarization (G).

3.5 Discussion

In the present study, we described a novel approach to differentiate hDPSCs towards cells with a neuronal phenotype. Apart from acquiring morphological features of neuronal cells, a subset of differentiated cells also showed a neurogenic associated electrophysiological profile. This was demonstrated by the presence of voltage-sensitive sodium and potassium currents that could be reversibly blocked by TTX and TEA respectively in addition to the firing of a single action potential upon current stimulation.

In order to neuronally differentiate hDPSCs, we combined protocols that have been applied in other studies into a two-step protocol. Previous protocols were able to differentiate hDPSCs to functional neuronal cells, as determined by the presence of voltage-dependent sodium and potassium currents. However, these studies did not observe action potential-firing by the differentiated cells, addressing the incomplete differentiation of hDPSCs to neuronal cells [98, 155]. Therefore, this two-step protocol was implemented to improve the differentiation outcome. First, we adopted the neuronal induction step based on EGF and FGF-2 signalling [155] and combined these essential signalling molecules with the formation of 3-dimensional neurosphere structures. Neurosphere formation is a common culturing technique for NSC as it is considered to create a favourable microenvironment for intercellular interactions [50, 152, 153, 215, 216]. Furthermore, it has been shown that a close physical contact between neural progenitor cells is essential for neuronal commitment, which can also be achieved by neurosphere generation [226, 227]. Secondly, we used a neuronal maturation protocol based on increased cAMP levels and NT-3 signalling that was previously implied by Kiràly *et al.* Elevated intracellular cAMP is thought to play an essential role in sustaining neurogenic differentiation of early neuronal

committed cells, whereas NT-3 signalling is essential for neurogenic maturation [217, 228, 229]. In the study by Kiràly *et al.*, neuronal induction was achieved by epigenetic reprogramming, which was replaced in this study by the formation of neurospheres [98].

To our knowledge, this paper presents the first ultrastructural data of the microenvironment within neurospheres derived from dental pulp stem cells. When comparing hDPSC-derived neurospheres with the scarce ultrastructural data on NSC-derived neurospheres, some differential and corresponding features were observed [230, 231]. In these studies, multiple apoptotic bodies were found inside the cytoplasm of intra-neurospheral cells. These were not observed in our neurosphere culture, although we observed loss of cell integrity with a subsequent loss of cells that could be used for neurogenic maturation. Moreover, in the present study, ECM deposits were found that presumably contributed to the microenvironment and structural integrity of the 3D neurospheres. A similar result of the present study compared to the studies by Bez *et al.* [230] and Zhao *et al.* [231], was the increase in intercellular communication inside the neurospheres, which reflects the augmented metabolic activity and demand that is observed within the spheres. However, in the studies by Bez *et al.* and Zhao *et al.* intercellular communication was achieved by means of gap junctions whereas in our culture, paracrine signalling via vesicular transport appeared to be the main form of cell communication. Nonetheless, it can be concluded that by forming neurospheres, a microenvironment is created that influences the metabolic activity of the intra-neurospheral cells and that allows the development of an improved intercellular communication network.

In determining the expression level of neuron-related markers, markers were chosen that were not already expressed in a large fraction of hDPSCs prior to differentiation [61]. Therefore, NeuN, MAP-2, NCAM and GAP.43 were selected as neuron-related markers to discriminate between hDPSCs and d-hDPSCs. In addition, Synapsin I and Synaptophysin were used to evaluate the production of synaptic vesicles. Furthermore, A2B5 was used to identify oligodendroglial cells while GFAP was used to evaluate differentiation of hDPSCs towards astrocytes, although GFAP is also found to be expressed by neuronal precursors [232]. Using these markers, a significant difference in marker expression between

hDPSCs and d-hDPSCs was observed, both in the percentage of immune-positive cells, as in the correlating MFI. The expression of neuronal and synaptic markers was significantly increased in d-hDPSCs, except for the MFI per cell for GAP.43 which showed high inter-patient variability. Nestin expression was significantly reduced following differentiation, suggesting that a subset of d-hDPSCs shifted towards a more mature neuronal phenotype. A2B5 expression was only detected in less than 2% of d-hDPSCs, indicating that d-hDPSCs did not differentiate towards oligodendroglial cells. Immune-reactivity for GFAP suggested that a subset of d-hDPSCs differentiated towards astrocytes, although the perinuclear staining pattern suggests incomplete differentiation. In addition to neural markers, the percentage of immune-positive cells and the MFI per cell was also assessed for the stem cell markers CD29, CD44 and Stro-1. Both the percentage of immune-positive cells and MFI per cell were not significantly reduced following neuronal differentiation, although the MFI per cell shows a declining trend. Although markers such as CD29 and CD44 are often used to characterise mesenchymal stem cell populations, it has been shown that neural stem/precursor cells also express these markers [233, 234]. Taken together, these results suggest that d-hDPSCs acquire a neuronal phenotype, based on an increase in the MFI per cell and the percentage of immune-positive cells for neuron-associated and synaptic markers. However, the percentage of NCAM-positive cells was lower than in a previous report of Arthur *et al.*, for both the basal expression in hDPSCs as in d-hDPSCs [155]. Nourbakhsh *et al.* also reported a higher percentage of NCAM positive cells before and after neuronal differentiation conditions, albeit in lower percentages than Arthur *et al.* and in stem cells derived from the pulp of human deciduous teeth [224]. This discrepancy between the present study and earlier reports can be attributed to the fact that we used a lower and upper fluorescent threshold when determining the percentage of immune-positive cells. Therefore, a very strict standardized quantification method was used, compared to non-standardized quantification methods such as the visual observation of the amount of immune-positive cells per field of view. In addition, other factors that might influence the outcome of NCAM reactivity are noted. First, to obtain their stem cell culture, Arthur *et al.* and Nourbakhsh *et al.* used an isolation method based on enzymatic digestion of the pulp tissue, whereas we opted for the explant method. Previously it was

shown that isolation methodology does not have an effect on the stem cell properties and multilineage differentiation potential of hDPSCS. However, the influence on neurogenic differentiation potential and basal neuronal marker expression has not been evaluated [92]. Second, the culture-medium in which the control cells were grown differed between the present study and the study of Arthur *et al.* and Nourbakhsh *et al.* We opted to culture the control cells in neurogenic maturation medium minus cAMP and NT-3 48h before harvesting the material or fixing the cells. Other studies cultured the control samples in standard culture medium by which they are unable to assess the influence of the basal medium without growth factors on which their differentiation promoting conditions are built. Nonetheless, the increased expression of both MAP-2 and NCAM was confirmed with PCR indicating active transcription of these proteins at the RNA level. Both hDPSCs and d-hDPSCs failed to express the early neuronal gene Mash-1 and the late neuronal gene SCG10. The failure of hDPSCs to express Mash-1 suggests that although hDPSCs are of neuro-ectodermal origin and that they express neuronal markers at the protein level, they should not be labelled as neural progenitor cells who are known to express Mash-1 [235, 236]. The absence of Mash-1 expression in d-hDPSCs can be explained by the advanced maturation stage of d-hDPSCs compared to hDPSCs. Although Mash-1 is frequently used as a genetic marker for cells with neuronal differentiation potential, Mash-1 is also expressed in tumour cells, such as the SH-SY5Y cells that were used as a positive control [237]. This explains why neuronally differentiated SH-SY5Y expressed both Mash-1 and SCG10. The lack of SCG10 expression in d-hDPSCs can be attributed to incomplete neuronal maturation as this gene is expressed in mature neurons [238, 239].

In addition to evaluating the neurogenic differentiation of hDPSCs based on protein and gene expression, the secretome of hDPSCs and d-hDPSCs was examined into more detail. Interestingly, an altered secretion pattern could be observed between hDPSCs and d-hDPSCs for the growth factors/neurotrophins BDNF, NGF and VEGF while the secretome of both cell populations contained a similar concentration of GDNF. Depending on the CNS pathology, these growth factors/neurotrophins are known to have diverse effects on the host tissue including neuroprotection and the stimulation of host NSC activation to improve endogenous repair [56, 207, 240-242]. The concentration of BDNF was

significantly higher in hDPSCs, compared to d-hDPSCs. It can be suggested that this decrease in BDNF secretion following neurogenic differentiation can be attributed to the characteristic BDNF secretion mechanism in neurons, assuming d-hDPSCs acquired neuronal characteristics. In neurons it was shown that endogenous release of BDNF is limited in unstimulated neurons [243, 244]. Following depolarization, BDNF secretion is triggered via calcium-influx dependent mechanisms [244-246]. In the present d-hDPSC-culture, it can be assumed that intercellular stimulation is insufficient to generate adequate calcium influx to activate BDNF secretion. Nonetheless, BDNF secretion by grafted cells can have potential applications in Alzheimer's disease in which BDNF secretion is known to be decreased in the hippocampus [247, 248] and in ischaemic stroke where BDNF signalling is thought to ameliorate the disease outcome [249, 250]. In addition to its trophic and protective effects, it has also been shown that BDNF can promote seizures when injected into the hippocampus due to increased excitatory signalling. Therefore, caution needs to be taken into account when using a BDNF-based therapeutic strategy [251]. Furthermore, NGF and VEGF secretion was enhanced following neurogenic differentiation compared to non-differentiated hDPSCs. Similar to BDNF, NGF is also thought to have potential applications in both Alzheimer's disease and ischaemic stroke. In ischaemic stroke, NGF is thought to have a beneficial effects [240, 252] whereas in Alzheimer's disease, the use of NGF as a therapeutic agent is a topic of debate [253, 254]. VEGF has been shown to have various effects in CNS-pathologies which improved disease symptoms and outcome. The potential mechanisms of action of VEGF were not limited to improving blood supply to brain lesions by inducing angiogenesis, but also due to increased neurogenesis and neuroprotection following VEGF treatment in animal models of neurological disorders [255-259]. Finally, GDNF is known for its ability to enhance survival of dopaminergic neurons, opening possibilities for treating Parkinson's disease [260-263]. Taken together, hDPSCs already secrete multiple growth factors/neurotrophins of which the secretion can be either promoted or downregulated by subjecting hDPSCs to neuronal differentiation. The differential secretome of these cells broadens potential applications should hDPSCs, d-hDPSCs, or a combination of both be used as a growth factor delivery vehicle in cell-based therapies.

In the present study, the assessment of neuronal maturation of hDPSCs was investigated more into detail with TEM in order to gain insight into the acquired neuron-specific characteristics of d-hDPSCs. d-hDPSCs were characterised by a large central nucleus with a prominent nucleolus and various cytoplasmic extensions that formed an intercellular network. In addition, these cytoplasmic extensions were aligned in parallel along with the cytoskeletal components within the extensions, suggesting the possibility of antero- and retrograde transport. Both vesicular- and electrical communication are potential communication mechanisms between adjacent d-hDPSCs. Electrical communication is suggested by gap junctions which were observed at cell-cell contact sites along cytoplasmic extensions. Furthermore, these contact sites appeared clustered at varicosities where mitochondria were found in close proximity to the intercellular contacts. Vesicular transport was demonstrated by the presence of both electron-dense and electron-lucent vesicles at the distal part of the cytoplasmic extensions. In addition, the active secretion and absorption of communicating vesicles was observed. Interestingly, MVB were found in the vicinity of coated pits. MVB are intracellular organelles that are comprised of multiple vesicles enclosed by an outer membrane that are thought to play an important role in endocytosis and protein trafficking in neurons and other non-neural cells [264, 265]. In neuronal cells, it is thought that MVB play an essential role in the retrograde transport of neurotrophic factors such as BDNF and GDNF [266]. The presence of these organelles confirmed the increased inter- and intracellular communication in d-hDPSCs. Together, these distinct neuronal features suggest a successful neuronal maturation of d-hDPSCs [264].

Although d-hDPSCs acquired morphological characteristics of neurons, this does not confirm a successful differentiation towards functional neurons. Therefore, a patch-clamp analysis was performed. The ion channel- and electrophysiological profile of human induced pluripotent stem cell-derived neurons is provided in addendum to this chapter. The electrophysiological recordings of d-hDPSCs showed that voltage-gated sodium and potassium currents were present after differentiation. The selective blocking of these currents by respectively TTX and TEA confirmed their ion specificity. Compared to previous studies by Arthur *et al.* and Kiràly *et al.* some corresponding observations can be made [98, 155]: both

studies were able to find TTX-sensitive sodium channels. However, Arthur *et al.* did not examine the presence of voltage-gated potassium channels. The voltage-gated potassium channels reported by Kiràly *et al.* could only be partially blocked by TEA suggesting that the concentration of TEA used in that study (5 mM compared to 35 mM TEA in our study) was insufficient to block all potassium channels. Moreover, in the study of Kiràly *et al.* it was not shown whether the observed ion channels could be reversibly blocked by TTX and TEA. Furthermore, the differentiated cell population was also split up based on their electrophysiological profile showing the presence of d-hDPSCs displaying sodium currents with premature and mature characteristics. In the present study, a subset of differentiated cells is seen that displayed larger inward or outward currents (peak values of -60.025 ± 18.0 pA/pF and +87.45 ± 18.21 pA/pF; n=4) together with cells displaying more premature characteristics. This mixture of cells in different developmental stages explains the large standard error on electrophysiological data and is also reflected in the PCR data for Mash-1 and SCG10. We decided to show the electrophysiological profile of the general d-hDPSCs population, providing a more realistic overview of the obtained cells being aware that it is a heterogenic population. Nonetheless, d-hDPSCs acquired voltage-sensitive sodium and potassium currents that could be reversibly blocked by TTX and TEA respectively. In addition to voltage-gated sodium and potassium currents, we were able to observe the firing of a single action potential by a subset of d-hDPSCs. However, a train of repeated action potential firing after stimulation was not observed, which would be the ultimate proof of functional neurons. The failure to fire repeated action potentials might be attributed to the gating kinetics of the delayed rectifier potassium channels, i.e. the high activation potential (-10 mV), resulting in an incomplete repolarization. The incomplete repolarization failed to deactivate sodium channels which would be necessary for repetitive firing. A similar observation was made in a study by Wislet-Gendebien *et al.* where MSC were co-cultured with cerebellar granule neurons [91]. In this study, the firing of an action potential by differentiated MSC was observed, but these cells also failed to fire repeated action potentials. Although differentiating cells were kept on maturation-promoting conditions for four weeks, this incubation period might be insufficient for hDPSCs to reach full neuronal maturation. It has been shown that there is a progressive increase in

current amplitude during neuronal maturation and ultimately, action potential firing [267]. Moreover, recent studies reported that differentiating human embryonic stem cells and induced pluripotent stem cells (iPSCs) to neurons take 30-70 days to acquire a functional neuronal culture [74, 268-271]. In addition, human embryonic stem cells and iPSCs are considered to be pluripotent, and thus more capable of differentiating towards other cell types, compared to hDPSCs which are considered multipotent although they express pluripotency markers [272, 273]. Therefore, it can be postulated that a four-week maturation period is insufficient for hDPSCs to acquire a fully functional neuronal phenotype.

Conclusion

The present study aimed to provide a new successful protocol to differentiate human dental pulp stem cells towards functionally active neurons. Although promising results were achieved, establishing a completely functional d-hDPSC culture remains a challenge. The results in this study demonstrated that hDPSCs are capable of neuronal commitment with distinct features of neuronal cells as demonstrated by morphological and electrophysiological characteristics. In addition, exposing hDPSCs to the neurogenic differentiation protocol altered the secretion of selected growth factors/neurotrophins. Future research is needed to identify to what extent and by which mechanism hDPSCs and/or d-hDPSCs could be used to ameliorate the disease outcome in neurological disorders.

Acknowledgements

Addendum

The ion channel- and electrophysiological profile of commercially available human induced pluripotent stem cell-derived neurons (iCell®; Cellular Dynamics International, Madison, WI,USA) is provided below. Traces and I–V relationship of voltage-dependent inward Na^+, outward K^+ and inward Ca^{2+} currents are presented in Addendum 3.1A-C. These currents were blocked by TTX, TEA and nifedipine respectively, showing a dose-response relationship in the case of Na^+ and K^+ currents. The presented findings were verified by Haythornthwaite *et al.* [274]. Maximum inward Na^+ currents were measured by depolarizing the cells from -50 mV to +70 mV with steps of 10 mV for a duration of 40 ms (Addendum 3.1A). To measure the maximum outward K^+ currents, iCell® neurons were first exposed to TTX to block TTX-sensitive voltage-gated Na^+ channels. Subsequently, TTX-sensitive inward Na^+ currents were blocked and only outward K^+ currents were measured. Afterwards, the cells were depolarized from -50 mV to +40 mV with steps of 10 mV for a duration of 1000 ms (Addendum 3.1B). In order to measure the maximum inward Ca^{2+} currents, TTX- and TEA-sensitive voltage-gated Na^+ and K^+ channels were blocked with TTX and TEA respectively. Consequently, TTX-sensitive inward Na^+ and TEA-sensitive outward K^+ currents were blocked. Next, the cells were depolarized from -60 mV to +50 mV with steps of 10 mV for a duration of 200 ms to determine inward Ca^{2+} currents (Addendum 3.1C). In Chapter 4, cadmium chloride ($CdCl_2$) is used to block Ca^{2+} currents instead of nifedipine. Data and image are courtesy of Cellular Dynamics International and are available online at https://cellulardynamics.com/.
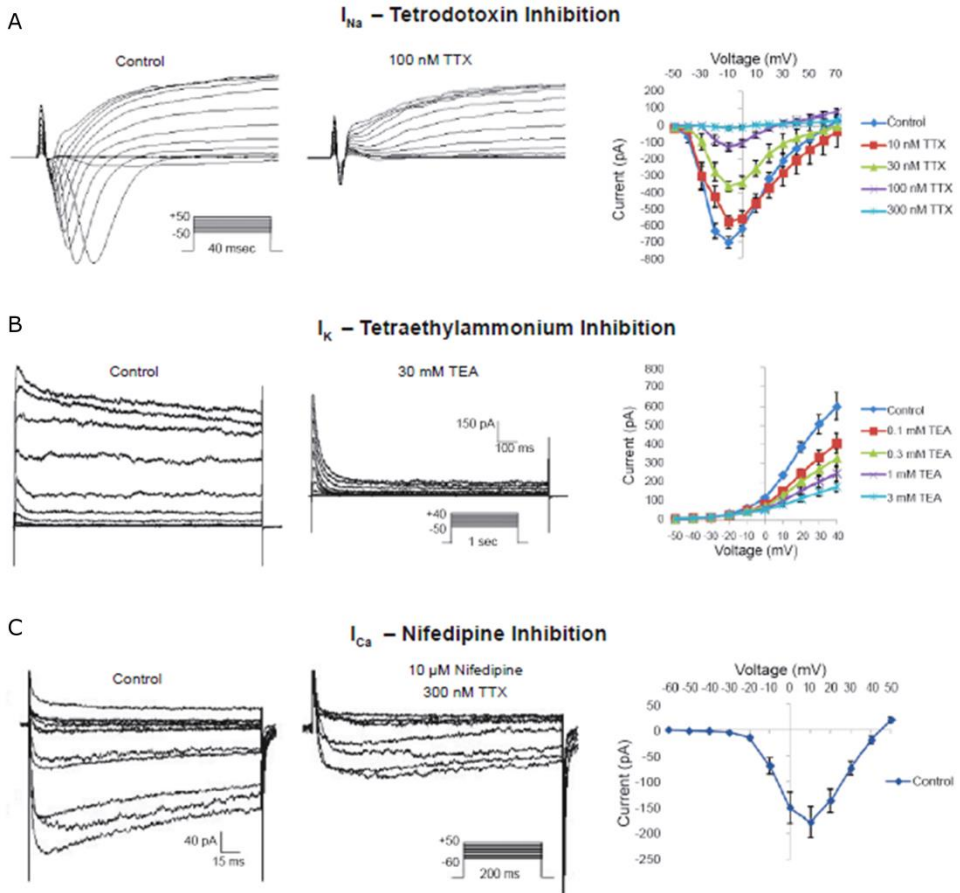
Addendum 3.1: Ion channel- and electrophysiological profile of commercially available human induced pluripotent stem cell-derived neurons. Traces and I–V relationship of voltage-dependent inward Na$^+$ (A), outward K$^+$ (B) and inward Ca2$^+$ (C) currents in iCell® Neurons. These currents were blocked by TTX, TEA and nifedipine respectively. Data and image are courtesy of Cellular Dynamics International.

Neurons derived from human induced pluripotent stem cells show functional maturation over time in which they gain the potential to fire a train of action potentials as demonstrated by the electrophysiological profile shown in Addendum 3.2. Whole-cell patch-clamp recordings were performed at 1 week, 2 weeks and 4-5 weeks of neuronal differentiation. During neuronal differentiation, neurons gradually acquired the ability to fire action potentials over time. Data were generated under current clamp conditions at a resting membrane potential of -65 mV. Currents were injected from -200 pA to +400 pA in steps of 50 pA to evoke spiking. Data and image are courtesy of Kuijlaars *et al*. [275]
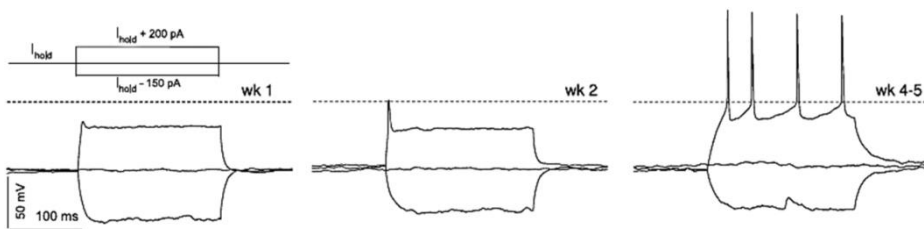
Addendum 3.2: Functional maturation of human induced pluripotent stem cell-derived neurons. Whole-cell patch-clamp generated traces of evoked potentials demonstrate a difference between early (1–2 weeks) and more mature stages (4-5 weeks) of neuronal differentiation. In early stages of neuronal differentiation, the cultured cells were only able to generate a single action potential after 2 weeks. After 4-5 weeks, the cultured cells were capable of repeated action potential firing upon current injection. Image was taken and adapted from [275].

Chapter 4 : Paracrine-mediated neuronal differentiation, neuritogenesis and migration of SH-SY5Y cells by human dental pulp stem cells

4.1 Abstract

Neurological disorders are characterised by neurodegeneration and/or loss of neuronal function which cannot be adequately repaired by the host. Therefore, there is need for novel treatment options such as cell-based therapies that aim to salvage or reconstitute the lost tissue, or that stimulate host repair. The present study aimed to evaluate the paracrine effects of human dental pulp stem cells (hDPSCs) on the migration and neural maturation of human SH-SY5Y neuroblastoma cells. The hDPSC-secretome had a significant chemoattractive effect on SH-SY5Y cells as shown by a transwell assay. To evaluate neural maturation, SH-SY5Y cells were first induced towards neuronal cells, after which they were exposed to the hDPSC-secretome. Additionally, SH-SY5Y cells subjected to the hDPSC-secretome showed increased neuritogenesis compared to non-exposed cells. Maturated cells were shown to increase immune-reactivity for neuronal markers compared to controls. Ultrastructurally, retinoic acid-signalling and subsequent exposure to the hDPSC-secretome induced a gradual rise in metabolic activity and neuronal features such as multivesicular bodies and cytoskeletal elements associated with cellular communication. In addition, electrophysiological recordings of differentiating cells demonstrated a transition towards a neuronal electrophysiological profile based on the maximum TTX-sensitive, Na^+-current. Moreover, CM-hDPSC-maturated SH-SY5Y cells developed distinct features including Cd^{2+}-sensitive currents, which suggests that CM-hDPSC maturated SH-SY5Y acquired voltage-gated Ca^{2+}-channels. The results reported in this study demonstrate the potential of hDPSCs to support differentiation and recruitment of cells with neuronal precursor characteristics in a paracrine manner. Moreover, this *in vitro* experimental design showed that the widely used SH-SY5Y cell line can improve and simplify the preclinical *in vitro* research on the molecular mechanisms of stem cell-mediated neuronal regeneration.

4.2 Introduction

Over 10% of deaths and new cases of permanent disabilities are caused by central nervous system (CNS) pathologies of which cerebrovascular- and Alzheimer's disease are the most important contributors [5]. Moreover, the highest incidence of these pathologies is observed in the elderly, increasing the socioeconomic burden in an aging population [276]. The common neuronal degeneration in these pathologies can only be partially reconstituted by endogenous repair mechanisms. Hence, novel strategies and therapies such as cell-based therapies are required for the treatment and prevention of CNS pathologies. The most ideal candidates for cell-based therapies following CNS damage, would be neural stem- or precursor cells (NSCs, NPCs). These cells are able to differentiate into the majority of cell types present in the adult brain [50] and have been successfully used in animal models of CNS pathologies (reviewed in [8]). Due to ethical [52] and practical issues [53] regarding the application of human NSCs and NPCs, an easy-accessible alternative stem cell-source with the capacity to stimulate endogenous repair by NSCs or NPCs is needed.

A promising cell source are human dental pulp stem cells (hDPSCs) which have been successfully differentiated into functionally active immature action potential-firing neurons [105]. However, their effect on NSCs/NPCs remains to be elucidated. hDPSCs are obtained with minimally invasive procedures and are believed to originate from migrating neural crest cells, supporting their potential efficacy in CNS disorders [85, 205]. hDPSCs are characterised by the expression of specific mesenchymal stem cell (MSC) markers and show tri-lineage differentiation potential, supporting their MSC characteristics [83, 92, 93, 95].

Multiple stem cell-mediated mechanisms have been proposed following hDPSC-transplantation, including neuroprotection, cell replacement, immunomodulation and the promotion of both neuroplasticity and angiogenesis in damaged CNS regions [41, 56, 207, 208, 277]. These mechanisms are mainly thought to be mediated by the effect of the cell-secretome on endogenous stem cells and the host microenvironment instead of replacing lost cells, although hDPSC-integration into the host brain has been reported [206]. hDPSCs and other MSC subtypes were found to secrete a broad spectrum of growth factors including neurotrophins, chemokines, pro-angiogenic growth factors and

immunomodulatory cytokines as previously shown and quantified by our group [77, 105, 106, 108] and others [68, 79]. Therefore, transplanted cells serve as a vehicle for sustained growth factor delivery at the injured site, a hypothesis that was most recently supported in an *in vivo* model for ischemic stroke [114].

To acquire more insight into the proposed *in vivo* mechanisms of transplanted hDPSCs, various *in vitro* models are available to study the different effects of paracrine mediated neuroregeneration by stem cells. SH-SY5Y neuroblastoma cells have been used as an alternative to human NPCs or cells with neuronal characteristics in *in vitro* models for Alzheimer's [278] and Parkinson's [279] disease and stroke [67], but also to investigate mechanisms that drive neurite outgrowth and differentiation [280]. This study evaluated the influence of the hDPSC-secretome on migration, neurite outgrowth, neurogenic maturation, and proliferation of neuroblastoma cells. Moreover, the electrophysiological profile of SH-SY5Y cells was determined during the differentiation process.

4.3 Materials and Methods

4.3.1 Cell culture media

Human Dental Pulp Stem Cells (hDPSCs) were cultured in alpha-modification of minimum essential medium (α-MEM) supplemented with 2 mM L-glutamine, 100 U/ml penicillin, 100 µg/ml streptomycin (all from Sigma-Aldrich St. Louis, Mo, USA) and 10% Fetal bovine serum (FBS; Biochrom AG, Berlin, Germany) which will be referred to as standard hDPSC medium. Standard SH-SY5Y medium consisted of Dulbecco's modified Eagle's and F12 medium (DMEM/F12; Thermo Fisher Scientific Inc.) supplemented with 2 mM L-glutamine, 100 U/ml penicillin, 100 µg/ml streptomycin and 10% FBS. Serum-poor medium consisted of DMEM/F12, 2 mM L-glutamine, 100 U/ml penicillin, 100 µg/ml streptomycin and 0.1% FBS instead of 10% FBS. This medium also serves as the base medium for the production and collection of conditioned medium from hDPSCs. For RA-induction of SH-SY5Y cells, medium consisting of DMEM/F12, 2 mM L-glutamine, 100 U/ml penicillin, 100 µg/ml streptomycin and 1% FBS was used.

4.3.2 Isolation and cell culture of hDPSCs

Human dental pulp tissue was obtained from patients of both sexes aged 14 to 19 (n=11) with informed consent of the patient or after approval of the legal guardian. This study was approved by the Medical Ethical Committee of Hasselt University (13/0104u). hDPSCs were isolated and cultured as described previously in Chapter 2 and 3 [92, 95]. All experiments were conducted with hDPSCs between passage 2-8. hDPSCs were routinely characterised for the MSC surface markers described in Chapter 2 [92], confirming their stem cell nature.

4.3.3 Preparation of conditioned medium of hDPSCs

In order to prepare the conditioned (secretome-containing) medium of hDPSCs (CM-hDPSC), cells were seeded at a density of 2 x 10^4 cells/cm² in standard culture medium. After 24h, the medium was changed to 1 ml/5 cm² of 0.1% FBS-containing serum-poor SH-SY5Y standard medium. 48h later, the medium was collected, centrifuged at 300 g, aliquoted and stored at -80°C for later use.

4.3.4 Cell culture and differentiation of SH-SY5Y neuroblastoma cells

The SH-SY5Y neuroblastoma cell line (Sigma-Aldrich) was grown in standard SH-SY5Y medium and incubated at 37°C in a humidified atmosphere containing 5% CO2. The cells were seeded at a density of 6 x 10^3 cells/cm² in culture flasks pre-coated with 50 µg/ml collagen type I (First Link, Wolverhampton, United Kingdom) and the culture medium was changed every 3-4 days. After reaching 70-80% confluence, the cells were harvested using 0.05% Trypsin with EDTA and expanded.

To induce neuronal differentiation, a two-step protocol based on RA and BDNF exposure, previously described by Encinas et al. was used [218]. Briefly, SH-SY5Y cells were seeded at a density of 2.5 x 10^4 cells/cm² in standard SH-SY5Y medium on collagen type I-coated glass- or Thermanox® coverslips for immunocytochemistry (ICC) and TEM analysis respectively. After 24h, the medium was changed to standard SH-SY5Y medium supplemented with 10 µM RA (Sigma-Aldrich) and 1% FBS instead of 10% to induce neuronal differentiation. These cells were then kept in culture for 5 days with one medium change after 3 days. Next, the cells were washed with phosphate buffered saline (PBS) and either CM-hDPSC or serum-poor DMEM/F12 supplemented with 50

ng/ml BDNF (Immunotools, Friesoythe, Germany), was added to the RA-induced SH-SY5Y cells to stimulate neuronal maturation. The cells were kept in culture for 7 days and the culture medium or CM-hDPSC was changed every 2-3 days. Samples of each differentiation step were used for electrophysiological recordings or were either fixed with 4% paraformaldehyde (PFA) or 2% glutaraldehyde for ICC or TEM analysis respectively. CM-hDPSC of all different hDPSC donors was used throughout this study. The fully BDNF-differentiated SH-SY5Y cells will be used as a reference for the neuronal features of maturated neuroblastoma cells throughout this study.

4.3.5 3-(4,5-dimethylthiazol-2-Yl)-2,5- diphenyltetrazolium bromide (MTT) assay

In order to determine the proliferation capacity of SH-SY5Y neuroblastoma cells after exposure to CM-hDPSC, a 3-(4,5-dimethylthiazol-2-Yl)-2,5-diphenyltetrazolium bromide (MTT) assay was performed. Cells were seeded at a density of 3×10^4 cells/cm² in a 96 well plate in quintuplicate per condition. After 24h incubation, the cells were exposed to CM-hDPSC of two donors of which the mean value was later calculated for each experiment. SH-SY5Y cells exposed to standard SH-SY5Y medium or serum-poor SH-SY5Y medium served as a positive and negative control respectively. After 24h, 48h and 72h, the culture medium was replaced with serum-poor SH-SY5Y culture medium and 500 µg/ml MTT. After 4h of incubation, the MTT-containing solution was removed and 0.01M of glycine in dimethylsulfoxide was added to the wells to dissolve the purple formazan crystals. The amount of absorbance was measured at 570 nm and corrected for the background signal at 655 nm with an iMark™ Microplate Reader (BIO-RAD, Nazareth, Belgium) after which all data were normalized to the SH-SY5Y cells exposed to standard SH-SY5Y medium with 0.1% FBS after 24h exposure.

4.3.6 Transswell migration assay

Tissue culture inserts (ThinCert™, 8 µm pore size, Greiner Bio-One, Frickenhausen, Germany) were seeded with SH-SY5Y cells in standard SH-SY5Y medium containing 0.1% FBS. The bottom, chemoattractive, compartment contained either CM-hDPSC or standard SH-SY5Y culture medium with 10% or

0.1% FBS which served as positive and negative control respectively (n=5). After 24h, transmigrated cells were fixed with 4% PFA and stained with 0.1% crystal violet. Two representative micrographs were taken per insert and migration was quantified with AxioVision software (Carl Zeiss, Aalen, Germany).

4.3.7 Immunocytochemistry

Cells seeded on glass coverslips were fixed in 4% PFA and immunostainings were performed according to a standardized protocol for immunofluorescence and light microscopy as described previously in Chapter 2 and 3 [92, 105]. Cells were incubated for 1h with primary antibodies listed in Table 4.1 and incubated for 30 min with the appropriate secondary antibody. Negative controls omitted the primary antibody. The mean fluorescence intensity (MFI) was quantified as described previously in Chapter 3 [105].

4.3.8 Neuritogenesis assay

The influence of RA, BDNF and CM-hDPSC (n=8) on neurite outgrowth of SH-SY5Y cells was evaluated by measuring the mean length of the longest neurite on neurite-bearing cells that were stained for ß-III tubulin using Nikon EclipseNet Imaging Software (Excel Technologies, Enfield, CT, USA).

4.3.9 Transmission electron microscopy

SH-SY5Y cells cultured on plastic Thermanox® coverslips were prepared for ultrastructural analysis and the evaluation was performed as previously described in Chapter 2 [92, 95].

4.3.10 Patch-clamp Recordings and Electrophysiological Measurements

Voltage clamp recordings were performed using the whole cell configuration of the patch-clamp technique [225]. For electrophysiological recordings, the bath solution contained 130 mM NaCl, 4 mM KCl, 2 mM $CaCl_2$, 1 mM $MgCl_2$, 10 mM HEPES, 10 mM glucose and 19 mM sucrose which was adjusted to pH 7.4 with NaOH (~311 mOsm/kg). When appropriate, this extracellular solution was supplemented with tetrodotoxin (1µM, TTX; Alomone Labs, Jerusalem, Israel) or TTX + $CdCl_2$ (200µM) to evaluate the responsiveness of the cells for these voltage-gated Na^+- and Ca^{2+}-channel blockers respectively. These chemicals were applied using a fast perfusion system (SF-77B, Warner Instruments,

Holliston, MA, USA) by rapidly moving the solution interface across the cell surface. Micropipettes (2-5 MΩ resistance) were fabricated from 1.5 mm (o.d.) borosilicate glass capillary tubes (Hilgenberg, Malsfeld, Germany). The pipette solution contained 140 mM KCl, 4 mM NaCl, 0.02 mM $CaCl_2$, 2 mM $MgCl_2$, 4 mM Mg-ATP, 10 mM HEPES, 0.8 mM EGTA and was adjusted to pH 7.2 with KOH, (~307 mOsm/kg). All recordings were carried out at room temperature using a computer-controlled patch-clamp amplifier (EPC-10; HEKA Electronics, Lambrecht, Germany) and Patchmaster software (HEKA Electronics). Residual capacitances and leak currents were eliminated by means of a P/6 protocol. Currents were filtered at 2.9 kHz, sampled at 20 kHz and stored on a computer hard disk for later analysis. Cells were clamped at a holding potential of -80 mV during 50 ms. Current patterns were obtained by depolarizing the cell membrane from the holding membrane potential to voltages between -80 mV and +60 mV at intervals of 10 mV. The pulse duration was 100 ms. Inward and outward current amplitudes were measured at the peak value and were additionally determined after applying TTX and TTX + $CdCl_2$. Data were analysed off-line with Fitmaster v2x69 software (HEKA Electronics).

4.3.11 Statistical analysis

Statistical analysis was performed using Graphpad Prism 5 software (Graphpad, San Diego, CA, USA). Datasets were tested for normality with D'Agostino and Pearson's test. Depending on the number of groups and normal distribution of the data, different experimental groups were compared by means of a paired or unpaired t-test or Mann-Whitney-U test, or a one-way ANOVA test followed by a Bonferroni post-test or Kruskall-Wallis or Friedman test followed by a Dunn's test for non-parametric data. Differences were considered statistically significant at p-values ≤ 0.05. Data were expressed as mean ± standard error of the mean (S.E.M).

Table 4.1: Primary and secondary antibodies for immunocytochemical analysis.
MAP-2: microtubule associated protein 2; NeuN: neuronal nuclei; MM: mouse monoclonal antibody; GAM: goat anti-mouse; DAM: donkey anti-mouse; DAR: donkey anti-rabbit; GP: goat polyclonal antibody; RTU: ready to use; DP: Donkey polyclonal; HRP: horseradish peroxidase

Marker	Species	Clone	Dilution	Label	Company
Primary Antibodies					
ß—III Tubulin	MM	2G10	1/2000		Sigma-Aldrich
MAP-2	MM	ab11267, HM-2	1/500		Abcam, Cambridge, UK
NeuN	MM	mAb377, A60	1/100		Millipore, Billerica, MA, USA
Neurofilament	MM	2F11	1/200		DakoCytomation, Glostrup, Denmark
Secondary Antibodies					
GAM	GP-IgG		RTU	HRP	DakoCytomation
DAM	DP IgG		1/500	Alexa Fluor 555	Invitrogen, Carlsbad, CA, USA
DAR	DP IgG		1/500	Alexa Fluor 488	Invitrogen

4.4 Results

4.4.1 The hDPSC-secretome promotes migration but not proliferation of SH-SY5Y cells

After establishing and characterizing the hDPSC culture and collecting the CM-hDPSC, a transwell assay was performed to evaluate the chemoattractive effect of the CM-hDPSC on SH-SY5Y cells (Fig 4.1). Crystal violet staining of migrated cells after exposure of SH-SY5Y cells to standard SH-SY5Y medium with 0.1% (Fig 4.1A) or 10% FBS (Fig 4.1C) or to CM-hDPSC (Fig 4.1B) for 24h, demonstrated that SH-SY5Y cell migration was significantly enhanced (1.93-fold; p-value = 0.0159) by CM-hDPSC (Fig 4.1D; n = 5). No significant increase in metabolic activity as a measure of proliferation of SH-SY5Y cells upon CM-hDPSC-exposure was observed after 24h (Fig 4.1E). Exposure of SH-SY5Y cells to standard SH-SY5Y medium with 0.1% FBS or CM-hDPSC had no significant effect on metabolic activity after 24h, 48h or 72h.
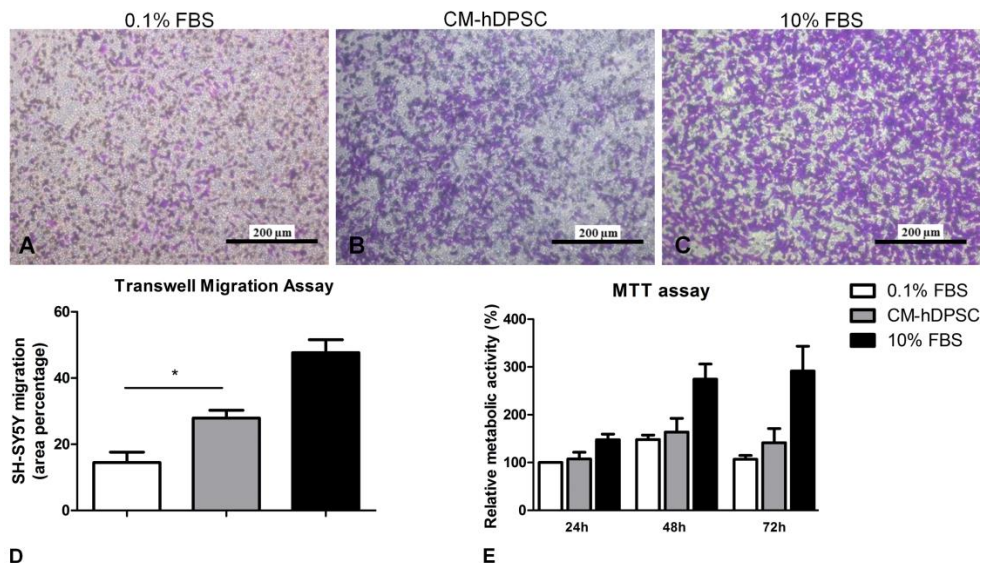
Figure 4.1: CM-hDPSC promotes SH-SY5Y migration. Crystal violet staining of transwell inserts (n=5) after 24h exposure to standard SH-SY5Y medium with 0.1% FBS (A), 10% FBS (C) or CM-hDPSC (B). CM-hDPSC had a significant chemoattractant effect on SH-SY5Y cell migration (D) but did not significantly enhance their relative metabolic activity after 24h, 48h or 72h compared to SH-SY5Y cells exposed to 0.1% FBS (E) as demonstrated by the MTT assay (n= 8). Standard SH-SY5Y medium with 10% FBS was included as a positive chemoattractant control and for increased metabolic activity. Scale bars A-C= 200µm; *= p-value ≤ 0.05.

4.4.2 CM-hDPSC exposure induces a neuronal morphology, neurite outgrowth and enhanced neuronal marker expression in SH-SY5Y cells

During the two-step differentiation process, SH-SY5Y cells underwent multiple morphological adaptations with a stepwise increase in neuronal features which was reflected by the changes in neurite outgrowth (Fig. 4.2) and the quantitative analysis of neuronal marker expression (Fig. 4.3). Both CM-hDPSC- and BDNF-maturated cells obtained a significant increase in the fraction of cells with neurites (Fig. 4.2E) compared to control and RA-induced SH-SY5Y cells (all p-values < 0.0001). The average neurite length (Fig. 4.2F) compared to control and RA-induced SH-SY5Y cells after ß-III staining (Fig. 4.2A-D) was significantly longer in CM-hDPSC- and BDNF-maturated cells (all p-values < 0.0001; CM-

hDPSC vs RA had a p-value of 0.0006). BDNF-maturated SH-SY5Y cells bear significantly longer neurites than CM-hDPSC-maturated cells (p-value = 0.0278).
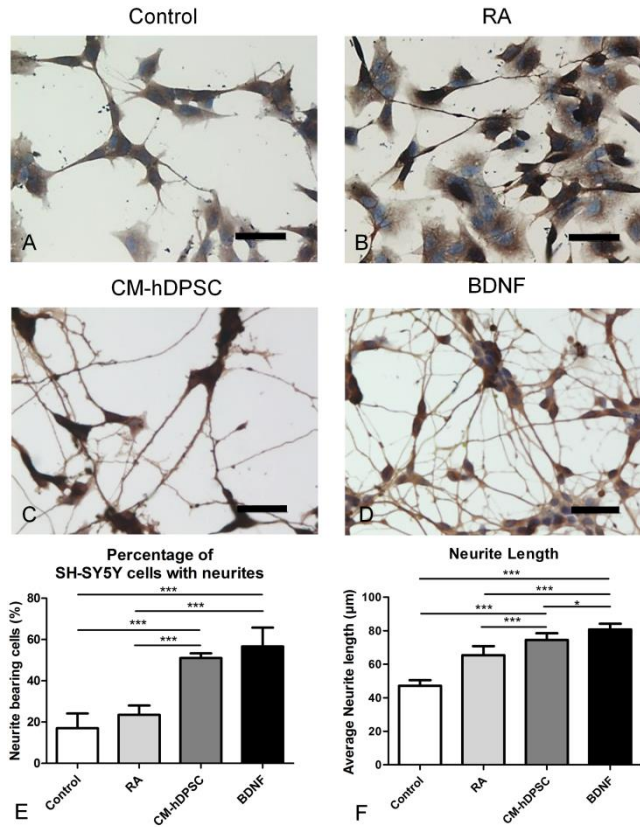
Figure 4.2: CM-hDPSC-induced maturation enhanced neurite outgrowth in SH-SY5Y neuroblastoma cells. ß-III tubulin staining of control (A), RA-induced (B), CM-hDPSC- (C) and BDNF-maturated (D) SH-SY5Y cells show a significant increase in the percentage of neurite bearing cells (E) and the average length of the longest neurite (F) after the maturation process (n=8; * = p-value ≤ 0.05; *** = p-value ≤ 0.001). Scale bars A-D= 50µm.

Quantitative analysis for the percentage of immune-reactive SH-SY5Y cells (Fig. 4.3M) and MFI/cell (Fig. 4.3N) was performed for NeuN (Fig. 4.3A-D), MAP-2 (Fig. 4.3E-H) and neurofilament (Fig. 4.3I-L). Negative staining controls were included in the top right corner of Fig. 3A, D and E. Both the fraction of

immunoreactive cells as the MFI/cell for NeuN were significantly increased in CM-hDPSC maturated SH-SY5Y cells compared to RA-induced neuroblastoma cells (Fig. 4.3B, C, M, N). While no significant difference was found between the fraction of immunoreactive SH-SY5Y cells for MAP-2, the MFI/cell showed an increase during the maturation process, as shown by the significant difference (p-value = 0.0476) between RA-induced and CM-hDPSC-maturated SH-SY5Y cells (Fig. 4.3F, G, M, N). RA-induction significantly decreased (p-value = 0.003) MFI/cell for neurofilament immunoreactivity compared to controls (Fig. 4.3I, J) which was restored by CM-hDPSC and BDNF-exposure (Fig. 4.3H, I, N) although not significantly. The fraction of immunopositive cells for neurofilament was significantly increased in CM-hDPSC-treated cells compared to RA-induced SH-SY5Y cells (p-value = 0.0120), but not compared to control cells. With the exception of the significant decrease in the MFI/cell for NF, no significant difference in MFI or percentage of immunopositive cells was observed between control cells and RA-induced SH-SY5Y cells. No significant difference between the MFI/cell and percentage of immunoreactive cells was found between CM-hDPSC- and BDNF-maturated cells for these markers.
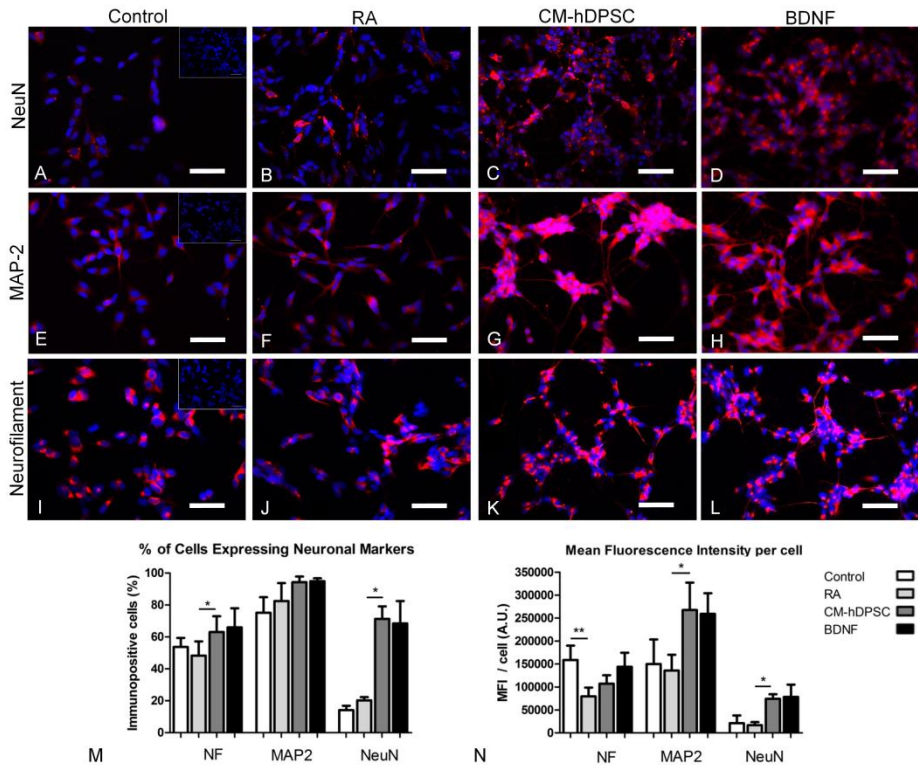
Figure 4.3: SH-SY5Y neuroblastoma cells upregulate neuronal marker expression after CM-hDPSC-induced maturation. NeuN (A-D), MAP-2 (E-H) and NF (I-L) staining revealed a significant increase in the percentage of NF and NeuN, immunoreactive cells after CM-hDPSC exposure compared to RA-induced cells (M). Inserts in control SH-SY5Y include the negative control staining. The MFI per cell was significantly increased after CM-hDPSC exposure compared to RA-induced cells for MAP-2 and NeuN (T). The MFI for NF was significantly decreased after RA-induction compared to control cells (T) (n=5, except for NeuN, n=4; * = p-value ≤ 0.05; ** = p-value ≤ 0.01). Scale bars A-L= 50µm.

4.4.3 SH-SY5Y cells acquire ultrastructural features of neuronal cells

SH-SY5Y cells were subjected to an ultrastructural analysis using TEM (Fig. 4.4) during the different phases of the differentiation process. Analysis of control (Fig. 4.4A-C), RA-induced (Fig. 4.4D-F) and CM-hDPSC- (Fig. 4.4G-I) or BDNF-maturated (Fig. 4.4J-L) SH-SY5Y cells showed that these cells acquired ultrastructural features of neuronal cells during the induction- and maturation phase. Naïve SH-SY5Y cells were characterised by a large central nucleus with

prominent nucleolus (Fig. 4.4A, white arrowheads). Upon RA-exposure and subsequent CM-hDPSC or BDNF-exposure, in addition to prominent nucleoli (Fig. 4.4D, G and J respectively; black arrows), these cells were characterised by abundant organelles associated with metabolic activity and protein synthesis. Upon the transition from control SH-SY5Y to RA-induced SH-SY5Y cells, a perinuclear distribution of the aforementioned organelles was observed (Fig. 4.4D; red bracket). This intracellular machinery was more pronounced in the RA-induced SH-SY5Y cells (Fig. 4.4D and E, asterisk) compared to control, and CM-hDPSC/BDNF-maturated cells (Fig. 4.4B, H, K respectively; asterisk).

The cytoplasm of RA-induced and CM-hDPSC/BDNF-maturated cells contained multivesicular bodies (MVB, Fig. 4.4E, H, K, inserts; I, L, black circles) which were absent in the control cells. In addition to small electron-dense vesicles, CM-hDPSC-maturated SH-SY5Y cells also produced larger electron-dense vesicles (Fig. 4.4G, black circle). Nonetheless, all SH-SY5Y subgroups showed the presence of small electron-dense vesicles in their cytoplasmic extensions (Fig. 4.4C, F, I, L; white circles). Cells subjected to CM-hDPSC- or BDNF signalling, but not control or RA-induced SH-SY5Y cells, acquired longitudinal aligned cytoskeletal elements (Fig. 4.4H, I, L, arrowheads). The intercellular contact zones between neighbouring cells showed the release of these electron-dense vesicles (Fig. 4.4G, insert; G, H, red arrow) between CM-hDPSC-maturated cells.
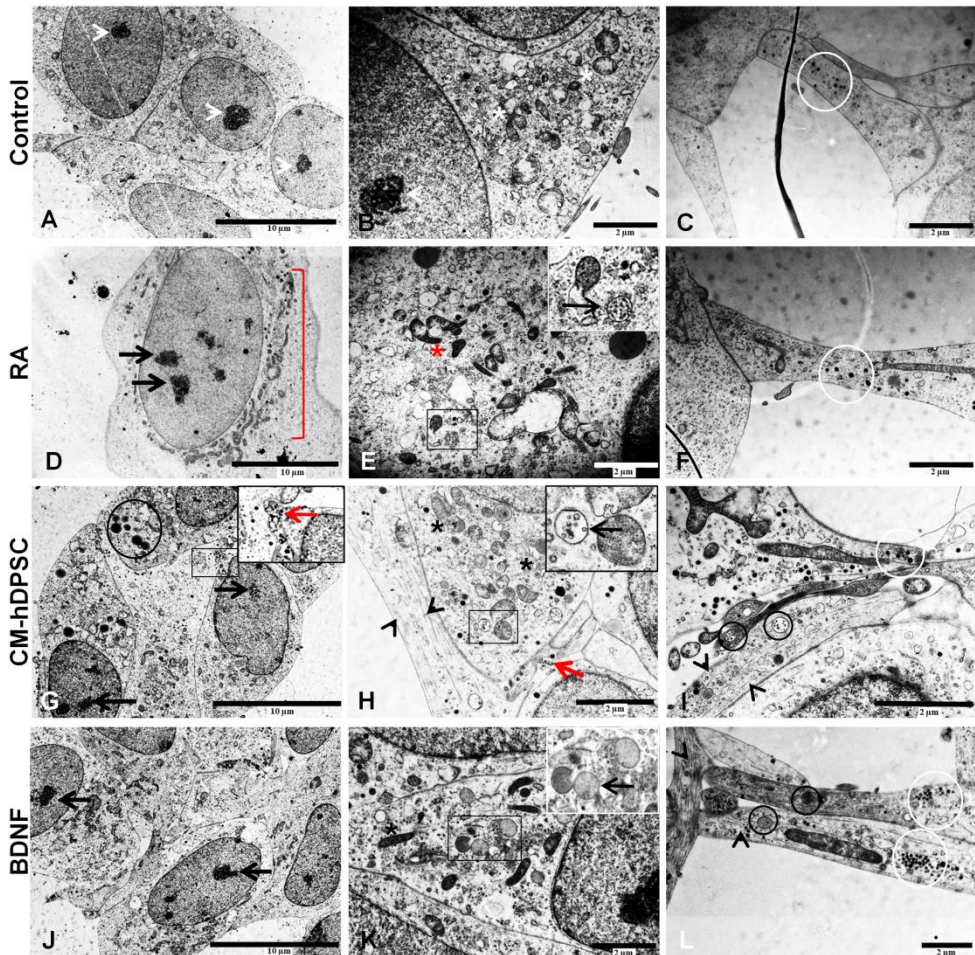
Figure 4.4: SH-SY5Y neuroblastoma cells acquired ultrastructural features of neuronal cells. Ultrastructural analysis of control (A-C), RA-induced (D-F) and CM-hDPSC- (G-I) or BDNF-maturated (J-L) SH-SY5Y cells showed that these cells acquired ultrastructural features of neuronal cells during the neuronal induction- and maturation phase. Control SH-SY5Y cells appeared as metabolically active cells with a large central nucleus with a nucleolus (A, white arrowheads). These metabolic features and requirements were increased upon RA-exposure and subsequent CM-hDPSC or BDNF exposure as demonstrated by the prominent nucleoli (D, G and J respectively; black arrows) and the abundance of organelles associated with metabolic activity. RA-signalling induced a perinuclear organization of these organelles (D; red bracket) which were more pronounced in the RA-induced SH-SY5Y cells (D and E, asterisk) compared to control (B; asterisk), CM-hDPSC and BDNF maturated cells (H, K; asterisks). The cytoplasm of RA-induced and CM-hDPSC/BDNF maturated cells contained multivesicular bodies (E, H, K, inserts; I, L, black

circles) which were absent in the control cells. All cells were characterised by small electron-dense vesicles in their cytoplasmic extensions (C, F, I, L; white circles) which were released at intercellular contact zones between CM-hDPSC-maturated cells (G, insert; G, H, red arrow). CM-hDPSC maturated SH-SY5Y cells also produced larger electron-dense vesicles (G, black circle). CM-hDPSC- or BDNF signalling enhanced the development of longitudinal aligned cytoskeletal elements along the course of the cytoplasmic extensions (H, I, L, arrowheads). Scale bars: (A, D, G, J)= 10 µm; (B, C, E, F, H, I, K, L)= 2 µm.

4.4.4 Electrophysiological properties of SH-SY5Y cells

SH-SY5Y neuroblastoma cells in the different stages of differentiation and maturation were subjected to electrophysiological analysis in order to gain additional insight into the degree of differentiation and functionality of the obtained cell populations (Fig. 4.5). A representative trace of a CM-hDPSC-maturated SH-SY5Y cell depolarized from a holding potential of -80 mV to -10mV with pulse duration 100 ms is presented in Fig. 4.5A. The resulting decrease in inward current upon 1µM TTX and 1µM TTX + 200µM $CdCl_2$ simulation are illustrated in the traces in Fig. 4.5B and Fig. 4.5C correspondingly, demonstrating the presence of TTX- and $CdCl_2$-senstive inward voltage-gated Na^{+-} and Ca^{2+}-channels respectively. The maximum inward currents, recorded at a membrane potential of -10 mV, in unstimulated, 1µM TTX and 1µM TTX + 200µM $CdCl_2$-stimulated control, RA-induced, CM-hDPSC- and BDNF-exposed SH-SY5Y cells were subjected to statistical analysis (Fig. 4.5D). These results show a significantly increased maximum inward current in unstimulated CM-hDPSC- (n=8) and BDNF exposed SH-SY5Y cells (n=7) compared to controls (n=7, ### and # marks). This inward current was also significantly different between RA-induced (n=8) and CM-hDPSC-maturated cells. Subsequent TTX stimulation significantly decreased maximum inward currents at a membrane potential of -10 mV in all conditions. The inward current that remained after TTX stimulation was significantly larger in CM-hDPSC-exposed SH-SY5Y cells (n=8) compared to TTX-stimulated controls (n=7; ##), RA-induced (n=8), and BDNF-exposed cells (n=7). The remaining current after TTX stimulation was significantly reduced by adding 200µM $CdCl_2$ on top of TTX stimulation in CM-hDPSC-maturated SH-SY5Y cells (n=3). Adding $CdCl_2$ had no significant effect in control (n=2), RA-induced (n=3) or BDNF-exposed (n=5)

SH-SY5Y cells and no difference between maximal inward currents after 1µM TTX + 200µM CdCl$_2$ stimulation could be observed between subgroups. The current/voltage relationship of inward currents in unblocked conditions and after adding 1µM TTX and 1µM TTX + 200µM CdCl$_2$ in control, RA-induced, CM-hDPSC- and BDNF-treated subgroups is presented in Fig. 4.5E-H respectively. No significant change in resting membrane potential or train of action potential-firing was observed over the differentiation process. No significant difference in maximum outward currents was observed over the tested membrane potentials.
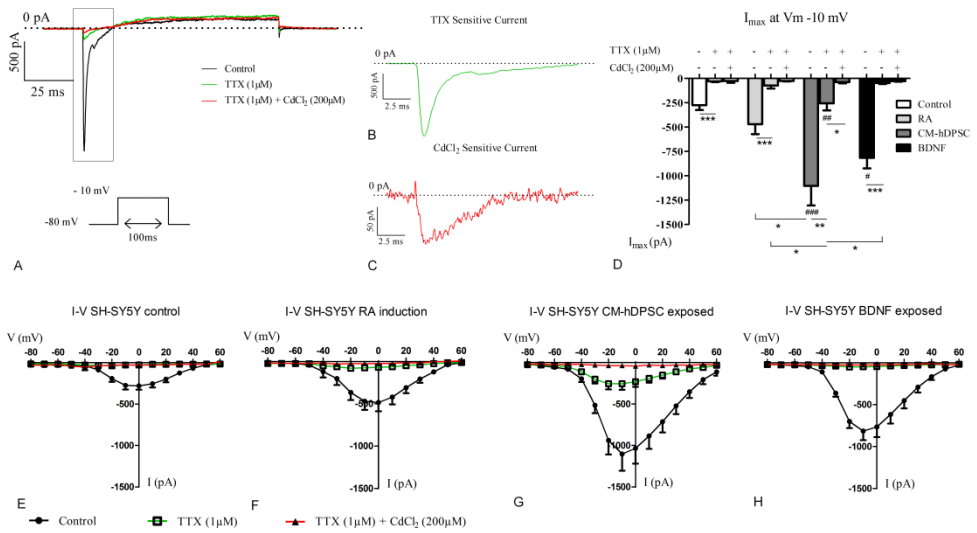
Figure 4.5: CM-hDPSC-maturated SH-SY5Y cells develop a distinct neuronal electrophysiological profile. (A) representative trace of a CM-hDPSC matured SH-SY5Y cell depolarized from a holding potential of -70 mV to -10mV with pulse duration 100 ms. Exposure to 1µM TTX or 1µM TTX + 200 µM $CdCl_2$ blocked inward currents by blocking Voltage-gated Na^+ and Na^+ + Ca^{2+} channels respectively. Detailed image of (A) showing representative traces of TTX-sensitive (B) and $CdCl_2$-sensitive (C) currents. (D) Maximum inward currents recorded at a membrane potential of -10 mV in control conditions (unstimulated) and after stimulating the different SH-SY5Y subsets with 1µM TTX and 1µM TTX + 200µM $CdCl_2$. These results show a significantly increased maximum inward current in unstimulated CM-hDPSC- (n=8) and BDNF exposed SH-SY5Y cells (n=7) compared to controls (n=8; ### and # marks). This inward current was also significantly different between RA-induced (n=8) and CM-hDPSC-maturated cells. Subsequent TTX stimulation significantly decreased maximum inward currents at a membrane potential of -10 mV in all conditions. The inward current that remained after TTX stimulation was significantly larger in CM-hDPSC-exposed SH-SY5Y compared to TTX-stimulated controls (##), RA-induced, and BDNF-exposed cells. The remaining current after TTX stimulation was significantly reduced by addition of 200µM $CdCl_2$ on top of the TTX in CM-hDPSC-maturated SH-SY5Y cells. $CdCl_2$ addition had no significant effect in other SH-SY5Y subgroups. The current/voltage relationship of inward currents in SH-SY5Y in unblocked condition and after addition of 1µM TTX and 1µM TTX + 200µM $CdCl_2$ in control (E), RA-induced (F), CM-hDPSC- (G) and BDNF- (H) treated subgroups shows these inward currents at different membrane potentials. Data are represented as mean ± S.E.M. *, #= p-value ≤ 0.05; **, ##= p-value ≤ 0.01; ***, ###= p-value ≤ 0.001.

4.5 Discussion

In the present study, the paracrine potential of hDPSCs to support recruitment and differentiation of cells with NPC-characteristics was described, using the human SH-SY5Y neuroblastoma cell-line. Furthermore, the data obtained in this study underscore the value of SH-SY5Y cells as an easy-to-use *in vitro* tool for preclinical research which allows the rapid evaluation of neurotrophic effects.

In the first part of this study, we investigated the chemoattractive properties of CM-hDPSC. These results showed that CM-hDPSC was able to stimulate migration of SH-SY5Y cells. As recruitment of endogenous cells with neuroregenerative characteristics to the site of neuronal injury is one of the goals in neuroregenerative medicine, hDPSCs can be considered as a delivery vehicle for chemoattractant factors. Moreover, NPCs and/or NSCs require blood vessels to migrate towards the site of injury [281]. Importantly, hDPSCs have been shown to stimulate endothelial cell migration and vessel formation *in vitro* and *in vivo* [77, 108] making them attractive candidates for stem cell-based therapies for neuronal injury.

In the second part of the study, we aimed to obtain neuronally differentiated SH-SY5Y cells after exposure to CM-hDPSC. Therefore, we adapted a protocol described by Encinas *et al.* [218] which is based on sequential RA- and BDNF-signalling. In our experimental setup, RA-treated SH-SY5Y cells were exposed to CM-hDPSC. In parallel, BDNF treatment was included as a positive control for neuronal maturation. RA stimulation prior to the addition of CM-hDPSC or BDNF is preferable since RA signalling increases the expression of Tyrosine Kinase A and B receptor (TrkA, B), improving the responsiveness for neurotrophins secreted by hDPSCs and for BDNF [68, 105, 218, 282].

To our knowledge, this paper is the first to report the effects of the hDPSC-secretome on migration, maturation and neuritogenesis of SH-SY5Y cells. In accordance with Mead *et al.* [68] who observed increased paracrine-mediated neuritogenesis in axotomized retinal ganglion cells by hDPSCs, CM-hDPSC promoted neurite outgrowth in SH-SY5Y cells. A similar, but methodological substantially different study by Pires *et al.* [280] used the CM of bone marrow (BMSCs)- and Wharton Jelly's-derived MSCs to evaluate neurite outgrowth and neuronal differentiation of SH-SY5Y cells. Although the mean length of the SH-

SY5Y cells exposed to the stem cells in the study by Pires *et al.* is comparable with the lengths described in this study, fewer neurites were counted and the percentage of neurite bearing cells was not evaluated [280]. In addition to stimulating neurite outgrowth, the CM-hDPSC was also capable of increasing the expression of neuronal-related markers in RA-induced neuroblastoma cells. In accordance with Pires *et al.* [280], the fraction of MAP-2 expressing cells was not altered, although a significant upregulation of this marker is reported after exposure to CM-hDPSC. Furthermore, a concomitant increase of MFI/cell and increased fraction of cells showing immunoreactivity for the late neuronal marker NeuN and the cytoskeletal marker neurofilament was observed after CM-hDPSC-exposure. The ultrastructural appearance of differentiating SH-SY5Y cells revealed that addition of RA to SH-SY5Y cells induced metabolic changes as indicated by the prominent nucleoli and perinuclear organisation of the cell organelles. More interestingly, supplementing RA to the culture medium of SH-SY5Y neuroblastoma cells induced the formation of MVBs, which is regarded as a structural hallmark of neuronal cells and cellular communication [265]. Following exposure of the RA-induced cells to CM-hDPSC or BDNF, additional changes included the appearance of longitudinally aligned cytoskeletal elements in which cell organelles associated with vesicular transport were observed, suggesting antero- and/or retrograde transport. A major difference between the CM-hDPSC and BDNF-exposed cells was the appearance of a different subset of electron-dense intracellular vesicles and the observed release of granular material in the intercellular cleft. With the exception of the latter observation, these findings are in agreement with the scarce data available on the ultrastructure of differentiated SH-SY5Y cells [283].

To verify neuronal differentiation and maturation of SH-SY5Y cells, electrophysiological recordings were performed. Both CM-hDPSC and BDNF exposure after RA-induction of SH-SY5Y cell significantly enhanced maximal inward currents, a prerequisite of repeated action potential firing which in itself was not observed. These enhanced maximal inward currents could be significantly inhibited by the addition of 1µM TTX, suggesting the functional activity of voltage-gated Na$^+$ channels in the neuroblastoma cell-membrane. After exposure to 1µM TTX, a significantly higher current remained in the CM-hDPSC-exposed SH-SY5Y cells. This current could be significantly inhibited by

adding 200µM CdCl$_2$ to 1µM TTX whereas this had no effect in the other SH-SY5Y subsets. These data suggest that adding CM-hDPSCs to RA-induced SH-SY5Y cells stimulated voltage-gated Ca^{2+}-channel generation in the SH-SY5Y membrane. Moreover, this effect is BDNF-independent as these currents were not observed in BDNF-exposed SH-SY5Y cells. Unfortunately, we were not able to identify the voltage-gated Ca^{2+}-channel subtype as low or high voltage-activated, as both types of these channels have been previously identified in SH-SY5Y cells [284]. Moreover, we did not distinguish between different subsets of voltage-gated Na$^+$-channels, which are also present in SH-SY5Y cells [285]. Nonetheless, these data indicate that the hDPSC-secretome can stimulate the electrophysiological heterogeneous SH-SY5Y cell-line [286] to increase the expression of TTX-sensitive voltage-gated Na$^+$- and CdCl$_2$-sensitive Ca^{2+}-channels.

Due to the absence of direct contacts between hDPSCs and SH-SY5Y cells, the observed effects are solely attributed to the plethora of paracrine factors produced by hDPSCs. Moreover, it seems unlikely that these effects can exclusively be attributed to BDNF present in the CM-hDPSC. Our group previously showed that, without concentrating the CM and at a seeding density and conditioned medium volume as used in this study, the concentration of BDNF is less than 10 ng/ml [105, 106] as compared to the positive control which used 50 ng/ml BDNF [218]. These findings are in line with Crigler et al. 2006 who demonstrated that the effect of BMSC-produced BDNF is only partially responsible for the observed effects on SH-SY5Y cells [101]. The paracrine factors secreted by the DPSCs include nerve growth factor, neurotrophin-3, BDNF, glial-derived growth factor and vascular endothelial growth factor [68, 105] which act via TrK receptors and via Stromal cell-derived factor 1, activating the Chemokine (C-X-C Motif) Receptor 4. These soluble factors have the capacity to induce migration as well as axonal and cytoskeletal changes [257, 287, 288] whereas Trk receptor-mediated signalling enhances neuronal differentiation [289].

SH-SY5Y cells are commonly used as *in vitro* tools to investigate the mechanisms of action of neuroprotective compounds [279] or to evaluate the role of a gene of interest in neurological disorders [290]. In this study, we used

SH-SY5Y cells to establish an *in vitro* model allowing us to examine paracrine mediated effects of hDPSCs on SH-SY5Y cells. This model can pave the way for more in depth studies of molecular pathways or signalling cascades that drive neuronal differentiation, neuritogenesis and migration of SH-SY5Y cells. This fundamental study aimed to contribute to the progress of preclinical MSC research for neurodegenerative disorders. However, before being considered as a therapy, several hurdles remain to be overcome. For instance, the route of administration, dose and type of MSCs are ongoing points of discussion (reviewed in [291, 292]. Moreover, although MSC transplantation is considered safe, it has been shown that MSC transplantation favours tumour growth when transplanted in allogeneic animals due to their immunomodulatory properties [293]. Despite these issues, MSCs continue to be an attractive candidate for cell-based therapies for neurological disorders of which the mechanisms of action remain largely unknown.

Conclusion

The present study aimed to provide a new successful *in vitro* tool to evaluate the paracrine effect of hDPSCs on cells with neural precursor characteristics. The results in this study demonstrated that the CM of hDPSCs is capable of stimulating neuronal maturation and neuritogenesis in RA-pretreated human SH-SY5Y neuroblastoma cells. Moreover, SH-SY5Y cells were clearly attracted towards the stem cell-secretome. This *in vitro* experimental design of a non-animal source of neuronal precursor cells shows the value of the easily available SH-SY5Y cell line and can improve and simplify the preclinical *in vitro* research on molecular mechanisms of stem cell-mediated neuronal regeneration.

Acknowledgements

Chapter 5 : The neuroprotective and neuroregenerative potential of human dental pulp stem cells on primary cortical neurons and neural stem cells is not enhanced by Leukocyte- and Platelet-Rich Fibrin priming

5.1 Abstract

Neurodegenerative disorders such as stroke are characterised by degeneration and/or loss in neuronal function which cannot be adequately restored by endogenous repair response. Therefore, there is a need of novel treatment options such as cell-based therapies that aim to salvage the lost tissue or that can stimulate host repair. This study primarily aimed to investigate the paracrine-mediated neuroregenerative potential of the conditioned medium of human dental pulp stem cells (CM-hDPSCs) on neural stem cell (NSC) proliferation and migration and on protecting primary cortical neurons (pCNs) against oxygen and glucose deprivation (OGD)-induced cell death and pCN neurite outgrowth. Next, the effect of Leukocyte- and Platelet-Rich Fibrin (L-PRF) 'priming' on the neuroregenerative effect of the hDPSC secretome (prCM-hDPSCs) on NSCs and pCNs was evaluated. L-PRF is an autologous blood-derived biomaterial that is being successfully applied clinically with beneficial results in wound- and bone healing. The mechanisms of action of L-PRF are unknown but it is suggested L-PRF creates a local inflammatory milieu that favours regeneration and that recruits and activates wound repairing- and stem cells in addition to secreting growth factors and extracellular matrix proteins. Moreover, this inflammatory microenvironment is also thought to play an important role in repairing central nervous degeneration by stimulating endogenous repair. In the present study, L-PRF is used as a tissue in a dish that can provide an inflammatory microenvironment to prime hDPSCs that could enhance their neuroregenerative properties. In addition, the effect of the two fractions (conditioned medium or L-PRF exudate) of the biomaterial itself on hDPSCs, NSC, pCNs and neuroregenerative mechanisms was investigated.

The results in this study demonstrated that the CM-hDPSC protects OGD-exposed pCNs against ischemic death and was capable to enhance neuritogenesis in pCNs. Moreover, this conditioned medium had a chemoattractant effect on NSCs but did not stimulate NSC proliferation. Unfortunately, although priming hDPSCs increased their secretion of the growth factor BDNF, no additional effect on the paracrine mediated mechanisms of regeneration described in this study were observed. Furthermore, the soluble factors present in L-PRF itself had detrimental effects on NSCs and pCNs in

higher concentration and only low concentrations of the conditioned medium of L-PRF stimulated NSC migration or was able to protect pCNs from ischemic death. These data support the paracrine mediated neuroregenerative potential of hDPSCs and suggest that L-PRF is a bioincompatible biomaterial on CNS-derived cells and caution is advised when applying this biomaterial clinically in the vicinity of CNS tissue.

5.2 Introduction

As previously mentioned, CNS pathologies, including stroke, are one of the main causes of deaths and new cases of permanent disabilities [5]. Moreover, the neuronal degeneration in these pathologies can only be partially reconstituted by the host itself. Novel therapies such as cell-based therapies are therefore being considered for the treatment of CNS disorders. Ideally, neural stem cells (NSCs) or neural precursor cells (NPCs) would be used as a (stem) cell source as these cells were shown to be able to differentiate into the majority of cell types present in the adult brain [50] but due to ethical and practical issues with NSCs, an easy-accessible alternative stem cell-source with a neuroregenerative potential is needed.

In Chapter 4, human dental pulp stem cells (hDPSCs) were proposed as an attractive alternative for NSCs or NPCs as they have been suggested to enhance neuroregeneration by multiple mechanisms, including cell replacement, neuroprotection, immunomodulation and promoting neuroplasticity and angiogenesis [41, 56, 207, 208, 277]. As these mechanisms were thought to be mediated by paracrine actions of the hDPSCs, Chapter 4 focused on investigating the effect of hDPSCs on cells with a neuronal predisposition, human SH-SY5Y neuroblastoma cells, with encouraging results. Although an easy-to-use model to investigate neuritogenesis and neuronal maturation of SH-SY5Y cells was provided, it remains to be determined if these effects can also be observed in a different subset of cells with neuronal predisposition which more closely resemble the physiology of the target cells.

The first and main focus of this study was to evaluate paracrine-mediated effects of hDPSCs on murine NSCs and primary cortical neurons (pCNs). The influence of the hDPSC secretome (CM-hDPSCs) on NSC proliferation and migration was determined. Moreover, the influence of the hDPSC factors on neurite outgrowth of primary cortical neurons was also evaluated in addition to an assessment of the neuroprotective properties of the hDPSC in an oxygen-glucose deprivation (OGD) assay. In this OGD assay, pCNs were first subjected to ischemic conditions consisting of 0.3% O_2 and low glucose concentrations, resembling the ischemic core of the stroke lesion. Afterwards, reperfusion damage was

mimicked by restoring nutrient flow by adding fresh medium and increasing the oxygen levels to 2.3% O_2, resembling the ischemic penumbra [294].

The second aim of this study was to evaluate whether preconditioning hDPSCs can enhance their neuroregenerative effect by boosting growth factor secretion of the hDPSCs. When hDPSCs are to be considered as a stem cell-based therapy for ischemic stroke, it is important to take into account the hypoxic/ischemic and inflammatory microenvironment in which the cells are situated to mediate or stimulate endogenous repair or that can influence cell survival. Therefore, several studies have tried to precondition or 'prime' stem cells with *in vitro* mimetics for *in vivo* situations such as hypoxia. Hypoxic preconditioning can be achieved by adding pharmacological agents such as deferoxamine to enhance their neuroregenerative effects [160] or hypoxia itself. Hypoxia enhanced the pro-angiogenic properties of hDPSCs [161] and their trophic effect on fibroblasts and SH-SY5Y cells [162]. Similarly, hypoxia mimetic agents increased VEGF secretion and stimulated hypoxia induced factor 1 alpha (HIF-1α) expression [163, 164].

A novel approach to prime hDPSCs is to expose them to key components of the inflammatory reaction which can be found in the blood. Therefore, we aimed to evaluate whether a clinically applied, blood-derived biomaterial, leukocyte- and platelet rich fibrin (L-PRF), can enhance the neuroregenerative effect of hDPSCs. L-PRF has shown great promise in wound healing and the restoration of bone defects in for instance craniomaxillofacial surgery [295, 296] and its therapeutic effect is thought to be mediated by the growth factors present in this material [166, 167]. In this study, L-PRF is hypothesized to contain inflammatory components that modify the stem cell properties and neuroregenerative potential of hDPSCs. For example L-PRF is known to contain factors such as tumour necrosis factor alpha (TNF-α) [297], insulin-like growth factor 1 (IGF-1) [167] and interleukin 1 beta (IL-1ß) [167] that can influence stem cell characteristics and behaviour. TNF-α was previously shown to enhance the stem cell properties of hDPSCs [298] and the neuronal fate of bone-marrow derived mesenchymal stem cells (BMSCs) [299], based on marker expression. Similarly, IGF-1 enhanced the proliferation of BMSCs [300]. In addition, TNF-α sigalling altered the secretome of adipose-derived stem cells which showed enhanced angiogenic properties compared to non-treated cells [301] and IL-1ß promoted

the immunomodulatory properties of human umbilical cord MSCs [302]. Moreover, TNF-α-, IGF-1- and IL-1ß-stimulated MSCs increased the expression of the stromal-derived factor-1 (SDF-1) receptor CXCR4, potentially enhancing the migratory capacity of MSCs towards the ischemic brain where SDF-1 is secreted [299, 300, 302, 303]. However, the effect of the L-PRF components on enhancing the neuroregenerative effect of hDPSCs or other MSC subtypes remains elusive, which will be investigated into more detail in this chapter.

L-PRF can be obtained from venous whole blood samples using a specialized centrifuge and collection tubes and has the form of a spongy clot that can be mechanically compressed in the form of a membrane, which is mainly used clinically. During this compression process, the fluid containing growth factors residing in the clot can be isolated and is termed the L-PRF exudate (EX L-PRF). Moreover, the factors present in the clot can also be isolated by keeping it in culture for 4 days after which the factors secreted by the L-PRF clot or that were bound to the fibrin matrix can be recovered from the conditioned culture medium (CM-LPRF). In this study, hDPSCs were exposed to various concentrations of EX/CM L-PRF in order to investigate the proliferative effect of L-PRF on hDPSCs. Additionally, hDPSCs were exposed to EX/CM L-PRF in different concentration for various time points in order to evaluate enhanced growth factor production. BDNF secretion was used as a measure for enhanced neuroregeneration as this factor was previously shown to be secreted by hDPSCs [63, 68, 106] and was demonstrated to enhance functional recovery and neurogenesis after ischemic stroke [249, 250]. The conditioned medium of primed hDPSCs (prCM-hDPSCs) was then collected and used in the assays on NSCs and pCNs (*vide supra*) in parallel with CM-hDPSCs. Finally, the L-PRF-derived fractions were also used in similar assays as it was previously shown that transforming growth factor ß (TGF-ß), platelet-derived growth factor (PDGF), IL-6 and vascular endothelial growth factor (VEGF) which are also contained in L-PRF [167, 304], and IGF-1 have neuroregenerative effects [256, 305-307]. However, the potential of L-PRF-derived therapeutics in neuroregeneration remains to be determined. Although L-PRF is currently being used as a biomaterial and contains multiple growth factors to which the major therapeutic effect is being attributed, its effect on different tissues such neuronal tissue is largely unknown. In order to assess the use of this promising

biomaterial for other applications, the influence of L-PRF on neuronal tissue was investigated.

5.3 Materials and Methods

5.3.1 Isolation and cell culture of hDPSCs

Human dental pulp tissue was obtained from patients of both sexes aged 14 to 26 (n=7) undergoing routine extraction of third molars for orthodontic reasons at the Department of Maxillofacial Surgery, Ziekenhuis Oost-Limburg (ZOL), Genk, Belgium or at the Campus St-Barbara of the ZOL located in Lanaken, Belgium. Dental pulp tissues were obtained with informed consent of the patient or after approval of the legal guardian. This study was approved by the Medical Ethical Committee of Hasselt University (13/0104u). Subsequently, hDPSCs were isolated and cultured as described in previous chapters [92, 95]. All experiments were conducted with hDPSCs between passage two and eight.

5.3.2 Isolation and culture of leukocyte- and platelet-rich fibrin

L-PRF was isolated from healthy volunteers aged 25 to 54 (n= 10) and isolation was approved by the Medical Ethical Committee of the University Hospital of Leuven and Hasselt University (S58789 / B322201628215 / I / U). L-PRF was prepared according to the guidelines of the IntraSpin™ Centrifuge, the only FDA approved centrifuge for the preparation of L-PRF (Intra-Lock International, Boca Raton, FL, USA). Briefly, 9ml blood samples were collected and spun down for 12 min at 400 g. Afterwards, L-PRF clots were collected and coagulated red blood cells were removed. The resulting clot was then transferred to the Xpression™ Box (Intra-Lock International) and a weighted press was put onto the clots. This device is designed to extract the exudate from the clot (EX L-PRF) in a controlled manner and to form a thin compressed layer of L-PRF with consistent thickness. The exudate was filtered, aliquoted and stored at -80°C for later use. L-PRF clots were transferred to 6 well plates and put in culture in α-MEM or Neurobasal-A medium without serum or serum replacement for 96h but containing 2mM L-glutamine and 100 U/ml penicillin, 100 μg/ml streptomycin. Afterwards the conditioned medium (CM L-PRF) was collected, aliquoted and stored at -80°C. Fig. 5.1 provides a schematic overview that describes CM L-PRF and EX L-PRF isolation.
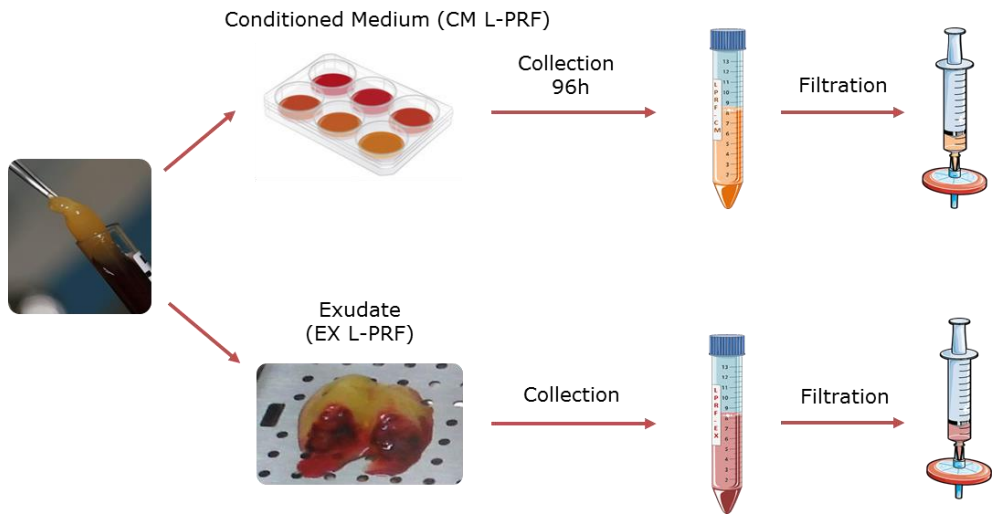
Figure 5.1: Workflow to isolate L-PRF subfractions. The L-PRF clot is isolated by centrifugation from blood samples that are subsequently processed for CM L-PRF and EX L-PRF isolation. L-PRF clots are transferred to 6-well plates in culture medium based on the downstream application. CM L-PRF was then collected after 96h 144h. The L-PRF clot is transferred to the Xpression™ Box and by gravitational compression of the clot, EX L-PRF is collected. Both CM- and EX L-PRF were filtered before use.

5.3.3 Metabolic activity and proliferation of CM/EX L-PRF-exposed hDPSCs: The MTT and Propidium iodide assay

The metabolic activity and proliferative activity of hDPSCs exposed to 1%, 2%,5% and10% CM/EX L-PRF (n=5) were evaluated by means of a MTT and propidium iodide (PI) assay respectively, the latter taking the amount of PI intercalating between DNA as a measure for the total number of cells. The MTT and PI test were performed by seeding hDPSCs at a density of 3×10^4 cells / cm² in 96 well plates in standard hDPSC medium. After 24h, the medium was discarded and hDPSCs were exposed to 1%, 2%, 5% and 10% CM/EX L-PRF for 24h, 48h or 72h. hDPSCs exposed to hDPSC standard medium without FBS and with 10% FBS were used as a negative and positive control respectively. At each time point, the MTT or PI assay was performed. In order to perform the MTT assay at each time point, the medium was removed and 500 µg/ml MTT was

added. After 4h of incubation, the MTT-containing solution was removed and 0.01M of glycine in DMSO was added to the wells in order to dissolve the insoluble formed formazan crystals. The absorbance was measured at 570 nm and corrected for the background signal at 655 nm with an iMark™ Microplate Reader (BIO-RAD).

The PI assay was performed by removing the medium and adding 75µl of lysis buffer to each well (Reagent A100, Chemometec, Allerod, Denmark) after which 75µl of stabilizing solution (Reagent B, Chemometec) containing PI (Sigma-Aldrich) in a final concentration of 10 µg/ml was added and incubated at room temperature in the dark for 15 min. Afterwards, the solution was transferred to a black 96 well plate and fluorescence was excited at 540 nm and measured at 612 nm with a Fluostar Optima (BMG Labtech, Ortenberg, Germany). All data were normalized to the values of hDPSCs exposed to standard hDPSC medium without FBS after 24h exposure.

5.3.4 Priming of hDPSCs with L-PRF exudate and conditioned medium

hDPSCs from two different donors were primed with four different CM/EX L-PRF donors in various concentrations (1%, 5% and 10%) in standard hDPSCs medium but without adding FBS. Cells were seeded at 1.5×10^4 cells / cm² in standard hDPSC medium. After the cells attached to the plastic surface, the medium was removed and serum-free hDPSC medium supplemented with the appropriate concentration of CM/EX L-PRF was added to prime the cells. After 24 or 48 hours, this priming medium was removed and the cells were washed with PBS. Next, serum-free Neurobasal-A medium supplemented with 2mM L-glutamine, 100 U/ml penicillin and 100 µg/ml streptomycin was added to the hDPSCs. 48h later, the medium was collected, centrifuged at 300g for 6 min, aliquoted and stored for later use. Moreover, the number of cells of all conditions was counted with a Moxi cell counter (ORFLO Technologies, Ketchum, ID, USA).

In order to evaluate the inductive effect of EX L-PRF and CM L-PRF on the growth factor production of hDPSCs, BDNF secretion was determined as a measure for increased neurotrophin production and for the potentially enhanced neuroregenerative capacity of hDPSCs. The BDNF concentration was determined by means of ELISA according to the instructions of the manufacturer (Raybiotech®; Norcross, GA, USA). Moreover, the BDNF concentration was

normalized to 1×10^5 cells to correct for variations in cell number due to the priming conditions. In addition to assessing the BDNF secretion in the cell secretome, the BDNF concentration in CM L-PRF (n=3) and EX L-PRF was also determined.

5.3.5 Preparation of conditioned medium of prCM-hDPSCs and hDPSCs

In order to prepare the conditioned (secretome-containing) medium of primed (prCM-hDPSCs), and non-primed hDPSCs (CM-hDPSCs), cells (n= 7 hDPSC donors) were seeded at a density of 1.4×10^4 cells/cm² in standard culture medium. After the cells adhered to the surface, the medium was changed to 1 ml/5 cm² of α-MEM supplemented with 2 mM L-glutamine, 100 U/ml penicillin, 100 µg/ml streptomycin and with or without 10% EX L-PRF from 3 different donors. 48 hours later, the cells were rinsed with PBS and the medium was changed to serum free Neurobasal-A medium, supplemented with 2 mM L-glutamine, 100 U/ml penicillin, and 100 µg/ml streptomycin for 48 hours to allow EX L-PRF induced secretion of growth factors. After 48 hours, the medium was collected, centrifuged at 300 g, aliquoted and stored at -80°C for later use. In addition, the cells were counted to later normalize prCM-hDPSC volumes to corresponding CM-hDPSC donors for the increased cell numbers of exudate-exposed cells compared to controls. All prCM-hDPSC samples were prepared in parallel with CM-hDPSCs. For each experiment, the average experimental output value of the effect of prCM-hDPSCs (CM of hDPSCs primed with 3 different L-PRF donors) was calculated and compared to CM-hDPSC.

5.3.6 Isolation and culture of mouse neural stem cells

Mouse NSCs were isolated from fetal mouse brains by a protocol previously described by Conti et al. [308] with minor modifications based on Reekmans et al. [309]. At gestational days 14-15, pregnant C57BL/6JOlaHsd mice (Envigo, Cambridgeshire, UK) were sacrificed by cervical dislocation and the fetuses were removed from the abdomen as approved by the ethical commission of Hasselt University (protocol number 201410K). Subsequently, the brains were removed and cut into small fragments in cold (4°C) phosphate buffered saline (PBS) with 100 U/ml penicillin and 100 µg/ml streptomycin. The brain fragments were then transferred to a new vial and centrifuged for 8 min at 200g. Afterwards, the supernatant was removed and incubated with 0.2% collagenase A (Roche, Basel,

Switzerland) and DNase-I (2000 Kunitz units / 50 ml; Sigma-Aldrich) in PBS for 1.5h at 37°C. The obtained dissociated tissue was subsequently washed and resuspended in Neurobasal A medium (Thermo Fisher Scientific Inc) supplemented with 1% N2 (Thermo Fisher Scientific Inc), 10 ng/ml epidermal growth factor (EGF) and basic fibroblast growth factor (both from Immunotools), 100 U/ml penicillin and 100 µg/ml streptomycin. The cell suspension was then rinsed through a 70 µm cell strainer and transferred to an uncoated culture flask to allow neurosphere formation and removal of unwanted, plastic adherent cells. The neurospheres were allowed to grow for 4-5 days at 37°C in a humidified atmosphere containing 5% CO_2 and the growth factors were replenished every other day. Afterwards, the floating neurospheres were collected, centrifuged at 200g for 6 min and dissociated with Accutase (Sigma-Aldrich) for 5 min. Subsequently, the obtained NSCs were seeded at 2.5 x 10^4 cells/cm² on a 5µg/ml fibronectin (R&D Systems, Minneapolis, MN, USA) coated surface in Neurobasal A medium supplemented with 2% B27 without vitamin A (Thermo Fisher Scientific Inc), 10 ng/ml EGF and bFGF, 2mM L-glutamine, 100 U/ml penicillin and 100 µg/ml streptomycin which will be referred to as standard NSC medium. The culture medium was changed every 3 to 4 days and cells were subcultured when 70- 80% confluence was reached. To passage the cells, NSCs were harvested by incubation with Accutase for 5 min (37°C) and centrifuged for 5 min at 300g. For immunocytochemical analysis, the NSCs were seeded at 2 x 10^4 cells/cm^2 on 5µg/ml fibronectin coated glass coverslips or on coated Thermanox® plastic coverslips for TEM processing. Immunophenotyping of NSCs was performed for the markers described in Reekmans et al. [309].

5.3.7 Immunocytochemistry

NSCs or pCNs seeded on glass coverslips were fixed in 4% PFA and immunostainings were performed according to a standardized protocol for immunofluorescence microscopy as described in the previous chapters [92, 105]. Cells were incubated for 1h with the primary antibodies listed in Table 5.1 and incubated for 30 min with the appropriate secondary antibody. Negative controls were included, omitting the primary antibody.

Table 5.1: Primary and secondary antibodies for immunocytochemical analysis. MM: Mouse Monoclonal antibody; RP: Rabbit Polyclonal antibody; GP: goat polyclonal DAM: Donkey anti-mouse; DAR: Donkey anti-rabbit; DAG: Donkey anti-goat; DP= Donkey Polyclonal

Marker	Species	Clone, Cat nr.	Dilution	Label	Company
Primary Antibodies					
A2B5	MM	MAB312R	1/200		Millipore Billerica, MA, USA
BLBP	RP	ABN14	1/250		Millipore
ß-III tubulin	RP	ab18207	1/50		Abcam, Cambridge, UK
ß-III tubulin	MM	2G10	1/2000		Sigma-Aldrich, St-Louis, MO, USA
CD45	RP	Ab63390	1/100		Abcam
GFAP	MM	Clone G-A-5	1/400		Sigma-Aldrich,
NCAM	RP	Ab5032	1/100		Millipore
NeuN	MM	A60, MAB377	1/100		Millipore
Sca-1	GP	AF1226	1/50		R&D, Minneapolis, MN, USA
Sox2	RP	Ab97959	1/1000		Abcam
Secondary Antibodies					
DAM	DP IgG	A31570	1/500	Alexa Fluor 555	Invitrogen, Carlsbad, CA, USA
DAR	DP IgG	A21206	1/500	Alexa Fluor 488	Invitrogen
DAG	DP IgG	A11055	1/500	Alexa Fluor 488	Invitrogen

5.3.8 Transmission electron microscopy

NSCs seeded on plastic coverslips for TEM analysis were prepared and processed as described previously [92] and in Chapter 2-4.

5.3.9 Transwell migration assay

Tissue culture inserts (ThinCert™, 8 µm pore size, Greiner Bio-One) were seeded with NSCs (5 x 10^4 cells/insert) in Neurobasal-A medium containing 0.2% B27 without Vit A, 2mM L-glutamine, 10ng/ml bFGF and EGF, 100 U/ml penicillin and 100 µg/ml streptomycin. The bottom, chemoattractant, compartment of the well plate contained either CM-hDPSCs or prCM-hDPSCs (n=4) to which 0.2% B27 without Vit A and 10ng/ml EGF and bFGF was freshly added. In addition to evaluating the migration-promoting effect of hDPSCs and prCM-hDPSC, the effect of EX/CM L-PRF (n=4) in various concentrations (0.1%, 1%, 2%, 5%) was also assessed. As a negative (non-promoting) control, Neurobasal-A medium containing 0.2% B27 without Vit A, 2mM L-glutamine, 10ng/ml bFGF and EGF, 100 U/ml penicillin and 100 µg/ml streptomycin was added. The same medium containing 2% B27 without Vitamin A, 10 ng/ml EGF and bFGF and 100 ng/ml SDF-1 (Immunotools) was used as a positive control. After 24h, the transmigrated cells were fixed with 4% PFA and stained with 0.1% crystal violet. Two representative micrographs were taken per insert and migration was quantified with AxioVision software (Carl Zeiss, Aalen, Germany).

5.3.10 Metabolic activity and proliferation of CM-hDPSCs, prCM-hDPSCs and CM/EX L-PRF-exposed NSCs

The metabolic activity and proliferative activity of NSCs exposed to CM-hDPSCs, prCM-hDPSCs (n=6) or 0.1, 1%, 2% and 5% CM/EX L-PRF (n=5) were evaluated by means of a MTT and PI assay respectively. NSCs were seeded in 96 well plates at a density of 1.5 x 10^4 cells/ cm² in standard NSC medium. After 24h, the cells were exposed to the experimental conditions and both assays were performed 24h, 48h and 72h later as described earlier in this chapter in section 5.2.3. To all experimental conditions, 0.2% B27 without Vitamin A and 10 ng/ml EGF and bFGF was added. As internal controls, NSCs were exposed to standard NSC medium with 0.2% B27 without Vitamin A instead of 2% and standard NSC medium with 20 ng/ml of EGF and bFGF to serve as a negative and positive control respectively. After collecting data, all data were normalized to NSCs exposed to standard NSC medium with 0.2% B27 without Vitamin A after 24h exposure.

5.3.11 Isolation of primary cortical neurons

Primary cortical neurons were isolated from fetal mouse brains by an adapted protocol, based on [310]. Briefly, at gestational days 17-18, pregnant C57BL/6JOlaHsd mice (Envigo) were sacrificed by cervical dislocation and the fetuses were removed from the abdomen as approved by the ethical commission of Hasselt University (protocol number 201410K). Subsequently, the brains were removed and put into preheated Hank's balanced salt solution (HBSS; Thermo Fisher Scientific Inc) supplemented with 7 mM 4-(2-hydroxyethyl)-1-piperazineethanesulfonic acid (HEPES; Thermo Fisher Scientific Inc) and 100 U/ml penicillin and 100 µg/ml streptomycin. Afterwards, the meninges were carefully removed with forceps under a Leica S6E stereomicroscope (Leica microsystems, Wetzlar, Germany) and the cortex was dissected clear from the hippocampus, thalamus and the striatum. The obtained cortices were collected in HBSS/HEPES and incubated with 0.05% trypsin for 15 min at 37°C. The cortices were then washed three times with minimum essential medium (MEM; Thermo Fisher Scientific Inc) supplemented with 10% horse serum (Thermo Fisher Scientific Inc), 0.6% glucose, 100 U/ml penicillin and 100 µg/ml streptomycin and were mechanically dissociated by pipetting up and down for about 30 times with a glass Pasteur pipet with decreasing diameter. The acquired cell suspension was centrifuged for 8 min at 300g. Then, the cells were resuspended in supplemented MEM medium and rinsed through a 70 µM cell strainer (Thermo Fisher Scientific Inc) to obtain a single cell suspension. Neurons were seeded at varying densities in culture plates or on coverslips previously coated with 20 µg/ml poly-d-lysine (Corning; Corning, NY, USA). After the neurons attached to the coated surface of the plates the medium was changed to Neurobasal medium (Thermo Fisher Scientific Inc) supplemented with 2 mM L-glutamine, 2% B27 with Vitamin A (Thermo Fisher Scientific Inc), 100 U/ml penicillin and 100 µg/ml streptomycin (referred to as standard pCN medium). Neurons were cultured for up to two weeks, without medium change (37°C, 5% CO_2).

5.3.12 Oxygen-glucose deprivation assay

An OGD assay was performed to evaluate the neuroprotective effect of CM-hDPSCs, prCM-hDPSCs and CM/EX L-PRF. The OGD assay mimics the ischemia

and subsequent reperfusion damage which is typical for stroke. Briefly, pCNs were seeded at a density of 6 x 10^4 cells/cm^2 in black 96-well plates with a translucent bottom (Greiner Bio-one) and cultured in standard pCN medium for five days to allow neuronal maturation. Consequently, the cells were exposed to OGD. Therefore, the medium was removed and OGD was initiated by incubating the cells in DMEM without glucose (Invitrogen) and placed inside an incubator with 0.3% O_2 for 6h. After exposure to OGD, the cells were washed with PBS and incubated for 24h at 2.3% O_2 with standard pCN medium, CM-hDPSCs, prCM-hDPSCs (n=7) and CM/EX L-PRF (n=6) in various concentrations (0.1%, 1% and 5%) to determine their protective effect post-OGD. A schematic overview of the OGD assay is provided in Fig. 5.2. Cell viability was determined with the PI assay as described previously. To gain insight in cellular survival, cells were subjected to the PI assay prior to OGD (T0), after 6h OGD (T1) and 24h after restoring nutrient and oxygen supply (T2).

Figure 5.2: Experimental setup of the OGD survival assay. The pCN culture is exposed to OGD for 6h (T0 to T1). After OGD the pCNs are exposed to the experimental conditions for 24h. Cell viability is measured at the starting point (T0), after 6h OGD (T1) to measure OGD-induced cell death and 24h after OGD (T2) to evaluate the post-OGD neuroprotective effect of the experimental treatments.

5.3.13 Neuritogenesis assay

After freshly isolated pCNs (2.5 x 10^4 cells / cm²) adhered to the glass coverslips, the plating medium that was previously described, was changed to CM-hDPSCs, prCM-hDPSCs (n=5) or CM/EX L-PRF (n=3) in various concentration to which 2% B27 with Vitamin A was freshly added before adding it to the cells. In parallel, pCNs were also kept in culture in standard pCN medium as controls. After 72h, the pCNs were fixed with 4 % PFA and an immunocytochemical staining was performed for ß-III tubulin. Subsequently, the mean length of the longest neurite on each neurite-bearing cell that was positively stained was calculated with Fiji software [311] with the NeuronJ plugin

[312]. For each sample, at least 50 neurites were counted and only clearly distinguishable neurites were measured. For prCM-hDPSCs, the average neurite length was calculated of primed CM of 5 different hDPSC donors, primed with 3 different L-PRF donors. Simultaneously, the fraction of ß-III tubulin positive cells was evaluated to determine the neuronal purity of the obtained pCN culture.

5.3.14 Statistical analysis

Statistical analysis was performed using Graphpad Prism 5 software (Graphpad, San Diego, CA, USA) (Appendix). Normality was checked with the Shapiro-Wilk test. Normal distributed data were tested with one way ANOVA and Bonferroni's multiple comparison post-test. Non-parametric data were analysed with the Kruskal-Wallis test followed by a Dunn's test. Differences were considered statistically significant at p-values ≤ 0.05. Data were expressed as mean ± standard error of the mean (S.E.M).

5.4 Results

5.4.1 CM and EX L-PRF had an inverse effect on hDPSC metabolism whereas both stimulated hDPSC proliferation

In order to evaluate the influence of CM- and EX L-PRF on hDPSC metabolism and proliferation, an MTT and PI test was performed 24h, 48h and 72h after exposure (Fig. 5.3). Remarkably, the CM L-PRF had an inverse effect on hDPSC metabolism (Fig 5.3A) and hDPSC proliferation (Fig. 5.3B) where higher concentrations of CM L-PRF (5% and 10%) significantly decreased hDPSC metabolism at all time points down to 51.25%- 65.05% of the Alpha-MEM + 0% FBS values measured after 24h (p-values * ≤ 0.05; ** ≤ 0.01 and *** ≤ 0.001), while 10% CM L-PRF significantly stimulated (p-value ≤ 0.01) hDPSC proliferation up to 2.5-fold after 72h. Next EX L-PRF was subjected to the same analysis and it appeared that low concentrations of EX L-PRF (1%, 2% and 5%) significantly decreased hDPSC metabolism down to 60.87% ± 9.538 after 24h (p-value ≤ 0.001), but this effect was diminished 48h and 72h later where only 1% EX L-PRF significantly decreased hDPSC metabolism (p-value * ≤ 0.05; ** ≤ 0.01) (Fig. 5.3C). The highest concentration of EX L-PRF that was used (10%) significantly increased (p-value ≤ 0.05) metabolism after 72h 1.43-fold. On the

other hand, when cell numbers were evaluated with PI, no decrease in cell numbers could be observed. While no effect was observed after 24h, 5% and 10% EX L-PRF significantly enhanced hDPSC proliferation (p-value * ≤ 0.05; ** ≤ 0.01) after 48h and 72h but in all tested concentrations a stimulating trend was observed (Fig. 5.3D). 10% EX L-PRF increased hDPSC proliferation 3.7-fold, while the positive control, Alpha-MEM + 10% FBS increased hDPSCs number 2.7-fold. All data were normalized to the values corresponding to hDPSCs exposed to Alpha-MEM with 0% FBS after 24h.
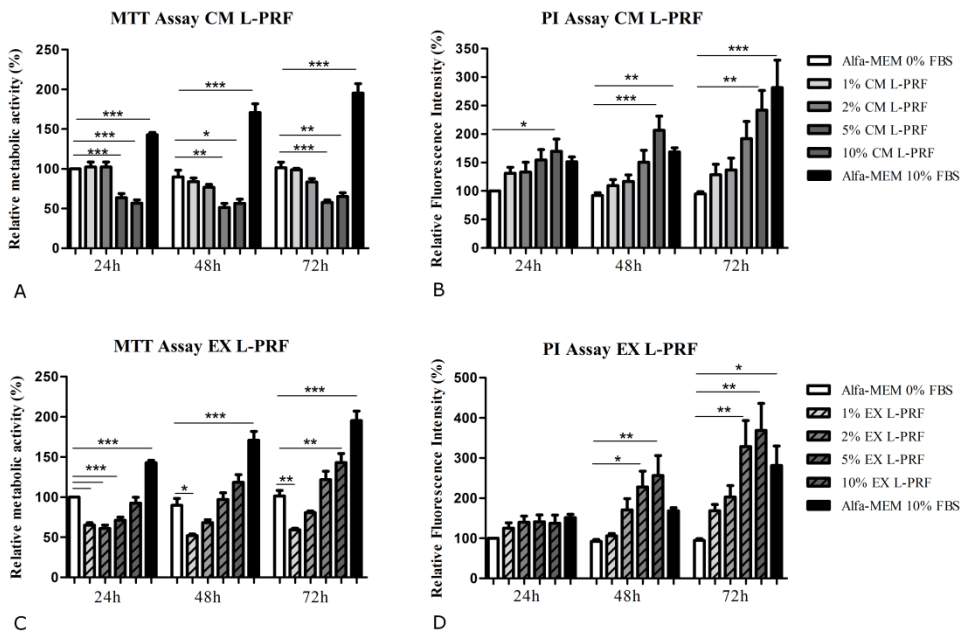
Figure 5.3: Metabolic and proliferative activity of hDPSCs exposed to CM and EX L-PRF. The metabolic (A, C) and proliferative (B, D) effect of hDPSCs that were exposed for 24h, 48h and72h to CM (A, B) or EX (C, D) L-PRF was evaluated by means of an MTT and PI assay respectively (n=5). CM and EX L-PRF had an inverse effect on hDPSC metabolism as high concentrations of CM significantly diminished, and high concentrations of EX L-PRF significantly stimulated hDPSC metabolism. Both CM as EX L-PRF had a dose-response effect on proliferation as higher concentrations significantly enhanced hDPSC proliferation. *; **; ***: p-value ≤ 0.05; 0.01 and 0.001 respectively. Data are expressed as mean ± S.E.M.

This effect of L-PRF on metabolic activity of hDPSCs was additionally investigated by estimating the relative metabolic activity per cell, as shown by the ratio of relative metabolic activity and relative cell numbers (Fig. 5.4). 5% and 10% CM L-PRF significantly decreased (p-values * ≤ 0.05; ** ≤ 0.01 and *** ≤ 0.001) the relative metabolic activity per cell on all time points to less than 50% of the Alpha-MEM + 0% FBS values measured after 24h (Fig. 5.4A). EX L-PRF significantly decreased the relative metabolic activity per cell on all time points (p-values * ≤ 0.05; ** ≤ 0.01) with all the tested EX L-PRF concentrations to ± 50% of the Alpha-MEM + 0% FBS values measured after 24h, except for 10% EX L-PRF, which did not significantly alter the relative metabolic activity per cell after 24h exposure (Fig. 5.4B). Also for this concentration of 10% EX L-PRF, the relative metabolic activity per cell decreased significantly after 48h and 72h (p-value * ≤ 0.05). Moreover, the presented data suggest that the decrease in metabolic activity that is observed, is an effect of CM and EX L-PRF on hDPSC-metabolism, as no effect of the L-PRF subfractions on cell death was observed in the PI assay.
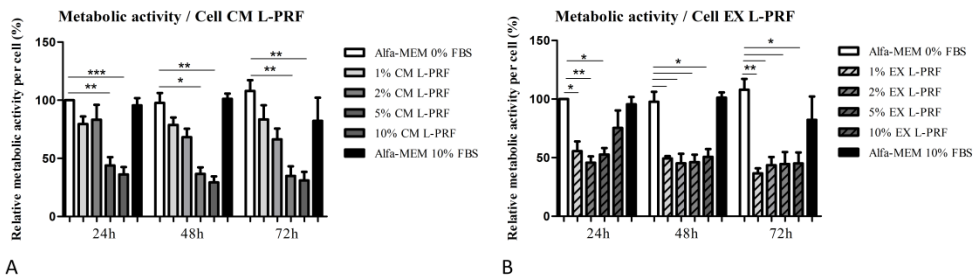
Figure 5.4: Relative metabolic activity per cell of hDPSCs exposed to CM/EX L-PRF. 5% and 10% CM L-PRF significantly decreased the relative metabolic activity per cell on all time points (A). EX L-PRF significantly decreased the relative metabolic activity per cell on all time points with all the tested EX L-PRF concentrations, except for 10% EX L-PRF, which did not significantly alter the relative metabolic activity per cell after 24h exposure. *; **; ***: p-value ≤ 0.05; 0.01 and 0.001 respectively. Data are expressed as mean ± S.E.M.

5.4.2 Priming of hDPSCs with CM and EX L-PRF For different time periods altered their BDNF secretion although with high variation

The CM of hDPSCs primed with various concentrations of CM and EX L-PRF for 24 or 48h was collected and subjected to an ELISA for BDNF as a measure for neurotrophin production (Fig. 5.5A). 24h priming with 10% CM L-PRF (p-value ≤ 0.01) and 5% and 10% EX L-PRF (p-values ≤ 0.05) significantly enhanced BDNF production from 0.1 ng/ml ± 0.15 ng/ml to maximum 0.64 ng/ml ± 0.39 ng/ml per 1×10^5 hDPSCs compared to non-primed (hDPSCs exposed to alpha-MEM with 0% FBS). A significant increase in BDNF production after 48h priming could only observed when hDPSCs were primed with 10% CM or EX L-PRF (p-value ≤ 0.05), increasing the BDNF concentration from 0.19 ng/ml ± 0.12 ng/ml to 0.54 ng/ml ± 0.59 ng/ml per 100.000 hDPSCs compared. Due to the negative effect of 5% and 10% CM L-PRF on hDPSC metabolism after 24h and 48h (vide supra), subsequent priming experiments were performed with hDPSCs primed with 10% EX L-PRF for 48h. In addition to the BDNF ELISA performed for primed hDPSCs, the BDNF content of EX (Fig. 5.5B) and CM collected at different incubation times (Fig. 5.5C) was evaluated. The EX L-PRF contained approximately 10 ng/ml BDNF while this concentration increased almost 20-fold in the CM L-PRF. No significant difference in BDNF concentration could be observed in CM L-PRF collected after 48h, 96h or 144h incubation.
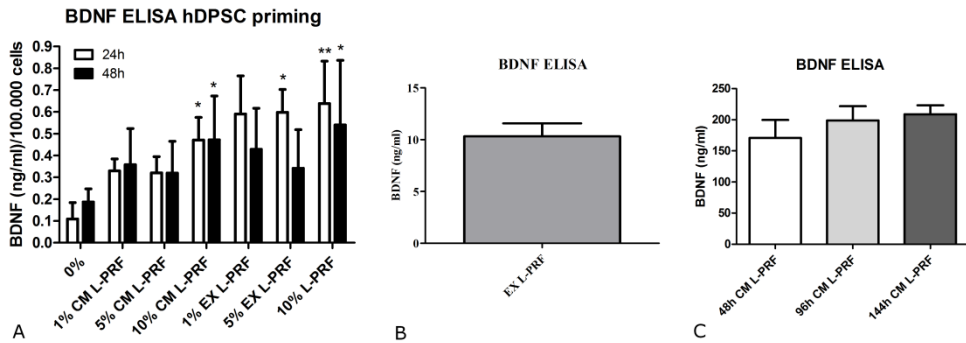
Figure 5.5: ELISA for BDNF production in hDPSCs primed with CM and EX L-PRF and BDNF present in EX and CM L-PRF. BDNF secretion was increased in hDPSCs primed (n=4) with 10% CM L-PRF or 5% and 10% EX L-PRF for 24h while significant BDNF secretion could only be observed when hDPSCs were primed for48h with 10% CM or EX L-PRF (A). The BDNF concentration in EX L-PRF (n=8) (B) is increased almost 20-fold in CM L-PRF, where the BDNF concentration did not increase with increasing incubation times prior to harvesting the CM L-PRF (n=3) (C). *; **: p-value ≤ 0.05 and 0.01. Data are expressed as mean ± S.E.M.

5.4.3 Morphological and immunocytological characteristics of NSCs

Mouse NSCs were isolated from fetal brains and cultured as neurospheres (Fig. 5.6A). During this neurosphere culturing phase, unwanted cell types (e.g. fibroblasts, endothelial cells etc.) were negatively selected. Next, neurospheres were dissociated and the single-cell suspension was transferred to fibronectin-coated flasks to allow adherent cell culture (Fig. 5.6B). NSCs present as cells with a large perikaryon with peripheral halo and typically acquired a bipolar or multipolar morphology with intercellular extensions. Ultrastructurally, these cells are characterised by a large nucleus with prominent nucleolus (Fig. 5.6C) and the cytoplasm contains several multivesicular bodies (MVBs) (Fig. 5.6D, insert). NSCs derived from different fetuses were cultured separately and were considered as distinct cell lines. NSCs (n=6) were subsequently immunophenotyped (Fig. 5.7) and showed reactivity for the NSC markers Sox2, neural cell adhesion molecule (NCAM), brain lipid-binding protein (BLBP), glial fibrillary acidic protein (GFAP) and A2B5 (Fig. 5.7A-E). Negative controls show no immunoreactivity (Fig. 5.7A, insert). It should be noted that 50% of the

obtained NSC lines did not express GFAP. The obtained NSCs did not express markers of a more mature neuronal phenotype such as ß-III Tubulin and neuronal nuclei (NeuN) (Fig. 5.7F, G) and did not express the hematopoietic marker CD45 and the mesenchymal marker Stem cells antigen-1 (Sca-1) (Fig. 5.7H, I). One representative NSC line was used in the subsequent experiments.
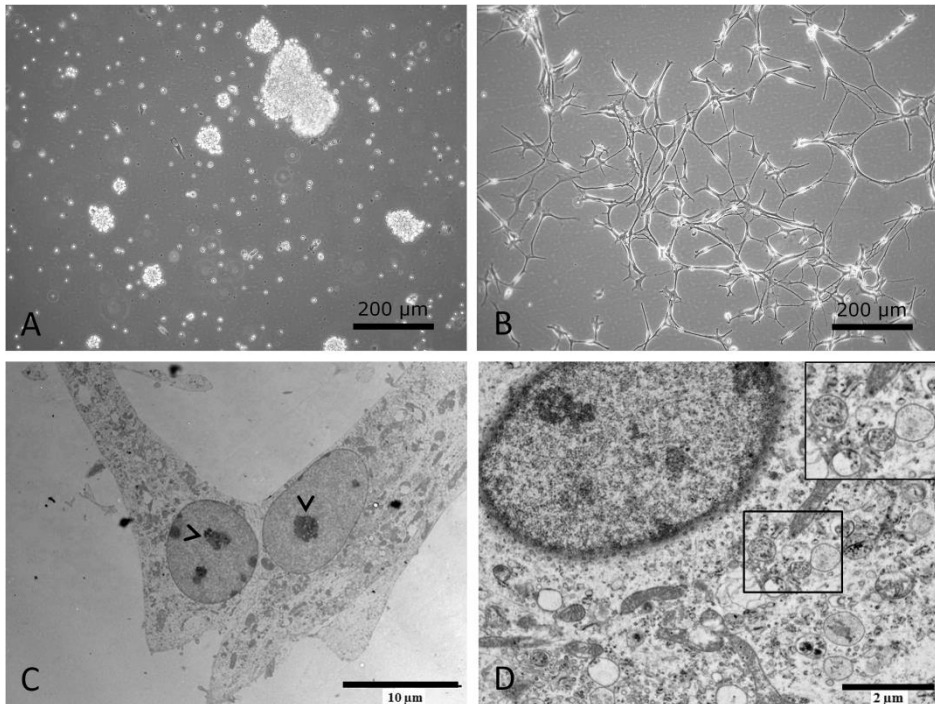
Figure 5.6: Morphological and ultrastructural features of NSCs. NSCs were initially cultured as neurospheres (A) which, after dissociation, formed an adherent cell culture characterised by a large perikaryon and intercellular extensions (B). Utrastructurally, NSCs were characterised by a large nucleolus (C) and by a cytoplasm rich in MVBs (D). Scale bars A, B: 200µm; C: 10µm; D: 2µm.
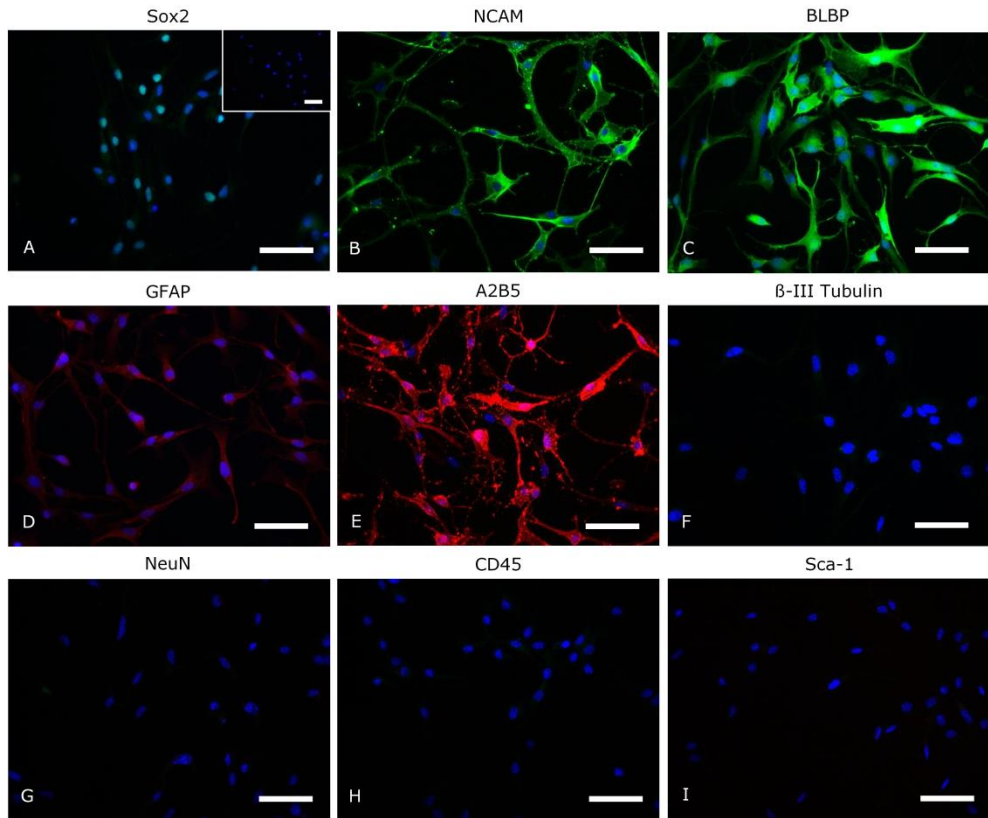
Figure 5.7: Immunophenotype of NSCs. NSCs showed immunoreactivity for the NSC markers Sox2 (A), NCAM (B), BLBP (C), GFAP (D) and A2B5 (E). NSCs did not show immune reactivity for late neuronal markers ß-III tubulin (F) and NeuN (G), or for the hematopoietic marker CD45 (H) and the mesenchymal marker Sca-1 (I). Images show representative micrographs of NSCs isolated from 6 different fetuses. Scale bars A-I: 50 µm.

5.4.4 NSC proliferation and metabolic activity were not stimulated by CM-hDPSCs, prCM-hDPSCs, CM L-PRF and EX L-PRF

The stimulating effect of CM-hDPSCs and prCM-hDPSCs on NSC metabolism and proliferation was evaluated by means of an MTT and PI assay respectively (n=6). CM-hDPSCs significantly stimulated NSC metabolism after 24h exposure (p-value ≤ 0.01) and although there appears to be a metabolism-stimulating effect after 48h, this was not significant (Fig. 5.8A) and the trend disappeared

after 72h exposure. Similarly, CM-hDPSCs and prCM-hDPSCs were not able to stimulate NSC proliferation (Fig. 5.8B). No significant difference between CM-hDPSCs and prCM-hDPSCs could be observed in either assay. To confirm these results, the influence of CM-hDPSC or prCM-hDPSC on relative metabolic activity per cell, as estimated by the ratio of the relative values of the MTT- and PI-assay, was determined. No significant influence of CM-hDPSC or prCM-hDPSC was observed (data not shown).
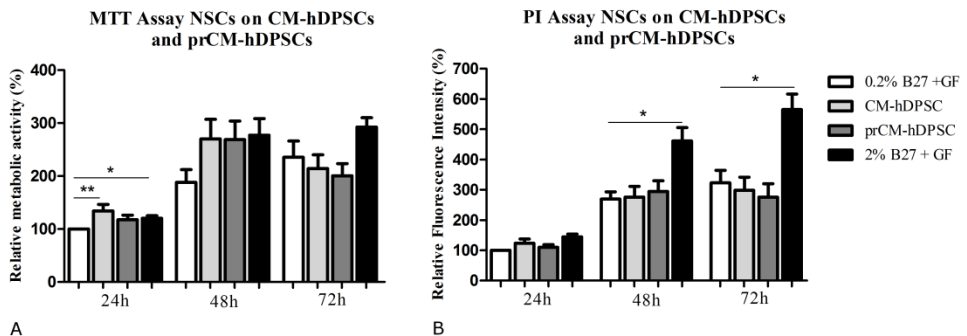
Figure 5.8: The influence of CM-hDPSCs and prCM-hDPSCs on NSC metabolism and proliferation. CM-hDPSCs and prCM-hDPSCs (n=6) did not significantly influence NSC metabolism (A) or proliferation (B) after 24h, 48h and 72h although CM-hDPSCs significantly stimulates NSC metabolism after 24h. No significant difference could be observed between CM-hDPSCs and prCM-hDPSCs. *; **: p-value ≤ 0.05 and 0.01 respectively. Data are expressed as mean ± S.E.M.

In addition, the potential of CM and EX L-PRF (n=5) to influence NSC metabolism and proliferation was also evaluated. Similar to CM-hDPSCs and prCM-hDPSCs, CM L-PRF did not have a significant effect on NSC metabolism (Fig. 5.9A) or proliferation (Fig. 5.9B) although a trend appears to be present that tends to decrease NSC metabolism with higher concentrations of CM L-PRF. Interestingly, 2% and 5% CM L-PRF significantly decreased the relative metabolic activity per cell after 24h exposure, but this effect was abolished after 48h and 72h. These data indicate that CM L-PRF does not influence cell numbers or the relative metabolic activity per cell.

EX L-PRF on the other hand, had detrimental effects on NSC metabolism (Fig. 5.9C) and proliferation (Fig. 5.9D) with increasing concentrations. After 24h, 5% EX L-PRF decreased the fraction of NSCs to 24.24% of the controls exposed to 0.2% B27 without Vitamin A and growth factors (10ng/ml EGF and bFGF). After 72h, this fraction recovers to 33.43% but is still drastically decreased. Similarly, the relative metabolic activity that was measured by the MTT assay decreases significantly to 26.73% of the control value after 24h incubation with 5% EX L-PRF and remains decreased at 40.81% of the control value after 72h. Only concentrations of EX L-PRF as low as 0.1% did not have a significant negative effect over the different time points. Remarkably, 0.1% and 1% EX L-PRF significantly decreased the relative metabolic activity per cell after 24h exposure, but this effect was eliminated after 48h and 72h. At 48h and 72h exposure to the EX L-PRF concentrations, no effect on relative metabolic activity per cell was observed. These data indicate that EX L-PRF has a detrimental effect on NSC numbers, and not on NSC metabolism (data not shown). All data were normalized to the values corresponding to NSCs exposed to Neurobasal-A with 0.2% B27 without Vitamin A and 10 ng/ml bFGF and EGF.
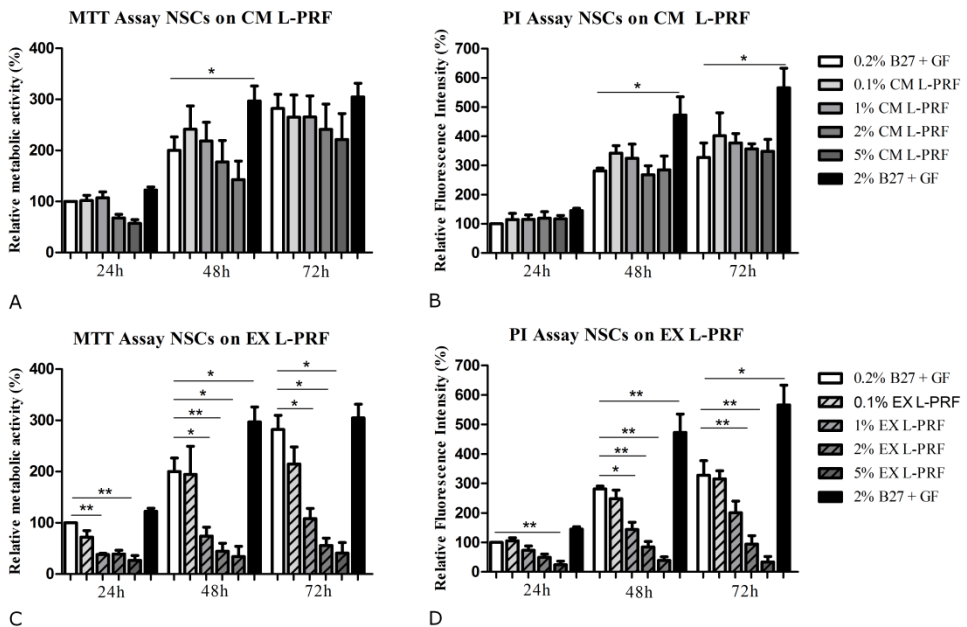
Figure 5.9: The influence of L-PRF-derived CM and EX on NSC metabolism and proliferation. CM L-PRF (n=5) did not have a significant effect on NSC metabolism (A) or proliferation (B) over the 72h testing period. EX L-PRF (n=5) on the other hand, significantly decreased NSC metabolism (C) and proliferation (D) with a dose-response effect. Only concentrations as low as 0.1% EX L-PRF had no significant effect on NSC metabolism or proliferation. *; **: p-value ≤ 0.05 and 0.01 respectively. Data are expressed as mean ± S.E.M.

5.4.5 The hDPSC-secretome and CM L-PRF act as a chemoattractant on NSCs

The chemoattractant properties of primed- and non-primed hDPSCs (n=4) was evaluated by means of a transwell migration assay. In addition, the chemoattractant potential of CM and EX L-PRF as an autologous biomaterial was similarly evaluated (Fig. 5.10). Both CM-hDPSCs and prCM-hDPSCs significantly attracted NSCs after 24h incubation (p-value * ≤ 0.05) (Fig. 5.10A). Moreover, no significant difference could be observed between CM-hDPSCs, prCM-hDPSCs and the positive control consisting of 2% B27 without Vitamin A, 10 ng/ml EGF and bFGF and 100 ng/ml SDF-1. No significant difference was detected between CM-hDPSCs and prCM-hDPSCs. CM L-PRF (n=4) was only able to significantly stimulate NSC migration when 2% CM L-PRF was used with no significant difference between 2% CM L-PRF and the positive control (Fig. 5.10B). EX L-PRF did not have a significant effect on NSC migration (n=4).

Transwell Migration Assay

A   B
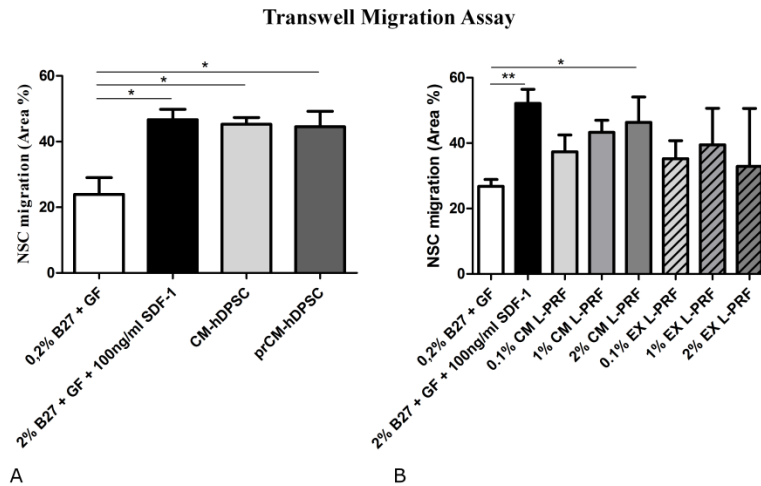
Figure 5.10: The chemoattractant properties of CM-hDPSCs, prCM-hDPSCs and L-PRF-derived CM and EX. Both CM-hDPSCs and prCM-hDPSCs (n=4) attract NSCs but priming did not have an additional effect (A). 2% CM L-PRF (n=4) significantly stimulated NSC migration (B). EX L-PRF (n=4) mediated NSC migration could not be observed. *; **: p-value ≤ 0.05 and 0.01 respectively. Data are expressed as mean ± S.E.M

5.4.6 CM-hDPSC but not prCM-hDPSC and low CM L-PRF concentration protect pCNs against OGD-induced neuronal death

In order to evaluate the neuroprotective effect of hDPSCs and of the soluble factors contained within L-PRF, pCNs were exposed to an OGD assay (Fig. 5.11). pCN survival was quantified by using the PI assay at baseline (=pre-OGD), immediately after OGD (=Post-OGD) and 24h after OGD. OGD led to a significant decrease in cell numbers during the OGD period after which only 47.24% ± 22.85% of pCNs survived (pre- vs post OGD). Moreover, cell death increased significantly to 26.5% ± 10.4%of the pre-OGD value over the 24h after OGD when pCNs were maintained in standard culture conditions (post-OGD vs pCN medium). Immediately after OGD, the experimental conditions were added to the cells and 24h survival was quantified with the PI assay as a measure for cell numbers. CM-hDPSCs, but not prCM-hDPSCs (n=7) significantly protects pCNs against OGD-induced cell death compared to controls on standard pCN medium (Fig. 5.11A) as 42.58 ± 17.87% of the pCNs survive 24h after the

OGD period when exposed to CM-hDPSC. The lowest concentration of CM L-PRF (0.1%) was able to protect pCNs against OGD-induced cell death (44.47% ± 15.84% survival) but higher concentrations of CM L-PRF and all concentrations of EX L-PRF were not able to exert a neuroprotective effect (Fig. 5.11B). All data were normalized to average PI values corresponding to Pre-OGD.

pCN Survival
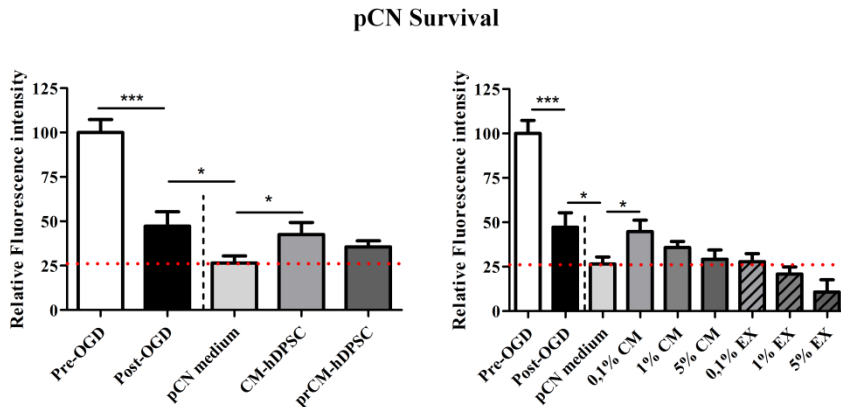
Figure 5.11: CM/EX L-PRF and CM-hDPSC/prCM-hDPSC mediated neuroprotection of primary cortical neurons after oxygen and glucose deprivation. CM-hDPSCs (n=7) significantly protected pCNs against neuronal death 24h after OGD but this effect could not be observed in L-PRF-primed hDPSCs (A). The lowest CM L-PRF concentration (n=5) showed a neuroprotective effect on pCNs, but this effect could not be determined in other concentrations of CM L-PRF or EX L-PRF. The red dashed line represents the fraction of pCNs that survives after OGD and 24h after OGD. The black dashed line demarcates where the experimental conditions were added to the pCNs. *; ***: p-value ≤ 0.05 and 0.001 respectively. Data are expressed as mean ± S.E.M

5.4.7 CM-hDPSCs but not prCM-hDPSCs promotes pCN neurite outgrowth whereas CM and EX L-PRF have a detrimental effect on pCNs

In addition to investigating the paracrine-mediated neuroprotective effect of primed and non-primed hDPSCs, their effect on pCN neurite outgrowth was evaluated (Fig. 5.12). CM-hDPSCs, but not prCM-hDPSCs (n=5) was able to stimulate neurite outgrowth in pCNs after 72h (Fig. 5.12A), increasing neurite outgrowth from 72.15 μm ± 10.35 μm in controls to 111.7 μm ± 13.78 μm after

CM-hDPSC-exposure. Moreover, the fraction of ß-III tubulin-positive cells (control: 92.56% ± 1.99%) was not significantly altered by adding CM-hDPSCS or prCM-hDPSCs to these cultures, maintaining the neuronal content of the culture (Fig. 5.12B). Additionally, to evaluate neuronal survival over the 72h period, the amount of pyknotic ß-III tubulin-positive cells was also evaluated. CM-hDPSCS or prCM-hDPSCs did not have an effect on pCN cell death (Fig. 5.12C). Representative micrographs of the control, CM-hDPSC stimulated and prCM-hDPSC exposed pCNs are presented in Fig. 5.12D-F respectively.
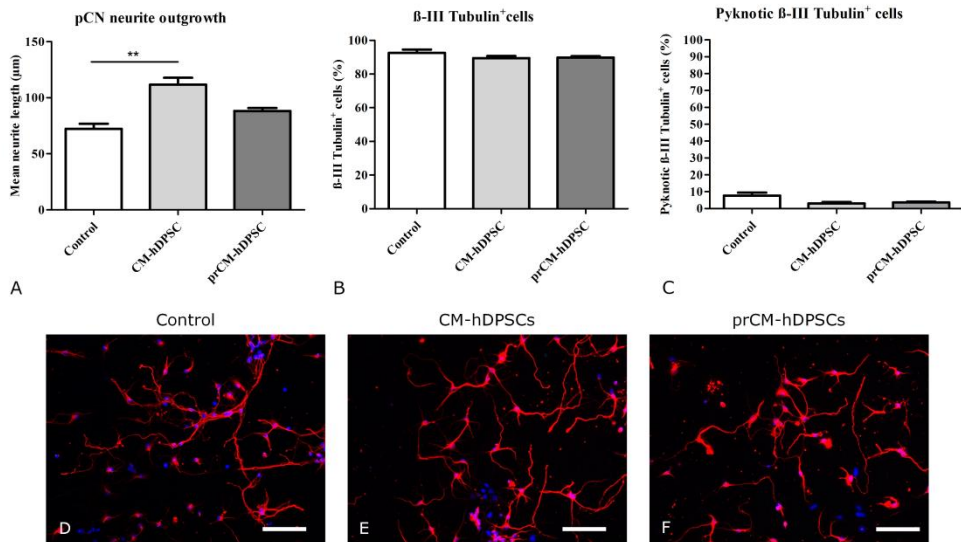
Figure 5.12: Neurite outgrowth and neuronal purity after pCN exposure to CM-hDPSCs and prCM-hDPSCs. CM-hDPSC, but not prCM-hDPSC (n=5) was able to stimulate neurite outgrowth in pCNs compared to controls (A). Exposure to CM-hDPSC or prCM-hDPSC did not have an influence on the neuronal content of the cell cultures (B) or neuronal death (C) 72h after exposure. Representative micrographs of ß-III tubulin stained pCNs after exposure to control medium (D), CM-hDPSCs (E) and prCM-hDPSCs (F). **: p-value ≤ 0.01. Data are expressed as mean ± S.E.M. Scale bars D-F: 50µm.

Similar to the assessment of neurite outgrowth and neuronal survival of pCNs exposed to CM-hDPSCs and prCM-hDPSCs, the influence of CM and EX L-PRF (n=3) on these parameters was evaluated (Fig. 5.13). None of the tested concentrations of CM and EX L-PRF was able to stimulate neurite outgrowth of

pCNs compared to controls (Fig. 5.13A). Moreover, with increasing concentrations of CM L-PRF, a significant decrease to 29.67% ± 5.69 % in the fraction of ß-III tubulin positive cells was observed when pCNs were exposed to 5% CM L-PRF for 72h (Fig. 5.13B). No significant effect in the fraction of ß-III tubulin positive cells was observed in pCNs exposed to 0.1%, 1% or 5% EX L-PRF, but higher concentrations of EX L-PRF increased the fraction of pyknotic ß-III tubulin positive cells in the culture (Fig. 5.13C). Due to the pyknotic appearance and deviating morphology of pCNs exposed to 1% and 5% EX L-PRF, quantification of mean neurite length was performed for these conditions. Representative images of pCNs on standard medium, 0.1%, 1%, 2% and 5% CM L-PRF and 0.1%, 1% and 5% EX L-PRF are presented in Fig. 5.13D-K respectively.
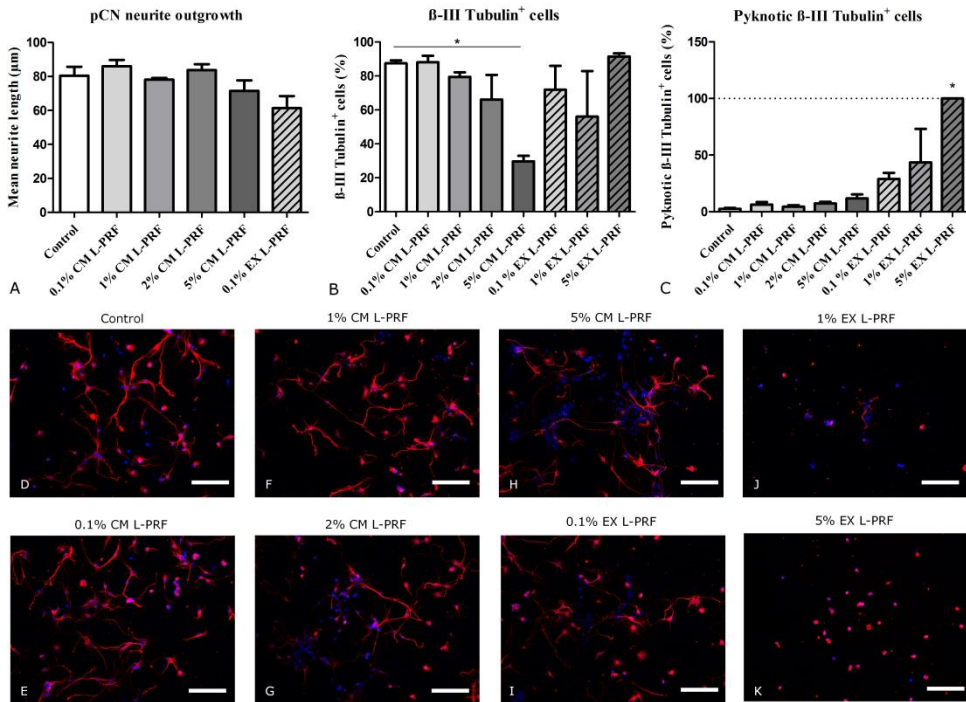
Figure 5.13: Neurite outgrowth and neuronal purity after pCN exposure to CM- and EX L-PRF. CM L-PRF and EX L-PRF (n=3) did not enhance neurite outgrowth in pCNs compared to controls (A). Exposure to 5% CM-L-PRF significantly decreased the number of ß-III tubulin positive cells in the neuronal culture (B). EX L-PRF did not significantly alter the fraction of ß-III tubulin positive cells in the culture, but had a dose-responsive effect on the fraction of pyknotic ß-III tubulin reactive cells in the culture (C). Representative micrographs of ß-III tubulin stained pCNs after exposure to control medium (D), 0.1% CM L-PRF (E), 1% CM L-PRF (F), 2% CM L-PRF (G), 5% CM L-PRF (H), 0.1% EX L-PRF (I), 1% EX L-PRF (J) and 5% EX L-PRF (K). *: p-value ≤ 0.05. Data are expressed as mean ± S.E.M. Scale bars D-F: 50µm.

5.5 Discussion

Plausible mechanisms of action of (mesenchymal) stem cell-mediated neuronal repair after stroke include paracrine-induced chemoattraction and proliferation of endogenous NSCs in addition to protecting damaged neurons against neuronal cell death and stimulating the formation of new neuronal connections. This chapter built further on Chapter 4, but instead of using SH-SY5Y cells to

study paracrine-mediated neuroregenerative mechanisms of hDPSCs, this chapter focused on using *in vitro* expanded and characterised NSCs and primary cortical neurons as an alternative to the SH-SY5Y cell line described earlier. In addition, this study aimed to invigorate the neuroregenerative potential of the hDPSC secretome by preconditioning or 'priming' the cells with L-PRF. This clinically applicable autologous biomaterial, that can also be seen as an inflammatory microenvironment in a dish, was hypothesized to enhance the growth factor secretion pattern of hDPSCs. The inflammatory cytokines present in the tissue resemble the hostile microenvironment of CNS disorders, such as stroke, where hDPSCs can be used as a potential therapy. Finally, L-PRF is being applied clinically [295, 296] although the underlying mechanisms of action of L-PRF-mediated healing are mostly unknown but are attributed to the growth factors contained in the biomaterial. Therefore, the different growth factor-containing fractions of L-PRF were isolated and used in the same assays that assessed the neuroregenerative potential of primed and non-primed hDPSCs.

In the first phase, the effect of L-PRF on hDPSCs was evaluated. It was shown that the CM and EX L-PRF had an inverse effect on hDPSC metabolism. High concentrations of CM L-PRF significantly decreased hDPSCs metabolism which was increased by high concentrations of EX L-PRF. Both subfractions of the L-PRF secretome stimulated hDPSC proliferation, which can be explained by the platelet-derived components that are present in CM and EX L-PRF. Platelet lysates are often used as serum replacement in cell culture [313-315] and as the concentration of platelet components is expected to be higher in EX L-PRF than in CM L-PRF this can explain for the larger effect of EX L-PRF on hDPSC proliferation than CM L-PRF. Moreover, the presented data suggest that the observed decrease in metabolic activity is truly an effect of CM and EX L-PRF on hDPSC-metabolism, as no effect of the L-PRF subfractions on cell death was observed in the PI assay. This statement should however be interpreted with caution as the significant increase in cell numbers, as determined by the PI assay, can also lead to overconfluency in the well-plate. This will lead to cellular contact inhibition, thereby reducing cellular metabolism, as read out by the MTT assay [316]. A reason for the discrepancy in metabolic activity is unknown. This discrepancy can be attributed to patient variability in L-PRF donor fractions, although previous reports that focus on patient variability in L-PRF potency or

content are scarce and are limited to the growth factor secretion pattern and the donor blood composition [317]. On the other hand, it is known that patient variability in DPSC donors exists, depending on age and the stem cell microenvironment [318, 319] and this can potentially have an effect on the hDPSC response to L-PRF exposure. Moreover, it can be postulated that the high fraction of leukocyte-derived factors in the CM L-PRF which were secreted over time by the L-PRF membrane, has a different composition than the factors in EX L-PRF which can be hypothesized to mainly contain factors secreted by the blood platelets that are activated during the L-PRF isolation process. However, since the composition and difference of both CM and EX L-PRF are mostly unknown, no clear statement on factors that are responsible for this effect can be made. Nonetheless, candidate factors might include those components that influence mitochondrial function such as leukocyte-derived myeloperoxidases [320], TNF-α [297] and IL-1ß [167] which lead to reactive oxygen species (ROS) production [321]. The MTT assay on which the metabolic evaluation of hDPSCs after CM and EX L-PRF exposure is based on, is based on an enzymatic conversion that takes place in the mitochondria. Therefore, CM L-PRF-derived stimulants of intracellular ROS production can influence the readout of the MTT. Consequently, it is advised to exclude this CM L-PRF effect by checking cellular ROS production with for example 2',7' –dichlorofluorescin diacetate based assays [322]. Although the morphology of the CM and EX L-PRF exposed cells did not differ from unstimulated hDPSCs (data not shown), the effect on mitochondrial health needs to be checked with TEM to exclude a possible negative effect of L-PRF components on mitochondrial morphology. Moreover, as it was previously shown by Alongi et al. that inflammation can influence the stem cell properties of hDPSCs and decreases their mineralisation potential, the effect of L-PRF subfractions on the stem cell properties of hDPSCs should be investigated [323]. Next, hDPSCs were primed with different concentrations of CM and EX L-PRF and BDNF secretion was taken as a measure for increased neurotrophin production. Priming hDPSCs for 24h or 48h with 10% CM or EX L-PRF significantly enhanced BDNF production by hDPSCs. However, due to the negative effect of CM L-PRF on hDPSC metabolism, 10% EX L-PRF was subsequently used to prime hDPSCs. Moreover, it was shown that CM and EX L-PRF contained a high concentration of BDNF and this concentration was 20-fold higher in CM as in EX L-PRF,

supporting the potential use of L-PRF as a biocompatible material for neurodegenerative disorders.

The proliferative and chemoattractant properties of CM-hDPSCs and prCM-hDPSCs or CM and EX L-PRF on NSCs were evaluated next. The NSCs that were used in this study showed the immunophenotype for the markers described in Reekmans et al. [309]. In accordance with the secretome studies of CM-hDPSCs on SH-SY5Y cells described in Chapter 4, CM-hDPSCs did not influence NSC proliferation or metabolic activity and priming hDPSCs with L-PRF did not alter this response. CM L-PRF also did not have an effect on NSC metabolism and/or proliferation. EX L-PRF on the other, had a detrimental effect on both NSC metabolism and proliferation. It can be postulated that EX L-PRF is a blood-derived biomaterial with a different composition than CM L-PRF that is added to NSCs that are not protected by a blood-brain barrier (BBB). As one of the functions of the BBB is to regulate molecular traffic and keep out neurotoxins to preserve neuronal survival and maintain neuronal connectivity [324], its absence exposes NSCs to potential neurotoxins in the EX L-PRF. For example, the EX L-PRF is expected to contain components from activated platelets that are not bound to the fibrin matrix. One of the factors secreted by activated platelets is glutamate [325]. Glutamate has previously been shown to promote excitotoxic neuronal death and is the central mediator in stroke-induced neuronal death (see Chapter 1) [12, 326]. Although no quantification of L-PRF-derived glutamate was performed, this glutamate signalling may be responsible for the NSC death that is observed in this study. Moreover, this mechanism can also be responsible for the dose-response increase in the fraction of pyknotic pCNs that was observed when pCNs were exposed to EX L-PRF. Other known factors that are present in L-PRF which influence NSC or pCN survival or function include IL 1ß [327, 328], and TNF-α [328-330]. These factors were shown to have pleiotropic effects as they were also able to stimulate NSC proliferation, depending on the activated pathways [331] and pCN survival [332]. On the other hand, the results described in this chapter did not show beneficial effects of the L-PRF fractions on NSC proliferation, as was expected by the presence of TGF-ß, IL-6, IGF-1, VEGF and PDGF [256, 305-307]. The relative contribution of these factors within CM L-PRF and EX L-PRF need to be determined and selective blocking experiments for NSC-damaging inflammatory mediators will provide

additional insight into the growth- and repair-promoting factors that are present in the L-PRF fractions. In addition to the influence on NSC metabolism and proliferation, CM-hDPSCs prCM-hDPSCs and the L-PRF-derived fractions were used to evaluate their chemoattractant properties on NSCs in a transwell assay. CM-hDPSCs significantly promoted NSC migration but this ability was not improved by L-PRF priming. Similarly, CM L-PRF was also able to stimulate NSC migration, but not EX L-PRF, presumably due to their negative effect on NSCs. Only 2% CM L-PRF was able to stimulate NSC chemoattraction. Higher concentrations of CM L-PRF were not evaluated due to the negative trend that was observed in NSC metabolism when these cells were exposed to concentrations of CM L-PRF ≥ 5%. Factors secreted by hDPSCs that can be responsible for this chemoattractant effect on NSCs include monocyte chemotactic protein-1 (MCP-1) [108, 333], Il-8 [108, 334] and SDF-1 [75, 335] although directed blocking experiments are required to verify this statement. The composition of CM L-PRF is mainly unidentified but it was shown that chemokines that attract neural precursor cells such as insulin-like growth factor-1 and IL-1ß [167, 336, 337] are present in L-PRF.

Finally, the neuroprotective and neuritogenic potential of L-PRF and the secretome of primed and non-primed hDPSCs on pCNs were evaluated as these are key aims for therapies targeting CNS regeneration. It was demonstrated that CM-hDPSCs, but not prCM-hDPSCs was able to protect pCNs from OGD-induced cell death. These results are in line with the studies by Kong et al. [338] who used human BMSCs and Scheibe et al. [69] who used human and murine BMSCs and showed the neuroprotective effect of these cells in an indirect co-culture system or of their conditioned medium on OGD-exposed pCNs. This neuroprotective effect was shown to be mediated by the inhibition of the programmed cell-death mechanisms parthanatos, necroptosis and apoptosis by Kong et al. [338]. Whether similar mechanisms are responsible for hDPSC-mediated attenuation of OGD-induced cell death remains to be elucidated but as hDPSCs have a similar secretome as BMSCs [68] it can be hypothesized that resembling mechanisms are responsible for the observed effect. In addition to protecting neurons, it was shown previously that hDPSCs and CM-hDPSCs protect ischemic human astrocytes in an OGD assay by mediating ROS production and by producing inflammatory mediators [339]. Moreover, this

neuroprotective effect of hDPSCs and CM-hDPSCs on ischemic human astrocytes was superior to commercial human BMSCs and their secretome [339]. When the neuroprotective effect of CM and EX L-PRF was evaluated, only the lowest concentration of CM L-PRF (0.1%) was able to protect pCNs against OGD-induced cell death. One of the factors present in the (CM) L-PRF that can be responsible for this neuroprotective effect is TGF-ß1 which was previously shown to protect against neuronal cell death [167, 340, 341]. In addition to protecting pCNs against OGD-induced cell death, CM-hDPSCs but not prCM-hDPSCs was able to promote neuritogenesis in pCNs compared to controls in standard pCN medium. Moreover, both conditioned media did not significantly influence the purity of the neuronal culture or the number of pyknotic cells, excluding cytotoxic effects of the conditioned media or the stimulation of proliferation of ß-III tubulin negative cells in the neuronal culture. The factors responsible in the CM-hDPSCs for enhanced neurite outgrowth include the factors working via tyrosine receptor kinases (Trk) which were described in Chapter 4. These include but are not limited to nerve growth factor, neurotrophin-3, BDNF, glial-derived growth factor and VEGF [68, 105, 287]. CM and EX L-PRF did not enhance neurite outgrowth despite the presence of BDNF in these L-PRF fractions. On the contrary, CM L-PRF had a dose-response decrease in the fraction of ß-III tubulin positive cells, while EX L-PRF induced pCN death as demonstrated by the increase in pyknotic ß-III tubulin positive cells in these cultures.

The results in this chapter support the paracrine mediated stimulation of neuroregenerative mechanisms of hDPSCs on NSCs and pCNs. In line with Chapter 4, no effect was seen on proliferation of NSCs but migration and neurite outgrowth of NSCs and pCNs was demonstrated respectively. In addition, CM-hDPSCs was shown to protect pCNs against OGD-induced cell death. It should be noted that in this study, paracrine-mediated neuronal differentiation and maturation is not reported. A similar approach to differentiate NSCs in multiple steps, comparable with the protocol described in Chapter 4, was used to differentiate NSCs exposed to CM-hDPSCs and prCM-hDPSCs. This protocol was based on Spiliotopoulos et al. [342] which over a period of 21 days increases BDNF signalling while decreasing EGF signalling in embryonic stem cell-derived neural stem cells. However, upon exposure to CM-hDPSCs or prCM-hDPSCs, NSCs did not acquire characteristics of mature neurons (data not shown)

implicating that differentiation process of NSCs can be inherently different than the process described in SH-SY5Y cells as described in Chapter 4. Despite the efforts that were made to enhance the secretome of hDPSCs by L-PRF priming that was used as an inflammatory tissue in a dish, only enhanced secretion of BDNF was determined. No additional effect on neuroregenerative mechanism was observed by priming hDPSCs with L-PRF. On the contrary, priming hDPSCs decreased their neuroprotective and neuritogenic effect, although not significantly. It can be postulated that L-PRF priming alters the hDPSC-secretome to a less favourable composition for neuroregeneration. As the concentration of other growth factors than BDNF was not determined, no additional information on the effect of L-PRF on the hDPSC secretome is available. Future studies should focus on other factors such as VEGF secretion and other mechanisms associated with wound healing such as angiogenesis. However, caution is advised when applying pro-angiogenic therapies in CNS disorders such as ischemic stroke and spinal cord injury due to the increased risk of secondary ischemia-reperfusion damage [11, 12, 343]. For example VEGF worsens stroke outcome by increasing BBB-leakage and ischemia-reperfusion damage [344-347] in the acute stroke phase whereas VEGF is generally considered to promote recovery following stroke when applied at later time points [256, 347]. The extent of CNS recovery due to angiogenesis is therefore not only dependent on restoration of the blood flow but also on repairing BBB or blood-spinal barrier integrity and the establishment of functional blood vessels to prevent leakage of CNS-damaging (macro)molecules [347-349]. Based on these studies and results from this chapter, these barriers need to be adequately restored for revascularisation to have a beneficial effect in CNS regeneration to rule out the influence of the damaging blood components on neuronal survival.

Clinically, it is very important to note that positive effects of L-PRF on neural cells were only observed with the conditioned medium of L-PRF and that the EX fraction of L-PRF had devastating effects on NSCs and pCNs. Moreover, only low concentrations of CM L-PRF had a positive effect on NSC migration and pCN protection. Therefore, it can be postulated that the inflammatory mediators with detrimental effects on neuronal survival such as TNF-α and IL 1ß exert their neurotoxic effect in higher concentration ranges of CM L-PRF. This could mask the potential beneficial effect of repair-promoting mediators, although the exact

composition of CM L-PRF and EX L-PRF remains to be determined and is crucial in understanding L-PRF-mediated effects after transplantation [328]. It should be stressed that concentrations this low will be highly unlikely in an *in vivo* setting should L-PRF be used near central nervous system (CNS) structures. For example, L-PRF has been used for treating skull base defects in the vicinity of the BBB [350]. Although no adverse effects were observed in this study, caution using L-PRF this close to the CNS is advised as cerebrospinal fluid leakage in this kind of defects is often seen and is an indication of BBB disruption which can lead to L-PRF secretome leakage into the CNS. Although caution is advised in using L-PRF in the vicinity of the CNS, the effect of L-PRF on the peripheral nervous system (PNS) is unknown. The PNS is not limited by a BBB, therefore it can be postulated that L-PRF-derived factors have a different effect on the PNS neuronal components although its effect still needs to be elucidated. For example, in contrast to CNS glutamate excitotoxicity, glutamate stimulates intracellular signalling and migration of Schwann cells in a rat nerve-crush injury model [351] although dorsal root ganglia remain susceptible to glutamate-induced excitotoxicity [352]. Encouraging results for PNS nerve regeneration come from studies using platelet rich fibrin (without leukocytes) and platelet rich plasma on a rat sciatic nerve injury model although no improvement was observed in the histomorphometric analysis [353]. L-PRF was used in a split-mouth study for the healing of postextraction sockets. It was shown that post-operative pain was attenuated, but no data are available on nerve regeneration in this clinical study [296]. In order to justify the use of L-PRF clinically for enhanced wound healing, additional preclinical research is mandatory, as its effect on different tissues is largely unknown and an autologous biomaterial might even bioincompatible depending on the application [354].

Conclusion

The present study primarily aimed to investigate the paracrine-mediated neuroregenerative potential of hDPSCs on NSCs proliferation and migration and on protecting pCNs against OGD-induced cell death and pCN neurite outgrowth. Moreover, the effect of preconditioning hDPSCs L-PRF - an autologous biomaterial that can be seen as inflammatory tissue in a dish - which was hypothesized to potentialise the neuroregenerative potential of the hDPSC

secretome was investigated. In addition, the effect of the biomaterial itself on hDPSCs, NSC, pCNs and neuroregenerative mechanisms was investigated. The results in this study demonstrated that the CM of hDPSCs had a neuroprotective effect on OGD-exposed pCNs and was capable to enhance neuritogenesis in pCN. Moreover, this conditioned medium had a chemoattractant effect on NSCs but did not stimulate NSC proliferation. Unfortunately, although priming hDPSCs increased the secretion of the growth factor BDNF, no additional effect on the paracrine mediated mechanisms of regeneration described in this study were observed. Furthermore, the soluble factors present in L-PRF itself had detrimental effects on NSCs and pCNs in higher conditions and only low concentrations of the conditioned medium of L-PRF stimulated NSC migration or was able to protect pCNs from ischemic death. These data suggest that L-PRF is a bioincompatible biomaterial on CNS-derived cells and caution is advised when applying this biomaterial in the vicinity of CNS tissue.

Chapter 6 : Optimization of the transient Middle Cerebral Artery Occlusion mouse stroke model – *in vivo* Pilot study of intravenous delivered human dental pulp stem cells

6.1 Abstract

Stroke is a major cause of death in the developed world and leaves a large fraction of surviving patients with a permanent handicap. Despite numerous efforts that report preclinical beneficial effects of experimental drugs and new surgical interventions, little success has been observed in clinical trials making thrombolytic agents the primary treatment option. Stem cell-based therapies emerged as a potential new treatment but it is essential that these studies take into account the multiple mechanisms underlying stroke pathology. Despite the ease of use of taking a reduction in lesion size as an indication of functional improvement, stroke-related behavioural impairments after stroke depend heavily on the affected brain region and extent of damage. In order to adequately assess functional improvement stimulated by transplanted stem cells or other therapies, the selection of individual tests that can distinguish characteristic stroke deficiencies are essential for the success of translational therapy. In addition to the need of a representative set of behavioural tests to evaluate post-stroke and stem cell-stimulated functional recovery, it is also essential to monitor the fate of the transplanted cells and the endogenous healing response over time as this allows temporospatial follow-up of the stem cell fate, behavioural changes and the endogenous response.

This chapter aimed to optimize the widely used transient middle cerebral artery occlusion (tMCAO) stroke model and to establish easy-to-use behavioural tests that allow follow-up of stroke mice up to one month. Moreover, a pilot study was conducted in which the neuroregenerative potential of intravenously delivered human dental pulp stem cells (hDPSCs) was evaluated, using the optimized behavioural tests and non-invasive magnetic resonance imaging (MRI) to determine changes in lesion volume. In addition, the stem cell fate was tracked with bioluminescence imaging (BLI). The results in this study indicate that 60 min occlusion of the middle cerebral artery is the optimal occlusion time. This provides a therapeutic window in which therapeutics can exert their effect on behavioural function up to one month after stroke induction. Suitable behavioural tests included the modified neurological severity score, the rotarod, corner- and cylinder test. The results from the *in vivo* pilot indicated unsuccessful induction of tMCAO in the experimental cohort and loss of signal

from the transplanted cells within 72 hours after transplantation. Therefore, no effect of the hDPSC-transplantation on stroke outcome could be evaluated. Despite these results, the tMCAO model was established in our lab, accompanied by a set of applicable behavioural tests. Future studies should focus on establishing standard operation procedures and early lesion verification to obtain standardized stroke lesions with reproducible deficits for this model to be implemented in translational stroke research in our lab.

6.2 Introduction

Stroke causes a high socioeconomic burden in the developed world and has a major impact on the quality of life for surviving stroke patients who end up with permanent disabilities [3, 355] . Current available therapies can only be applied within the first 4.5 hours after stroke onset stressing the need for a therapy for this devastating disease that can be applied in a broader time window [29]. However, despite numerous efforts that report preclinical beneficial effects of experimental drugs and new surgical interventions, little success has been observed in clinical trials making thrombolytic agents the primary treatment option, as discussed in Chapter 1 [356]. Therefore, stem cell-based therapies have emerged as a potential treatment for ischemic stroke. Whereas the ideal candidates for stroke would be *ex vivo* expanded and manipulated neural stem cells (NSCs) or neural precursor cells (NPCs), there are ethical considerations with regard to the isolation of NSCs from embryonic or fetal tissue together with isolation and culturing complications of adult NSCs [52, 53], stressing the need for an alternative stem cell source that can be used as a therapy in ischemic stroke.

A promising cell source to promote neuroregeneration are a subtype of mesenchymal stem cells (MSC), human dental pulp stem cells (hDPSCs) [85, 92], as discussed in previous chapters. These cells have shown to stimulate neuroplasticity and angiogenesis, show immunomodulatory and neuroprotective effects and have been postulated to replace the lost cells after transplantation in damaged central nervous system (CNS) regions, although these mechanisms are mainly mediated by the influence of the paracrine factors secreted by the stem cells on the endogenous microenvironment [41, 56, 207, 208, 277]. However, one of the explanations for apparent failure of bench-to-bedside translation of potential therapies that showed great preclinical potential, is that several preclinical studies focus on post-mortem histological analysis of lesion size to evaluate the therapeutic effect without looking into other mechanisms underlying the stroke pathology [12, 356, 357]. Although lesion size was shown - and remains to be - a good predictor of motor- and sensorimotor impairment in stroke mice [358-360], other studies tone down this statement [361] as cognitive impairments were observed independent of lesion size. Nonetheless,

the level of behavioural impairments after stroke depend on the affected brain region and extent of damage. Therefore, to adequately assess functional improvement stimulated by the transplanted stem cells, the selection of proper individual tests is essential for the success of translational research. These tests need to be able to detect the different deficiencies after stroke, but should also be able to provide an effect range in between potential treatments can ameliorate functional behaviour over time.

In addition to the need of a representative set of behavioural tests to evaluate post-stroke and stem cell-stimulated functional recovery, it is also essential to monitor the fate of the transplanted cells over time. One of the major issues in determining the fate of the transplanted cells and determining the exact onset of functional recovery, is that most studies described in Table 1.1 and 1.2 in Chapter 1 used traditional histopathological techniques to determine the fate of the transplanted cells and to visualize possible methods of action of the transplanted cells. Therefore, it is necessary to non-invasively and temporospatially track the transplanted cells.

The first phase of this study will focus on the optimization of the proximal filament transient middle cerebral artery occlusion (tMCAO) model [362] as it most closely resembles the *in vivo* situation. This endovascular tMCAO model allows for a controlled transient occlusion time of the middle cerebral artery and is chosen over the distal tMCAO model as it avoids intracranial operative procedures [363-365]. Moreover, it circumvents the use of chemicals such as endothelin-1 and photothrombotic stroke which do not resemble the *in vivo* situation [65, 365]. Therefore, filament occlusion will be performed for 30, 45 and 60 min after which the stroke lesion will be verified. Additionally, the modified neurological severity score (mNSS) [366], rotarod [358], cylinder test [367] and open field test [368] will be used to evaluate the applicability of these tests to evaluate 1-week post-stroke recovery after 30, 45 and 60 min tMCAO.

The second phase of this study will use the acquired information to subject mice to the optimal tMCAO time and evaluate the use of these behavioural tests for follow-up to one month. Moreover, the corner test [369] is introduced in this part of the study. In the final part of this study, hDPSCs will be intravenously (I.V.) delivered 24h after stroke onset in mice subjected to the tMCAO time

determined in the first phase of this study. These cells will be transduced to express firefly luciferase (*fluc*) and will monitored with bioluminescence imaging (BLI) to track the stem cell fate *in vivo* [370, 371]. Lesion size will be monitored over time to verify induction of the stroke lesion and to evaluate the effect of the hDPSC transplantation on lesion size.

Finally, the optimal behavioural tests as determined in the second phase will be used to assess functional improvements following stem cell transplantation. By combining these results, the stem cell fate, reduction in lesion size and behavioural changes can all be monitored concomitantly without the need of *ex vivo* analysis. After the study, the fate of the stem cells is determined with immunohistochemistry in the lung, spleen, liver and brain of the animals to confirm the results from the BLI measurements.

This study aims to optimize the frequently used tMCAO model in our lab in parallel with establishing representative and user-friendly behavioural tests that are able to distinguish between general motor- and sensorimotor dysfunction in healthy controls and stroke mice. The *in vivo* pilot study hopes to combine

6.3 Materials and Methods

6.3.1 Isolation and culture of hDPSCs

Human dental pulp tissue was obtained from patients aged 19 and 26 (n=2) undergoing routine extraction of third molars for orthodontic reasons at the Department of Maxillofacial Surgery, Ziekenhuis Oost-Limburg (ZOL), Genk, Belgium or at the Campus St-Barbara of the ZOL located in Lanaken, Belgium. Dental pulp tissues were obtained with informed consent of the patient or after approval of the legal guardian. This study was approved by the Medical Ethical Committee of Hasselt University (13/0104u). Subsequently, hDPSCs were isolated and cultured as described previously [92, 95]. The pilot experiment was conducted with hDPSCs in passage 8. Two days prior to transplantation, hDPSCs were transduced with a lentiviral vector encoding triple flag-tagged firefly luciferase (*fluc*) driven by the EF1a promoter (*fluc*-hDPSCs) for subsequent BLI and histology.

6.3.2 Transient middle cerebral artery occlusion and intravenous transplantation of hDPSCs

C57/bl6 mice (n=29) of 8 weeks old (Janvier Labs, Le Genest-Saint-Isle, France) were subjected to tMCAO as described previously [362] and as approved by the ethical committee of Hasselt University (protocol number 201428A1V1). Briefly, Mice were anesthetized with 2% isoflurane, fixed into position and an eye ointment (Terramycine + Polymyxine B, Pfizer, NY, USA) was applied to the eyes to prevent dehydration. Next a longitudinal cervical midline incision was made under an operating microscope. Subcutaneous tissue was blunt dissected and the salivary glands were separated similarly. Subsequently, self-retaining retractors were placed behind the left salivary gland and behind the sternocleidomastoid muscle. During this phase, 0.05mg/kg atropine (Sterop, Brussels, Belgium) was injected intraperitoneally to decrease mucus production and 1% xylocaine (AstraZeneca, Brussels, Belgium) was applied as a local analgesic. A self-retaining retractor was applied behind the oesophagus with low tension and the common carotid artery (CCA) was blunt dissected from the vagal nerve and the internal jugular vein. Next the CCA was ligated as caudal as possible and the bifurcation of the internal carotid artery (ICA) and external carotid artery (ECA) was exposed. The ECA was lightly occluded and a vascular clip was applied as cranial to the bifurcation as possible. A second loose ligation was made caudal to the vascular clip and a hemi section of the CCA between the first ligation and the vascular clip was made. Next, a 7-0 silicone-tipped monofilament (7019PK5Re; Doccol, Sharon, MA, USA) was inserted in the hemisected CCA and advanced towards the vascular clip. At this point, the second CCA ligation is tightened around the filament to prevent backflow as the vascular clip is removed. The filament is subsequently advanced into the ICA to occlude the MCA (Fig. 6.1). Care is taken not to occlude the posterior communicating artery (PCA). The filament was kept in place for 30 or 45 min while the animals remained under anaesthesia, or for 60 mins during which the wound was sutured and the animals were allowed to recover. After 60 min MCAO, the animals were anaesthetised, sutures were removed and the filament was retracted. After the surgery the wound was sutured and animals were allowed to recover in a heat cage. During surgery, mouse temperature is maintained by keeping the mice on a heat pad. Postoperatively, 0.015 mg/kg

buprenorphine (Vetergesic) and 0,5ml 5% glucose in NaCl are administered intraperitoneally. After the study period, the mice are euthanized by an overdose of 100 mg/kg pentobarbital (Nembutal®, Ceva, Libourne, France) and depending on the application, transcardially perfused with 4% paraformaldehyde (PFA). All mice were kept in a temperature-controlled room (20°C ± 3°C) with a 12 h day-night cycle and food and water were available *ad libitum*.
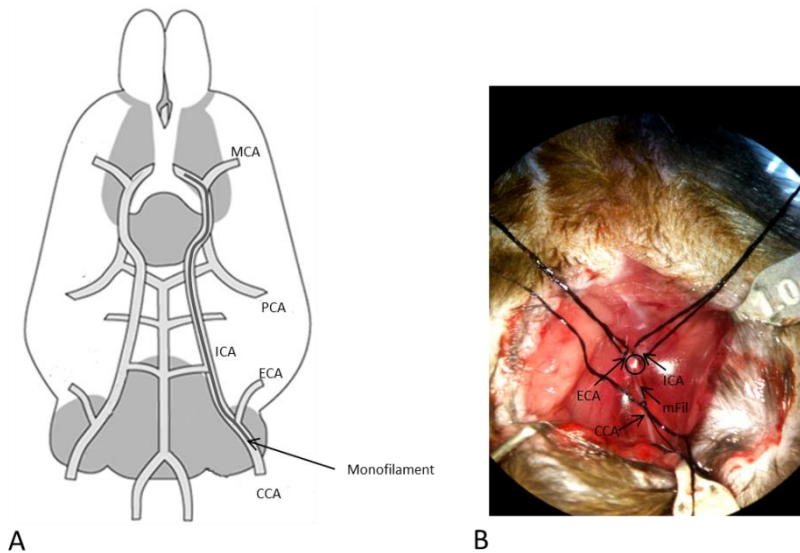
Figure 6.1: Schematic ventral overview of the tMCAO procedure. A silicon-coated monofilament is inserted in the left common carotid artery (CCA) and propagated along the internal carotid artery (ICA) towards the origin of the middle cerebral artery (MCA). The external carotid artery (ECA) is ligated and care is taken not to occlude the posterior communicating artery (PCA) (A). A detailed image of the filament being kept in place by a ligation on the CCA while inserted in the CCA is shown in (B). The silicon coating can be observed at the bifurcation of the ICA and the ECA (encircled). The filament will be subsequently advanced in the ICA to occlude the MCA. (A) Adapted from O'Neill and Clemens, 2001 [372]. (B) Original image is courtesy of dr. Tom Struys.

These studies were approved by the Ethical Committee of Hasselt University (201428A1V1) and were performed according to the guidelines described on the protection of animals used for scientific purposes at Hasselt University (EU Directives 2010/63). tMCAO was performed in 3 cohort studies. Cohort 1:

optimization of the tMCAO time and behavioural tests. 30 min (n=3), 45 min (n=3) and 60 min (n=3) MCAO was performed. One sham animal was included in this first cohort. Cohort 2:1 month follow up of 60 min tMCAO (n=4) compared to sham-operated animals (n=3) and assessment of behavioural test applicability. Cohort 3: *in vivo* pilot of intravenous hDPSC transplantation. Sham operated (n=3), untreated tMCAO controls (n=3) and tMCAO mice receiving *fluc*-hDPSCs from two donors (n= 3 per hDPSC donor) were monitored for two weeks to evaluate post-stroke recovery and stem cell fate.

6.3.3 Verification of stroke lesion: TTC staining and *in vivo* magnetic resonance imaging

To verify the lesion induced by 30, 45 and 60 min tMCAO, mouse brains were isolated, cut into 500 µm coronal sections with a vibratome (Leica, Wetzlar, Germany) and stained with 2% TTC (Triphenyl tetrazolium chloride, Sigma-Aldrich, St. Louis, MO, USA) for 30 min at 37°C. Afterwards, the stained slices were fixed with 4% PFA for 24h and images were acquired with a digital camera. In addition to the TTC staining, stroke lesions were verified with MRI after 60min tMCAO. Axial T2*-weighted images (RARE sequence, repetition time: 2500 ms; echo time 40 ms; rare factor: 8) were made with a Biospec 70/30 USR 7 Tesla small animal MR scanner (Bruker; Billerica, MA, USA) equipped with corresponding Topspin 3.1 (Bruker) and Paravision 6.0.1 software (Bruker). Prior to scanning, mice were anesthetized with 2% isoflurane. Temperature and respiration were monitored and controlled for throughout the experiment.

6.3.4 Behavioural tests after tMCAO

To optimize the transient MCA occlusion time, different behavioural tests were applied to mice subjected to 30, 45 or 60 min tMCAO in order to determine behavioural tests that provide an effect window and that can be used for both short-term (1 week) and midlong-term (4 weeks) follow up. As a general measure for neurological dysfunction, the mNSS was used. This test contains both sensory, motor and sensorimotor components and was described previously by Chen et al. [366]. Next, mice were put on a rotarod [358] which accelerated from 5 to 60 rpm over 5 min. Mice were tested twice non-consecutively on each experimental time point. All mice were trained for 3

consecutive days, with 2 trials each day, prior to stroke. The results of the final training day were taken as a baseline measure for the rotarod.

Another test that was used is the corner test. In this test, described by Zhang et al. [369], mice are allowed to walk into a corner of 30° degrees between non-translucent plastic walls separated by a 5mm opening. In the corner, mice turn left or right, depending on sensorimotor input or laterality of the mouse. Baseline values were measured to take into account any residual left- or right preference of the tested mice. On each testing day, 10 turns in 2 non-consecutive trials were counted.

The cylinder test [367] measures spatial and motor behaviour. The mouse is placed in a transparent plastic cylinder (9 cm diameter, 30 cm height) and actively starts to explore vertical areas by rearing and exploring the environment with their vibrissae and forelimbs. The number of separate paw placements observed for the left- and right forelimb, and both forelimbs were recorded. Mice with unilateral brain damage will then show asymmetric forelimb placing. Baseline measurements were taken for each mouse and all mice were observed for 2 non-consecutive trials for 3 min or until 25 touches were recorded. Cylinder touches were interpreted and counted as described by Li et al. [367]. Finally, an open field test was used to evaluate spontaneous locomotion behaviour in stroke mice [368]. Mice were placed in a 50 cm x 50 cm field and their movement was recorder with a digital camera. EthoVision XT software (Noldus, Wageningen, The Netherlands) was used to track the movement of the mice and the total distance covered and average velocity were evaluated.

6.3.5 Intravenous transplantation and *in vivo* tracking of *fluc*-hDPSCs

In a pilot experiment, I.V. injection of *fluc*-hDPSCs (n=2 different donors) was performed 24h after 60 min tMCAO. 2.5×10^5 *fluc*-hDPSCs were injected in the tail vein in a total volume of 250 µl (n=3 mice per *fluc*-hDPSC donor). In addition to the mice transplanted with fluc-hDPSCs, sham operated (n=3) and untreated tMCAO (n=3) mice receiving 250µl PBS were included as controls. 24h and 3 days post-injection, the fate of the transplanted cells was monitored with BLI. Mice were injected I.V. with 126 mg/kg body weight luciferin-D^{TM} (Promega,

Madison, WI, USA) in PBS. Consecutive 1 minute frames were acquired with an IVIS Spectrum *In vivo* Imaging System (Caliper Life Sciences/Perkin Elmer, Waltham, MA, USA) until the maximum signal intensity was reached. Image analysis was performed with Living Image 4.5.2 software (Perkin Elmer, Waltham, Massachusetts, United States).

6.3.6 *Ex vivo fluc*-hDPSC tracking with immunohistochemistry

Two weeks after tMCAO the liver, spleen, lungs and brain hemispheres were isolated from all animals after transcardial perfusion with 4% PFA. The collected organs were additionally fixed in 4% PFA for 72h after which they were embedded in paraffin to obtain 7 μm sections. Prior to staining, paraffin embedded sections were exposed to xylene and decreasing concentrations of ethanol and washed in PBS. Heat-induced antigen retrieval was performed by heating the sections in citrate buffer (Dako, Glostrup, Denmark) for 10 min. To reduce non-specific staining by endogenous peroxidase, sections were incubated with peroxidase block solution (Dako) for 30 min. at room temperature. Thereafter, blocking for non-specific binding was performed by incubating the sections with protein block (Dako) for 30 min. Consequently, the cells were washed three times with PBS and incubated with primary antibodies for flag (1/200; F7425, Sigma-Aldrich) for 1h at room temperature to detect cells of human origin in the samples. Afterwards, samples were washed with PBS and incubated with a goat-anti rabbit Alexa fluor 555-conjugated (1/500; A21430, Life Technologies, Carlsbad, CA, USA) secondary antibody. Sections were then stained with DAPI for 10 min. Finally, sections were mounted using Dako anti-fade mounting medium.

6.3.7 Statistical analysis

Statistical analysis was performed using Graphpad Prism 5 software (Graphpad, San Diego, CA, USA). Data were analysed with a one-tailed Mann-Whitney test or with the Kruskal-Wallis test followed by a Dunn's test. Differences were considered statistically significant at p-values ≤ 0.05. Data were expressed as mean ± standard error of the mean (S.E.M.).

6.4 Results

6.4.1 One-week follow up of tMCAO mice: behavioural tests and lesion assessment

In the first cohort, the occlusion time of the tMCAO model was optimized. Mice were observed for one week after 30, 45 and 60 min tMCAO during which the open field test, rotarod, mNSS and cylinder test was used to evaluate the influence of the occlusion time on behavioural deficits (Fig. 6.2). Although 60 min tMCAO animals appear to have a higher mNSS (4.33 ± 1.15 vs 0.0 ± 0.0), run on the rotarod for a shorter time (195.2 ± 64.02 s vs 300 ± 0 s) and run slower (78.4 ± 14.93 % vs 99% of baseline) and less far (72.13 ±19.5% vs 100.6%) in the open field test compared to shams (Fig. 6.2A-D), this effect was not significant but is attributed to the small sample size in the sham operated animals. These results show a significant effect (p-value ≤ 0.05) of 60 min tMCAO on behavioural function in the cylinder test compared to the baseline value of the same animals, 7 days post stroke as demonstrated by 56.36 ± 37.91% vs 6.67% left forepaw placing (Fig. 6.2E). Despite the lack of statistical power due to low sample sizes, the described tests were taken into account in cohort 2, due to the visually observed stroke-related deficits that were discerned using these tests. Sham operated animals and animals subjected to 30-or 45 min tMCAO did not develop significant functional deficits compared to the baseline value.
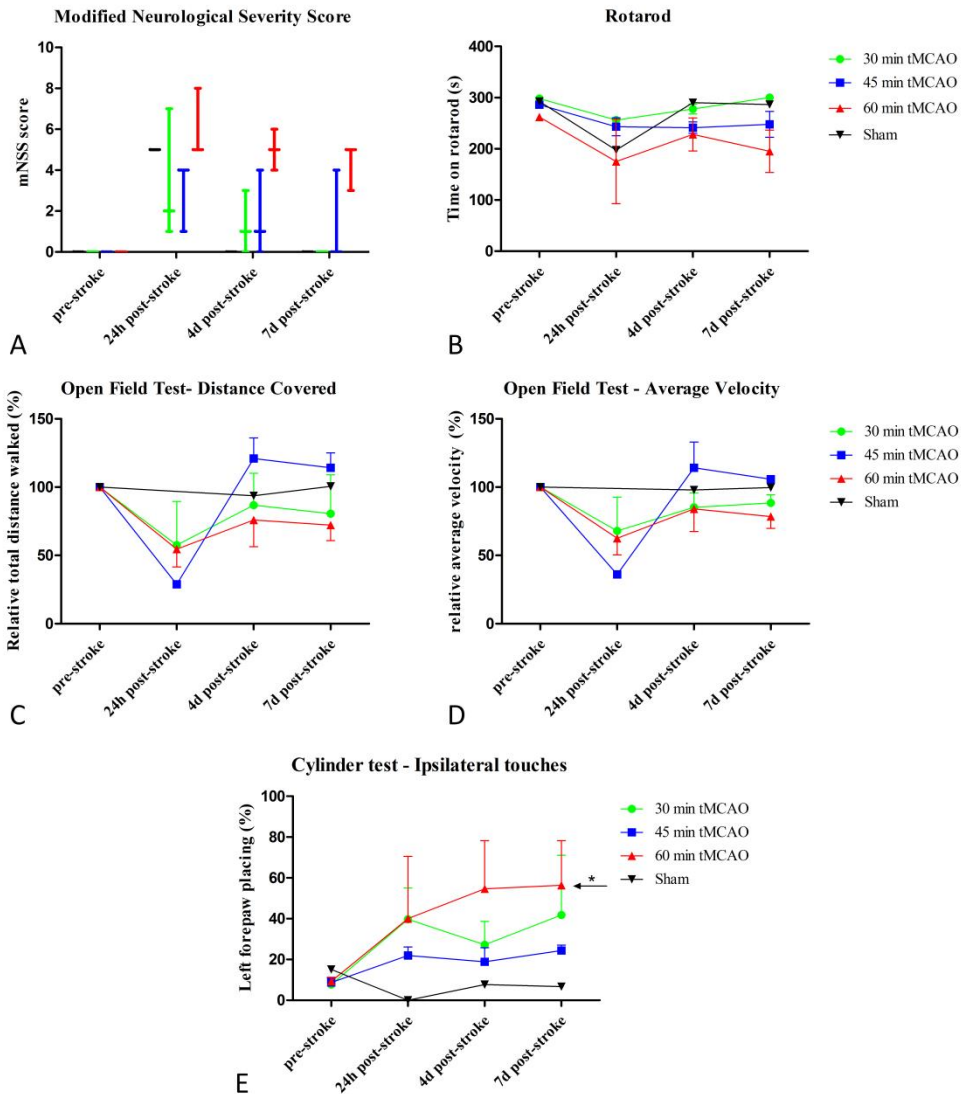
Figure 6.2: Behavioural tests show stroke-related decrease in function after 60 min tMCAO. Behavioural deficits were evaluated with the mNSS (A), rotarod (B), open field test (C, D) and the cylinder test (E) for one week following 30, 45 or 60 min tMCAO. A significant difference after 7 days could only be observed in the cylinder test between sham-operated animals and animals subjected to 60 min tMCAO. *= p-value ≤ 0.05. Data are expressed as mean ± S.E.M.

After one week, mice were sacrificed and the induction and location of the lesion was verified with a TTC staining (Fig. 6.3). This staining shows the mild striatocortical lesion in 30- and 45 min tMCAO (Fig. 6.3A, B; arrowheads), whereas the lesion is more extensive in the 60 minute tMCAO subgroup (Fig. 6.3C; arrowheads). No lesion was observed in sham operated animals (Fig. 6.3D).
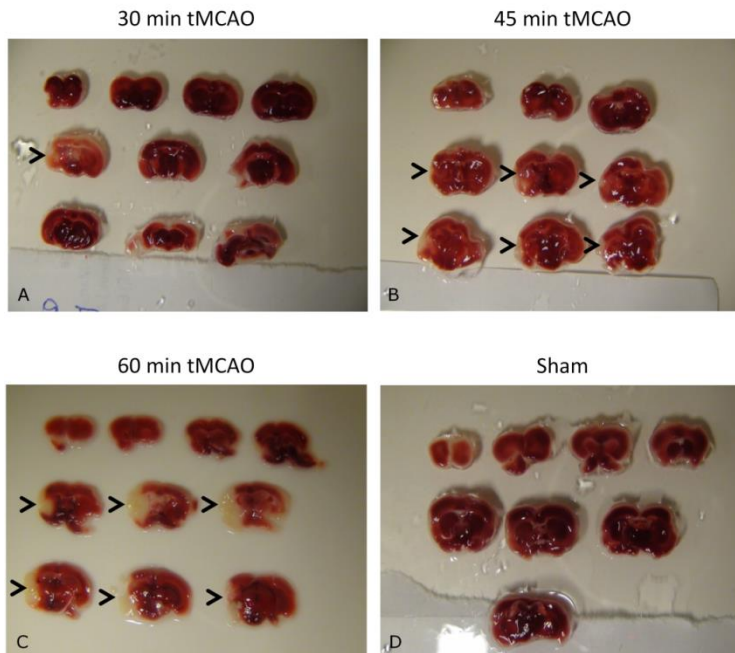
Figure 6.3: Lesion verification after tMCAO. After 7 days of 30 min (A), 45 min (B) and 60 min (C) tMCAO, the presence of the generated lesions was evaluated with a TTC staining. These stainings show the mild striatocortical lesion after 30 min and 45 min tMCAO (A, B; arrowheads) which is expanded by increasing the tMCAO time to 60 min (C; arrowheads). In sham operated animals (D), no lesion was observed.

6.4.2 Behavioural test applicability one month post 60 min-tMCAO

Based on the results of the first cohort, 60 min tMCAO was chosen as the optimal occlusion time. The second cohort aimed to determine which behavioural tests, introduced in section 6.3.1, could be used to evaluate stroke-induced alterations in behavioural function up to one month after stroke induction (Fig. 6.4). In addition, the corner test was introduced as an additional behavioural test to assess sensorimotor function. All time points were compared individually between sham-operated animals and mice subjected to 60 min tMCAO with a one tailed Mann-Whitney test. These results showed that the open field test could not provide an effect window during the one month follow-up. Both the distance covered by the animals as the velocity at which they were moving did not significantly differ during the testing period (Fig 6.4A, B). The mNSS was significantly higher (all p-values $\leq$ 0.05) in the 60 minute tMCAO group compared to shams at all post-stroke time points (Fig. 6.4C). The maximum score in the 60 min tMCAO subjected mice was 7.25 $\pm$ 2.21 24h after stroke was significantly higher (p-value 0.0249 $\leq$ 0.05) compared to 0.33 $\pm$ 0.47 in the sham operated animals. After 4 weeks, the mNSS score in 60 min tMCAO subjected mice was 4.0 $\pm$ 1.0 and remained significantly elevated (p-value 0.05 $\leq$ 0.05) compared to a score of 0 $\pm$ 0 in the sham treated mice.

60 min tMCAO subjected mice had a significantly higher (p-value $\leq$ 0.05) percentage of ipsilateral forepaw placing in the cylinder test up to 3 weeks post-stroke (Fig. 6.4D). The highest percentage of ipsilateral touches was reached 4 days post-tMCAO (67.68 $\pm$ 32.04% vs 11.09 $\pm$ 5.34%; p-value 0.029 $\leq$ 0.05) and remained significantly elevated up to 3 weeks post-stroke (31.39 $\pm$ 5.39% vs 7.2 $\pm$ 6.46%; p-value 0.05 $\leq$ 0.05). Moreover, mice subjected to 60 min tMCAO dropped off the rotarod faster than sham-operated animals (Fig. 6.4E). 60 min tMCAO mice dropped after 175.33 $\pm$ 96.85 s compared to sham operated mice that remained 258.00 $\pm$ 29.3 s on the rotarod 24h post-tMCAO (p-value 0.029 $\leq$ 0.05. After 4 weeks, mice subjected to 60 min tMCAO remained on the rotarod for 191.5 $\pm$ 4.33 s compared to sham operated animals that kept running for 259.17 $\pm$ 25.04 s (p-value 0.038 $\leq$ 0.05). Finally, 60 min tMCAO mice showed a significantly higher propensity to turn unilaterally in the corner test up to 14 days after stroke induction (p-values $\leq$ 0.05), after which their

turning behaviour started to converge with sham-treated animals (Fig. 6.4F). 24h After stroke induction, 60 min tMCAO treated mice have a 97.5 ± 5.0 % propensity to make unilateral turns compared to 50.0 ± 5.0 % in sham-operated animals (p-value 0.022 ≤ 0.05). After two weeks, the propensity for unilateral turns is 95.0% ± 8.7 % in 60 min tMCAO treated mice compared to 46.67 ± 20.0 % in sham-operated animals (p-value 0.038 ≤ 0.05). These data demonstrate, that with the exception of the open field test, all behavioural tests provide an effect window for a potential treatment for up to one-month post-tMCAO. These tests were subsequently used in the following cohort to evaluate the influence of I.V. delivered *fluc*-hDPSCs on behavioural function in mice subjected to 60 min tMCAO.
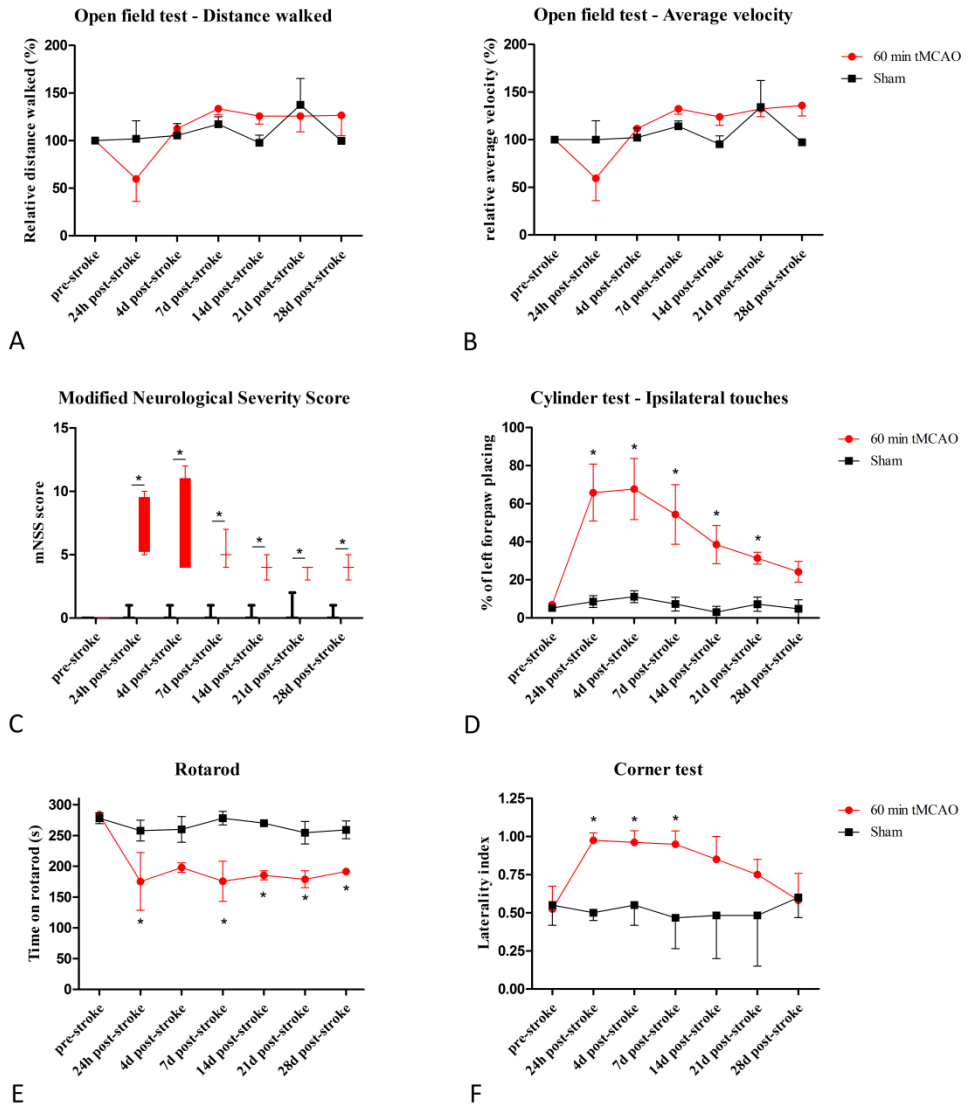
Figure 6.4: One month follow-up of behavioural tests after 60 min tMCAO. The open field test was not able to discern an influence of the tMCAO on the distance walked (A), or on the velocity (B) of the mice compared to shams. A significant effect of stroke on animal behaviour was observed in the mNSS (C), cylinder test (D), rotarod (E) and corner test (F). Moreover, these effects could be observed up to four weeks in the mNSS and rotarod test. Both tests that took laterality into account show significant stroke-induced behavioural symptoms for up to three weeks in the cylinder test and up to 7 days in the corner test. *= p-value ≤ 0.05. Data are expressed as mean ± S.E.M.

6.4.3 I.V. delivery of *fluc*-hDPSCs did not improve behavioural function after 60 min of tMCAO

In the final cohort, mice received I.V.-delivered *fluc*-hDPSCs 24 hours after 60 min tMCAO stroke onset and follow-up of stem cell fate and functional recovery with behavioural tests was performed for 2 weeks (Fig. 6.5). None of the behavioural tests demonstrated the stroke-induced symptoms that were shown in cohort 2 (Fig. 6.5A-D). Therefore, no difference could be observed between animals that received the stem cell graft and untreated tMCAO controls, although the low sample sizes in this pilot cohort can also account for the absence of a trend in clinical effect. After three and five days, one animal in the tMCAO-hDPSC group was sacrificed due to establishing humane endpoints as determined by the ethical committee.
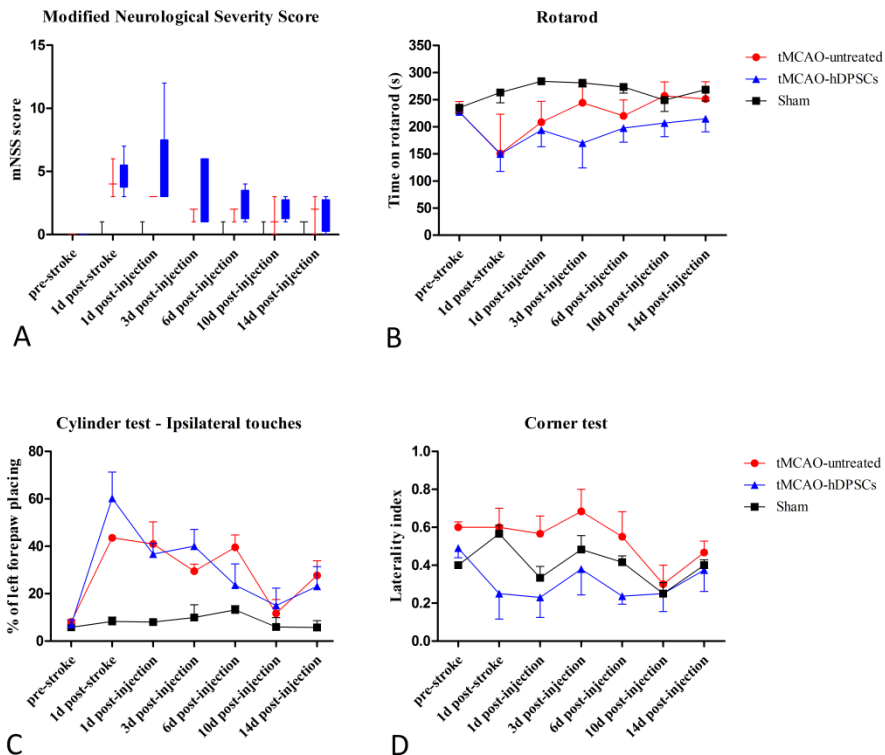
Figure 6.5: Functional assessment after I.V. delivery of *fluc*-hDPSCs in 60 min tMCAO mice. No influence of the hDPSC transplantation on functional behaviour after 60 min tMCAO could be observed in the mNSS (A), rotarod (B), cylinder test (C) and corner test (D). Moreover, no stroke-related symptoms were observed in untreated tMCAO mice compared to shams in these tests. Data are expressed as mean ± S.E.M.

Animals were scanned with MRI five days post-stroke to verify lesion induction. Severe corticostriatal damage was observed in 1/8 animals (Fig. 6.6A, red dashed circles) which subsequently needed to be sacrificed and mild striatal damage was observed in 1/8 animals. These data suggest incomplete induction of 60 min tMCAO due to experimental errors. A BLI signal from the transplanted cells was observed in 1/6 mice that received a *fluc*-hDPSC graft 24h after I.V. injection (Fig. 6.6B; red circle). This signal was generated from subcutaneously injected *fluc*-hDPSCs. No signal generated from the anatomical position of the lungs, spleen, liver or brain was detected. After 3 days, no BLI signal could be detected from the same animal (Fig. 6.6C).

To exclude dispersion of the cells throughout the animal body lowering the signal under the BLI detection limit, the liver, spleen, lungs and brain were isolated after the study and were subjected to an immunohistochemical staining for the flag-tag (Fig. 6.6D-G) which was included in the lentiviral vector. However, no flag-positive *fluc*-hDPSCs could be identified in the brain (Fig. 6.6D), the liver (Fig. 6.6E), the lungs (Fig. 6.6F) or the spleen (Fig. 6.6G) from mice that received the cell transplant.
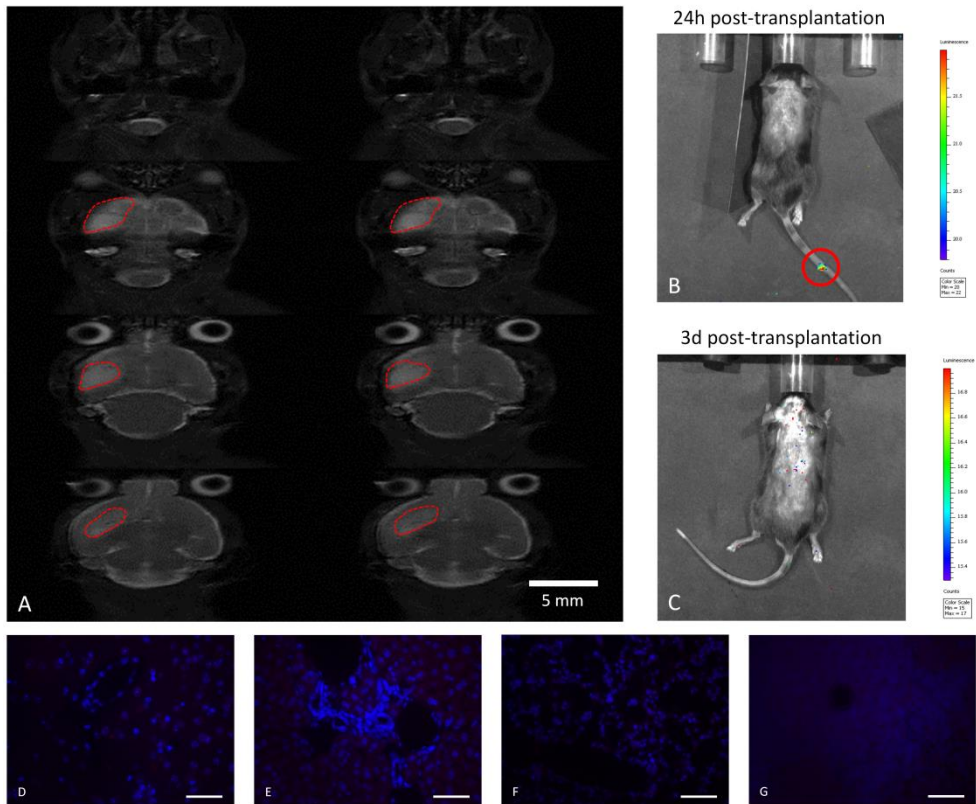
Figure 6.6: MRI of 60 min tMCAO and BLI to detect *fluc*-hDPSCs. T2* weighted horizontal images were made of mice subjected to 60 min tMCAO 5 days post-stroke (A). In 1/8 mice, corticostriatal damage was observed in the left hemisphere (A, red dashed circles). The fate of the transplanted *fluc*-hDPSCs was evaluated by means of BLU (B, C). One day after transplantation, a BLI signal was generated from the injection site in the tail (B, red circle). This signal was lost 3d post-transplantation. (C). No flag immunoreactivity could be observed in the brain (D), liver (E), Lungs (F) or spleen (G) of animals that received a *fluc*-hDPSCs graft two weeks after transplantation. Scale bar A: 5 mm; D-G: 50 μm

6.5 Discussion

In order to evaluate the therapeutic effect of transplanted hDPSCs or other stem cells or therapeutics, it is essential to obtain a representative animal model for ischemic stroke. Together with this model, there is also a need of assays that are able to measure stroke-related symptoms and that can be used over a period of time to evaluate the attenuation of symptoms by potential therapies. Therefore, this study aimed to optimize the tMCAO model in our lab that provides a therapeutic effect window, and to establish a set of behavioural tests that are able to assess stroke-related functional deficits over a prolonged period of time. This study consisted of three cohort studies, in which the first focused on determining the optimal tMCAO time that reflected in stroke-related functional symptoms that could be evaluated by means of behavioural tests for up to one week. The second cohort then focused on whether the optimal occlusion time was able to induce functional deficits that could be observed up to one month and that allow a therapeutic effect window. Finally, a proof-of-principle *in vivo* pilot study was performed in which *fluc*-hDPSCs were I.V. delivered 24h after stroke onset and were tracked with BLI. Behavioural function was monitored for two weeks after hDPSC transplantation.

Although multiple animal models for stroke are available, each with their strengths and weaknesses [65, 365], the first part of the study optimized the proximal filament tMCAO. The filament tMCAO model is the physiologically most relevant model as it most closely resembles the *in vivo* situation. This endovascular tMCAO model allows for a controlled transient occlusion time of the middle cerebral artery and is chosen over the distal tMCAO model as it avoids intracranial operative procedures [363-365]. Moreover, this model circumvents the use of chemicals which are needed to induce photothrombotic stroke [373] or endothelin-1 induced thromboembolisms [374]. The results from this study indicated that 60 min tMCAO produced lesions that were reflected in the functional behaviour of the animals compared to shams, although a significant effect was only observed in the cylinder test after 7 days. This can be explained by the low number of sham operated animals in this first cohort. Nonetheless, due to the visually observed stroke-related deficits that were discerned using these tests, all tests described in the first cohort were taken into account in the

second phase of the study where 60 min tMCAO was induced and stroke mice were monitored for one month. To verify the induction of stroke lesions in the 30-, 45- and 60 min tMCAO mice, a TTC staining was performed. This staining showed the severest lesion in the 60 min tMCAO subgroup. Lesion volume was not quantified because of the limited applicability and representability of this staining method for lesion volume as it only stains the ischemic core containing necrotic cells [375] and does not take into account the penumbra. Despite these shortcomings, the TTC staining remains a valuable method to verify lesion induction in optimization strategies and can potentially be combined with pimonidazole, a hypoxia marker, to identify the tissue at risk in the penumbra [376].

In the second cohort, the behavioural tests that were applied in the first part of this study were used to evaluate the ability of these tests to identify stroke-related symptoms and whether an effect window is present in the 60 min tMCAO mice for a potential therapy to exert its effect. These results showed that with the exception of the open field test, all other tests could be used to evaluate stroke-related behavioural deficits. The rotarod and mNSS could be used for up to four weeks post-stroke, whereas the cylinder test and corner test were able to show a significant effect of 60 min tMCAO up to three and one week after stroke induction. In the open field test, only the total distance walked and the velocity at which the animals were moving were recorded and were used as a measure for voluntary motor movement. However, Doeppner et al. used a different approach to interpret open field test data and they were able to use this test as a reliable test to evaluate post-stroke behaviour after neural precursor cell transplantation [377]. In this study, described by Doeppner et al., the time the animals spend in certain areas of the arena was recorded and the time the animals are resting, scanning or actively progressing in the arena was measured. In this study by Doeppner et al., similar results were observed with the rotarod and corner test although this study was able to show prolonged stroke effects in the corner test [377]. The results from the mNSS were according to Chen et al. [366] and the cylinder test and corner were in line with Li et al. and Zhang et al. who also showed a gradual gain of function over time with these tests [367, 369]. Therefore, with the exception of the open field test,

these tests were included in the *in vivo* pilot study using I.V. delivered *fluc*-hDPSCs.

In the third part of this study, *fluc*-hDPSCs were delivered I.V. 24h after stroke onset. However, no influence of the stem cell graft on behavioural function could be observed over the two-week testing period. Moreover, no influence of 60 min tMCAO on behavioural deficits could be demonstrated, compared to sham-operated controls. This was apparent when the mice that were subjected to 60 min tMCAO were scanned with MRI to verify the stroke lesion 5 days post-stroke. From this data it was shown that only two out of eight mice had a T2-weighted MRI detectable stroke lesion of which one was limited to the striatum and the other lesion was in line with the severe corticostriatal damage that was observed in the first part of the study. These data indicate unsuccessful induction of stroke lesions in the *in vivo* pilot. Remarkably, the tMCAO subjected mice showed a higher mNSS compared to sham animals prior to the stem cell transplantation, which may indicate a transient functional defect due to non-lethal reduced perfusion. These findings stress the use of a standardized operation procedure that is supported by a method to verify reduced blood flow in the area of interest using Laser Doppler or laser speckle contrast imaging [378], or by verifying induction of the lesion immediately post-stroke using non-invasive imaging methods [379]. Moreover, it also important to take into account the variation in collateral flow from the external carotid artery and the posterior communicating artery (PCA) that is present in the mouse brain vasculature that can influence the outcome of lesion formation in experimental stroke models [379-381].

Despite the failure to induce proper stroke lesions and subsequent unrepresentative behavioural analysis, the fate of the I.V.-delivered *fluc*-hDPSCs was tracked with BLI. Unfortunately, a *fluc*-hDPSC signal could only be detected in one out of six graft-receiving mice 24h after injection. Moreover, this signal was generated from subcutaneously injected *fluc*-hDPSCs. No signal from the anatomical position of the lungs, spleen, liver or brain was detected. This signal was lost 3 days post-injection and no flag signal could be detected from the immunohistochemical stainings that were performed after the study, implicating that the grafted cells did not survive the first 24h after transplantation. This

contradicts earlier studies that demonstrated the survival and migration of a small fraction of the I.V.- delivered MSCs towards the ischemic lesion, although these studies were performed in rats [117, 121, 123, 124, 137, 382], but is in line with several other studies that were also not able to demonstrate the presence of grafted cells after injection [57, 119]. I.V.- delivered cells are known to be present in the spleen, lungs and liver after transplantation [383], but even in these organs, no BLI signal or flag-immunoreactive cells could be detected. In order to determine or verify the fate of the administered cells, a human gene-specific PCR can be used as the genetic material from dead human cells can still be distinguished from the host DNA [384, 385]. However, due to the high probability of contaminated DNA samples, low sample size (n=1 for each experimental group in cohort 3) and missing of donor tissue where transplanted cells are not expected to end up in, i.e. muscle tissue, a human-specific PCR was not conducted in this study.

The results from the first two parts of this study demonstrated the optimization of the tMCAO stroke model in our lab and the application of a range of behavioural tests that can be used to monitor stroke-related functional deficits over time. The composite score used in this study, the mNSS was chosen over the Bederson test. While the latter is simpler to perform, it is more subjective in nature and fails to detect long-term deficits after stroke [110, 111]. The rotarod, corner test, cylinder test and open field test, evaluate motor- and sensorimotor behaviour. Although the open field test was not applicable as a test to follow up stroke-induced loss of function, only this test is able to evaluate voluntary movement and exploring behaviour due to the minimal interference of the research during the evaluation period. Therefore, it is important to note that the rotarod, cylinder and corner test all evaluate motor- and sensorimotor function by researcher-induced stimulation of activity. In addition to these trials, other tests that are widely used to asses post-stroke behaviour include the adhesive-removal test, wire hanging test, pole test, staircase test [110, 111]. Gait analysis tests are also frequently used and the main advantage with these tests is that these can be computer-aided, allowing for an objective assessment of stroke-induced gait aberrations [386]. Moreover, the presented behavioural tests in this study did not take cognitive impairment into account. Therefore, future studies should include a cognitive test such as the Morris water maze or

[387] radial arm maze [388] to complete the set of tests to include a composite score, motor-, sensorimotor- and cognitive tests.

Conclusion

This study showed that 60 min occlusion of the middle cerebral artery is the optimal occlusion time to provide a therapeutic window for potential therapies to stimulate behavioural improvement up to one month after stroke. The results from the *in vivo* pilot indicated unsuccessful induction of tMCAO in the experimental cohort and loss of signal from the transplanted cells within 72 hours after transplantation. Therefore, no effect of the hDPSC transplantation on stroke outcome could be evaluated. Despite these results, the tMCAO model was introduced in our lab accompanied by a set of applicable behavioural tests. Future studies should nonetheless focus on establishing standard operation procedures and early lesion verification to obtain standardized stroke lesions with reproducible deficits for this model to be implemented in translational stroke research in our lab.

Acknowledgements

Chapter 7 : General Discussion, Perspectives and Conclusion

General discussion

Stroke is the second single most common cause of death, worldwide, accounting for 10-15% of deaths each year. Moreover, 90 % of patients that survive from a stroke are left with residual deficits leading to permanent disabilities, increasing health care-related costs. As the highest stroke incidence is observed in people over 65 years of age, and given the current demographic trend of an ageing population, the social and economic burden caused by these pathologies is expected to rise [2, 3, 6, 7, 276].

Despite the increased stroke incidence, current available therapies fail to sufficiently ameliorate the disease outcome and the time window after stroke onset after which they can be applied is limited to 4.5 h post-ischemia. Therefore, new therapeutic strategies are needed for treating and preventing stroke that can be applied in a broader time frame. While several clinical advances in stroke management [23, 25-28] and treatment have been developed as promising new treatment options, stem cell-based therapies have also emerged as a potential candidate to promote functional recovery in patients suffering from stroke [8, 41, 357, 389]. In spite of the promising results achieved with cell-based therapies in stroke, the most suitable stem cell type, the host response, the precise mechanisms of action of these therapies and the fate of the donor cells remain largely unknown [357, 382, 389, 390]. The most ideally suited candidates for such cell-based therapies would be neural stem cells (NSCs) or neural precursor cells. These cells are able to differentiate into the majority of cell types present in the adult brain [50] and have already been successfully used in animal models of central nervous system pathologies [8, 51, 390, 391]. Unfortunately, due to ethical considerations [52] and practical issues [53] with human NSCs and NPCs an easy-accessible alternative stem cell-source that is able to aid reconstituting the lost neural tissue is needed. Multiple mechanisms have been proposed for stem cell-mediated therapies, including neuroprotection, cell replacement, immunomodulation and promoting both neuroplasticity and angiogenesis in damaged brain regions (Figure 1.2) [41]. Interestingly, these mechanisms are mainly thought to be mediated by the effect of the stem cell-secretome on endogenous stem cells and on the host microenvironment instead of directly replacing the lost cells although

encouraging results have also been achieved with cell-replacement studies [41, 54, 74, 76, 80, 357, 390].

This work focused on exploring the neuroregenerative effect of human dental pulp stem cells (hDPSCs) and used this interesting stem cell population in an *in vivo* pilot study in a filament transient middle cerebral artery occlusion mouse stroke model (tMCAO). These cells were previously shown to possess mesenchymal stem cell (MSC) characteristics [85] and have shown beneficial effects in *in vivo* models for central nervous system pathologies [41, 56, 207, 208, 277] although the precise mechanisms of action are unknown but are postulated to be paracrine-mediated. In this study, multiple effector mechanisms of hDPSCs were evaluated. The potential of hDPSCs to differentiate into functional neuronal cells as a cell replacement strategy was investigated. Moreover, as cell replacement by engrafted cells is only one of the potential mechanisms for cell-based therapies to ameliorate stroke outcome, the paracrine mediated effect of hDPSCs on human SH-SY5Y neuroblastoma cells with NPC characteristics and mouse NSCs was evaluated.

What is the effect of isolation methodology on the stem cell properties and multilineage differentiation potential of hDPSCs?

Before delving deeper into the neuroregenerative capacity of hDPSCs, a long-lasting issue regarding the isolation method of these cells was evaluated. The two most widely applied isolation methods to harvest hDPSCs are enzymatic digestion of the tissue and the explant method. Both techniques have been used successfully with hDPSCs [85, 95], but the influence of both isolation techniques on the stem cells properties and multilineage differentiation potential of hDPSCs is unknown. In **Chapter 2**, we isolated hDPSCs using both isolation methods and compared their MSC characteristics. Our study revealed that there is no difference in cellular morphology, proliferation rate, stem cell marker expression and mesenchymal differentiation potential between hDPSCs, isolated by means of the enzymatic digestion or the outgrowth method, when these cells are kept in the same culture conditions and are derived from the same donors. Keeping culture conditions equal when comparing isolation methods is critical as it has been shown that culture media, additives, oxygen tension but also passage

number can have an effect on gene expression or differentiation potential of MSCs [392-399]. Both isolation methods yielded stem cell populations that are particularly capable of differentiation into osteoblasts and chondroblasts, but incomplete adipose differentiation, leading to the conclusion that these stem cells provide a promising strategy for the treatment of bone and cartilage injuries. Secretome analysis of hDPSCs obtained by means of both isolation methods was not performed. Although the isolation methodology had no effect on the MSC characteristics of hDPSCs, it cannot be excluded that the isolation procedure can have an influence on the growth factor secretion profile of hDPSCs but this was beyond the scope of the study.

Can hDPSCs be differentiated into neuronal cells that are capable of firing action potentials?

After confirming the applicability and validity of the outgrowth method for isolating hDPSCs, the potential of these cells to differentiate to cells with functional neuronal characteristics was evaluated in **Chapter 3**. Previous studies that aimed to differentiate hDPSCs towards neuronal cells used multistep differentiation protocols that were based on specific growth factor signalling [155] or epigenetic reprogramming [98]. These studies were able to show the presence of voltage-gated Na^+ and K^+ channels in the differentiated cells cultures. However, the firing of action potentials was not observed, which is a hallmark of functional neuronal cells.

In our study, we hypothesized that hDPSCs could be more successfully differentiated to neuronal cells *in vitro* when neurosphere formation precedes neuronal maturation. Neurosphere formation is epidermal growth factor- and basic fibroblast growth factor-dependent and is considered to be a standard cell culture procedure in which NSCs are propagated [50]. Furthermore, neurospheres are used to investigate neural precursor characteristics and it is assumed that neurospheres create a suitable 3-dimensional microenvironment in which the intra-neurospheral cells differentiate towards neuronal and/or glial precursors [209]. Neuronal maturation was subsequently based on increasing cyclic adenosine monophosphate and neurotrophin-3 signalling which are thought to play a role in sustaining neuronal commitment and neurogenic

maturation [217, 228, 229]. Although promising results were achieved using this two-step protocol, establishing a completely functional neuronally differentiated hDPSC culture remains a challenge as the generation of only one action potential could be observed. Nonetheless, the results in this study demonstrated that hDPSCs are capable of neuronal commitment with distinct features of neuronal cells as demonstrated by morphological and electrophysiological characteristics. No further characterization of the neuronal subtype of the differentiated hDPSC culture was performed. In addition, exposing hDPSCs to the neurogenic differentiation protocol altered the secretion of selected growth factors/neurotrophins. In conclusion, hDPSCs could be successfully differentiated into functionally active immature action potential-firing neuronal cells [63] with tetrodotoxin- and tetraethylammonium-sensitive voltage-gated Na^+ and K^+ channels. A study by Ellis et al. used mouse hDPSCs and was able to observe protein expression of cholinergic, dopaminergic and GABAergic neurons in the differentiated cells culture using immunocytochemistry. Moreover, this study also showed the presence of voltage-gated L-type Ca^{2+} channels as demonstrated by whole cell patch-clamp recordings. However, this study was not able to demonstrate the presence of voltage-gated Na^+ and K^+ channels and the firing of action potentials [400].

While these are encouraging results, it has been shown that directed differentiation towards neuronal cells with a precise identity is necessary to obtain region-specific cell-based therapies. It has been suggested that damaged areas in the brain can only be successfully reconstituted by the equivalent homotopic neurons, which stresses that adequate pre-transplantation targeted differentiation of stem cells grafts towards specific types of neurons is required for direct cell replacement by the stem cells themselves [401-403]. For example, it has been shown that grafting cortical donor tissue into the damaged motor cortex re-established cortical and even subcortical circuitry [402], a feature that was not observed when using heterotopical tissue such as occipital cortex [404]. More recently, a study by Michelsen et al. demonstrated that *in vitro* differentiated mouse embryonal stem cell (ESC)-derived visual cortical neurons were able to re-establish connections with the damaged visual cortex with reciprocal axonal projections and synaptic integration [401]. Interestingly, grafting these cells in the damaged motor cortex or ESC-derived motor neurons

in the damaged visual cortex did not lead to graft integration [401]. In addition, targeted differentiated induced pluripotent stem cells (iPSCs) to pyramidal cortical neurons have been shown to integrate in the host circuitry after transplantation into to the neonatal mouse brain [74], and have been used in preclinical stroke research [54]. Similarly, it has been suggested that potential donor cells for Parkinson's disease should be of the correct nigral dopaminergic neuron phenotype to improve functional engraftment with the appropriate targets [403]. Integration of differentiated hDPSCs into the host brain has been reported [206], but based on these observations with ESC- and iPSC- derived therapies, it remains questionable whether predifferentiated hDPSCs can adequately replace lost neurons.

Can the hDPSC secretome stimulate neuronal differentiation, migration and neuritogenesis in SH-SY5Y cells?

As direct cell replacement by stem cell-based therapies is only one plausible mechanism of action, other cell-mediated regenerative processes were evaluated. These focused on the paracrine action of the stem cell secretome on human SH-SY5Y neuroblastoma cells and mouse NSCs. In **Chapter 4**, the influence of the hDPSC secretome on migration, neurite outgrowth, neurogenic maturation, and proliferation of neuroblastoma cells was evaluated. Moreover, the electrophysiological profile of SH-SY5Y cells was determined during the differentiation process. To evaluate the outcome of the SH-SY5Y cells exposed to conditioned medium (CM) of hDPSCs (CM-hDPSCs), a previously established protocol by Encinas et al., based on retinoic acid (RA) and brain derived neurotrophic factor (BDNF) was included in this study as a positive control for neuronal differentiation [218]. The results from this study showed that the hDPSC-secretome did not stimulate SH-SY5Y proliferation, but contained chemoattractant factors that stimulated SH-SY5Y migration in a transwell migration assay. Additionally, SH-SY5Y cells subjected to the hDPSC secretome showed increased neuritogenesis compared to non-exposed cells. Maturated cells were shown to increase immune-reactivity for neuronal markers neuronal nuclei and microtubule-associated protein 2 compared to controls. Ultrastructurally, RA-signalling and subsequent exposure to the hDPSC secretome induced a gradual rise in metabolic activity and neuronal features

such as multivesicular bodies and cytoskeletal elements associated with cellular communication, findings that were in line with Lee at al. [283]. In addition, electrophysiological recordings of differentiating cells demonstrated a transition towards a neuronal electrophysiological profile based on the maximum tetrodotoxin-sensitive, Na^+-current. Moreover, CM-hDPSC-matured SH-SY5Y cells developed distinct features including Cd^{2+}-sensitive currents, which suggests that CM-hDPSC matured SH-SY5Y acquired voltage-gated Ca^{2+}-channels. We did not identify the voltage-gated Ca^{2+}-channel subtype as low or high voltage-activated, but both types of these channels have been previously identified in SH-SY5Y cells [284]. Similarly, we also did not distinguish between different subsets of voltage-gated Na^+-channels, which are also present in SH-SY5Y cells [285]. In addition to these neuroregenerative mechanisms, we also investigated the neuroprotective effect of CM-hDPSC in a glutamate excitotoxicity- and hypoxia, induced by a GasPak (BD), assay, but we were not able to induce sufficient neuronal death to observe CM-hDPSC mediated neuroprotection (data not shown). This is in contrast with a previous study by Egashira et al. that was able to observe a neuroprotective effect of adipose stem cell (ASC)-derived conditioned medium on SH-SY5Y cells exposed to glutamate [67]. In addition, the Gaspak anaerobic environment might not have created a sufficient reduction in O_2 concentration, as it was shown that SH-SY5Y cells are sensitive to 24h oxygen-glucose deprivation (OGD) [405] although it can be argued that 24h OGD at 0.3-0.5% O_2 does not represent physiological stroke conditions [294]. Nonetheless, the results reported in this study demonstrated the potential of hDPSCs to support differentiation and recruitment of cells with neuronal precursor characteristics in a paracrine manner. Moreover, this *in vitro* experimental design showed that the widely used SH-SY5Y cell line can improve and simplify the preclinical *in vitro* research on the molecular mechanisms of stem cell-mediated neuronal regeneration.

Are hDPSCs able to exert neuroprotective and neuroregenerative effects on primary cortical neurons and neural stem cells in a paracrine manner?

Given these promising data with a human cell line with NPC characteristics, we next aimed to extrapolate these findings to mouse NSCs and primary cortical neurons (pCNs) to confirm the paracrine effects of the hDPSC-secretome. Moreover, it is important to take into account the hypoxic and inflammatory stroke microenvironment in which the transplanted cells are situated to exert their therapeutic effect, which can influence the secretome content and survival rate of the engrafted cells [159]. Therefore, efforts are being made to prepare or 'prime' stem cells for the microenvironment they are to be transplanted in prior to transplantation which aims to alter and/or enhance the growth factor content of the stem cell-derived secretome. Stem cells are being primed by for example using hypoxia [162] or hypoxia mimetics [160, 406]. We used a novel approach by exposing hDPSCs to key components of the inflammatory reaction which can be found in the blood. To achieve this priming process, we evaluated whether a clinically applied, blood-derived biomaterial, leukocyte- and platelet rich fibrin (L-PRF), can enhance the neuroregenerative effect of hDPSCs by altering their secretome. This biomaterial showed great promise in wound healing and the restoration of bone defects [295, 296] and its therapeutic effect is thought to be mediated by the growth factors present in this material [166, 167]. These growth factors were isolated and divided into two fractions, namely the L-PRF exudate (EX L-PRF) and the conditioned medium from L-PRF (CM-LPRF). EX L-PRF was isolated by compressing the L-PRF clot and collecting the obtained fluid from the compressed matrix and CM L-PRF was obtained by keeping L-PRF in culture and collecting the medium which contained the growth factors that were secreted by the cells residing in the L-PRF membrane.

The study presented in **Chapter 5** primarily aimed to investigate the paracrine-mediated neuroregenerative potential of CM-hDPSCs on NSC proliferation and migration and on protecting pCNs against OGD-induced cell death and pCN neurite outgrowth. Next, the effect of L-PRF 'priming' on the neuroregenerative effect of the hDPSC secretome on NSCs and pCNs was evaluated. The results in this study demonstrated that the CM-hDPSC protects OGD-exposed pCNs against ischemic death and was capable to enhance neuritogenesis in pCNs. Moreover, this conditioned medium had a chemoattractant effect on NSCs but did not stimulate NSC proliferation which was also observed in human SH-SY5Y neuroblastoma cells in Chapter 4. Unfortunately, although L-PRF priming of

hDPSCs increased the secretion of the growth factor BDNF, no additional effect on the paracrine-mediated mechanisms of regeneration described in this study were observed. It should be noted that only neuroregenerative mechanisms were evaluated with primed- and non-primed CM-hDPSC. No information is available on the effect of primed hDPSCs on other regenerative processes involved in for instance wound healing and bone defects.

Simultaneous with the experiments that evaluated the paracrine effect of the secretome of primed- and non-primed hDPSCs on NSCs and pCNs, the effect of the different growth factor-containing fractions that were isolated from L-PRF on these cells was evaluated. Remarkably, the soluble factors present in L-PRF itself had detrimental effects on NSCs and pCNs in higher concentrations and only low concentrations of the conditioned medium of L-PRF stimulated NSC migration or was able to protect pCNs from ischemic death. Several candidate components in CM/EX L-PRF can be responsible for the observed effects, including myeloperoxidase [320], glutamate [12, 407] and pro-inflammatory cytokines such as tumour necrosis factor alpha (TNF-α) but quantification of these factors in L-PRF needs to be performed to identify possible harmful components. In addition, after determining the relative contribution of these factors within CM L-PRF and EX L-PRF, selective blocking experiments for NSC/pCN-damaging inflammatory mediators will provide additional insight into the growth- and repair-promoting factors that are present in the L-PRF fractions. Moreover, by performing these blocking experiments, additional insights are obtained which can provide the basis for novel therapeutic strategies for ischemic stroke. For instance, Anti TNF-α therapies or IL-1 receptor antagonist were previously applied in preclinical studies for ischemic stroke where they improved stroke outcome [329, 408-410]. These therapies are hypothesized to mainly influence non-neuronal cells, microglial activation and the peripheral immune response, although additional preclinical research is suggested to gain additional insight in anti-TNF-α and anti-IL-1 strategies and their effect on neural cells [408, 411, 412]. Nonetheless, these data suggest that caution is advised when applying this biomaterial clinically in the vicinity of CNS tissue such as when treating defects at the skull base, or after brain surgery when L-PRF is considered as a therapy to help heal the cranial window. Although no clinical adverse effects are

observed momentarily, based on our data, leakage of L-PRF-derived fluids into the cerebrospinal fluid should be avoided.

Taken together, the *in vitro* data from Chapter 3 suggest that hDPSCs have the potential to differentiate into cells with neuronal characteristics when applying the two-step differentiation protocol where neurosphere formation preceding neuronal maturation induces morphological and electrophysiological characteristics of functional neurons. Despite these promising results, the yield of cells that acquired these neuronal features is limited. Nearly half of the cells do not survive the neurosphere induction step and based on the immunocytochemical stainings and electrophysiological data, less than half of the surviving cells acquires the immunophenotype or electrophysiological profile of neuronal cells.

Based on the *in vitro* data from Chapter 4 and 5, it was shown that the hDPSC secretome is rich in factors that are able to promote migration of NSCs and SH-SY5Y neuroblastoma cells which was not enhanced by L-PRF priming. As recruitment of endogenous cells with neuroregenerative characteristics to the site of neuronal injury is one of the goals in neuroregenerative medicine, hDPSCs can be considered as a delivery vehicle for chemoattractant factors. Additionally, hDPSCs have been shown to stimulate endothelial cell migration and vessel formation *in vitro* and *in vivo* [77, 108] which are mandatory for NPCs and/or NSCs require to migrate towards the site of injury [281]. Furthermore, the hDPSC secretome was able to stimulate neurite outgrowth in both SH-SY5Y cells and pCNs. Stimulation of neuronal maturation was only observed in SH-SY5Y cells exposed to CM-hDPSCs. A similar approach that aimed to differentiate NSCs was also initiated based on a previously published study by Spiliotopoulos et al. [342], but these cells did not acquire neuronal characteristics after prolonged culture in CM-hDPSC, demonstrating that the intracellular machinery that drives neuronal differentiation is different in SH-SY5Y cells and NSCs. Moreover, SH-SY5Y cells are tumour-derived cells of human origin and are by definition not stem cells, whereas the NSC line described in this study was isolated from C57/Bl6 mice and is more representative for studies that focus on stem cell-induced NSC development. Finally, pCNs were protected from OGD-induced neuronal death by CM-hDPSC,

demonstrating a neuroprotective effect of the hDPSC-secretome on primary neurons. Taken together, these data suggest that non-primed, non-predifferentiated hDPSCs are attractive candidates for stem cell-based therapies for neuronal injury as was evaluated in an *in vivo* pilot study.

Can the transient middle cerebral artery occlusion mouse stroke model be optimized and implemented in our lab with representative functional behavioural tests?

In the final research chapter, **Chapter 6**, we aimed to optimize the transient middle cerebral artery occlusion (tMCAO) mouse stroke model and conduct an *in vivo* pilot study by injecting *firefly luciferase (fluc)*-transduced hDPSCs intravenously (I.V.) in the optimized model. In order to adequately assess functional improvement stimulated by stem cell transplantation we additionally aimed to optimize individual behavioural tests that can distinguish characteristic stroke deficiencies. Moreover, we evaluated post-stroke and stem cell-stimulated functional recovery, and monitored the fate of the transplanted cells over time. The results in this study indicated that 60 minutes occlusion of the middle cerebral artery is the optimal occlusion time. This provides a therapeutic window in which therapeutics can exert their effect on behavioural function up to one month after stroke induction. Suitable behavioural tests included the modified neurological severity score, the rotarod, corner- and cylinder test. The results from the *in vivo* pilot indicated unsuccessful induction of tMCAO in the experimental cohort as shown by MRI and loss of bioluminescent signal from the transplanted cells within 72 hours after transplantation, although the low sample sizes in this pilot cohort can also account for the absence of a trend in clinical effect in the experimental groups. Therefore, no effect of the hDPSC transplantation on stroke outcome could be evaluated. These findings stress the need of establishing standard operation procedures and early lesion verification to obtain standardized stroke lesions with reproducible deficits for this model to be implemented.

Perspectives and Future directions

Due to the promising preclinical results of stem cell-based therapies in *in vivo* models of ischemic stroke, small-scale human trials were performed using IV delivered autologous MSCs [382, 413, 414] and a small trial using hDPSCs has already been started in the TOOTH study (The Open study Of dental pulp stem cell Therapy in Humans), which evaluates the safety and feasibility of autologous human adult hDPSC therapy in patients with chronic disability after stroke [415]. The outcome of these studies showed that MSC transplantation improved the disease outcome but stress that the underlying mechanisms of action need to be determined to provide a more directed approach. Therefore it is important that in the preclinical phase the potential of stem cell-based therapies is thoroughly investigated in animal models of ischemic stroke which should take the ARRIVE guidelines into account to ensure scientific quality, reproducibility and transparency of preclinical stroke research reports [416].

When considering the optimal transplantation route, each model and route of administration has its own advantages to investigate specific mechanisms of action of the donor cells [417]. Intra-arterial (I.A.) - and I.V.-delivered donor cells would be the preferred method of administration in human applications but this administration route requires a substantial amount of donor cells compared to intracranially delivered stem cells and are hindered by several limitations. These include high morbidity and cells ending up in the spleen after I.A. delivery [119, 418] and pulmonary obstruction after I.V. delivery of donor cells [121, 383]. However, several reports are available that state that donor cell migration towards the spleen is a possible mechanism of action of stem cell-mediated regeneration following stroke. Acosta et al. demonstrated that I.V.-delivered bone marrow mesenchymal stem cells (BMSCs) end up in the spleen, but that BMSC migration to the spleen inversely correlated with a reduced infarct-, peri-infarct size, and the number of MHC-II positive activated cells in the striatum [135]. Although the influence of MSCs themselves on post-stroke immunosuppression was not investigated, Doeppner et al. reported that post-stroke immunosuppression was attenuated after MSC extracellular vesicles were injected in stroke mice [114]. Supporting this hypothesis, Vendrame et al. investigated the immunomodulatory effects of the mononuclear cell fraction of

umbilical cord blood cells [419]. In this study it was demonstrated that I.V. transplantation of these cells diminished spleen reduction and rescued CD8^{+} T-cell counts in addition to a reduction in brain damage. Moreover, it was shown that the cell transplant increased IL-10 and interferon gamma mRNA expression and decreased TNF-α mRNA expression [419]. Donor cells applied to the host circulation migrate towards and integrate in low numbers into the brain lesion and ameliorate the disease outcome (See Table 1.1) presumably by neurotrophic effects as the cerebral level of neurotrophins was found to be elevated in some studies [117, 132, 133]. Moreover, I.A. or I.V. delivery of donor cells allows the interaction of the BBB with donor cells to be studied which can contribute to knowledge of the neuro-immunological response after ischemic stroke [113]. Intracranial delivery of donor cells is the most invasive route of transplantation but a thorough meta-analysis of preclinical data by Vu et al. showed that intracranial delivery of MSCs provided greater clinical benefit although this mode of administration is less favourable for human applications due to the highly invasive nature of the transplantation procedure [420]. In addition to these three most-studied routes of administration, intranasal delivery of BMSCs [129, 421] and intrathecal cell delivery [422, 423] improved the functional outcome after stroke and attenuated ischemic damage. However, it remains debatable whether intranasal cell delivery is a realistic option for human applications due to the immunological barrier function of the nasal mucosa and size of the human brain, elongating the migration pathway along the olfactory tract on which intranasal cell delivery is based on [424, 425]. Intrathecal cell administration is associated with many side-effects, including lumbosacral neuropathies, headache and glioproliferative lesions of the spinal cord [426-428]. Therefore, additional preclinical research that assesses the safety and efficacy of these alternative administration routes is essential.

Another topic of debate is the most suitable source of stem cells as a potential therapy in stroke research. Comparative studies are needed to highlight differences in therapeutic potential of stem cells from different sources in an analogous experimental setup. For example, studies comparing different subtypes of MSCs showed that ASCs are more suitable as a candidate MSC than BMSCs [133] while another study compared the same subsets of MSC and could not observe any difference [57]. Moreover, the studies listed in Table 1.1,

describe both xenogeneic transplantation of human MSCs as allogeneic-derived MSCs in animal models for ischemic stroke. Studies that compare xenogeneic and allogeneic MSCs in ischemic stroke are limited to the study by Yasuhara et al. [126] and Balseanu et al. [124] who compared human and rat BMSCs and Guttiérrez-Fernández et al. who compared human ASCs with rat ASCs [139]. In the study by Yasuhara et al., it was shown that the allogeneic BMSC graft showed a higher survival rate and a higher number of neurogenic differentiated cells. In both engrafted groups, improvement in locomotor and neurological function and a reduced loss of striatal peri-infarct cells was observed [126]. Although Balseanu et al. used both rat and human BMSC in their study, no direct comparison was made between the xeno- and allograft [124]. Preclinical studies with autologous-derived stem cells are scarce and were only described in Jiang et al. [116] who transplanted autologous rat ASCs in ischemic rats whereas for other subtypes of MSCs, preclinical studies with autologous stem cells are not available. This study by Jiang et al. did not compare the outcome of the transplantation between autologous and allogeneic ASCs, which would provide additional information on extrapolability of their results. Although xenogeneic stem cell transplants are not likely to be used in human studies, preclinical studies using xenogeneic grafts provide insight in the potential of human stem cell sources in ischemic stroke.

To date, no studies have been performed that compare the therapeutic potential of iPSCs with a subtype of MSCs. Although the most thoroughly studied stem cell type in stroke research are MSCs, the potential of iPSCs and iPSC-derived neural progenitor cells is currently being intensively investigated with several very promising results when iPSCs are predifferentiated towards neuronal precursor cells or committed cortical neurons [54, 55, 429-432]. In contrast to MSCs, where the paracrine effects of the stem cell secretome have been investigated thoroughly, there is a lack of stroke-related *in vitro* evidence of the (neuro)protective, regenerative and angiogenic properties of iPSCs [433, 434]. All transplantation studies with iPSCs have been performed with intracranially administered iPSCs. I.A. or I.V. delivery of iPSC-derived neuronal precursor or committed cells has not been performed to date. When considering iPSCs as a therapy for ischemic stroke it is important to note that non-differentiated iPSCs can remain present within an iPSC-derived progenitor cell pool, which can result

in teratoma formation. This teratoma formation was not observed when fully committed iPSC-derived cells were transplanted [46, 435]. Moreover, Choi et al. demonstrated the ability of the iPSC-derived neural precursor cells to return towards their pluripotent and thus tumorigenic state by transgene reactivation during differentiation [436]. Therefore, adequate screening of fully neuronal committed cells preceding engraftment is recommended. Another safety issue with the use of iPSCs, and more specifically with retrovirally transduced iPSCs, is the retroviral gene integration in the host, which may promote tumourigenicity [437]. Therefore, additional approaches have been developed to generate iPSCs with a lower risk for tumourigenicity such as omitting c-myc from the reprogramming factors, or using the non-integrating Sendai virus to develop transgene-free iPSCs, although with lower yield [438, 439]. Moreover, it has been shown that iPSCs retain an epigenetic memory related to the somatic donor tissue, leading to spontaneous redifferentiation to the cells of the tissue of origin [440-442] although it has been shown that this epigenetic memory and redifferentiation rate can vary between the somatic cells of origin with different tumorigenic propensities between the somatic donor cells [441, 442]. The tumourigenicity of human iPSCs (and ESCs), was thoroughly reviewed by Ben-David and Benvenisty [443]. As an alternative to iPSCs in which the Yamanaka factors [44, 45] are transduced, exogenous gene-free iPSCs can be used [444]. Another option is to additionally engineer iPSC-derived cells to express suicide genes to eradicate the cells after they exerted their therapeutic effect, an approach that was successfully used in ESCs and BMSCs [445, 446].

It should be noted that in addition to various MSC sources and iPSCs, encouraging results have also been achieved by using bone marrow mononuclear cells (BMMNCs) in animal models of ischemic stroke [447, 448] where this subset of cells was found to stimulate endogenous angiogenesis [58, 59] and neurogenesis by improving the NPC-vascular niche [60] or modulate the immune system [449]. The scarce *in vitro* data on the effect of BMMNCs on regenerative processes showed that BMMNCs exerted protective effects on rat hippocampal brain slices subjected to oxygen- and glucose deprivation [450] and that the BMMNC-secretome induced neuronal differentiation of SH-SY5Y neuroblastoma cells [451]. Nonetheless, additional *in vitro* data supporting the mechanism of action of BMMNC-based therapy for ischemic stroke are required.

In addition to the discussion on the most suitable stem cell source for cell-based therapies for ischemic stroke, there are additional factors that can influence stroke outcome. For example, the host strain (i.e. Nude rats vs immunocompetent rats) and species [381, 452-454] can have an influence on the stroke outcome and cell survival rates [55]. Another factor that can influence cell survival and amelioration is the time after stroke onset the transplantation is performed as cell transplantation at later time-points exposes the cells to the established immune-response [455] whereas cell transplantation early after stroke onset, or too close to the ischemic core can expose the cells to limited blood supply, oxidative stress and trophic factor deficiency [11]. Another well-studied factor that can influence stroke outcome in preclinical studies is age. As stroke is a disease that mainly affects the elderly [355], it is important to take into account the effect of the aged microenvironment, age-related co-morbidities and the aged immune system on the outcome of stem cell-based therapies [456-458]. Some reports argue that the altered stroke microenvironment in aged animals might be less favourable for cell transplantation [429, 459]. Indeed, the formation of the glial scar is accelerated after stroke which hinders functional repair in aged rats [460]. Moreover, co-morbidities such as hypertension, hyperlipidemia and diabetes mellitus appear to play a role in age-related stroke severity [461, 462]. Buga et al. demonstrated that angiogenesis in aged rat brains was similar to their younger counterparts but this study also showed an upregulation of pro-inflammatory- and scar-promoting genes in the aged rats compared to the younger brains, supporting the accelerated scar formation and increased neuro-inflammation in aged stroke subjects [463]. Of the studies listed in Table 1.1, two studies by Shen et al. [130, 138] and studies by Taguchi et al. [134], Balseanu et al.[124] and Zhang et al. [123] used aged rats to perform MSC-transplantation studies in ischemic stroke. Although these studies did not directly compare the outcome of their transplantation study between young and aged rats, several encouraging results were found in these studies. These included, but are not limited to, enhanced functional recovery [123, 124, 134, 138], a reduction of the glial scar thickness [130, 138] and improved angiogenesis [123, 124, 134]. The use of iPSCs in aged rats was described by Tatarishivili et al. who showed that almost 50% of the engrafted iPSC-derived long-term expendable neuroepithelial cells survived

8 weeks post-transplantation and caused functional improvement in the aged rats [429]. Moreover, these cells differentiated towards neuroblast-like cells, compared to the BMSCs described in [130, 138] where the few surviving cells predominantly differentiated towards astrocytes. These studies support the use of aged animals for *in vivo* stroke studies in which they were able to observe cell-mediated improvements in brain regeneration and functional recovery. Nonetheless, a direct comparison in stroke outcome and of the molecular effect after cell transplantation between young and aged animals for the various age-related differences in (brain) microenvironment could provide additional information on which processes are mainly responsible for stem cell-mediated brain repair.

Despite the promising results achieved with cell-based therapies in stroke, the host response, the precise mechanisms of action of these therapies and the fate of the donor cells remain largely unknown [389]. Therefore, non-invasive imaging modalities have been developed that are able to provide detailed temporospatial and functional information on the donor cell fate, the host microenvironment and endogenous repair mechanisms [464].

To track the donor cells, several strategies can be used. Non-invasive imaging methods of donor cells are based on magnetic resonance imaging (MRI), positron emission tomography (PET), single-photon emission computed tomography (SPECT) and optical methods such as bioluminescence imaging (BLI) and fluorescence imaging. Labelling strategies include direct- and indirect methods. Direct pre-transplantation donor cell labels such as superparamagnetic iron oxide (SPIO) particles [57, 465-467] and radionuclides [120, 121] have been used to track donor cell fate, but are also subjected to several disadvantages [468], including label transfer to non-specific cells or the limited radionuclide half-life. For indirect labelling, imaging reporter genes are introduced into the host cells that encode for proteins or molecules that will lead to the accumulation of a specific substrate or ligand within the cells in which the reporter is expressed that can then be detected with a non-invasive imaging modality [370, 468, 469].

Similar to tracking the fate of donor cells, non-invasive imaging modalities based on MRI, radionuclide imaging or optical methods can be applied to monitor the

physiological and/or functional properties of the host environment. These methods allow visualization of neurovascular processes and neurological function but can also be used to study endogenous stem cells responses to treatment. For example BLI-based methods have been used to track endogenous neuronal stem cells and neurogenesis after stroke [470]. In addition, *fluc* under the control of the vascular endothelial growth factor receptor 2 promoter has been used to evaluate post-stroke angiogenesis with BLI [471] and when put under control of the toll-like receptor 2, the response of microglia could be observed after photothrombotic stroke [472]. Another approach is to use PET or SPECT compatible radionuclides have been used in animal models of stroke to evaluate stroke outcome with PET after transplanting iPSCs and ESCs [473]. This study by Wang et al. was able to correlate the PET signal with functional improvement as shown by a decrease in mNSS score in animals that received a non-predifferentiated iPSC- or ESC graft. The timing and expression of the endocannabinnoid receptors CB1 and CB2, which are though to play a neuroprotective role after ischemic stroke, was also investigated with PET. These results showed that CB1 plays a role in photothrombotic stroke and is a potential target for pharmacological interventions [474]. More recently, a study by Zinnhardt et al. combined a multitracer PET study with MRI to link the spatio-temporal relationship of MMP- and microglial activation after tMCAO providing more detailed information on early and delayed endogenous stroke responses [475].

MR-based methods have the advantage that they can couple physiological information with anatomical characteristics of the region of interest. Blood oxygenation level-dependent functional MRI (BOLD fMRI) depends on the haemodynamic response to neuronal activity which are directly related to the energy demand of the studied brain areas [476]. In small-animal stroke research, BOLD-fMRI after electric forepaw stimulation has been successfully used to assess functional recovery and electric brain activity [477]. As stated in Chapter 1, current therapies for ischemic stroke aim to salvage the ischemic penumbra. Therefore it is important to have an adequate monitoring tool to evaluate the size of the penumbra before and after therapeutic intervention. By using Diffusion- and Perfusion weighted MRI, the size of the ischemic penumbra can be determined based on the area of diffusion/perfusion mismatch [478].

While the diffusion/perfusion ratio is mainly used clinically, it has also been successfully applied in a rat model of ischemic stroke [479, 480]. The architectural information of the affected brain region can also be visualized with MR-modalities. Diffuse tensor imaging (DTI) images the anisotropy of water molecules in different tissues and is mainly used in stroke research to study and visualize white matter tracts [481]. Although its use in experimental stroke in animal models is limited, DTI has been used to study the MRI evolution of stroke macaques [482]. Manganese-enhanced MRI can be used to image synaptic connectivity and neuronal connectivity during stroke and recovery has been evaluated in MCAO models using this technique [483, 484]. Finally, arterial spin labeling can be used to monitor reperfusion and had been used in small animal models of ischemic stroke to visualize perfusion in the ischemic brain, allowing the potential longitudinal follow-up of therapeutic interventions that aim to enhance reperfusion [485, 486].

Although post-mortem cell tracking methods provide detailed spatial information on the donor cell fate and host microenvironment, they are unable to deliver dynamic information on these subjects. A longitudinal follow-up with non-invasive imaging methods allows donor cell-fate and changes in host microenvironment to be linked with behavioural and functional improvements which can lead to additional insight in the mechanisms responsible for functional recovery in stroke after donor cell transplantation, which will most likely be the next step in stem cell-based translational stroke research.

Conclusion

Although multiple clinical advances have been made to improve the clinical diagnosis and outcome after acute ischemic stroke, beneficial long-term or delayed interventions are currently not available. Stem cell-based therapies with MSCs have shown great promise in *in vivo* models of ischemic stroke through various administration routes. Nonetheless, the mechanisms of action of the transplanted cells remain poorly understood. This thesis aimed to explore the neuroregenerative potential of a subtype of MSCs, hDPSCs, that were isolated by the explant method. It was shown that these cells could be differentiated towards single action potential-firing immature neurons, albeit with a low success rate. The therapeutic potential of this stem cell source and *modus*

operandi can be attributed to the plethora of factors that are secreted that are able to stimulate neuroregenerative processes. The hDPSC-secretome was shown to enhance neuritogenesis, and neuronal differentiation in addition to containing chemoattractant factors for NSCs and cells with NPC characteristics. Moreover, hDPSCs were able to protect primary cortical neurons against oxygen-glucose deprivation. Preconditioning hDPSCs with L-PRF did not enhance their neuroregenerative potential and it was shown that L-PRF itself has a negative effect on neuronal cells. In order to explore the *in vivo* effect of hDPSCs in a preclinical stroke model, the tMCAO model was optimized in our lab together with suitable and representative behavioural tests. In a pilot study, the necessity of standard operative procedures in order to obtain reproducible stroke lesions became clear, as no stem cell mediated effect in behavioural function could be observed due to low cell survival and inconsistent stroke induction. Nonetheless, the work in this thesis paves the way for preclinical studies that focus on hDPSC-based stem cell therapies for ischemic stroke. Future studies should aim to establish longitudinal follow-up with non-invasive imaging methods in order to allow donor cell-fate and changes in host microenvironment to be linked with behavioural and functional improvements which can lead to additional insight in the mechanisms responsible for functional recovery in stroke after donor cell transplantation.

Summary

Worldwide, stroke is the second most common cause of death, accounting for 10-15% of deaths each year. Moreover, stroke is an important cause of adult disability as 90% of patients that survive from a stroke are left with a residual deficit. In addition, the highest incidence of these pathologies is observed in the elderly, increasing the socioeconomic burden in an aging population. In ischemic stroke, the blood supply to certain brain areas is compromised which triggers a cascade of deleterious events ultimately leading to neuronal cell death. The resulting severe neurological dysfunction clinically translates into paralysis, sensory disturbances, aphasia, urinary incontinence and cognitive impairment. Limited stroke-induced endogenous neurogenesis can be observed in patients but adequate functional recovery is not achieved. Recombinant tissue plasminogen activator is the only FDA-approved pharmacological treatment for ischemic stroke and has to be administered within 4.5 hours after the ischemic insult, limiting its use to 2-4% of the patients and is unable to sufficiently improve the functional outcome. These indications highlight the urgent need for improved treatment of stroke patients. Stem cell therapy is a promising approach to minimize neurological damage and enhance functional recovery after stroke. The ideal source of stem cells for ischemic stroke would be neural stem cells (NSCs) or neural precursor cells (NPCS), but due to practical and ethical considerations, a stem cell source that is able to reconstitute the tissue or stimulate endogenous repair is needed.

This thesis evaluated the neuroregenerative potential of human dental pulp stem cells (hDPSCs), a subtype of mesenchymal stem cells that can easily be isolated from extracted third molars with low invasiveness. Multiple mechanisms of action of stem cell-based therapies for ischemic stroke have been suggested. These include differentiation towards neuronal cells and integration in the host tissue, but more likely, paracrine-mediated mechanisms are responsible for stem cell-induced functional recovery after transplantation into animal stroke models. Therefore, the neuronal differentiation potential of hDPSCs was investigated and the paracrine actions of the hDPSC secretome were assessed.

Before exploring the mechanisms of hDPSC-induced neuroregeneration, the optimal isolation method for these stem cells was determined (**Chapter 2**). Two commonly used isolation methods, the enzymatic digestion and outgrowth

method, were used to isolate hDPSCs and the stem cell properties and multilineage differentiation potential was investigated. Both isolation methods could be used to obtain an hDPSC population for downstream applications as no influence of isolation methodology on the stem cell properties and multilineage differentiation potential of hDPSCs was observed.

Next, the ability of hDPSCs to differentiate towards neuronal cells was investigated (**Chapter 3**). The results in this chapter showed that hDPSCs are able to differentiate into cells with functional and immunocytochemical properties of immature neurons albeit with a low success rate.

In addition to the potential of hDPSCs to differentiate into neuronal cells, the capacity of the hDPSC secretome to stimulate neuroregenerative mechanisms was evaluated. The commonly used SH-SY5Y neuroblastoma cell line which is known to possess NPC characteristics was used to determine the potential of the hDPSCs secretome to stimulate migration, proliferation, neurite outgrowth and neuronal differentiation of SH-SY5Y cells (**Chapter 4**). With the exception of SH-SY5Y proliferation, these important neuroregenerative mechanisms were stimulated by the hDPSC secretome. Moreover, this *in vitro* experimental design showed that the widely used SH-SY5Y cell line can improve and simplify the preclinical *in vitro* research on the molecular mechanisms of stem cell-mediated neuronal regeneration. Although these data were encouraging and showed the *in vitro* potential of SH-SY5Y cells, these immortalised tumour cells are by definition not NSCs or NPCs. Therefore, the influence of the hDPSC secretome was also evaluated on NSCs and primary cortical neurons (**Chapter 5**). Moreover, as efforts are being made to prepare or 'prime' stem cells for the microenvironment they are to be transplanted in prior to transplantation which aims to alter and/or enhance the growth factor content of the stem cell-derived secretome, we used a novel priming approach by exposing hDPSCs to key components of the inflammatory reaction which can be found in the blood. To achieve this priming process, we evaluated whether a clinically successfully applied, blood-derived biomaterial, leukocyte- and platelet rich fibrin (L-PRF), can enhance the neuroregenerative effect of hDPSCs by altering their secretome. The results in this chapter demonstrated that the hDPSC secretome protects primary cortical neurons against ischemic death and was capable to

enhance neuritogenesis in these cells. Moreover, the secretome had a chemoattractant effect on NSCs but did not stimulate NSC proliferation. Unfortunately no additional effect on the paracrine-mediated mechanisms of regeneration described in this study were observed when hDPSCs were primed with L-PRF.

Finally, the transient middle cerebral artery occlusion (tMCAO) mouse stroke model was optimized together with a battery of behavioural tests that can distinguish stroke-related symptoms up to one month. In addition, a pilot study using intravenous delivered hDPSCs to evaluate functional improvement after transplantation was conducted (**Chapter 6**). Although the mouse stroke model was successfully optimized and implemented, no effect of the hDPSC transplantation on functional improvement was observed. The results from the *in vivo* pilot indicated unsuccessful induction of tMCAO in the experimental cohort as shown by magnetic resonance imaging and loss of bioluminescent signal from the transplanted cells within 72 hours after transplantation. Therefore, no effect of the hDPSC transplantation on stroke outcome could be evaluated. These findings stress the need of establishing standard operation procedures and early lesion verification to obtain standardized stroke lesions with reproducible deficits for this model to be implemented.

Nonetheless, the work in this thesis paves the way for preclinical studies that focus on hDPSC-based stem cell therapies for ischemic stroke. Future studies should aim to establish longitudinal follow-up with non-invasive imaging methods in order to allow donor cell-fate and changes in host microenvironment to be linked with behavioural and functional improvements which can lead to additional insight in the mechanisms responsible for functional recovery in stroke after donor cell transplantation.

Samenvatting

Het herseninfarct is wereldwijd de tweede meest voorkomende doodsoorzaak waarbij 10-15% van de overlijdens jaarlijks hieraan te wijten zijn. Daarenboven blijft 90% van de patiënten die het infarct overleven achter met een permanente handicap. Aangezien de hoogste incidentie in herseninfarcten wordt waargenomen bij ouderen, leidt dit tot een verhoogde socio-economische last in een vergrijzende populatie. In het ischemisch herseninfarct is de bloedsvoorziening naar bepaalde hersengebieden verstoord welke een cascade van schadelijke effecten veroorzaakt die uiteindelijk voor neuronale celdood zorgen. De daaropvolgende ernstige afwijking in neurologische functie vertaalt zich klinisch in paralyse, sensorische uitval, afasie, urinaire incontinentie en cognitieve problemen. Het endogeen herstel na een herseninfarct is beperkt waardoor er geen functioneel herstel meer kan optreden. Recombinant weefsel plasminogeen activator is momenteel de enige FDA-goedgekeurde farmacologische behandeling voor het ischemisch herseninfarct en dit dient binnen de 4.5 uur na de start van de ischemie te worden toegediend. Hierdoor kan dit geneesmiddel slechts bij 2-4% van de patiënten gebruikt worden en is er sprake van onvoldoende functioneel herstel. Deze indicaties tonen de dringende nood aan voor een betere behandeling voor patiënten met een herseninfarct. Stamceltherapie is een veelbelovende aanpak om neurologische schade te beperken en om functioneel herstel na het herseninfarct te stimuleren. De ideale stamcelbron voor het ischemisch herseninfarct zouden neurale stamcellen (NSCs) of neurale precursorcellen (NPCs) zijn, maar wegens praktische en ethische overwegingen is er nood aan een alternatieve stamcelbron die in staat is het verloren weefsel te vervangen of endogeen herstel te stimuleren.

In dit doctoraatsproefschrift werd het neuroregeneratief potentieel onderzocht van humane dentale pulpastamcellen (hDPSCs), een subtype van mesenchymale stamcellen dat eenvoudig en niet-invasief uit geëxtraheerde wijsheidstanden kan worden geïsoleerd. Het therapeutische effect van stamcelgebaseerde therapieën wordt aan meerdere mechanismen gekoppeld. Hierbij werd verondersteld dat dit te wijten was aan differentiatie van de stamcellen naar neuronale cellen en de integratie in het gastheerweefsel, maar waarschijnlijk zijn vooral de paracriene mechanismen verantwoordelijk voor stemcel-geïnduceerd functioneel herstel. Daarom werden in deze studie zowel het neuronaal diferentiatiepotentieel van hDPSCs als de paracriene effecten van het hDPSC secretoom onderzocht.

Vooraleer de mechanismen van hDPSC-geïnduceerde neuroregeneratie werden onderzocht, werd de optimale isolatiemethode voor hDPSCs bepaald (**Hoofdstuk 2**). Hiervoor werden twee vaak gebruikte methoden, de enzymatische digestie- en uitgroei methode, gebruikt om hDPSCs te isoleren uit wijsheidstanden. Nadien werden de stamceleigenschappen en het typische differentiatiepatroon van de cellen bepaald. Zo werd duidelijk dat beide isolatiemethoden gebruikt kunnen worden om hDPSCs te isoleren voor verdere toepassingen aangezien de isolatiemethode geen invloed had op de stamceleigenschappen van hDPSCs of op hun differentiatiepotentieel naar meerdere celtypes.

Hierna werd het vermogen van hDPSCs om naar neuronale cellen te differentiëren onderzocht (**Hoofdstuk 3**). De resultaten in dit hoofdstuk toonden aan dat hDPSCs kunnen differentiëren tot cellen met functionele en immunocytochemische eigenschappen van immature neuronen maar met een lage succesratio.

Naast het neuronale differentiatiepotentieel van hDPSCs, werd de capaciteit van het hDPSC secretoom om neuroregeneratieve mechanismen te stimuleren, geëvalueerd. De vaak gebruikte SH-SY5Y neuroblastoma cellijn waarvan geweten is dat deze NPC karakteristieken vertoont, werd hierbij gebruikt om het potentieel van het hDPSC secretoom op migratie, proliferatie, neurietuitgroei en neuronale differentiatie van SH-SY5Y cellen te onderzoeken (**Hoofdstuk 4**). Met uitzondering van SH-SY5Y proliferatie, werden deze neuroregeneratieve mechanismen gestimuleerd door het hDPSC secretoom. Daarenboven toont deze *in vitro* experimentele opzet aan dat de SH-SY5Y cellijn het preklinisch *in vitro* onderzoek naar de moleculaire mechanismen van stamcelgemedieerde neuronale regeneratie kan verbeteren en versimpelen. Ondanks de bemoedigende *in vitro* resultaten van de SH-SY5Y cellen, moet opgemerkt worden dat deze geïmmortaliseerde tumorcellen per definitie geen NSCs/NPCs zijn. Daarom werd de invloed van het hDPSC secretoom ook geëvalueerd op NSCs en primaire corticale neuronen (**Hoofdstuk 5**). Momenteel worden pogingen ondernomen om stamcellen voor te bereiden of te 'primen' voor de micro-omgeving waarin ze getransplanteerd zullen worden met als doel het stamcelsecretoom aan te passen of de inhoud aan groeifactoren te verrijken. In

deze studie gebruikten wij een nieuwe priming aanpak door hDPSCs bloot te stellen aan componenten van de ontstekingsreactie die teruggevonden kunnen worden in bloed. Om dit primingsproces te optimaliseren, evalueerden we of een klinisch succesvol toegepast biomateriaal dat wordt afgeleid uit het bloed, "leukocyt- en plaatjes-rijk fibrine" (L-PRF), het neuroregeneratief effect van hDPSCs kan verbeteren door hun secretoom aan te passen. De resultaten in dit hoofdstuk toonden aan dat het hDPSC secretoom primaire corticale neuronen beschermt tegen ischemische celdood en ook de neuritogenese in deze cellen werd bevorderd. Daarenboven had het hDPSC secretoom een chemoattractief effect op NSCs, maar werd NSC proliferatie niet gestimuleerd. Helaas werd er geen additioneel effect waargenomen op de beschreven paracrien-gemedieerde mechanismen van neuroregeneratie wanneer hDPSCs werden geprimed met L-PRF.

Als laatste werd het transient a. cerebri media occlusie (tMCAO) muismodel voor het ischemisch herseninfarct geoptimaliseerd samen met een reeks gedragstesten die infarctgerelateerde symptomen tot één maand kunnen onderscheiden. Daarenboven werd een pilootstudie uitgevoerd waarbij hDPSCs intraveneus werden toegediend om functioneel herstel na transplantatie te beoordelen (**Hoofdstuk 6**). Ondanks dat het tMCAO model succesvol kon worden geoptimaliseerd en geïmplementeerd, kon geen effect van de getransplanteerde hDPSCs op functioneel herstel worden geobserveerd. De resultaten van de *in vivo* pilootstudie toonden via magnetische resonantie beeldvorming aan dat het infarct onsuccesvol werd geïnduceerd en dat de stamcellen niet meer gedetecteerd konden worden met bioluminescentiebeeldvorming 72 uur na de transplantatie. Daarom kon er geen effect van de hDPSC transplantatie op de infarctuitkomst worden geëvalueerd. Deze bevindingen tonen de nood aan om een gestandaardiseerd operatieprotocol te hanteren en vlak na de operatie de laesie te verifiëren om gestandaardiseerde infarctlaesies te verkrijgen met reproduceerbare functionele tekortkomingen om dit model te kunnen implementeren.

Desalniettemin effent het werk in dit doctoraatsproefschrift de weg naar preklinische studies die zich toespitsen op het gebruikt van hDPSC-gebaseerde stamceltherapiën voor het ischemisch herseninfarct. Vervolgstudies dienen zich

te richten op het gebruik van niet-invasieve beeldvormingsmethoden om het lot van de donorcellen en veranderingen in de micro-omgeving van de gastheer te kunnen correleren met gedrags- en functioneel herstel. Deze kunnen leiden tot nieuwe inzichten in de mechanismen die verantwoordelijk zijn voor functioneel herstel in het herseninfarct na transplantatie van de donorcellen

.

References

References

1. Nichols, M., N. Townsend, R. Luengo-Fernandez, J. Leal, A. Gray, P. Scarborough, and M. Rayner, European Cardiovascular Disease Statistics 2012. European Heart Network, Brussels, European Society of Cardiology, Sophia Antipolis. 2012.

2. Go, A.S., D. Mozaffarian, V.L. Roger, E.J. Benjamin, J.D. Berry, M.J. Blaha, S.F. Dai, E.S. Ford, C.S. Fox, S. Franco, H.J. Fullerton, C. Gillespie, S.M. Hailpern, J.A. Heit, V.J. Howard, M.D. Huffman, S.E. Judd, B.M. Kissela, S.J. Kittner, D.T. Lackland, J.H. Lichtman, L.D. Lisabeth, R.H. Mackey, D.J. Magid, G.M. Marcus, A. Marelli, D.B. Matchar, D.K. McGuire, E.R. Mohler, C.S. Moy, M.E. Mussolino, R.W. Neumar, G. Nichol, D.K. Pandey, N.P. Paynter, M.J. Reeves, P.D. Sorlie, J. Stein, A. Towfighi, T.N. Turan, S.S. Virani, N.D. Wong, D. Woo, M.B. Turner, A.H.A.S. Comm, and S.S. Subcomm, Heart Disease and Stroke Statistics-2014 Update A Report From the American Heart Association. Circulation, 2014. **129**(3): p. E28-E292.

3. Mozaffarian, D., E.J. Benjamin, A.S. Go, D.K. Arnett, M.J. Blaha, M. Cushman, S.R. Das, S. de Ferranti, J.P. Despres, H.J. Fullerton, V.J. Howard, M.D. Huffman, C.R. Isasi, M.C. Jimenez, S.E. Judd, B.M. Kissela, J.H. Lichtman, L.D. Lisabeth, S. Liu, R.H. Mackey, D.J. Magid, D.K. McGuire, E.R. Mohler, 3rd, C.S. Moy, P. Muntner, M.E. Mussolino, K. Nasir, R.W. Neumar, G. Nichol, L. Palaniappan, D.K. Pandey, M.J. Reeves, C.J. Rodriguez, W. Rosamond, P.D. Sorlie, J. Stein, A. Towfighi, T.N. Turan, S.S. Virani, D. Woo, R.W. Yeh, M.B. Turner, C. American Heart Association Statistics, and S. Stroke Statistics, Heart Disease and Stroke Statistics-2016 Update: A Report From the American Heart Association. Circulation, 2016. **133**(4): p. e38-360.

4.   Hinkle, J.L. and M.M. Guanci, Acute ischemic stroke review. J Neurosci Nurs, 2007. **39**(5): p. 285-93, 310.

5.   Dua, T., M. Cumbrera, C. Mathers, and S. Saxena, Global Burden Of Neurological Disorders: Estimates And Projections, in *Neurological Disorders: Public Health Challenges*, B. Campanini, Editor. 2006, World Health Organization: Geneva, Switzerland. p. 27-40.

6.   United Nations, Department of Economic and Social Affairs. (2002). Magnitude And Speed Of Poplation Ageing, in *World Population Ageing 1950-2050*. Population Division, DESA, United Nations New York, NY, USA p. 11-13.

7.   Norrving, B. and B. Kissela, The global burden of stroke and need for a continuum of care. Neurology, 2013. **80**(3 Suppl 2): p. S5-12.

8.   Lindvall, O. and Z. Kokaia, Stem cells for the treatment of neurological disorders. Nature, 2006. **441**(7097): p. 1094-6.

9.   Goldstein, M., H.J.M. Barnett, J.M. Orgogozo, N. Sartorius, L. Symon, and N.V. Vereshchagin, Stroke—1989: Recommendations on stroke prevention, diagnosis, and therapy. Report of the WHO Task Force on Stroke and other Cerebrovascular Disorders. Stroke, 1989. **20**(10): p. 1407-1431.

10.   Donnan, G.A., M. Fisher, M. Macleod, and S.M. Davis, Stroke. Lancet, 2008. **371**(9624): p. 1612-23.

11.   White, B.C., J.M. Sullivan, D.J. DeGracia, B.J. O'Neil, R.W. Neumar, L.I. Grossman, J.A. Rafols, and G.S. Krause, Brain ischemia and reperfusion: molecular mechanisms of neuronal injury. J Neurol Sci, 2000. **179**(S 1-2): p. 1-33.

12.   Dirnagl, U., C. Iadecola, and M.A. Moskowitz, Pathobiology of ischaemic stroke: an integrated view. Trends Neurosci, 1999. **22**(9): p. 391-7.

13.   Bandera, E., M. Botteri, C. Minelli, A. Sutton, K.R. Abrams, and N. Latronico, Cerebral blood flow threshold of ischemic penumbra and infarct core in acute ischemic stroke: a systematic review. Stroke, 2006. **37**(5): p. 1334-9.

14.   Fisher, M., The ischemic penumbra: identification, evolution and treatment concepts. Cerebrovasc Dis, 2004. **17 Suppl 1**: p. 1-6.

15.   Moretti, A., F. Ferrari, and R.F. Villa, Neuroprotection for ischaemic stroke: current status and challenges. Pharmacol Ther, 2015. **146**: p. 23-34.

16.   Muir, K.W., A. Buchan, R. von Kummer, J. Rother, and J.C. Baron, Imaging of acute stroke. Lancet Neurol, 2006. **5**(9): p. 755-68.

17.   Goyal, M., B.K. Menon, and C.P. Derdeyn, Perfusion imaging in acute ischemic stroke: let us improve the science before changing clinical practice. Radiology, 2013. **266**(1): p. 16-21.

18.   Pan, J., A.A. Konstas, B. Bateman, G.A. Ortolano, and J. Pile-Spellman, Reperfusion injury following cerebral ischemia: pathophysiology, MR imaging, and potential therapies. Neuroradiology, 2007. **49**(2): p. 93-102.

19.   Dominguez, C., P. Delgado, A. Vilches, P. Martin-Gallan, M. Ribo, E. Santamarina, C. Molina, N. Corbeto, V. Rodriguez-Sureda, A. Rosell, J. Alvarez-Sabin, and J. Montaner, Oxidative stress after thrombolysis-induced reperfusion in human stroke. Stroke, 2010. **41**(4): p. 653-60.

20. Jickling, G.C., D. Liu, B. Stamova, B.P. Ander, X. Zhan, A. Lu, and F.R. Sharp, Hemorrhagic transformation after ischemic stroke in animals and humans. J Cereb Blood Flow Metab, 2014. **34**(2): p. 185-99.

21. Warach, S. and L.L. Latour, Evidence of reperfusion injury, exacerbated by thrombolytic therapy, in human focal brain ischemia using a novel imaging marker of early blood-brain barrier disruption. Stroke, 2004. **35**(11 Suppl 1): p. 2659-61.

22. Paciaroni, M., G. Agnelli, F. Corea, W. Ageno, A. Alberti, A. Lanari, V. Caso, S. Micheli, L. Bertolani, M. Venti, F. Palmerini, S. Biagini, G. Comi, P. Previdi, and G. Silvestrelli, Early hemorrhagic transformation of brain infarction: rate, predictive factors, and influence on clinical outcome: results of a prospective multicenter study. Stroke, 2008. **39**(8): p. 2249-56.

23. Langhorne, P. and S.U.T. Collaborati, Organised inpatient (stroke unit) care for stroke. Cochrane Database of Systematic Reviews, 2013(9).

24. The National Institute of Neurological Disorders and Stroke rt-PA Stroke Study Group. Tissue plasminogen activator for acute ischemic stroke. . N Engl J Med, 1995. **333**(24): p. 1581-7.

25. Hacke, W., M. Kaste, C. Fieschi, D. Toni, E. Lesaffre, R. von Kummer, G. Boysen, E. Bluhmki, G. Hoxter, M.H. Mahagne, and et al., Intravenous thrombolysis with recombinant tissue plasminogen activator for acute hemispheric stroke. The European Cooperative Acute Stroke Study (ECASS). JAMA, 1995. **274**(13): p. 1017-25.

26. Emberson, J., K.R. Lees, P. Lyden, L. Blackwell, G. Albers, E. Bluhmki, T. Brott, G. Cohen, S. Davis, G. Donnan, J. Grotta, G. Howard, M. Kaste, M. Koga, R. von Kummer, M. Lansberg, R.I. Lindley, G. Murray, J.M.

Olivot, M. Parsons, B. Tilley, D. Toni, K. Toyoda, N. Wahlgren, J. Wardlaw, W. Whiteley, G.J. Del Zoppo, C. Baigent, P. Sandercock, W. Hacke, and G. Stroke Thrombolysis Trialists' Collaborative, Effect of treatment delay, age, and stroke severity on the effects of intravenous thrombolysis with alteplase for acute ischaemic stroke: a meta-analysis of individual patient data from randomised trials. Lancet, 2014. **384**(9958): p. 1929-35.

27.   Sandercock, P., R. Collins, C. Counsell, B. Farrell, R. Peto, J. Slattery, C. Warlow, S. Anderson, A. Bowie, J. Boyle, A. Brownlie, D. Charlton, G. Cranswick, L. Day, M. Dennis, P. Dorman, H. Fraser, M. Kaye, R. Lindley, M. Liu, C. MacDonald, I. McCrindle, G. Middleton, D. Perry, V. Scoltock, B. Smith, H. Taylor, F. Waddell, J. Wardlaw, J. Crowther, J. Heineman, S. Knight, A. Radley, R. Ripley, S. Richards, S. Wilberforce, Z.M. Chen, J. vanGijn, M. Harrison, and L. Wilhelmsen, The International Stroke Trial (IST): A randomised trial of aspirin, subcutaneous heparin, both, or neither among 19 435 patients with acute ischaemic stroke. Lancet, 1997. **349**(9065): p. 1569-1581.

28.   Vahedi, K., J. Hofmeijer, E. Juettler, E. Vicaut, B. George, A. Algra, G.J. Amelink, P. Schmiedeck, S. Schwab, P.M. Rothwell, M.G. Bousser, H.B. van der Worp, W. Hacke, D. Decimal, and H. investigators, Early decompressive surgery in malignant infarction of the middle cerebral artery: a pooled analysis of three randomised controlled trials. Lancet Neurol, 2007. **6**(3): p. 215-22.

29.   Ropper, A.H., M.A. Samuels, and J.P. Klein, Chapter 34: Cerebrovascular Diseases, in *Adams and Victor's Principles of Neurology*. 2014, McGraw-Hill: New York, USA. p. 778-884.

30.   Hacke, W., G. Donnan, C. Fieschi, M. Kaste, R. von Kummer, J.P. Broderick, T. Brott, M. Frankel, J.C. Grotta, E.C. Haley, Jr., T. Kwiatkowski, S.R. Levine, C. Lewandowski, M. Lu, P. Lyden, J.R. Marler, S. Patel, B.C. Tilley, G. Albers, E. Bluhmki, M. Wilhelm, S. Hamilton, A.T. Investigators, E.T. Investigators, and N.r.-P.S.G. Investigators, Association of outcome with early stroke treatment: pooled analysis of ATLANTIS, ECASS, and NINDS rt-PA stroke trials. Lancet, 2004. **363**(9411): p. 768-74.

31.   Frank, J.I., Large hemispheric infarction, deterioration, and intracranial pressure. Neurology, 1995. **45**(7): p. 1286-90.

32.   von Kummer, R., G.W. Albers, E. Mori, and D.S. Committees, The Desmoteplase in Acute Ischemic Stroke (DIAS) clinical trial program. Int J Stroke, 2012. **7**(7): p. 589-96.

33.   Barreto, A.D., A.V. Alexandrov, L. Shen, A. Sisson, A.W. Bursaw, P. Sahota, H. Peng, M. Ardjomand-Hessabi, R. Pandurengan, M.H. Rahbar, K. Barlinn, H. Indupuru, N.R. Gonzales, S.I. Savitz, and J.C. Grotta, CLOTBUST-Hands Free: pilot safety study of a novel operator-independent ultrasound device in patients with acute ischemic stroke. Stroke, 2013. **44**(12): p. 3376-81.

34.   Smith, W.S., G. Sung, S. Starkman, J.L. Saver, C.S. Kidwell, Y.P. Gobin, H.L. Lutsep, G.M. Nesbit, T. Grobelny, M.M. Rymer, I.E. Silverman, R.T. Higashida, R.F. Budzik, M.P. Marks, and M.T. Investigators, Safety and efficacy of mechanical embolectomy in acute ischemic stroke: results of the MERCI trial. Stroke, 2005. **36**(7): p. 1432-8.

References

35. Dirnagl, U., J. Klehmet, J.S. Braun, H. Harms, C. Meisel, T. Ziemssen, K. Prass, and A. Meisel, Stroke-induced immunodepression: experimental evidence and clinical relevance. Stroke, 2007. **38**(2 Suppl): p. 770-3.

36. Chouchani, E.T., V.R. Pell, E. Gaude, D. Aksentijevic, S.Y. Sundier, E.L. Robb, A. Logan, S.M. Nadtochiy, E.N. Ord, A.C. Smith, F. Eyassu, R. Shirley, C.H. Hu, A.J. Dare, A.M. James, S. Rogatti, R.C. Hartley, S. Eaton, A.S. Costa, P.S. Brookes, S.M. Davidson, M.R. Duchen, K. Saeb-Parsy, M.J. Shattock, A.J. Robinson, L.M. Work, C. Frezza, T. Krieg, and M.P. Murphy, Ischaemic accumulation of succinate controls reperfusion injury through mitochondrial ROS. Nature, 2014. **515**(7527): p. 431-5.

37. Ishiguro, M., K. Mishiro, Y. Fujiwara, H. Chen, H. Izuta, K. Tsuruma, M. Shimazawa, S. Yoshimura, M. Satoh, T. Iwama, and H. Hara, Phosphodiesterase-III inhibitor prevents hemorrhagic transformation induced by focal cerebral ischemia in mice treated with tPA. PLoS One, 2010. **5**(12): p. e15178.

38. Hawkins, K.E., K.M. DeMars, J. Singh, C. Yang, H.S. Cho, J.C. Frankowski, S. Dore, and E. Candelario-Jalil, Neurovascular protection by post-ischemic intravenous injections of the lipoxin A4 receptor agonist, BML-111, in a rat model of ischemic stroke. J Neurochem, 2014. **129**(1): p. 130-42.

39. van der Worp, H.B., M.R. Macleod, P.M. Bath, J. Demotes, I. Durand-Zaleski, B. Gebhardt, C. Gluud, R. Kollmar, D.W. Krieger, K.R. Lees, C. Molina, J. Montaner, R.O. Roine, J. Petersson, D. Staykov, I. Szabo, J.M. Wardlaw, S. Schwab, and H.Y.P.i. Euro, EuroHYP-1: European multicenter, randomized, phase III clinical trial of therapeutic

hypothermia plus best medical treatment vs. best medical treatment alone for acute ischemic stroke. Int J Stroke, 2014. **9**(5): p. 642-5.

40.   Polderman, K.H., Mechanisms of action, physiological effects, and complications of hypothermia. Crit Care Med, 2009. **37**(7 Suppl): p. S186-202.

41.   Burns, T.C., C.M. Verfaillie, and W.C. Low, Stem cells for ischemic brain injury: a critical review. J Comp Neurol, 2009. **515**(1): p. 125-44.

42.   Weissman, I.L., Stem cells: units of development, units of regeneration, and units in evolution. Cell, 2000. **100**(1): p. 157-68.

43.   Wagers, A.J. and I.L. Weissman, Plasticity of adult stem cells. Cell, 2004. **116**(5): p. 639-48.

44.   Takahashi, K. and S. Yamanaka, Induction of pluripotent stem cells from mouse embryonic and adult fibroblast cultures by defined factors. Cell, 2006. **126**(4): p. 663-76.

45.   Takahashi, K., K. Tanabe, M. Ohnuki, M. Narita, T. Ichisaka, K. Tomoda, and S. Yamanaka, Induction of pluripotent stem cells from adult human fibroblasts by defined factors. Cell, 2007. **131**(5): p. 861-872.

46.   Liu, Z., Y. Tang, S. Lu, J. Zhou, Z. Du, C. Duan, Z. Li, and C. Wang, The tumourigenicity of iPS cells and their differentiated derivates. J Cell Mol Med, 2013. **17**(6): p. 782-91.

47.   Lundberg, C., A. Martinez-Serrano, E. Cattaneo, R.D. McKay, and A. Bjorklund, Survival, integration, and differentiation of neural stem cell lines after transplantation to the adult rat striatum. Exp Neurol, 1997. **145**(2 Pt 1): p. 342-60.

48.   Liu, S., Y. Qu, T.J. Stewart, M.J. Howard, S. Chakrabortty, T.F. Holekamp, and J.W. McDonald, Embryonic stem cells differentiate into

oligodendrocytes and myelinate in culture and after spinal cord transplantation. Proc Natl Acad Sci U S A, 2000. **97**(11): p. 6126-31.

49.   Johansson, C.B., S. Momma, D.L. Clarke, M. Risling, U. Lendahl, and J. Frisen, Identification of a neural stem cell in the adult mammalian central nervous system. Cell, 1999. **96**(1): p. 25-34.

50.   Reynolds, B.A. and S. Weiss, Generation of neurons and astrocytes from isolated cells of the adult mammalian central nervous system. Science, 1992. **255**(5052): p. 1707-10.

51.   Mine, Y., J. Tatarishvili, K. Oki, E. Monni, Z. Kokaia, and O. Lindvall, Grafted human neural stem cells enhance several steps of endogenous neurogenesis and improve behavioral recovery after middle cerebral artery occlusion in rats. Neurobiol Dis, 2013. **52**: p. 191-203.

52.   McLaren, A., Ethical and social considerations of stem cell research. Nature, 2001. **414**(6859): p. 129-31.

53.   Nunes, M.C., N.S. Roy, H.M. Keyoung, R.R. Goodman, G. McKhann, 2nd, L. Jiang, J. Kang, M. Nedergaard, and S.A. Goldman, Identification and isolation of multipotential neural progenitor cells from the subcortical white matter of the adult human brain. Nat Med, 2003. **9**(4): p. 439-47.

54.   Tornero, D., S. Wattananit, M. Gronning Madsen, P. Koch, J. Wood, J. Tatarishvili, Y. Mine, R. Ge, E. Monni, K. Devaraju, R.F. Hevner, O. Brustle, O. Lindvall, and Z. Kokaia, Human induced pluripotent stem cell-derived cortical neurons integrate in stroke-injured cortex and improve functional recovery. Brain, 2013. **136**(Pt 12): p. 3561-77.

55.   Oki, K., J. Tatarishvili, J. Wood, P. Koch, S. Wattananit, Y. Mine, E. Monni, D. Tornero, H. Ahlenius, J. Ladewig, O. Brustle, O. Lindvall, and Z. Kokaia, Human-induced pluripotent stem cells form functional

neurons and improve recovery after grafting in stroke-damaged brain. Stem Cells, 2012. **30**(6): p. 1120-33.

56. Leong, W.K., T.L. Henshall, A. Arthur, K.L. Kremer, M.D. Lewis, S.C. Helps, J. Field, M.A. Hamilton-Bruce, S. Warming, J. Manavis, R. Vink, S. Gronthos, and S.A. Koblar, Human adult dental pulp stem cells enhance poststroke functional recovery through non-neural replacement mechanisms. Stem Cells Transl Med, 2012. **1**(3): p. 177-87.

57. Gutierrez-Fernandez, M., B. Rodriguez-Frutos, J. Ramos-Cejudo, M. Teresa Vallejo-Cremades, B. Fuentes, S. Cerdan, and E. Diez-Tejedor, Effects of intravenous administration of allogenic bone marrow- and adipose tissue-derived mesenchymal stem cells on functional recovery and brain repair markers in experimental ischemic stroke. Stem Cell Res Ther, 2013. **4**(1): p. 11.

58. Shyu, W.C., S.Z. Lin, M.F. Chiang, C.Y. Su, and H. Li, Intracerebral peripheral blood stem cell (CD34+) implantation induces neuroplasticity by enhancing beta1 integrin-mediated angiogenesis in chronic stroke rats. J Neurosci, 2006. **26**(13): p. 3444-53.

59. Taguchi, A., T. Soma, H. Tanaka, T. Kanda, H. Nishimura, H. Yoshikawa, Y. Tsukamoto, H. Iso, Y. Fujimori, D.M. Stern, H. Naritomi, and T. Matsuyama, Administration of CD34+ cells after stroke enhances neurogenesis via angiogenesis in a mouse model. J Clin Invest, 2004. **114**(3): p. 330-8.

60. Nakano-Doi, A., T. Nakagomi, M. Fujikawa, N. Nakagomi, S. Kubo, S. Lu, H. Yoshikawa, T. Soma, A. Taguchi, and T. Matsuyama, Bone marrow mononuclear cells promote proliferation of endogenous neural

stem cells through vascular niches after cerebral infarction. Stem Cells, 2010. **28**(7): p. 1292-302.

61.   Martens, W., E. Wolfs, T. Struys, C. Politis, A. Bronckaers, and I. Lambrichts, Expression pattern of basal markers in human dental pulp stem cells and tissue. Cells Tissues Organs, 2012. **196**(6): p. 490-500.

62.   Fujimura, J., R. Ogawa, H. Mizuno, Y. Fukunaga, and H. Suzuki, Neural differentiation of adipose-derived stem cells isolated from GFP transgenic mice. Biochem Biophys Res Commun, 2005. **333**(1): p. 116-21.

63.   Gervois, P., T. Struys, P. Hilkens, A. Bronckaers, J. Ratajczak, C. Politis, B. Brone, I. Lambrichts, and W. Martens, Neurogenic maturation of human dental pulp stem cells following neurosphere generation induces morphological and electrophysiological characteristics of functional neurons. Stem Cells Dev, 2015. **24**(3): p. 296-311.

64.   Bederson, J.B., L.H. Pitts, M. Tsuji, M.C. Nishimura, R.L. Davis, and H. Bartkowski, Rat middle cerebral artery occlusion: evaluation of the model and development of a neurologic examination. Stroke, 1986. **17**(3): p. 472-6.

65.   Bacigaluppi, M., G. Comi, and D.M. Hermann, Animal models of ischemic stroke. Part two: modeling cerebral ischemia. Open Neurol J, 2010. **4**: p. 34-8.

66.   Chen, S.T., C.Y. Hsu, E.L. Hogan, H. Maricq, and J.D. Balentine, A model of focal ischemic stroke in the rat: reproducible extensive cortical infarction. Stroke, 1986. **17**(4): p. 738-43.

67.   Egashira, Y., S. Sugitani, Y. Suzuki, K. Mishiro, K. Tsuruma, M. Shimazawa, S. Yoshimura, T. Iwama, and H. Hara, The conditioned medium of murine and human adipose-derived stem cells exerts

neuroprotective effects against experimental stroke model*. Brain Res, 2012. **1461**: p. 87-95.

68.   Mead, B., A. Logan, M. Berry, W. Leadbeater, and B.A. Scheven, *Paracrine-mediated neuroprotection and neuritogenesis of axotomised retinal ganglion cells by human dental pulp stem cells: comparison with human bone marrow and adipose-derived mesenchymal stem cells*. PLoS One, 2014. **9**(10): p. e109305.

69.   Scheibe, F., O. Klein, J. Klose, and J. Priller, *Mesenchymal stromal cells rescue cortical neurons from apoptotic cell death in an in vitro model of cerebral ischemia*. Cell Mol Neurobiol, 2012. **32**(4): p. 567-76.

70.   Eriksson, P.S., E. Perfilieva, T. Bjork-Eriksson, A.M. Alborn, C. Nordborg, D.A. Peterson, and F.H. Gage, *Neurogenesis in the adult human hippocampus*. Nat Med, 1998. **4**(11): p. 1313-7.

71.   Reumers, V., C.M. Deroose, O. Krylyshkina, J. Nuyts, M. Geraerts, L. Mortelmans, R. Gijsbers, C. Van den Haute, Z. Debyser, and V. Baekelandt, *Noninvasive and quantitative monitoring of adult neuronal stem cell migration in mouse brain using bioluminescence imaging*. Stem Cells, 2008. **26**(9): p. 2382-90.

72.   Arvidsson, A., T. Collin, D. Kirik, Z. Kokaia, and O. Lindvall, *Neuronal replacement from endogenous precursors in the adult brain after stroke*. Nat Med, 2002. **8**(9): p. 963-70.

73.   Thored, P., A. Arvidsson, E. Cacci, H. Ahlenius, T. Kallur, V. Darsalia, C.T. Ekdahl, Z. Kokaia, and O. Lindvall, *Persistent production of neurons from adult brain stem cells during recovery after stroke*. Stem Cells, 2006. **24**(3): p. 739-47.

74. Espuny-Camacho, I., K.A. Michelsen, D. Gall, D. Linaro, A. Hasche, J. Bonnefont, C. Bali, D. Orduz, A. Bilheu, A. Herpoel, N. Lambert, N. Gaspard, S. Peron, S.N. Schiffmann, M. Giugliano, A. Gaillard, and P. Vanderhaeghen, *Pyramidal neurons derived from human pluripotent stem cells integrate efficiently into mouse brain circuits in vivo.* Neuron, 2013. **77**(3): p. 440-56.

75. Arthur, A., S. Shi, A.C. Zannettino, N. Fujii, S. Gronthos, and S.A. Koblar, *Implanted adult human dental pulp stem cells induce endogenous axon guidance.* Stem Cells, 2009. **27**(9): p. 2229-37.

76. Bronckaers, A., P. Hilkens, W. Martens, P. Gervois, J. Ratajczak, T. Struys, and I. Lambrichts, *Mesenchymal stem/stromal cells as a pharmacological and therapeutic approach to accelerate angiogenesis.* Pharmacol Ther, 2014. **143**(2): p. 181-96.

77. Hilkens, P., Y. Fanton, W. Martens, P. Gervois, T. Struys, C. Politis, I. Lambrichts, and A. Bronckaers, *Pro-angiogenic impact of dental stem cells in vitro and in vivo.* Stem Cell Res, 2014. **12**(3): p. 778-90.

78. Kusuma, S., Y.I. Shen, D. Hanjaya-Putra, P. Mali, L. Cheng, and S. Gerecht, *Self-organized vascular networks from human pluripotent stem cells in a synthetic matrix.* Proc Natl Acad Sci U S A, 2013. **110**(31): p. 12601-6.

79. Pierdomenico, L., L. Bonsi, M. Calvitti, D. Rondelli, M. Arpinati, G. Chirumbolo, E. Becchetti, C. Marchionni, F. Alviano, V. Fossati, N. Staffolani, M. Franchina, A. Grossi, and G.P. Bagnara, *Multipotent mesenchymal stem cells with immunosuppressive activity can be easily isolated from dental pulp.* Transplantation, 2005. **80**(6): p. 836-42.

80. Uccelli, A., L. Moretta, and V. Pistoia, Mesenchymal stem cells in health and disease. Nat Rev Immunol, 2008. **8**(9): p. 726-36.

81. Scheibe, F., J. Ladhoff, J. Huck, M. Grohmann, K. Blazej, A. Oersal, N. Baeva, M. Seifert, and J. Priller, Immune effects of mesenchymal stromal cells in experimental stroke. J Cereb Blood Flow Metab, 2012. **32**(8): p. 1578-88.

82. Friedenstein, A.J., R.K. Chailakhjan, and K.S. Lalykina, The development of fibroblast colonies in monolayer cultures of guinea-pig bone marrow and spleen cells. Cell Tissue Kinet, 1970. **3**(4): p. 393-403.

83. Pittenger, M.F., A.M. Mackay, S.C. Beck, R.K. Jaiswal, R. Douglas, J.D. Mosca, M.A. Moorman, D.W. Simonetti, S. Craig, and D.R. Marshak, Multilineage potential of adult human mesenchymal stem cells. Science, 1999. **284**(5411): p. 143-7.

84. Zuk, P.A., M. Zhu, P. Ashjian, D.A. De Ugarte, J.I. Huang, H. Mizuno, Z.C. Alfonso, J.K. Fraser, P. Benhaim, and M.H. Hedrick, Human adipose tissue is a source of multipotent stem cells. Mol Biol Cell, 2002. **13**(12): p. 4279-95.

85. Gronthos, S., M. Mankani, J. Brahim, P.G. Robey, and S. Shi, Postnatal human dental pulp stem cells (DPSCs) in vitro and in vivo. Proc Natl Acad Sci U S A, 2000. **97**(25): p. 13625-30.

86. Weiss, M.L., S. Medicetty, A.R. Bledsoe, R.S. Rachakatla, M. Choi, S. Merchav, Y. Luo, M.S. Rao, G. Velagaleti, and D. Troyer, Human umbilical cord matrix stem cells: preliminary characterization and effect of transplantation in a rodent model of Parkinson's disease. Stem Cells, 2006. **24**(3): p. 781-92.

87. Erices, A., P. Conget, and J.J. Minguell, Mesenchymal progenitor cells in human umbilical cord blood. Br J Haematol, 2000. **109**(1): p. 235-42.

88. Miura, M., S. Gronthos, M. Zhao, B. Lu, L.W. Fisher, P.G. Robey, and S. Shi, SHED: stem cells from human exfoliated deciduous teeth. Proc Natl Acad Sci U S A, 2003. **100**(10): p. 5807-12.

89. Lee, K.D., T.K. Kuo, J. Whang-Peng, Y.F. Chung, C.T. Lin, S.H. Chou, J.R. Chen, Y.P. Chen, and O.K. Lee, In vitro hepatic differentiation of human mesenchymal stem cells. Hepatology, 2004. **40**(6): p. 1275-84.

90. Toma, C., M.F. Pittenger, K.S. Cahill, B.J. Byrne, and P.D. Kessler, Human mesenchymal stem cells differentiate to a cardiomyocyte phenotype in the adult murine heart. Circulation, 2002. **105**(1): p. 93-8.

91. Wislet-Gendebien, S., G. Hans, P. Leprince, J.M. Rigo, G. Moonen, and B. Rogister, Plasticity of cultured mesenchymal stem cells: switch from nestin-positive to excitable neuron-like phenotype. Stem Cells, 2005. **23**(3): p. 392-402.

92. Hilkens, P., P. Gervois, Y. Fanton, J. Vanormelingen, W. Martens, T. Struys, C. Politis, I. Lambrichts, and A. Bronckaers, Effect of isolation methodology on stem cell properties and multilineage differentiation potential of human dental pulp stem cells. Cell Tissue Res, 2013. **353**(1): p. 65-78.

93. Dominici, M., K. Le Blanc, I. Mueller, I. Slaper-Cortenbach, F. Marini, D. Krause, R. Deans, A. Keating, D. Prockop, and E. Horwitz, Minimal criteria for defining multipotent mesenchymal stromal cells. The International Society for Cellular Therapy position statement. Cytotherapy, 2006. **8**(4): p. 315-7.

94.   Kaiser, S., B. Hackanson, M. Follo, A. Mehlhorn, K. Geiger, G. Ihorst, and U. Kapp, BM cells giving rise to MSC in culture have a heterogeneous CD34 and CD45 phenotype. Cytotherapy, 2007. **9**(5): p. 439-50.

95.   Struys, T., M. Moreels, W. Martens, R. Donders, E. Wolfs, and I. Lambrichts, Ultrastructural and immunocytochemical analysis of multilineage differentiated human dental pulp- and umbilical cord-derived mesenchymal stem cells. Cells Tissues Organs, 2011. **193**(6): p. 366-78.

96.   Anghileri, E., S. Marconi, A. Pignatelli, P. Cifelli, M. Galie, A. Sbarbati, M. Krampera, O. Belluzzi, and B. Bonetti, Neuronal differentiation potential of human adipose-derived mesenchymal stem cells. Stem Cells Dev, 2008. **17**(5): p. 909-16.

97.   Yang, H., Z. Xie, L. Wei, H. Yang, S. Yang, Z. Zhu, P. Wang, C. Zhao, and J. Bi, Human umbilical cord mesenchymal stem cell-derived neuron-like cells rescue memory deficits and reduce amyloid-beta deposition in an AbetaPP/PS1 transgenic mouse model. Stem Cell Res Ther, 2013. **4**(4): p. 76.

98.   Kiraly, M., B. Porcsalmy, A. Pataki, K. Kadar, M. Jelitai, B. Molnar, P. Hermann, I. Gera, W.D. Grimm, B. Ganss, A. Zsembery, and G. Varga, Simultaneous PKC and cAMP activation induces differentiation of human dental pulp stem cells into functionally active neurons. Neurochem Int, 2009. **55**(5): p. 323-32.

99.   Hau, S., D.M. Reich, M. Scholz, W. Naumann, F. Emmrich, M. Kamprad, and J. Boltze, Evidence for neuroprotective properties of human

umbilical cord blood cells after neuronal hypoxia in vitro. BMC Neurosci, 2008. **9**: p. 30.

100. Liu, Y., Y. Zhang, L. Lin, F. Lin, T. Li, H. Du, R. Chen, W. Zheng, and N. Liu, Effects of bone marrow-derived mesenchymal stem cells on the axonal outgrowth through activation of PI3K/AKT signaling in primary cortical neurons followed oxygen-glucose deprivation injury. PLoS One, 2013. **8**(11): p. e78514.

101. Crigler, L., R.C. Robey, A. Asawachaicharn, D. Gaupp, and D.G. Phinney, Human mesenchymal stem cell subpopulations express a variety of neuro-regulatory molecules and promote neuronal cell survival and neuritogenesis. Exp Neurol, 2006. **198**(1): p. 54-64.

102. Kingham, P.J., M.K. Kolar, L.N. Novikova, L.N. Novikov, and M. Wiberg, Stimulating the neurotrophic and angiogenic properties of human adipose-derived stem cells enhances nerve repair. Stem Cells Dev, 2014. **23**(7): p. 741-54.

103. Wilkins, A., K. Kemp, M. Ginty, K. Hares, E. Mallam, and N. Scolding, Human bone marrow-derived mesenchymal stem cells secrete brain-derived neurotrophic factor which promotes neuronal survival in vitro. Stem Cell Res, 2009. **3**(1): p. 63-70.

104. Nosrat, I.V., C.A. Smith, P. Mullally, L. Olson, and C.A. Nosrat, Dental pulp cells provide neurotrophic support for dopaminergic neurons and differentiate into neurons in vitro; implications for tissue engineering and repair in the nervous system. Eur J Neurosci, 2004. **19**(9): p. 2388-98.

105. Gervois, P., T. Struys, P. Hilkens, A. Bronckaers, J. Ratajczak, C. Politis, B. Brone, I. Lambrichts, and W. Martens, Neurogenic Maturation of Human Dental Pulp Stem Cells Following Neurosphere Generation

Induces Morphological and Electrophysiological Characteristics of Functional Neurons. Stem Cells Dev, 2014.

106. Martens, W., K. Sanen, M. Georgiou, T. Struys, A. Bronckaers, M. Ameloot, J. Phillips, and I. Lambrichts, Human dental pulp stem cells can differentiate into Schwann cells and promote and guide neurite outgrowth in an aligned tissue-engineered collagen construct in vitro. FASEB J, 2014. **28**(4): p. 1634-43.

107. Choi, M., H.S. Lee, P. Naidansaren, H.K. Kim, E. O, J.H. Cha, H.Y. Ahn, P.I. Yang, J.C. Shin, and Y.A. Joe, Proangiogenic features of Wharton's jelly-derived mesenchymal stromal/stem cells and their ability to form functional vessels. Int J Biochem Cell Biol, 2013. **45**(3): p. 560-70.

108. Bronckaers, A., P. Hilkens, Y. Fanton, T. Struys, P. Gervois, C. Politis, W. Martens, and I. Lambrichts, Angiogenic properties of human dental pulp stem cells. PLoS One, 2013. **8**(8): p. e71104.

109. Hung, S.C., R.R. Pochampally, S.C. Chen, S.C. Hsu, and D.J. Prockop, Angiogenic effects of human multipotent stromal cell conditioned medium activate the PI3K-Akt pathway in hypoxic endothelial cells to inhibit apoptosis, increase survival, and stimulate angiogenesis. Stem Cells, 2007. **25**(9): p. 2363-70.

110. Schaar, K.L., M.M. Brenneman, and S.I. Savitz, Functional assessments in the rodent stroke model. Exp Transl Stroke Med, 2010. **2**(1): p. 13.

111. Balkaya, M., J.M. Krober, A. Rex, and M. Endres, Assessing post-stroke behavior in mouse models of focal ischemia. J Cereb Blood Flow Metab, 2013. **33**(3): p. 330-8.

112. Toyoshima, A., T. Yasuhara, M. Kameda, J. Morimoto, H. Takeuchi, F. Wang, T. Sasaki, S. Sasada, A. Shinko, T. Wakamori, M. Okazaki, A.

Kondo, T. Agari, C.V. Borlongan, and I. Date, *Intra-Arterial Transplantation of Allogeneic Mesenchymal Stem Cells Mounts Neuroprotective Effects in a Transient Ischemic Stroke Model in Rats: Analyses of Therapeutic Time Window and Its Mechanisms.* PLoS One, 2015. **10**(6): p. e0127302.

113.   Ishizaka, S., N. Horie, K. Satoh, Y. Fukuda, N. Nishida, and I. Nagata, *Intra-arterial cell transplantation provides timing-dependent cell distribution and functional recovery after stroke.* Stroke, 2013. **44**(3): p. 720-6.

114.   Doeppner, T.R., J. Herz, A. Gorgens, J. Schlechter, A.K. Ludwig, S. Radtke, K. de Miroschedji, P.A. Horn, B. Giebel, and D.M. Hermann, *Extracellular Vesicles Improve Post-Stroke Neuroregeneration and Prevent Postischemic Immunosuppression.* Stem Cells Transl Med, 2015. **4**(10): p. 1131-43.

115.   Liao, W., J. Xie, J. Zhong, Y. Liu, L. Du, B. Zhou, J. Xu, P. Liu, S. Yang, J. Wang, Z. Han, and Z.C. Han, *Therapeutic effect of human umbilical cord multipotent mesenchymal stromal cells in a rat model of stroke.* Transplantation, 2009. **87**(3): p. 350-9.

116.   Jiang, W., G. Liang, X. Li, Z. Li, X. Gao, S. Feng, X. Wang, M. Liu, and Y. Liu, *Intracarotid transplantation of autologous adipose-derived mesenchymal stem cells significantly improves neurological deficits in rats after MCAo.* J Mater Sci Mater Med, 2014. **25**(5): p. 1357-66.

117.   Leu, S., Y.C. Lin, C.M. Yuen, C.H. Yen, Y.H. Kao, C.K. Sun, and H.K. Yip, *Adipose-derived mesenchymal stem cells markedly attenuate brain infarct size and improve neurological function in rats.* J Transl Med, 2010. **8**: p. 63.

118.   Lee, S.H., K.S. Jin, O.Y. Bang, B.J. Kim, S.J. Park, N.H. Lee, K.H. Yoo, H.H. Koo, and K.W. Sung, Differential Migration of Mesenchymal Stem Cells to Ischemic Regions after Middle Cerebral Artery Occlusion in Rats. PLoS One, 2015. **10**(8): p. e0134920.

119.   Walczak, P., J. Zhang, A.A. Gilad, D.A. Kedziorek, J. Ruiz-Cabello, R.G. Young, M.F. Pittenger, P.C. van Zijl, J. Huang, and J.W. Bulte, Dual-modality monitoring of targeted intraarterial delivery of mesenchymal stem cells after transient ischemia. Stroke, 2008. **39**(5): p. 1569-74.

120.   Mitkari, B., E. Kerkela, J. Nystedt, M. Korhonen, V. Mikkonen, T. Huhtala, and J. Jolkkonen, Intra-arterial infusion of human bone marrow-derived mesenchymal stem cells results in transient localization in the brain after cerebral ischemia in rats. Exp Neurol, 2013. **239**: p. 158-62.

121.   Detante, O., A. Moisan, J. Dimastromatteo, M.J. Richard, L. Riou, E. Grillon, E. Barbier, M.D. Desruet, F. De Fraipont, C. Segebarth, A. Jaillard, M. Hommel, C. Ghezzi, and C. Remy, Intravenous administration of 99mTc-HMPAO-labeled human mesenchymal stem cells after stroke: in vivo imaging and biodistribution. Cell Transplant, 2009. **18**(12): p. 1369-79.

122.   Lin, Y.C., T.L. Ko, Y.H. Shih, M.Y. Lin, T.W. Fu, H.S. Hsiao, J.Y. Hsu, and Y.S. Fu, Human umbilical mesenchymal stem cells promote recovery after ischemic stroke. Stroke, 2011. **42**(7): p. 2045-53.

123.   Zhang, L., L. Yi, M. Chopp, B.C. Kramer, M. Romanko, A. Gosiewska, and K. Hong, Intravenous administration of human umbilical tissue-derived cells improves neurological function in aged rats after embolic stroke. Cell Transplant, 2013. **22**(9): p. 1569-76.

124. Balseanu, A.T., A.M. Buga, B. Catalin, D.C. Wagner, J. Boltze, A.M. Zagrean, K. Reymann, W. Schaebitz, and A. Popa-Wagner, *Multimodal Approaches for Regenerative Stroke Therapies: Combination of Granulocyte Colony-Stimulating Factor with Bone Marrow Mesenchymal Stem Cells is Not Superior to G-CSF Alone.* Front Aging Neurosci, 2014. **6**: p. 130.

125. Zhao, L.R., W.M. Duan, M. Reyes, C.D. Keene, C.M. Verfaillie, and W.C. Low, *Human bone marrow stem cells exhibit neural phenotypes and ameliorate neurological deficits after grafting into the ischemic brain of rats.* Exp Neurol, 2002. **174**(1): p. 11-20.

126. Yasuhara, T., N. Matsukawa, K. Hara, M. Maki, M.M. Ali, S.J. Yu, E. Bae, G. Yu, L. Xu, M. McGrogan, K. Bankiewicz, C. Case, and C.V. Borlongan, *Notch-induced rat and human bone marrow stromal cell grafts reduce ischemic cell loss and ameliorate behavioral deficits in chronic stroke animals.* Stem Cells Dev, 2009. **18**(10): p. 1501-14.

127. Kubis, N., Y. Tomita, A. Tran-Dinh, V. Planat-Benard, M. Andre, B. Karaszewski, L. Waeckel, L. Penicaud, J.S. Silvestre, L. Casteilla, J. Seylaz, and E. Pinard, *Vascular fate of adipose tissue-derived adult stromal cells in the ischemic murine brain: A combined imaging-histological study.* Neuroimage, 2007. **34**(1): p. 1-11.

128. Zhou, F., S. Gao, L. Wang, C. Sun, L. Chen, P. Yuan, H. Zhao, Y. Yi, Y. Qin, Z. Dong, L. Cao, H. Ren, L. Zhu, Q. Li, B. Lu, A. Liang, G.T. Xu, H. Zhu, Z. Gao, J. Ma, J. Xu, and X. Chen, *Human adipose-derived stem cells partially rescue the stroke syndromes by promoting spatial learning and memory in mouse middle cerebral artery occlusion model.* Stem Cell Res Ther, 2015. **6**: p. 92.

129.   Wei, N., S.P. Yu, X. Gu, T.M. Taylor, D. Song, X.F. Liu, and L. Wei, Delayed intranasal delivery of hypoxic-preconditioned bone marrow mesenchymal stem cells enhanced cell homing and therapeutic benefits after ischemic stroke in mice. Cell Transplant, 2013. **22**(6): p. 977-91.

130.   Shen, L.H., Y. Li, J. Chen, Y. Cui, C. Zhang, A. Kapke, M. Lu, S. Savant-Bhonsale, and M. Chopp, One-year follow-up after bone marrow stromal cell treatment in middle-aged female rats with stroke. Stroke, 2007. **38**(7): p. 2150-6.

131.   Shen, L.H., Y. Li, J. Chen, J. Zhang, P. Vanguri, J. Borneman, and M. Chopp, Intracarotid transplantation of bone marrow stromal cells increases axon-myelin remodeling after stroke. Neuroscience, 2006. **137**(2): p. 393-9.

132.   Wakabayashi, K., A. Nagai, A.M. Sheikh, Y. Shiota, D. Narantuya, T. Watanabe, J. Masuda, S. Kobayashi, S.U. Kim, and S. Yamaguchi, Transplantation of human mesenchymal stem cells promotes functional improvement and increased expression of neurotrophic factors in a rat focal cerebral ischemia model. J Neurosci Res, 2010. **88**(5): p. 1017-25.

133.   Ikegame, Y., K. Yamashita, S. Hayashi, H. Mizuno, M. Tawada, F. You, K. Yamada, Y. Tanaka, Y. Egashira, S. Nakashima, S. Yoshimura, and T. Iwama, Comparison of mesenchymal stem cells from adipose tissue and bone marrow for ischemic stroke therapy. Cytotherapy, 2011. **13**(6): p. 675-85.

134.   Taguchi, A., P. Zhu, F. Cao, A. Kikuchi-Taura, Y. Kasahara, D.M. Stern, T. Soma, T. Matsuyama, and R. Hata, Reduced ischemic brain injury by partial rejuvenation of bone marrow cells in aged rats. J Cereb Blood Flow Metab, 2011. **31**(3): p. 855-67.

135.   Acosta, S.A., N. Tajiri, J. Hoover, Y. Kaneko, and C.V. Borlongan, Intravenous Bone Marrow Stem Cell Grafts Preferentially Migrate to Spleen and Abrogate Chronic Inflammation in Stroke. Stroke, 2015. **46**(9): p. 2616-27.

136.   Liu, H., O. Honmou, K. Harada, K. Nakamura, K. Houkin, H. Hamada, and J.D. Kocsis, Neuroprotection by PlGF gene-modified human mesenchymal stem cells after cerebral ischaemia. Brain, 2006. **129**(Pt 10): p. 2734-45.

137.   Yu, X., D. Chen, Y. Zhang, X. Wu, Z. Huang, H. Zhou, Y. Zhang, and Z. Zhang, Overexpression of CXCR4 in mesenchymal stem cells promotes migration, neuroprotection and angiogenesis in a rat model of stroke. J Neurol Sci, 2012. **316**(1-2): p. 141-9.

138.   Shen, L.H., Y. Li, J. Chen, A. Zacharek, Q. Gao, A. Kapke, M. Lu, K. Raginski, P. Vanguri, A. Smith, and M. Chopp, Therapeutic benefit of bone marrow stromal cells administered 1 month after stroke. J Cereb Blood Flow Metab, 2007. **27**(1): p. 6-13.

139.   Gutierrez-Fernandez, M., B. Rodriguez-Frutos, J. Ramos-Cejudo, L. Otero-Ortega, B. Fuentes, M.T. Vallejo-Cremades, B.E. Sanz-Cuesta, and E. Diez-Tejedor, Comparison between xenogeneic and allogeneic adipose mesenchymal stem cells in the treatment of acute cerebral infarct: proof of concept in rats. J Transl Med, 2015. **13**: p. 46.

140.   Sonoyama, W., Y. Liu, T. Yamaza, R.S. Tuan, S. Wang, S. Shi, and G.T. Huang, Characterization of the apical papilla and its residing stem cells from human immature permanent teeth: a pilot study. J Endod, 2008. **34**(2): p. 166-71.

141. Seo, B.M., M. Miura, S. Gronthos, P.M. Bartold, S. Batouli, J. Brahim, M. Young, P.G. Robey, C.Y. Wang, and S. Shi, Investigation of multipotent postnatal stem cells from human periodontal ligament. Lancet, 2004. **364**(9429): p. 149-55.

142. Morsczeck, C., W. Gotz, J. Schierholz, F. Zeilhofer, U. Kuhn, C. Mohl, C. Sippel, and K.H. Hoffmann, Isolation of precursor cells (PCs) from human dental follicle of wisdom teeth. Matrix Biol, 2005. **24**(2): p. 155-65.

143. Ikeda, E., K. Yagi, M. Kojima, T. Yagyuu, A. Ohshima, S. Sobajima, M. Tadokoro, Y. Katsube, K. Isoda, M. Kondoh, M. Kawase, M.J. Go, H. Adachi, Y. Yokota, T. Kirita, and H. Ohgushi, Multipotent cells from the human third molar: feasibility of cell-based therapy for liver disease. Differentiation, 2008. **76**(5): p. 495-505.

144. Xiong, J., K. Mrozik, S. Gronthos, and P.M. Bartold, Epithelial cell rests of Malassez contain unique stem cell populations capable of undergoing epithelial-mesenchymal transition. Stem Cells Dev, 2012. **21**(11): p. 2012-25.

145. Zhang, Q., S. Shi, Y. Liu, J. Uyanne, Y. Shi, S. Shi, and A.D. Le, Mesenchymal stem cells derived from human gingiva are capable of immunomodulatory functions and ameliorate inflammation-related tissue destruction in experimental colitis. J Immunol, 2009. **183**(12): p. 7787-98.

146. Matsubara, T., K. Suardita, M. Ishii, M. Sugiyama, A. Igarashi, R. Oda, M. Nishimura, M. Saito, K. Nakagawa, K. Yamanaka, K. Miyazaki, M. Shimizu, U.K. Bhawal, K. Tsuji, K. Nakamura, and Y. Kato, Alveolar bone marrow as a cell source for regenerative medicine: differences between

alveolar and iliac bone marrow stromal cells. J Bone Miner Res, 2005. **20**(3): p. 399-409.

147. Silverio, K.G., T.L. Rodrigues, R.D. Coletta, L. Benevides, J.S. Da Silva, M.Z. Casati, E.A. Sallum, and F.H. Nociti, Jr., Mesenchymal stem cell properties of periodontal ligament cells from deciduous and permanent teeth. J Periodontol, 2010. **81**(8): p. 1207-15.

148. Liu, J., F. Yu, Y. Sun, B. Jiang, W. Zhang, J. Yang, G.T. Xu, A. Liang, and S. Liu, Concise reviews: Characteristics and potential applications of human dental tissue-derived mesenchymal stem cells. Stem Cells, 2015. **33**(3): p. 627-38.

149. Decup, F., N. Six, B. Palmier, D. Buch, J.J. Lasfargues, E. Salih, and M. Goldberg, Bone sialoprotein-induced reparative dentinogenesis in the pulp of rat's molar. Clin Oral Investig, 2000. **4**(2): p. 110-9.

150. Gronthos, S., J. Brahim, W. Li, L.W. Fisher, N. Cherman, A. Boyde, P. DenBesten, P.G. Robey, and S. Shi, Stem cell properties of human dental pulp stem cells. J Dent Res, 2002. **81**(8): p. 531-5.

151. Shi, S., P.G. Robey, and S. Gronthos, Comparison of human dental pulp and bone marrow stromal stem cells by cDNA microarray analysis. Bone, 2001. **29**(6): p. 532-9.

152. Sasaki, R., S. Aoki, M. Yamato, H. Uchiyama, K. Wada, T. Okano, and H. Ogiuchi, Neurosphere generation from dental pulp of adult rat incisor. Eur J Neurosci, 2008. **27**(3): p. 538-48.

153. Stevens, A., T. Zuliani, C. Olejnik, H. LeRoy, H. Obriot, J. Kerr-Conte, P. Formstecher, Y. Bailliez, and R.R. Polakowska, Human dental pulp stem cells differentiate into neural crest-derived melanocytes and have label-

retaining and sphere-forming abilities. Stem Cells Dev, 2008. **17**(6): p. 1175-84.

154.   Knecht, A.K. and M. Bronner-Fraser, Induction of the neural crest: a multigene process. Nat Rev Genet, 2002. **3**(6): p. 453-61.

155.   Arthur, A., G. Rychkov, S. Shi, S.A. Koblar, and S. Gronthos, Adult human dental pulp stem cells differentiate toward functionally active neurons under appropriate environmental cues. Stem Cells, 2008. **26**(7): p. 1787-95.

156.   Nosrat, I.V., J. Widenfalk, L. Olson, and C.A. Nosrat, Dental pulp cells produce neurotrophic factors, interact with trigeminal neurons in vitro, and rescue motoneurons after spinal cord injury. Dev Biol, 2001. **238**(1): p. 120-32.

157.   Apel, C., O.V. Forlenza, V.J. de Paula, L.L. Talib, B. Denecke, C.P. Eduardo, and W.F. Gattaz, The neuroprotective effect of dental pulp cells in models of Alzheimer's and Parkinson's disease. J Neural Transm, 2009. **116**(1): p. 71-8.

158.   Huang, A.H., B.R. Snyder, P.H. Cheng, and A.W. Chan, Putative dental pulp-derived stem/stromal cells promote proliferation and differentiation of endogenous neural cells in the hippocampus of mice. Stem Cells, 2008. **26**(10): p. 2654-63.

159.   Macrez, R., C. Ali, O. Toutirais, B. Le Mauff, G. Defer, U. Dirnagl, and D. Vivien, Stroke and the immune system: from pathophysiology to new therapeutic strategies. Lancet Neurol, 2011. **10**(5): p. 471-80.

160.   Liu, G.S., H.M. Peshavariya, M. Higuchi, E.C. Chan, G.J. Dusting, and F. Jiang, Pharmacological priming of adipose-derived stem cells for

paracrine VEGF production with deferoxamine. J Tissue Eng Regen Med, 2016. **10**(3): p. E167-76.

161.   Aranha, A.M., Z. Zhang, K.G. Neiva, C.A. Costa, J. Hebling, and J.E. Nor, Hypoxia enhances the angiogenic potential of human dental pulp cells. J Endod, 2010. **36**(10): p. 1633-7.

162.   Ahmed, N.E., M. Murakami, S. Kaneko, and M. Nakashima, The effects of hypoxia on the stemness properties of human dental pulp stem cells (DPSCs). Sci Rep, 2016. **6**: p. 35476.

163.   Muller, H.D., B. Cvikl, R. Gruber, G. Watzek, and H. Agis, Prolyl hydroxylase inhibitors increase the production of vascular endothelial growth factor in dental pulp-derived cells. J Endod, 2012. **38**(11): p. 1498-503.

164.   Kim, M.K., H.J. Park, Y.D. Kim, M.H. Ryu, T. Takata, S.K. Bae, and M.K. Bae, Hinokitiol increases the angiogenic potential of dental pulp cells through ERK and p38MAPK activation and hypoxia-inducible factor-1alpha (HIF-1alpha) upregulation. Arch Oral Biol, 2014. **59**(2): p. 102-10.

165.   Choukroun, J., A. Diss, A. Simonpieri, M.O. Girard, C. Schoeffler, S.L. Dohan, A.J. Dohan, J. Mouhyi, and D.M. Dohan, Platelet-rich fibrin (PRF): a second-generation platelet concentrate. Part IV: clinical effects on tissue healing. Oral Surg Oral Med Oral Pathol Oral Radiol Endod, 2006. **101**(3): p. e56-60.

166.   Dohan Ehrenfest, D.M., T. Bielecki, R. Jimbo, G. Barbe, M. Del Corso, F. Inchingolo, and G. Sammartino, Do the fibrin architecture and leukocyte content influence the growth factor release of platelet concentrates? An evidence-based answer comparing a pure platelet-rich plasma (P-PRP)

gel and a leukocyte- and platelet-rich fibrin (L-PRF)*. Curr Pharm Biotechnol, 2012. **13**(7): p. 1145-52.

167. Schar, M.O., J. Diaz-Romero, S. Kohl, M.A. Zumstein, and D. Nesic, *Platelet-rich concentrates differentially release growth factors and induce cell migration in vitro*. Clin Orthop Relat Res, 2015. **473**(5): p. 1635-43.

168. Huang, G.T., W. Sonoyama, J. Chen, and S.H. Park, *In vitro characterization of human dental pulp cells: various isolation methods and culturing environments*. Cell Tissue Res, 2006. **324**(2): p. 225-36.

169. Friedenstein, A.J., *Osteogenetic activity of transplanted transitional epithelium*. Acta Anat (Basel), 1961. **45**: p. 31-59.

170. Mitchell, K.E., M.L. Weiss, B.M. Mitchell, P. Martin, D. Davis, L. Morales, B. Helwig, M. Beerenstrauch, K. Abou-Easa, T. Hildreth, D. Troyer, and S. Medicetty, *Matrix cells from Wharton's jelly form neurons and glia*. Stem Cells, 2003. **21**(1): p. 50-60.

171. Zuk, P.A., M. Zhu, H. Mizuno, J. Huang, J.W. Futrell, A.J. Katz, P. Benhaim, H.P. Lorenz, and M.H. Hedrick, *Multilineage cells from human adipose tissue: implications for cell-based therapies*. Tissue Eng, 2001. **7**(2): p. 211-28.

172. Shi, S. and S. Gronthos, *Perivascular niche of postnatal mesenchymal stem cells in human bone marrow and dental pulp*. J Bone Miner Res, 2003. **18**(4): p. 696-704.

173. Frego, M., M. Bertin, A. Brolese, R. Ragazzi, C. Ruffolo, and D.F. D'Amico, *Endovascular treatment of acute pseudoaneurysm associated to pancreaticoduodenectomy*. Hepatogastroenterology, 2009. **56**(96): p. 1738-41.

References

174. Pellicelli, A.M., C. D'Ambrosio, R. Villani, G. Cerasari, P. Ialongo, A. Cortese, L.R. Grillo, and F. Soccorsi, Liver cirrhosis and rhino-orbital mucormycosis, a possible but rare association: description of a clinical case and literature review. Braz J Infect Dis, 2009. **13**(4): p. 314-6.

175. Huang, G.T., T. Yamaza, L.D. Shea, F. Djouad, N.Z. Kuhn, R.S. Tuan, and S. Shi, Stem/progenitor cell-mediated de novo regeneration of dental pulp with newly deposited continuous layer of dentin in an in vivo model. Tissue Eng Part A, 2010. **16**(2): p. 605-15.

176. Karaoz, E., P.C. Demircan, O. Saglam, A. Aksoy, F. Kaymaz, and G. Duruksu, Human dental pulp stem cells demonstrate better neural and epithelial stem cell properties than bone marrow-derived mesenchymal stem cells. Histochem Cell Biol, 2011. **136**(4): p. 455-73.

177. Roobrouck, V.D., F. Ulloa-Montoya, and C.M. Verfaillie, Self-renewal and differentiation capacity of young and aged stem cells. Exp Cell Res, 2008. **314**(9): p. 1937-44.

178. Nakashima, M., K. Iohara, and M. Sugiyama, Human dental pulp stem cells with highly angiogenic and neurogenic potential for possible use in pulp regeneration. Cytokine Growth Factor Rev, 2009. **20**(5-6): p. 435-40.

179. Tjwa, M., N. Sidenius, R. Moura, S. Jansen, K. Theunissen, A. Andolfo, M. De Mol, M. Dewerchin, L. Moons, F. Blasi, C. Verfaillie, and P. Carmeliet, Membrane-anchored uPAR regulates the proliferation, marrow pool size, engraftment, and mobilization of mouse hematopoietic stem/progenitor cells. J Clin Invest, 2009. **119**(4): p. 1008-18.

180. Zhang, W., X.F. Walboomers, S. Shi, M. Fan, and J.A. Jansen, Multilineage differentiation potential of stem cells derived from human

dental pulp after cryopreservation. Tissue Eng, 2006. **12**(10): p. 2813-23.

181.   Jing, W., J. Xiao, Z. Xiong, X. Yang, Y. Huang, M. Zhou, S. Chen, Y. Lin, and W. Tian, Explant culture: an efficient method to isolate adipose-derived stromal cells for tissue engineering. Artif Organs, 2011. **35**(2): p. 105-12.

182.   Wang, H.S., S.C. Hung, S.T. Peng, C.C. Huang, H.M. Wei, Y.J. Guo, Y.S. Fu, M.C. Lai, and C.C. Chen, Mesenchymal stem cells in the Wharton's jelly of the human umbilical cord. Stem Cells, 2004. **22**(7): p. 1330-7.

183.   Couble, M.L., J.C. Farges, F. Bleicher, B. Perrat-Mabillon, M. Boudeulle, and H. Magloire, Odontoblast differentiation of human dental pulp cells in explant cultures. Calcif Tissue Int, 2000. **66**(2): p. 129-38.

184.   Bakopoulou, A., G. Leyhausen, J. Volk, A. Tsiftsoglou, P. Garefis, P. Koidis, and W. Geurtsen, Assessment of the impact of two different isolation methods on the osteo/odontogenic differentiation potential of human dental stem cells derived from deciduous teeth. Calcif Tissue Int, 2011. **88**(2): p. 130-41.

185.   Abraham, R. and C.M. Verfaillie, Neural differentiation and support of neuroregeneration of non-neural adult stem cells. Prog Brain Res, 2012. **201**: p. 17-34.

186.   Gupta, S., C. Verfaillie, D. Chmielewski, S. Kren, K. Eidman, J. Connaire, Y. Heremans, T. Lund, M. Blackstad, Y. Jiang, A. Luttun, and M.E. Rosenberg, Isolation and characterization of kidney-derived stem cells. J Am Soc Nephrol, 2006. **17**(11): p. 3028-40.

187. Stanford, C.M., P.A. Jacobson, E.D. Eanes, L.A. Lembke, and R.J. Midura, Rapidly forming apatitic mineral in an osteoblastic cell line (UMR 106-01 BSP). J Biol Chem, 1995. **270**(16): p. 9420-8.

188. Bretschneider, A., W. Burns, and A. Morrison, "Pop-off" technic. The ultrastructure of paraffin-embedded sections. Am J Clin Pathol, 1981. **76**(4): p. 450-3.

189. Luo, M., Z. Liu, G. Chen, H. Hao, T. Lu, Y. Cui, M. Lei, C.M. Verfaillie, and Z. Liu, High glucose enhances TGF-beta1 expression in rat bone marrow stem cells via ERK1/2-mediated inhibition of STAT3 signaling. Life Sci, 2012. **90**(13-14): p. 509-18.

190. Luyckx, A., L. De Somer, S. Jacobs, O. Rutgeerts, C. Lenaerts, V.D. Roobrouck, C.M. Verfaillie, M. Waer, S.W. Van Gool, and A.D. Billiau, Oct4-negative multipotent adult progenitor cells and mesenchymal stem cells as regulators of T-cell alloreactivity in mice. Immunol Lett, 2011. **137**(1-2): p. 78-81.

191. Spath, L., V. Rotilio, M. Alessandrini, G. Gambara, L. De Angelis, M. Mancini, T.A. Mitsiadis, E. Vivarelli, F. Naro, A. Filippini, and G. Papaccio, Explant-derived human dental pulp stem cells enhance differentiation and proliferation potentials. J Cell Mol Med, 2010. **14**(6B): p. 1635-44.

192. Carinci, F., L. Lo Muzio, A. Piattelli, C. Rubini, F. Chiesa, F. Ionna, A. Palmieri, E. Maiorano, A. Pastore, G. Laino, M. Dolci, and F. Pezzetti, Potential markers of tongue tumor progression selected by cDNA microarray. Int J Immunopathol Pharmacol, 2005. **18**(3): p. 513-24.

193. Carinci, F., A. Piattelli, M. Degidi, A. Palmieri, V. Perrotti, L. Scapoli, M. Martinelli, G. Laino, and F. Pezzetti, Genetic effects of anorganic bovine

bone (Bio-Oss) on osteoblast-like MG63 cells. Arch Oral Biol, 2006. **51**(2): p. 154-63.

194. Caracino, V., G. D'Amico, R. Di Mizio, and F. D'Amario, Rare cases of bowel obstruction: internal hernias. Chir Ital, 2009. **61**(5-6): p. 617-21.

195. Genovesi, D., G.A. Cefaro, A. Vinciguerra, A. Augurio, M. D'Alessandro, V. Borzillo, R. Marchese, and M. Di Nicola, Retrospective long-term results and prognostic factors of postoperative treatment for UICC stages II and III rectal cancer. Tumori, 2009. **95**(6): p. 675-82.

196. Gagari, E., M.K. Rand, L. Tayari, H. Vastardis, P. Sharma, P.V. Hauschka, and P.D. Damoulis, Expression of stem cell factor and its receptor, c-kit, in human oral mesenchymal cells. Eur J Oral Sci, 2006. **114**(5): p. 409-15.

197. Laino, G., A. Graziano, R. d'Aquino, G. Pirozzi, V. Lanza, S. Valiante, A. De Rosa, F. Naro, E. Vivarelli, and G. Papaccio, An approachable human adult stem cell source for hard-tissue engineering. J Cell Physiol, 2006. **206**(3): p. 693-701.

198. Moore, E.G., A. D'Aleo, J. Xu, and K.N. Raymond, Eu(III) Complexes of Octadentate 1-Hydroxy-2-pyridinones: Stability and Improved Photophysical Performance[]. Aust J Chem, 2009. **62**(10): p. 1300-1307.

199. Karaoz, E., B.N. Dogan, A. Aksoy, G. Gacar, S. Akyuz, S. Ayhan, Z.S. Genc, S. Yuruker, G. Duruksu, P.C. Demircan, and A.E. Sariboyaci, Isolation and in vitro characterisation of dental pulp stem cells from natal teeth. Histochem Cell Biol, 2010. **133**(1): p. 95-112.

200. Laino, G., R. d'Aquino, A. Graziano, V. Lanza, F. Carinci, F. Naro, G. Pirozzi, and G. Papaccio, A new population of human adult dental pulp

stem cells: a useful source of living autologous fibrous bone tissue (LAB). J Bone Miner Res, 2005. **20**(8): p. 1394-402.

201. Iohara, K., L. Zheng, H. Wake, M. Ito, J. Nabekura, H. Wakita, H. Nakamura, T. Into, K. Matsushita, and M. Nakashima, A novel stem cell source for vasculogenesis in ischemia: subfraction of side population cells from dental pulp. Stem Cells, 2008. **26**(9): p. 2408-18.

202. Malone, A.M., C.T. Anderson, P. Tummala, R.Y. Kwon, T.R. Johnston, T. Stearns, and C.R. Jacobs, Primary cilia mediate mechanosensing in bone cells by a calcium-independent mechanism. Proc Natl Acad Sci U S A, 2007. **104**(33): p. 13325-30.

203. National Institute of Neurological Disorders and Stroke rt-PA Study Group. (1995). Tissue Plasminogen Activator for Acute Ischemic Stroke. New England Journal of Medicine. **333**(24): p. 1581-1588.

204. Nygaard, H.B., Current and emerging therapies for Alzheimer's disease. Clin Ther, 2013. **35**(10): p. 1480-9.

205. Waddington, R.J., S.J. Youde, C.P. Lee, and A.J. Sloan, Isolation of distinct progenitor stem cell populations from dental pulp. Cells Tissues Organs, 2009. **189**(1-4): p. 268-74.

206. Kiraly, M., K. Kadar, D.B. Horvathy, P. Nardai, G.Z. Racz, Z. Lacza, G. Varga, and G. Gerber, Integration of neuronally predifferentiated human dental pulp stem cells into rat brain in vivo. Neurochem Int, 2011. **59**(3): p. 371-81.

207. Sakai, K., A. Yamamoto, K. Matsubara, S. Nakamura, M. Naruse, M. Yamagata, K. Sakamoto, R. Tauchi, N. Wakao, S. Imagama, H. Hibi, K. Kadomatsu, N. Ishiguro, and M. Ueda, Human dental pulp-derived stem cells promote locomotor recovery after complete transection of the rat

spinal cord by multiple neuro-regenerative mechanisms. J Clin Invest, 2012. **122**(1): p. 80-90.

208. Yamamoto, A., K. Sakai, K. Matsubara, F. Kano, and M. Ueda, Multifaceted neuro-regenerative activities of human dental pulp stem cells for functional recovery after spinal cord injury. Neurosci Res, 2013.

209. Jensen, J.B. and M. Parmar, Strengths and limitations of the neurosphere culture system. Mol Neurobiol, 2006. **34**(3): p. 153-61.

210. Gritti, A., P. Frolichsthal-Schoeller, R. Galli, E.A. Parati, L. Cova, S.F. Pagano, C.R. Bjornson, and A.L. Vescovi, Epidermal and fibroblast growth factors behave as mitogenic regulators for a single multipotent stem cell-like population from the subventricular region of the adult mouse forebrain. J Neurosci, 1999. **19**(9): p. 3287-97.

211. Reynolds, B.A. and R.L. Rietze, Neural stem cells and neurospheres--re-evaluating the relationship. Nat Methods, 2005. **2**(5): p. 333-6.

212. Xiong, F., H. Gao, Y. Zhen, X. Chen, W. Lin, J. Shen, Y. Yan, X. Wang, M. Liu, and Y. Gao, Optimal time for passaging neurospheres based on primary neural stem cell cultures. Cytotechnology, 2011. **63**(6): p. 621-31.

213. Caldwell, M.A., X. He, N. Wilkie, S. Pollack, G. Marshall, K.A. Wafford, and C.N. Svendsen, Growth factors regulate the survival and fate of cells derived from human neurospheres. Nat Biotechnol, 2001. **19**(5): p. 475-9.

214. Morsczeck, C., F. Vollner, M. Saugspier, C. Brandl, T.E. Reichert, O. Driemel, and G. Schmalz, Comparison of human dental follicle cells (DFCs) and stem cells from human exfoliated deciduous teeth (SHED)

after neural differentiation in vitro. Clin Oral Investig, 2010. **14**(4): p. 433-40.

215.   Widera, D., W.D. Grimm, J.M. Moebius, I. Mikenberg, C. Piechaczek, G. Gassmann, N.A. Wolff, F. Thevenod, C. Kaltschmidt, and B. Kaltschmidt, Highly efficient neural differentiation of human somatic stem cells, isolated by minimally invasive periodontal surgery. Stem Cells Dev, 2007. **16**(3): p. 447-60.

216.   Osathanon, T., N. Nowwarote, and P. Pavasant, Basic fibroblast growth factor inhibits mineralization but induces neuronal differentiation by human dental pulp stem cells through a FGFR and PLCgamma signaling pathway. J Cell Biochem, 2011. **112**(7): p. 1807-16.

217.   Tatard, V.M., G. D'Ippolito, S. Diabira, A. Valeyev, J. Hackman, M. McCarthy, T. Bouckenooghe, P. Menei, C.N. Montero-Menei, and P.C. Schiller, Neurotrophin-directed differentiation of human adult marrow stromal cells to dopaminergic-like neurons. Bone, 2007. **40**(2): p. 360-73.

218.   Encinas, M., M. Iglesias, Y. Liu, H. Wang, A. Muhaisen, V. Cena, C. Gallego, and J.X. Comella, Sequential treatment of SH-SY5Y cells with retinoic acid and brain-derived neurotrophic factor gives rise to fully differentiated, neurotrophic factor-dependent, human neuron-like cells. J Neurochem, 2000. **75**(3): p. 991-1003.

219.   Constantinescu, R., A.T. Constantinescu, H. Reichmann, and B. Janetzky, Neuronal differentiation and long-term culture of the human neuroblastoma line SH-SY5Y. J Neural Transm Suppl, 2007(72): p. 17-28.

220. Seidenfaden, R., A. Krauter, and H. Hildebrandt, The neural cell adhesion molecule NCAM regulates neuritogenesis by multiple mechanisms of interaction. Neurochem Int, 2006. **49**(1): p. 1-11.

221. Rogers, D.A. and N.F. Schor, Kidins220/ARMS depletion is associated with the neural-to Schwann-like transition in a human neuroblastoma cell line model. Exp Cell Res, 2013. **319**(5): p. 660-9.

222. Gerhardt, L.C., K.L. Widdows, M.M. Erol, A. Nandakumar, I.S. Roqan, T. Ansari, and A.R. Boccaccini, Neocellularization and neovascularization of nanosized bioactive glass-coated decellularized trabecular bone scaffolds. J Biomed Mater Res A, 2013. **101**(3): p. 827-41.

223. Mikulowska-Mennis, A., T.B. Taylor, P. Vishnu, S.A. Michie, R. Raja, N. Horner, and S.T. Kunitake, High-quality RNA from cells isolated by laser capture microdissection. Biotechniques, 2002. **33**(1): p. 176-9.

224. Nourbakhsh, N., M. Soleimani, Z. Taghipour, K. Karbalaie, S.B. Mousavi, A. Talebi, F. Nadali, S. Tanhaei, G.A. Kiyani, M. Nematollahi, F. Rabiei, M. Mardani, H. Bahramiyan, M. Torabinejad, M.H. Nasr-Esfahani, and H. Baharvand, Induced in vitro differentiation of neural-like cells from human exfoliated deciduous teeth-derived stem cells. Int J Dev Biol, 2011. **55**(2): p. 189-95.

225. Hamill, O.P., A. Marty, E. Neher, B. Sakmann, and F.J. Sigworth, Improved patch-clamp techniques for high-resolution current recording from cells and cell-free membrane patches. Pflugers Arch, 1981. **391**(2): p. 85-100.

226. Schlett, K., A. Czirok, K. Tarnok, T. Vicsek, and E. Madarasz, Dynamics of cell aggregation during in vitro neurogenesis by immortalized neuroectodermal progenitors. J Neurosci Res, 2000. **60**(2): p. 184-94.

227.   Tarnok, K., A. Pataki, J. Kovacs, K. Schlett, and E. Madarasz, Stage-dependent effects of cell-to-cell connections on in vitro induced neurogenesis. Eur J Cell Biol, 2002. **81**(7): p. 403-12.

228.   Sharma, S.K. and A.B. Raj, Transient increase in intracellular concentration of adenosine 3':5'-cyclic monophosphate results in morphological and biochemical differentiation of C6 glioma cells in culture. J Neurosci Res, 1987. **17**(2): p. 135-41.

229.   Deng, W., M. Obrocka, I. Fischer, and D.J. Prockop, In vitro differentiation of human marrow stromal cells into early progenitors of neural cells by conditions that increase intracellular cyclic AMP. Biochem Biophys Res Commun, 2001. **282**(1): p. 148-52.

230.   Bez, A., E. Corsini, D. Curti, M. Biggiogera, A. Colombo, R.F. Nicosia, S.F. Pagano, and E.A. Parati, Neurosphere and neurosphere-forming cells: morphological and ultrastructural characterization. Brain Res, 2003. **993**(1-2): p. 18-29.

231.   Zhao, Y., T. Zhang, Q. Huang, A. Wang, J. Dong, Q. Lan, and Z. Qin, Ultrastructure of human neural stem/progenitor cells and neurospheres. Neural Regen Res, 2009. **4**(5): p. 365-370.

232.   Casper, K.B. and K.D. McCarthy, GFAP-positive progenitor cells produce neurons and oligodendrocytes throughout the CNS. Mol Cell Neurosci, 2006. **31**(4): p. 676-84.

233.   Naruse, M., K. Shibasaki, S. Yokoyama, M. Kurachi, and Y. Ishizaki, Dynamic changes of CD44 expression from progenitors to subpopulations of astrocytes and neurons in developing cerebellum. PLoS One, 2013. **8**(1): p. e53109.

234. Pruszak, J., W. Ludwig, A. Blak, K. Alavian, and O. Isacson, CD15, CD24, and CD29 define a surface biomarker code for neural lineage differentiation of stem cells. Stem Cells, 2009. **27**(12): p. 2928-40.

235. Castro, D.S., B. Martynoga, C. Parras, V. Ramesh, E. Pacary, C. Johnston, D. Drechsel, M. Lebel-Potter, L.G. Garcia, C. Hunt, D. Dolle, A. Bithell, L. Ettwiller, N. Buckley, and F. Guillemot, A novel function of the proneural factor Ascl1 in progenitor proliferation identified by genome-wide characterization of its targets. Genes Dev, 2011. **25**(9): p. 930-45.

236. Kim, E.J., J.L. Ables, L.K. Dickel, A.J. Eisch, and J.E. Johnson, Ascl1 (Mash1) defines cells with long-term neurogenic potential in subgranular and subventricular zones in adult mouse brain. PLoS One, 2011. **6**(3): p. e18472.

237. Kosari, F., C.M. Ida, M.C. Aubry, L. Yang, I.V. Kovtun, J.L. Klein, Y. Li, S. Erdogan, S.C. Tomaszek, S.J. Murphy, L.C. Bolette, C.P. Kolbert, P. Yang, D.A. Wigle, and G. Vasmatzis, ASCL1 and RET expression defines a clinically relevant subgroup of lung adenocarcinoma characterized by neuroendocrine differentiation. Oncogene, 2013.

238. Stein, R., N. Mori, K. Matthews, L.C. Lo, and D.J. Anderson, The NGF-inducible SCG10 mRNA encodes a novel membrane-bound protein present in growth cones and abundant in developing neurons. Neuron, 1988. **1**(6): p. 463-76.

239. Wuenschell, C.W., N. Mori, and D.J. Anderson, Analysis of SCG10 gene expression in transgenic mice reveals that neural specificity is achieved through selective derepression. Neuron, 1990. **4**(4): p. 595-602.

240. Saito, A., P. Narasimhan, T. Hayashi, S. Okuno, M. Ferrand-Drake, and P.H. Chan, Neuroprotective role of a proline-rich Akt substrate in

apoptotic neuronal cell death after stroke: relationships with nerve growth factor. J Neurosci, 2004. **24**(7): p. 1584-93.

241. McTigue, D.M., P.J. Horner, B.T. Stokes, and F.H. Gage, Neurotrophin-3 and brain-derived neurotrophic factor induce oligodendrocyte proliferation and myelination of regenerating axons in the contused adult rat spinal cord. J Neurosci, 1998. **18**(14): p. 5354-65.

242. Lindsay, R.M., Nerve growth factors (NGF, BDNF) enhance axonal regeneration but are not required for survival of adult sensory neurons. J Neurosci, 1988. **8**(7): p. 2394-405.

243. Ghosh, A., J. Carnahan, and M.E. Greenberg, Requirement for BDNF in activity-dependent survival of cortical neurons. Science, 1994. **263**(5153): p. 1618-23.

244. Wetmore, C., L. Olson, and A.J. Bean, Regulation of brain-derived neurotrophic factor (BDNF) expression and release from hippocampal neurons is mediated by non-NMDA type glutamate receptors. J Neurosci, 1994. **14**(3 Pt 2): p. 1688-700.

245. Balkowiec, A. and D.M. Katz, Cellular mechanisms regulating activity-dependent release of native brain-derived neurotrophic factor from hippocampal neurons. J Neurosci, 2002. **22**(23): p. 10399-407.

246. Hartmann, M., R. Heumann, and V. Lessmann, Synaptic secretion of BDNF after high-frequency stimulation of glutamatergic synapses. EMBO J, 2001. **20**(21): p. 5887-97.

247. Hock, C., K. Heese, C. Hulette, C. Rosenberg, and U. Otten, Region-specific neurotrophin imbalances in Alzheimer disease: decreased levels of brain-derived neurotrophic factor and increased levels of nerve growth

factor in hippocampus and cortical areas. Arch Neurol, 2000. **57**(6): p. 846-51.

248.   Phillips, H.S., J.M. Hains, M. Armanini, G.R. Laramee, S.A. Johnson, and J.W. Winslow, BDNF mRNA is decreased in the hippocampus of individuals with Alzheimer's disease. Neuron, 1991. **7**(5): p. 695-702.

249.   Ploughman, M., V. Windle, C.L. MacLellan, N. White, J.J. Dore, and D. Corbett, Brain-derived neurotrophic factor contributes to recovery of skilled reaching after focal ischemia in rats. Stroke, 2009. **40**(4): p. 1490-5.

250.   Schabitz, W.R., T. Steigleder, C.M. Cooper-Kuhn, S. Schwab, C. Sommer, A. Schneider, and H.G. Kuhn, Intravenous brain-derived neurotrophic factor enhances poststroke sensorimotor recovery and stimulates neurogenesis. Stroke, 2007. **38**(7): p. 2165-72.

251.   Scharfman, H.E., J.H. Goodman, A.L. Sollas, and S.D. Croll, Spontaneous limbic seizures after intrahippocampal infusion of brain-derived neurotrophic factor. Exp Neurol, 2002. **174**(2): p. 201-14.

252.   Ding, J., Y. Cheng, S. Gao, and J. Chen, Effects of nerve growth factor and Noggin-modified bone marrow stromal cells on stroke in rats. J Neurosci Res, 2011. **89**(2): p. 222-30.

253.   Barker, P.A., p75NTR is positively promiscuous: novel partners and new insights. Neuron, 2004. **42**(4): p. 529-33.

254.   Masoudi, R., M.S. Ioannou, M.D. Coughlin, P. Pagadala, K.E. Neet, O. Clewes, S.J. Allen, D. Dawbarn, and M. Fahnestock, Biological activity of nerve growth factor precursor is dependent upon relative levels of its receptors. J Biol Chem, 2009. **284**(27): p. 18424-33.

255. Storkebaum, E. and P. Carmeliet, VEGF: a critical player in neurodegeneration. J Clin Invest, 2004. **113**(1): p. 14-8.

256. Sun, Y., K. Jin, L. Xie, J. Childs, X.O. Mao, A. Logvinova, and D.A. Greenberg, VEGF-induced neuroprotection, neurogenesis, and angiogenesis after focal cerebral ischemia. J Clin Invest, 2003. **111**(12): p. 1843-51.

257. Jin, K., Y. Zhu, Y. Sun, X.O. Mao, L. Xie, and D.A. Greenberg, Vascular endothelial growth factor (VEGF) stimulates neurogenesis in vitro and in vivo. Proc Natl Acad Sci U S A, 2002. **99**(18): p. 11946-50.

258. Wang, Y., E. Kilic, U. Kilic, B. Weber, C.L. Bassetti, H.H. Marti, and D.M. Hermann, VEGF overexpression induces post-ischaemic neuroprotection, but facilitates haemodynamic steal phenomena. Brain, 2005. **128**(Pt 1): p. 52-63.

259. Lambrechts, D., E. Storkebaum, M. Morimoto, J. Del-Favero, F. Desmet, S.L. Marklund, S. Wyns, V. Thijs, J. Andersson, I. van Marion, A. Al-Chalabi, S. Bornes, R. Musson, V. Hansen, L. Beckman, R. Adolfsson, H.S. Pall, H. Prats, S. Vermeire, P. Rutgeerts, S. Katayama, T. Awata, N. Leigh, L. Lang-Lazdunski, M. Dewerchin, C. Shaw, L. Moons, R. Vlietinck, K.E. Morrison, W. Robberecht, C. Van Broeckhoven, D. Collen, P.M. Andersen, and P. Carmeliet, VEGF is a modifier of amyotrophic lateral sclerosis in mice and humans and protects motoneurons against ischemic death. Nat Genet, 2003. **34**(4): p. 383-94.

260. Lin, L.F., D.H. Doherty, J.D. Lile, S. Bektesh, and F. Collins, GDNF: a glial cell line-derived neurotrophic factor for midbrain dopaminergic neurons. Science, 1993. **260**(5111): p. 1130-2.

261. Choi-Lundberg, D.L., Q. Lin, Y.N. Chang, Y.L. Chiang, C.M. Hay, H. Mohajeri, B.L. Davidson, and M.C. Bohn, Dopaminergic neurons protected from degeneration by GDNF gene therapy. Science, 1997. **275**(5301): p. 838-41.

262. Beck, K.D., J. Valverde, T. Alexi, K. Poulsen, B. Moffat, R.A. Vandlen, A. Rosenthal, and F. Hefti, Mesencephalic dopaminergic neurons protected by GDNF from axotomy-induced degeneration in the adult brain. Nature, 1995. **373**(6512): p. 339-41.

263. Kordower, J.H., M.E. Emborg, J. Bloch, S.Y. Ma, Y. Chu, L. Leventhal, J. McBride, E.Y. Chen, S. Palfi, B.Z. Roitberg, W.D. Brown, J.E. Holden, R. Pyzalski, M.D. Taylor, P. Carvey, Z. Ling, D. Trono, P. Hantraye, N. Deglon, and P. Aebischer, Neurodegeneration prevented by lentiviral vector delivery of GDNF in primate models of Parkinson's disease. Science, 2000. **290**(5492): p. 767-73.

264. Palay, S.L. and G.E. Palade, The fine structure of neurons. J Biophys Biochem Cytol, 1955. **1**(1): p. 69-88.

265. Babst, M., D.J. Katzmann, W.B. Snyder, B. Wendland, and S.D. Emr, Endosome-associated complex, ESCRT-II, recruits transport machinery for protein sorting at the multivesicular body. Dev Cell, 2002. **3**(2): p. 283-9.

266. Rind, H.B., R. Butowt, and C.S. von Bartheld, Synaptic targeting of retrogradely transported trophic factors in motoneurons: comparison of glial cell line-derived neurotrophic factor, brain-derived neurotrophic factor, and cardiotrophin-1 with tetanus toxin. J Neurosci, 2005. **25**(3): p. 539-49.

267.   Biella, G., F. Di Febo, D. Goffredo, A. Moiana, V. Taglietti, L. Conti, E. Cattaneo, and M. Toselli, Differentiating embryonic stem-derived neural stem cells show a maturation-dependent pattern of voltage-gated sodium current expression and graded action potentials. Neuroscience, 2007. **149**(1): p. 38-52.

268.   Zhang, X.Q. and S.C. Zhang, Differentiation of neural precursors and dopaminergic neurons from human embryonic stem cells. Methods Mol Biol, 2010. **584**: p. 355-66.

269.   Elkabetz, Y., G. Panagiotakos, G. Al Shamy, N.D. Socci, V. Tabar, and L. Studer, Human ES cell-derived neural rosettes reveal a functionally distinct early neural stem cell stage. Genes Dev, 2008. **22**(2): p. 152-65.

270.   Lee, H., G.A. Shamy, Y. Elkabetz, C.M. Schofield, N.L. Harrsion, G. Panagiotakos, N.D. Socci, V. Tabar, and L. Studer, Directed differentiation and transplantation of human embryonic stem cell-derived motoneurons. Stem Cells, 2007. **25**(8): p. 1931-9.

271.   Shi, Y., P. Kirwan, and F.J. Livesey, Directed differentiation of human pluripotent stem cells to cerebral cortex neurons and neural networks. Nat Protoc, 2012. **7**(10): p. 1836-46.

272.   Liu, L., X. Wei, J. Ling, L. Wu, and Y. Xiao, Expression pattern of Oct-4, Sox2, and c-Myc in the primary culture of human dental pulp derived cells. J Endod, 2011. **37**(4): p. 466-72.

273.   Atari, M., C. Gil-Recio, M. Fabregat, D. Garcia-Fernandez, M. Barajas, M.A. Carrasco, H.S. Jung, F.H. Alfaro, N. Casals, F. Prosper, E. Ferres-Padro, and L. Giner, Dental pulp of the third molar: a new source of pluripotent-like stem cells. J Cell Sci, 2012. **125**(Pt 14): p. 3343-56.

274.   Haythornthwaite, A., S. Stoelzle, A. Hasler, A. Kiss, J. Mosbacher, M. George, A. Bruggemann, and N. Fertig, Characterizing human ion channels in induced pluripotent stem cell-derived neurons. J Biomol Screen, 2012. **17**(9): p. 1264-72.

275.   Kuijlaars, J., T. Oyelami, A. Diels, J. Rohrbacher, S. Versweyveld, G. Meneghello, M. Tuefferd, P. Verstraelen, J.R. Detrez, M. Verschuuren, W.H. De Vos, T. Meert, P.J. Peeters, M. Cik, R. Nuydens, B. Brone, and A. Verheyen, Sustained synchronized neuronal network activity in a human astrocyte co-culture system. Sci Rep, 2016. **6**: p. 36529.

276.   Olesen, J., A. Gustavsson, M. Svensson, H.U. Wittchen, B. Jonsson, C.s. group, and C. European Brain, The economic cost of brain disorders in Europe. Eur J Neurol, 2012. **19**(1): p. 155-62.

277.   Fang, C.Z., Y.J. Yang, Q.H. Wang, Y. Yao, X.Y. Zhang, and X.H. He, Intraventricular injection of human dental pulp stem cells improves hypoxic-ischemic brain damage in neonatal rats. PLoS One, 2013. **8**(6): p. e66748.

278.   Gatta, V., D. Drago, K. Fincati, M.T. Valenti, L. Dalle Carbonare, S.L. Sensi, and P. Zatta, Microarray analysis on human neuroblastoma cells exposed to aluminum, beta(1-42)-amyloid or the beta(1-42)-amyloid aluminum complex. PLoS One, 2011. **6**(1): p. e15965.

279.   Zhang, Z., L. Hou, X. Li, C. Ju, J. Zhang, X. Li, X. Wang, C. Liu, Y. Lv, and Y. Wang, Neuroprotection of inositol hexaphosphate and changes of mitochondrion mediated apoptotic pathway and alpha-synuclein aggregation in 6-OHDA induced parkinsons disease cell model. Brain Res, 2015.

280.   Pires, A.O., A. Neves-Carvalho, N. Sousa, and A.J. Salgado, The Secretome of Bone Marrow and Wharton Jelly Derived Mesenchymal Stem Cells Induces Differentiation and Neurite Outgrowth in SH-SY5Y Cells. Stem Cells Int, 2014. **2014**: p. 438352.

281.   Kojima, T., Y. Hirota, M. Ema, S. Takahashi, I. Miyoshi, H. Okano, and K. Sawamoto, Subventricular zone-derived neural progenitor cells migrate along a blood vessel scaffold toward the post-stroke striatum. Stem Cells, 2010. **28**(3): p. 545-54.

282.   Wyatt, S., R. Andres, H. Rohrer, and A.M. Davies, Regulation of neurotrophin receptor expression by retinoic acid in mouse sympathetic neuroblasts. J Neurosci, 1999. **19**(3): p. 1062-71.

283.   Lee, M.C., B.W. Kim, J.S. Kim, J.S. Lee, K.S. Kim, J.H. Lee, J.H. Nam, S.M. Rowe, and S.U. Kim, Neuronal differentiation of human neuroblastoma SH-SY5Y cells by gangliosides. Brain Tumor Pathol, 1997. **14**(1): p. 5-11.

284.   Sousa, S.R., I. Vetter, L. Ragnarsson, and R.J. Lewis, Expression and pharmacology of endogenous Cav channels in SH-SY5Y human neuroblastoma cells. PLoS One, 2013. **8**(3): p. e59293.

285.   Vetter, I., C.A. Mozar, T. Durek, J.S. Wingerd, P.F. Alewood, M.J. Christie, and R.J. Lewis, Characterisation of Na(v) types endogenously expressed in human SH-SY5Y neuroblastoma cells. Biochem Pharmacol, 2012. **83**(11): p. 1562-71.

286.   Santillo, S., A. Schiano Moriello, and V. Di Maio, Electrophysiological variability in the SH-SY5Y cellular line. Gen Physiol Biophys, 2014. **33**(1): p. 121-9.

287. Davies, A.M., Neurotrophins: neurotrophic modulation of neurite growth. Curr Biol, 2000. **10**(5): p. R198-200.

288. Geminder, H., O. Sagi-Assif, L. Goldberg, T. Meshel, G. Rechavi, I.P. Witz, and A. Ben-Baruch, A possible role for CXCR4 and its ligand, the CXC chemokine stromal cell-derived factor-1, in the development of bone marrow metastases in neuroblastoma. J Immunol, 2001. **167**(8): p. 4747-57.

289. Takahashi, J., T.D. Palmer, and F.H. Gage, Retinoic acid and neurotrophins collaborate to regulate neurogenesis in adult-derived neural stem cell cultures. J Neurobiol, 1999. **38**(1): p. 65-81.

290. Xu, J., X.Z. Zhang, Y.J. Zhang, X.M. Li, Z.L. Cai, and X.M. Li, Silencing of SIAH1 in SH-SY5Y affects alpha-synuclein degradation pathway. Int J Clin Exp Pathol, 2015. **8**(10): p. 12885-92.

291. Lindvall, O. and Z. Kokaia, Stem cells in human neurodegenerative disorders--time for clinical translation? J Clin Invest, 2010. **120**(1): p. 29-40.

292. Joyce, N., G. Annett, L. Wirthlin, S. Olson, G. Bauer, and J.A. Nolta, Mesenchymal stem cells for the treatment of neurodegenerative disease. Regen Med, 2010. **5**(6): p. 933-46.

293. Djouad, F., P. Plence, C. Bony, P. Tropel, F. Apparailly, J. Sany, D. Noel, and C. Jorgensen, Immunosuppressive effect of mesenchymal stem cells favors tumor growth in allogeneic animals. Blood, 2003. **102**(10): p. 3837-44.

294. Liu, S., H. Shi, W. Liu, T. Furuichi, G.S. Timmins, and K.J. Liu, Interstitial pO2 in ischemic penumbra and core are differentially affected following

transient focal cerebral ischemia in rats. J Cereb Blood Flow Metab, 2004. **24**(3): p. 343-9.

295. Munoz, F., C. Jimenez, D. Espinoza, A. Vervelle, J. Beugnet, and Z. Haidar, Use of leukocyte and platelet-rich fibrin (L-PRF) in periodontally accelerated osteogenic orthodontics (PAOO): Clinical effects on edema and pain. J Clin Exp Dent, 2016. **8**(2): p. e119-24.

296. Marenzi, G., F. Riccitiello, M. Tia, A. di Lauro, and G. Sammartino, Influence of Leukocyte- and Platelet-Rich Fibrin (L-PRF) in the Healing of Simple Postextraction Sockets: A Split-Mouth Study. Biomed Res Int, 2015. **2015**: p. 369273.

297. Dohan, D.M., J. Choukroun, A. Diss, S.L. Dohan, A.J. Dohan, J. Mouhyi, and B. Gogly, Platelet-rich fibrin (PRF): a second-generation platelet concentrate. Part III: leucocyte activation: a new feature for platelet concentrates? Oral Surg Oral Med Oral Pathol Oral Radiol Endod, 2006. **101**(3): p. e51-5.

298. Ueda, M., T. Fujisawa, M. Ono, E.S. Hara, H.T. Pham, R. Nakajima, W. Sonoyama, and T. Kuboki, A short-term treatment with tumor necrosis factor-alpha enhances stem cell phenotype of human dental pulp cells. Stem Cell Res Ther, 2014. **5**(1): p. 31.

299. Egea, V., L. von Baumgarten, C. Schichor, B. Berninger, T. Popp, P. Neth, R. Goldbrunner, Y. Kienast, F. Winkler, M. Jochum, and C. Ries, TNF-alpha respecifies human mesenchymal stem cells to a neural fate and promotes migration toward experimental glioma. Cell Death Differ, 2011. **18**(5): p. 853-63.

300. Huang, Y.L., R.F. Qiu, W.Y. Mai, J. Kuang, X.Y. Cai, Y.G. Dong, Y.Z. Hu, Y.B. Song, A.P. Cai, and Z.G. Jiang, Effects of insulin-like growth factor-

1 on the properties of mesenchymal stem cells in vitro. J Zhejiang Univ Sci B, 2012. **13**(1): p. 20-8.

301.   Kwon, Y.W., S.C. Heo, G.O. Jeong, J.W. Yoon, W.M. Mo, M.J. Lee, I.H. Jang, S.M. Kwon, J.S. Lee, and J.H. Kim, Tumor necrosis factor-alpha-activated mesenchymal stem cells promote endothelial progenitor cell homing and angiogenesis. Biochim Biophys Acta, 2013. **1832**(12): p. 2136-44.

302.   Fan, H., G. Zhao, L. Liu, F. Liu, W. Gong, X. Liu, L. Yang, J. Wang, and Y. Hou, Pre-treatment with IL-1beta enhances the efficacy of MSC transplantation in DSS-induced colitis. Cell Mol Immunol, 2012. **9**(6): p. 473-81.

303.   Hill, W.D., D.C. Hess, A. Martin-Studdard, J.J. Carothers, J. Zheng, D. Hale, M. Maeda, S.C. Fagan, J.E. Carroll, and S.J. Conway, SDF-1 (CXCL12) is upregulated in the ischemic penumbra following stroke: association with bone marrow cell homing to injury. J Neuropathol Exp Neurol, 2004. **63**(1): p. 84-96.

304.   Masuki, H., T. Okudera, T. Watanebe, M. Suzuki, K. Nishiyama, H. Okudera, K. Nakata, K. Uematsu, C.Y. Su, and T. Kawase, Growth factor and pro-inflammatory cytokine contents in platelet-rich plasma (PRP), plasma rich in growth factors (PRGF), advanced platelet-rich fibrin (A-PRF), and concentrated growth factors (CGF). Int J Implant Dent, 2016. **2**(1): p. 19.

305.   Mohapel, P., H. Frielingsdorf, J. Haggblad, O. Zachrisson, and P. Brundin, Platelet-derived growth factor (PDGF-BB) and brain-derived neurotrophic factor (BDNF) induce striatal neurogenesis in adult rats

with 6-hydroxydopamine lesions. Neuroscience, 2005. **132**(3): p. 767-76.

306. Dobolyi, A., C. Vincze, G. Pal, and G. Lovas, The neuroprotective functions of transforming growth factor beta proteins. Int J Mol Sci, 2012. **13**(7): p. 8219-58.

307. Zhu, W., Y. Fan, Q. Hao, F. Shen, T. Hashimoto, G.Y. Yang, M. Gasmi, R.T. Bartus, W.L. Young, and Y. Chen, Postischemic IGF-1 gene transfer promotes neurovascular regeneration after experimental stroke. J Cereb Blood Flow Metab, 2009. **29**(9): p. 1528-37.

308. Conti, L., S.M. Pollard, T. Gorba, E. Reitano, M. Toselli, G. Biella, Y. Sun, S. Sanzone, Q.L. Ying, E. Cattaneo, and A. Smith, Niche-independent symmetrical self-renewal of a mammalian tissue stem cell. PLoS Biol, 2005. **3**(9): p. e283.

309. Reekmans, K.P., J. Praet, N. De Vocht, B.R. Tambuyzer, I. Bergwerf, J. Daans, V. Baekelandt, G. Vanhoutte, H. Goossens, P.G. Jorens, D.K. Ysebaert, S. Chatterjee, P. Pauwels, E. Van Marck, Z.N. Berneman, A. Van der Linden, and P. Ponsaerts, Clinical potential of intravenous neural stem cell delivery for treatment of neuroinflammatory disease in mice? Cell Transplant, 2011. **20**(6): p. 851-69.

310. Banker, G. and K. Goslin, Culturing Nerve Cells. 2nd ed. 1998, Cambridge, MA: MIT Press. 666.

311. Schindelin, J., I. Arganda-Carreras, E. Frise, V. Kaynig, M. Longair, T. Pietzsch, S. Preibisch, C. Rueden, S. Saalfeld, B. Schmid, J.Y. Tinevez, D.J. White, V. Hartenstein, K. Eliceiri, P. Tomancak, and A. Cardona, Fiji: an open-source platform for biological-image analysis. Nat Methods, 2012. **9**(7): p. 676-82.

312.   Meijering, E., M. Jacob, J.C. Sarria, P. Steiner, H. Hirling, and M. Unser, Design and validation of a tool for neurite tracing and analysis in fluorescence microscopy images. Cytometry A, 2004. **58**(2): p. 167-76.

313.   Hemeda, H., B. Giebel, and W. Wagner, Evaluation of human platelet lysate versus fetal bovine serum for culture of mesenchymal stromal cells. Cytotherapy, 2014. **16**(2): p. 170-80.

314.   Doucet, C., I. Ernou, Y. Zhang, J.R. Llense, L. Begot, X. Holy, and J.J. Lataillade, Platelet lysates promote mesenchymal stem cell expansion: a safety substitute for animal serum in cell-based therapy applications. J Cell Physiol, 2005. **205**(2): p. 228-36.

315.   Schallmoser, K., C. Bartmann, E. Rohde, A. Reinisch, K. Kashofer, E. Stadelmeyer, C. Drexler, G. Lanzer, W. Linkesch, and D. Strunk, Human platelet lysate can replace fetal bovine serum for clinical-scale expansion of functional mesenchymal stromal cells. Transfusion, 2007. **47**(8): p. 1436-46.

316.   Bereiter-Hahn, J., A. Munnich, and P. Woiteneck, Dependence of energy metabolism on the density of cells in culture. Cell Struct Funct, 1998. **23**(2): p. 85-93.

317.   Lundquist, R., K. Holmstrom, C. Clausen, B. Jorgensen, and T. Karlsmark, Characteristics of an autologous leukocyte and platelet-rich fibrin patch intended for the treatment of recalcitrant wounds. Wound Repair Regen, 2013. **21**(1): p. 66-76.

318.   Kellner, M., M.M. Steindorff, J.F. Strempel, A. Winkel, M.P. Kuhnel, and M. Stiesch, Differences of isolated dental stem cells dependent on donor age and consequences for autologous tooth replacement. Arch Oral Biol, 2014. **59**(6): p. 559-67.

319.   Ma, D., Z. Ma, X. Zhang, W. Wang, Z. Yang, M. Zhang, G. Wu, W. Lu, Z. Deng, and Y. Jin, Effect of age and extrinsic microenvironment on the proliferation and osteogenic differentiation of rat dental pulp stem cells in vitro. J Endod, 2009. **35**(11): p. 1546-53.

320.   Finkel, T., Oxidant signals and oxidative stress. Curr Opin Cell Biol, 2003. **15**(2): p. 247-54.

321.   Yang, D., S.G. Elner, Z.M. Bian, G.O. Till, H.R. Petty, and V.M. Elner, Pro-inflammatory cytokines increase reactive oxygen species through mitochondria and NADPH oxidase in cultured RPE cells. Exp Eye Res, 2007. **85**(4): p. 462-72.

322.   Elkharaz, J., A. Ugun-Klusek, D. Constantin-Teodosiu, K. Lawler, R.J. Mayer, E. Billett, J. Lowe, and L. Bedford, Implications for oxidative stress and astrocytes following 26S proteasomal depletion in mouse forebrain neurones. Biochim Biophys Acta, 2013. **1832**(12): p. 1930-8.

323.   Alongi, D.J., T. Yamaza, Y. Song, A.F. Fouad, E.E. Romberg, S. Shi, R.S. Tuan, and G.T. Huang, Stem/progenitor cells from inflamed human dental pulp retain tissue regeneration potential. Regen Med, 2010. **5**(4): p. 617-31.

324.   Abbott, N.J. and A. Friedman, Overview and introduction: the blood-brain barrier in health and disease. Epilepsia, 2012. **53 Suppl 6**: p. 1-6.

325.   Tremolizzo, L., J.C. DiFrancesco, V. Rodriguez-Menendez, E. Sirtori, M. Longoni, A. Cassetti, M. Bossi, S. El Mestikawy, G. Cavaletti, and C. Ferrarese, Human platelets express the synaptic markers VGLUT1 and 2 and release glutamate following aggregation. Neurosci Lett, 2006. **404**(3): p. 262-5.

326.   Brown, G.C. and A. Bal-Price, Inflammatory neurodegeneration mediated by nitric oxide, glutamate, and mitochondria. Mol Neurobiol, 2003. **27**(3): p. 325-55.

327.   Guadagno, J., P. Swan, R. Shaikh, and S.P. Cregan, Microglia-derived IL-1beta triggers p53-mediated cell cycle arrest and apoptosis in neural precursor cells. Cell Death Dis, 2015. **6**: p. e1779.

328.   Downen, M., T.D. Amaral, L.L. Hua, M.L. Zhao, and S.C. Lee, Neuronal death in cytokine-activated primary human brain cell culture: role of tumor necrosis factor-alpha. Glia, 1999. **28**(2): p. 114-27.

329.   Barone, F.C., B. Arvin, R.F. White, A. Miller, C.L. Webb, R.N. Willette, P.G. Lysko, and G.Z. Feuerstein, Tumor necrosis factor-alpha. A mediator of focal ischemic brain injury. Stroke, 1997. **28**(6): p. 1233-44.

330.   Chen, N.N., F. Wei, L. Wang, S. Cui, Y. Wan, and S. Liu, Tumor Necrosis Factor Alpha Induces Neural Stem Cell Apoptosis Through Activating p38 MAPK Pathway. Neurochem Res, 2016. **41**(11): p. 3052-3062.

331.   Marques-Fernandez, F., L. Planells-Ferrer, R. Gozzelino, K.M. Galenkamp, S. Reix, N. Llecha-Cano, J. Lopez-Soriano, V.J. Yuste, R.S. Moubarak, and J.X. Comella, TNFalpha induces survival through the FLIP-L-dependent activation of the MAPK/ERK pathway. Cell Death Dis, 2013. **4**: p. e493.

332.   Ma, L., X.W. Li, S.J. Zhang, F. Yang, G.M. Zhu, X.B. Yuan, and W. Jiang, Interleukin-1 beta guides the migration of cortical neurons. J Neuroinflammation, 2014. **11**: p. 114.

333. Widera, D., W. Holtkamp, F. Entschladen, B. Niggemann, K. Zanker, B. Kaltschmidt, and C. Kaltschmidt, MCP-1 induces migration of adult neural stem cells. Eur J Cell Biol, 2004. **83**(8): p. 381-7.

334. Weiss, N., C. Deboux, N. Chaverot, F. Miller, A. Baron-Van Evercooren, P.O. Couraud, and S. Cazaubon, IL8 and CXCL13 are potent chemokines for the recruitment of human neural precursor cells across brain endothelial cells. J Neuroimmunol, 2010. **223**(1-2): p. 131-4.

335. Li, Y., J. Huang, X. He, G. Tang, Y.H. Tang, Y. Liu, X. Lin, Y. Lu, G.Y. Yang, and Y. Wang, Postacute stromal cell-derived factor-1alpha expression promotes neurovascular recovery in ischemic mice. Stroke, 2014. **45**(6): p. 1822-9.

336. Nieto-Estevez, V., C. Defterali, and C. Vicario-Abejon, IGF-I: A Key Growth Factor that Regulates Neurogenesis and Synaptogenesis from Embryonic to Adult Stages of the Brain. Front Neurosci, 2016. **10**: p. 52.

337. Wu, Y., Q. Chen, H. Peng, H. Dou, Y. Zhou, Y. Huang, and J.C. Zheng, Directed migration of human neural progenitor cells to interleukin-1beta is promoted by chemokines stromal cell-derived factor-1 and monocyte chemotactic factor-1 in mouse brains. Transl Neurodegener, 2012. **1**(1): p. 15.

338. Kong, D., J. Zhu, Q. Liu, Y. Jiang, L. Xu, N. Luo, Z. Zhao, Q. Zhai, H. Zhang, M. Zhu, and X. Liu, Mesenchymal stem cells protect neurons against hypoxic-ischemic injury via inhibiting parthanatos, necroptosis, and apoptosis, but not autophagy. Cell Mol Neurobiol, 2016.

339. Song, M., S.S. Jue, Y.A. Cho, and E.C. Kim, Comparison of the effects of human dental pulp stem cells and human bone marrow-derived

mesenchymal stem cells on ischemic human astrocytes in vitro. J Neurosci Res, 2015. **93**(6): p. 973-83.

340. Zhu, Y., G.Y. Yang, B. Ahlemeyer, L. Pang, X.M. Che, C. Culmsee, S. Klumpp, and J. Krieglstein, Transforming growth factor-beta 1 increases bad phosphorylation and protects neurons against damage. J Neurosci, 2002. **22**(10): p. 3898-909.

341. Braunger, B.M., S. Pielmeier, C. Demmer, V. Landstorfer, D. Kawall, N. Abramov, M. Leibinger, I. Kleiter, D. Fischer, H. Jagle, and E.R. Tamm, TGF-beta signaling protects retinal neurons from programmed cell death during the development of the mammalian eye. J Neurosci, 2013. **33**(35): p. 14246-58.

342. Spiliotopoulos, D., D. Goffredo, L. Conti, F. Di Febo, G. Biella, M. Toselli, and E. Cattaneo, An optimized experimental strategy for efficient conversion of embryonic stem (ES)-derived mouse neural stem (NS) cells into a nearly homogeneous mature neuronal population. Neurobiol Dis, 2009. **34**(2): p. 320-31.

343. Dumont, R.J., D.O. Okonkwo, S. Verma, R.J. Hurlbert, P.T. Boulos, D.B. Ellegala, and A.S. Dumont, Acute spinal cord injury, part I: pathophysiologic mechanisms. Clin Neuropharmacol, 2001. **24**(5): p. 254-64.

344. Hansen, T.M., A.J. Moss, and N.P. Brindle, Vascular endothelial growth factor and angiopoietins in neurovascular regeneration and protection following stroke. Curr Neurovasc Res, 2008. **5**(4): p. 236-45.

345. van Bruggen, N., H. Thibodeaux, J.T. Palmer, W.P. Lee, L. Fu, B. Cairns, D. Tumas, R. Gerlai, S.P. Williams, M. van Lookeren Campagne, and N. Ferrara, VEGF antagonism reduces edema formation and tissue damage

after ischemia/reperfusion injury in the mouse brain. J Clin Invest, 1999. **104**(11): p. 1613-20.

346. Zhang, Z.G., L. Zhang, Q. Jiang, R. Zhang, K. Davies, C. Powers, N. Bruggen, and M. Chopp, VEGF enhances angiogenesis and promotes blood-brain barrier leakage in the ischemic brain. J Clin Invest, 2000. **106**(7): p. 829-38.

347. Sandoval, K.E. and K.A. Witt, Blood-brain barrier tight junction permeability and ischemic stroke. Neurobiol Dis, 2008. **32**(2): p. 200-19.

348. Mautes, A.E., M.R. Weinzierl, F. Donovan, and L.J. Noble, Vascular events after spinal cord injury: contribution to secondary pathogenesis. Phys Ther, 2000. **80**(7): p. 673-87.

349. Whetstone, W.D., J.Y. Hsu, M. Eisenberg, Z. Werb, and L.J. Noble-Haeusslein, Blood-spinal cord barrier after spinal cord injury: relation to revascularization and wound healing. J Neurosci Res, 2003. **74**(2): p. 227-39.

350. Soldatova, L., R.G. Campbell, A.H. Elkhatib, T.W. Schmidt, N.R. Pinto, J.M. Pinto, D.M. Prevedello, L.F. Ditzel Filho, B.A. Otto, and R.L. Carrau, Role of Leukocyte–Platelet-Rich Fibrin in Endoscopic Endonasal Skull Base Surgery Defect Reconstruction. J Neurol Surg B, (EFirst).

351. Campana, W.M., E. Mantuano, P. Azmoon, K. Henry, M. Banki, J.H. Kim, D.P. Pizzo, and S.L. Gonias, Ionotropic glutamate receptors activate cell signaling in response to glutamate in Schwann cells. FASEB J, 2017.

352. Yue, W., L. Song, G. Fu, Y. Li, and H. Liu, Neuregulin-1beta regulates tyrosine kinase receptor expression in cultured dorsal root ganglion

neurons with excitotoxicity induced by glutamate. Regul Pept, 2013. **180**: p. 33-42.

353. Lichtenfels, M., L. Colome, A.D. Sebben, and J. Braga-Silva, Effect of Platelet Rich Plasma and Platelet Rich Fibrin on sciatic nerve regeneration in a rat model. Microsurgery, 2013. **33**(5): p. 383-90.

354. Anderson, J.M., Biological responses to materials. Annual Review of Materials Research, 2001. **31**: p. 81-110.

355. Feigin, V.L., M.H. Forouzanfar, R. Krishnamurthi, G.A. Mensah, M. Connor, D.A. Bennett, A.E. Moran, R.L. Sacco, L. Anderson, T. Truelsen, M. O'Donnell, N. Venketasubramanian, S. Barker-Collo, C.M. Lawes, W. Wang, Y. Shinohara, E. Witt, M. Ezzati, M. Naghavi, C. Murray, I. Global Burden of Diseases, S. Risk Factors, and G.B.D.S.E.G. the, Global and regional burden of stroke during 1990-2010: findings from the Global Burden of Disease Study 2010. Lancet, 2014. **383**(9913): p. 245-54.

356. Endres, M., B. Engelhardt, J. Koistinaho, O. Lindvall, S. Meairs, J.P. Mohr, A. Planas, N. Rothwell, M. Schwaninger, M.E. Schwab, D. Vivien, T. Wieloch, and U. Dirnagl, Improving outcome after stroke: overcoming the translational roadblock. Cerebrovasc Dis, 2008. **25**(3): p. 268-78.

357. Gervois, P., E. Wolfs, J. Ratajczak, Y. Dillen, T. Vangansewinkel, P. Hilkens, A. Bronckaers, I. Lambrichts, and T. Struys, Stem Cell-Based Therapies for Ischemic Stroke: Preclinical Results and the Potential of Imaging-Assisted Evaluation of Donor Cell Fate and Mechanisms of Brain Regeneration. Med Res Rev, 2016. **36**(6): p. 1080-1126.

358. Rogers, D.C., C.A. Campbell, J.L. Stretton, and K.B. Mackay, Correlation between motor impairment and infarct volume after permanent and

transient middle cerebral artery occlusion in the rat. Stroke, 1997. **28**(10): p. 2060-5; discussion 2066.

359.   Freret, T., V. Bouet, C. Leconte, S. Roussel, L. Chazalviel, D. Divoux, P. Schumann-Bard, and M. Boulouard, Behavioral deficits after distal focal cerebral ischemia in mice: Usefulness of adhesive removal test. Behav Neurosci, 2009. **123**(1): p. 224-30.

360.   Zhang, L., J. Chen, Y. Li, Z.G. Zhang, and M. Chopp, Quantitative measurement of motor and somatosensory impairments after mild (30 min) and severe (2 h) transient middle cerebral artery occlusion in rats. J Neurol Sci, 2000. **174**(2): p. 141-6.

361.   Hattori, K., H. Lee, P.D. Hurn, B.J. Crain, R.J. Traystman, and A.C. DeVries, Cognitive deficits after focal cerebral ischemia in mice. Stroke, 2000. **31**(8): p. 1939-44.

362.   Longa, E.Z., P.R. Weinstein, S. Carlson, and R. Cummins, Reversible middle cerebral artery occlusion without craniectomy in rats. Stroke, 1989. **20**(1): p. 84-91.

363.   Morancho, A., L. Garcia-Bonilla, V. Barcelo, D. Giralt, M. Campos-Martorell, S. Garcia, J. Montaner, and A. Rosell, A new method for focal transient cerebral ischaemia by distal compression of the middle cerebral artery. Neuropathol Appl Neurobiol, 2012. **38**(6): p. 617-27.

364.   Iadecola, C., F. Zhang, R. Casey, M. Nagayama, and M.E. Ross, Delayed reduction of ischemic brain injury and neurological deficits in mice lacking the inducible nitric oxide synthase gene. J Neurosci, 1997. **17**(23): p. 9157-64.

365. Fluri, F., M.K. Schuhmann, and C. Kleinschnitz, Animal models of ischemic stroke and their application in clinical research. Drug Des Devel Ther, 2015. **9**: p. 3445-54.

366. Chen, J., C. Zhang, H. Jiang, Y. Li, L. Zhang, A. Robin, M. Katakowski, M. Lu, and M. Chopp, Atorvastatin induction of VEGF and BDNF promotes brain plasticity after stroke in mice. J Cereb Blood Flow Metab, 2005. **25**(2): p. 281-90.

367. Li, X., K.K. Blizzard, Z. Zeng, A.C. DeVries, P.D. Hurn, and L.D. McCullough, Chronic behavioral testing after focal ischemia in the mouse: functional recovery and the effects of gender. Exp Neurol, 2004. **187**(1): p. 94-104.

368. Crawley, J.N., Exploratory behavior models of anxiety in mice. Neurosci Biobehav Rev, 1985. **9**(1): p. 37-44.

369. Zhang, L., T. Schallert, Z.G. Zhang, Q. Jiang, P. Arniego, Q. Li, M. Lu, and M. Chopp, A test for detecting long-term sensorimotor dysfunction in the mouse after focal cerebral ischemia. J Neurosci Methods, 2002. **117**(2): p. 207-14.

370. Massoud, T.F. and S.S. Gambhir, Molecular imaging in living subjects: seeing fundamental biological processes in a new light. Genes Dev, 2003. **17**(5): p. 545-80.

371. Kim, D.E., D. Schellingerhout, K. Ishii, K. Shah, and R. Weissleder, Imaging of stem cell recruitment to ischemic infarcts in a murine model. Stroke, 2004. **35**(4): p. 952-7.

372. O'Neill, M.J. and J.A. Clemens, Rodent models of global cerebral ischemia. Curr Protoc Neurosci, 2001. **Chapter 9**: p. Unit9 5.

373.   Watson, B.D., W.D. Dietrich, R. Busto, M.S. Wachtel, and M.D. Ginsberg, *Induction of reproducible brain infarction by photochemically initiated thrombosis.* Ann Neurol, 1985. **17**(5): p. 497-504.

374.   Horie, N., A.L. Maag, S.A. Hamilton, H. Shichinohe, T.M. Bliss, and G.K. Steinberg, *Mouse model of focal cerebral ischemia using endothelin-1.* J Neurosci Methods, 2008. **173**(2): p. 286-90.

375.   Popp, A., N. Jaenisch, O.W. Witte, and C. Frahm, *Identification of ischemic regions in a rat model of stroke.* PLoS One, 2009. **4**(3): p. e4764.

376.   Hennings, L.J., R. Flores, P.K. Roberson, A. Brown, J. Lowery, M. Borrelli, and W.C. Culp, *Persistent penumbra in a rabbit stroke model: incidence and histologic characteristics.* Stroke Res Treat, 2011. **2011**: p. 764830.

377.   Doeppner, T.R., B. Kaltwasser, M. Bahr, and D.M. Hermann, *Effects of neural progenitor cells on post-stroke neurological impairment-a detailed and comprehensive analysis of behavioral tests.* Front Cell Neurosci, 2014. **8**: p. 338.

378.   Cuccione, E., G. Padovano, A. Versace, C. Ferrarese, and S. Beretta, *Cerebral collateral circulation in experimental ischemic stroke.* Exp Transl Stroke Med, 2016. **8**: p. 2.

379.   Leithner, C., M. Fuchtemeier, D. Jorks, S. Mueller, U. Dirnagl, and G. Royl, *Infarct Volume Prediction by Early Magnetic Resonance Imaging in a Murine Stroke Model Depends on Ischemia Duration and Time of Imaging.* Stroke, 2015. **46**(11): p. 3249-59.

380.   Beretta, S., E. Cuccione, A. Versace, D. Carone, M. Riva, G. Padovano, V. Dell'Era, R. Cai, L. Monza, L. Presotto, D. Rousseau, F. Chauveau, G.

Paterno, G.B. Pappada, C. Giussani, E.P. Sganzerla, and C. Ferrarese, Cerebral collateral flow defines topography and evolution of molecular penumbra in experimental ischemic stroke. Neurobiol Dis, 2015. **74**: p. 305-13.

381. Majid, A., Y.Y. He, J.M. Gidday, S.S. Kaplan, E.R. Gonzales, T.S. Park, J.D. Fenstermacher, L. Wei, D.W. Choi, and C.Y. Hsu, Differences in vulnerability to permanent focal cerebral ischemia among 3 common mouse strains. Stroke, 2000. **31**(11): p. 2707-14.

382. Lee, J.S., J.M. Hong, G.J. Moon, P.H. Lee, Y.H. Ahn, O.Y. Bang, and S. collaborators, A long-term follow-up study of intravenous autologous mesenchymal stem cell transplantation in patients with ischemic stroke. Stem Cells, 2010. **28**(6): p. 1099-106.

383. Fischer, U.M., M.T. Harting, F. Jimenez, W.O. Monzon-Posadas, H. Xue, S.I. Savitz, G.A. Laine, and C.S. Cox, Jr., Pulmonary passage is a major obstacle for intravenous stem cell delivery: the pulmonary first-pass effect. Stem Cells Dev, 2009. **18**(5): p. 683-92.

384. Schneider, T., F. Osl, T. Friess, H. Stockinger, and W.V. Scheuer, Quantification of human Alu sequences by real-time PCR--an improved method to measure therapeutic efficacy of anti-metastatic drugs in human xenotransplants. Clin Exp Metastasis, 2002. **19**(7): p. 571-82.

385. Meyerrose, T.E., D.A. De Ugarte, A.A. Hofling, P.E. Herrbrich, T.D. Cordonnier, L.D. Shultz, J.C. Eagon, L. Wirthlin, M.S. Sands, M.A. Hedrick, and J.A. Nolta, In vivo distribution of human adipose-derived mesenchymal stem cells in novel xenotransplantation models. Stem Cells, 2007. **25**(1): p. 220-7.

386. Hetze, S., C. Romer, C. Teufelhart, A. Meisel, and O. Engel, Gait analysis as a method for assessing neurological outcome in a mouse model of stroke. J Neurosci Methods, 2012. **206**(1): p. 7-14.

387. Morris, R., Developments of a water-maze procedure for studying spatial learning in the rat. J Neurosci Methods, 1984. **11**(1): p. 47-60.

388. Brown, M.F., R.F. Farley, and E.J. Lorek, Remembrance of places you passed: social spatial working memory in rats. J Exp Psychol Anim Behav Process, 2007. **33**(3): p. 213-24.

389. Lindvall, O. and Z. Kokaia, Stem cell research in stroke: how far from the clinic? Stroke, 2011. **42**(8): p. 2369-75.

390. Kim, S.U. and J. de Vellis, Stem cell-based cell therapy in neurological diseases: a review. J Neurosci Res, 2009. **87**(10): p. 2183-200.

391. Rossi, F. and E. Cattaneo, Opinion: neural stem cell therapy for neurological diseases: dreams and reality. Nat Rev Neurosci, 2002. **3**(5): p. 401-9.

392. Patel, M., A.J. Smith, A.J. Sloan, G. Smith, and P.R. Cooper, Phenotype and behaviour of dental pulp cells during expansion culture. Arch Oral Biol, 2009. **54**(10): p. 898-908.

393. Roobrouck, V.D., K. Vanuytsel, and C.M. Verfaillie, Concise review: culture mediated changes in fate and/or potency of stem cells. Stem Cells, 2011. **29**(4): p. 583-9.

394. Boquest, A.C., A. Shahdadfar, K. Fronsdal, O. Sigurjonsson, S.H. Tunheim, P. Collas, and J.E. Brinchmann, Isolation and transcription profiling of purified uncultured human stromal stem cells: alteration of gene expression after in vitro cell culture. Mol Biol Cell, 2005. **16**(3): p. 1131-41.

395.   Holzwarth, C., M. Vaegler, F. Gieseke, S.M. Pfister, R. Handgretinger, G. Kerst, and I. Muller, Low physiologic oxygen tensions reduce proliferation and differentiation of human multipotent mesenchymal stromal cells. BMC Cell Biol, 2010. **11**: p. 11.

396.   Roobrouck, V.D., C. Clavel, S.A. Jacobs, F. Ulloa-Montoya, S. Crippa, A. Sohni, S.J. Roberts, F.P. Luyten, S.W. Van Gool, M. Sampaolesi, M. Delforge, A. Luttun, and C.M. Verfaillie, Differentiation potential of human postnatal mesenchymal stem cells, mesoangioblasts, and multipotent adult progenitor cells reflected in their transcriptome and partially influenced by the culture conditions. Stem Cells, 2011. **29**(5): p. 871-82.

397.   LeBlon, C.E., M.E. Casey, C.R. Fodor, T. Zhang, X. Zhang, and S.S. Jedlicka, Correlation between in vitro expansion-related cell stiffening and differentiation potential of human mesenchymal stem cells. Differentiation, 2015. **90**(1-3): p. 1-15.

398.   Shahdadfar, A., K. Fronsdal, T. Haug, F.P. Reinholt, and J.E. Brinchmann, In vitro expansion of human mesenchymal stem cells: choice of serum is a determinant of cell proliferation, differentiation, gene expression, and transcriptome stability. Stem Cells, 2005. **23**(9): p. 1357-66.

399.   Di Battista, J.A., W. Shebaby, O. Kizilay, E. Hamade, R. Abou Merhi, S. Mebarek, D. Abdallah, B. Badran, F. Saad, K.A. E, and W.H. Faour, Proliferation and differentiation of human adipose-derived mesenchymal stem cells (ASCs) into osteoblastic lineage are passage dependent. Inflamm Res, 2014. **63**(11): p. 907-17.

400. Ellis, K.M., D.C. O'Carroll, M.D. Lewis, G.Y. Rychkov, and S.A. Koblar, Neurogenic potential of dental pulp stem cells isolated from murine incisors. Stem Cell Res Ther, 2014. **5**(1): p. 30.

401. Michelsen, K.A., S. Acosta-Verdugo, M. Benoit-Marand, I. Espuny-Camacho, N. Gaspard, B. Saha, A. Gaillard, and P. Vanderhaeghen, Area-specific reestablishment of damaged circuits in the adult cerebral cortex by cortical neurons derived from mouse embryonic stem cells. Neuron, 2015. **85**(5): p. 982-97.

402. Gaillard, A., L. Prestoz, B. Dumartin, A. Cantereau, F. Morel, M. Roger, and M. Jaber, Reestablishment of damaged adult motor pathways by grafted embryonic cortical neurons. Nat Neurosci, 2007. **10**(10): p. 1294-9.

403. Thompson, L., P. Barraud, E. Andersson, D. Kirik, and A. Bjorklund, Identification of dopaminergic neurons of nigral and ventral tegmental area subtypes in grafts of fetal ventral mesencephalon based on cell morphology, protein expression, and efferent projections. J Neurosci, 2005. **25**(27): p. 6467-77.

404. Ebrahimi-Gaillard, A., J. Guitet, C. Garnier, and M. Roger, Topographic distribution of efferent fibers originating from homotopic or heterotopic transplants: heterotopically transplanted neurons retain some of the developmental characteristics corresponding to their site of origin. Brain Res Dev Brain Res, 1994. **77**(2): p. 271-83.

405. Kogel, D., B. Svensson, E. Copanaki, S. Anguissola, C. Bonner, N. Thurow, D. Gudorf, H. Hetschko, T. Muller, M. Peters, H.G. Konig, and J.H. Prehn, Induction of transcription factor CEBP homology protein

mediates hypoglycaemia-induced necrotic cell death in human neuroblastoma cells. J Neurochem, 2006. **99**(3): p. 952-64.

406. Ratajczak, J., P. Hilkens, P. Gervois, E. Wolfs, R. Jacobs, I. Lambrichts, and A. Bronckaers, Angiogenic Capacity of Periodontal Ligament Stem Cells Pretreated with Deferoxamine and/or Fibroblast Growth Factor-2. PLoS One, 2016. **11**(12): p. e0167807.

407. Paschen, W., Glutamate excitotoxicity in transient global cerebral ischemia. Acta Neurobiol Exp (Wars), 1996. **56**(1): p. 313-22.

408. Clausen, B.H., M. Degn, N.A. Martin, Y. Couch, L. Karimi, M. Ormhoj, M.L. Mortensen, H.B. Gredal, C. Gardiner, Sargent, II, D.E. Szymkowski, G.H. Petit, T. Deierborg, B. Finsen, D.C. Anthony, and K.L. Lambertsen, Systemically administered anti-TNF therapy ameliorates functional outcomes after focal cerebral ischemia. J Neuroinflammation, 2014. **11**: p. 203.

409. Tuttolomondo, A., R. Pecoraro, and A. Pinto, Studies of selective TNF inhibitors in the treatment of brain injury from stroke and trauma: a review of the evidence to date. Drug Des Devel Ther, 2014. **8**: p. 2221-38.

410. Mulcahy, N.J., J. Ross, N.J. Rothwell, and S.A. Loddick, Delayed administration of interleukin-1 receptor antagonist protects against transient cerebral ischaemia in the rat. Br J Pharmacol, 2003. **140**(3): p. 471-6.

411. Ignatowski, T.A., R.N. Spengler, K.M. Dhandapani, H. Folkersma, R.F. Butterworth, and E. Tobinick, Perispinal etanercept for post-stroke neurological and cognitive dysfunction: scientific rationale and current evidence. CNS Drugs, 2014. **28**(8): p. 679-97.

412. Pinteaux, E., N.J. Rothwell, and H. Boutin, Neuroprotective actions of endogenous interleukin-1 receptor antagonist (IL-1ra) are mediated by glia. Glia, 2006. **53**(5): p. 551-6.

413. Bang, O.Y., J.S. Lee, P.H. Lee, and G. Lee, Autologous mesenchymal stem cell transplantation in stroke patients. Ann Neurol, 2005. **57**(6): p. 874-82.

414. Honmou, O., K. Houkin, T. Matsunaga, Y. Niitsu, S. Ishiai, R. Onodera, S.G. Waxman, and J.D. Kocsis, Intravenous administration of auto serum-expanded autologous mesenchymal stem cells in stroke. Brain, 2011. **134**(Pt 6): p. 1790-807.

415. Nagpal, A., K.L. Kremer, M.A. Hamilton-Bruce, X. Kaidonis, A.G. Milton, C. Levi, S. Shi, L. Carey, S. Hillier, M. Rose, A. Zacest, P. Takhar, and S.A. Koblar, TOOTH (The Open study Of dental pulp stem cell Therapy in Humans): Study protocol for evaluating safety and feasibility of autologous human adult dental pulp stem cell therapy in patients with chronic disability after stroke. Int J Stroke, 2016. **11**(5): p. 575-85.

416. Kilkenny, C., W. Browne, I.C. Cuthill, M. Emerson, D.G. Altman, and N.C.R.R.G.W. Group, Animal research: reporting in vivo experiments: the ARRIVE guidelines. Br J Pharmacol, 2010. **160**(7): p. 1577-9.

417. Rodriguez-Frutos, B., L. Otero-Ortega, M. Gutierrez-Fernandez, B. Fuentes, J. Ramos-Cejudo, and E. Diez-Tejedor, Stem Cell Therapy and Administration Routes After Stroke. Transl Stroke Res, 2016. **7**(5): p. 378-87.

418. Li, L., Q. Jiang, G. Ding, L. Zhang, Z.G. Zhang, Q. Li, S. Panda, M. Lu, J.R. Ewing, and M. Chopp, Effects of administration route on migration and distribution of neural progenitor cells transplanted into rats with

focal cerebral ischemia, an MRI study. J Cereb Blood Flow Metab, 2010. **30**(3): p. 653-62.

419. Vendrame, M., C. Gemma, K.R. Pennypacker, P.C. Bickford, C. Davis Sanberg, P.R. Sanberg, and A.E. Willing, Cord blood rescues stroke-induced changes in splenocyte phenotype and function. Exp Neurol, 2006. **199**(1): p. 191-200.

420. Vu, Q., K. Xie, M. Eckert, W. Zhao, and S.C. Cramer, Meta-analysis of preclinical studies of mesenchymal stromal cells for ischemic stroke. Neurology, 2014. **82**(14): p. 1277-86.

421. Donega, V., C.H. Nijboer, G. van Tilborg, R.M. Dijkhuizen, A. Kavelaars, and C.J. Heijnen, Intranasally administered mesenchymal stem cells promote a regenerative niche for repair of neonatal ischemic brain injury. Exp Neurol, 2014. **261**: p. 53-64.

422. Lim, J.Y., C.H. Jeong, J.A. Jun, S.M. Kim, C.H. Ryu, Y. Hou, W. Oh, J.W. Chang, and S.S. Jeun, Therapeutic effects of human umbilical cord blood-derived mesenchymal stem cells after intrathecal administration by lumbar puncture in a rat model of cerebral ischemia. Stem Cell Res Ther, 2011. **2**(5): p. 38.

423. Jozwiak, S., A. Habich, K. Kotulska, A. Sarnowska, T. Kropiwnicki, M. Janowski, E. Jurkiewicz, B. Lukomska, T. Kmiec, J. Walecki, M. Roszkowski, M. Litwin, T. Oldak, D. Boruczkowski, and K. Domanska-Janik, Intracerebroventricular Transplantation of Cord Blood-Derived Neural Progenitors in a Child With Severe Global Brain Ischemic Injury. Cell Med, 2010. **1**(2): p. 71-80.

424. Lochhead, J.J. and R.G. Thorne, Intranasal delivery of biologics to the central nervous system. Adv Drug Deliv Rev, 2012. **64**(7): p. 614-28.

425. Danielyan, L., S. Beer-Hammer, A. Stolzing, R. Schafer, G. Siegel, C. Fabian, P. Kahle, T. Biedermann, A. Lourhmati, M. Buadze, A. Novakovic, B. Proksch, C.H. Gleiter, W.H. Frey, and M. Schwab, *Intranasal delivery of bone marrow-derived mesenchymal stem cells, macrophages, and microglia to the brain in mouse models of Alzheimer's and Parkinson's disease.* Cell Transplant, 2014. **23 Suppl 1**: p. S123-39.

426. Karussis, D., C. Karageorgiou, A. Vaknin-Dembinsky, B. Gowda-Kurkalli, J.M. Gomori, I. Kassis, J.W. Bulte, P. Petrou, T. Ben-Hur, O. Abramsky, and S. Slavin, Safety and immunological effects of mesenchymal stem cell transplantation in patients with multiple sclerosis and amyotrophic lateral sclerosis. Arch Neurol, 2010. **67**(10): p. 1187-94.

427. Hurst, R.W., E.P. Bosch, J.M. Morris, P.J. Dyck, and R.K. Reeves, *Inflammatory hypertrophic cauda equina following intrathecal neural stem cell injection.* Muscle Nerve, 2013. **48**(5): p. 831-5.

428. Berkowitz, A.L., M.B. Miller, S.A. Mir, D. Cagney, V. Chavakula, I. Guleria, A. Aizer, K.L. Ligon, and J.H. Chi, *Glioproliferative Lesion of the Spinal Cord as a Complication of "Stem-Cell Tourism".* N Engl J Med, 2016. **375**(2): p. 196-8.

429. Tatarishvili, J., K. Oki, E. Monni, P. Koch, T. Memanishvili, A.M. Buga, V. Verma, A. Popa-Wagner, O. Brustle, O. Lindvall, and Z. Kokaia, Human induced pluripotent stem cells improve recovery in stroke-injured aged rats. Restor Neurol Neurosci, 2014. **32**(4): p. 547-58.

430. Polentes, J., P. Jendelova, M. Cailleret, H. Braun, N. Romanyuk, P. Tropel, M. Brenot, V. Itier, C. Seminatore, K. Baldauf, K. Turnovcova, D. Jirak, M. Teletin, J. Come, J. Tournois, K. Reymann, E. Sykova, S.

Viville, and B. Onteniente, Human induced pluripotent stem cells improve stroke outcome and reduce secondary degeneration in the recipient brain. Cell Transplant, 2012. **21**(12): p. 2587-602.

431. Yuan, T., W. Liao, N.H. Feng, Y.L. Lou, X. Niu, A.J. Zhang, Y. Wang, and Z.F. Deng, Human induced pluripotent stem cell-derived neural stem cells survive, migrate, differentiate, and improve neurologic function in a rat model of middle cerebral artery occlusion. Stem Cell Res Ther, 2013. **4**(3): p. 73.

432. Eckert, A., L. Huang, R. Gonzalez, H.S. Kim, M.H. Hamblin, and J.P. Lee, Bystander Effect Fuels Human Induced Pluripotent Stem Cell-Derived Neural Stem Cells to Quickly Attenuate Early Stage Neurological Deficits After Stroke. Stem Cells Transl Med, 2015. **4**(7): p. 841-51.

433. Song, G., X. Li, Y. Shen, L. Qian, X. Kong, M. Chen, K. Cao, and F. Zhang, Transplantation of iPSc Restores Cardiac Function by Promoting Angiogenesis and Ameliorating Cardiac Remodeling in a Post-infarcted Swine Model. Cell Biochem Biophys, 2014.

434. Zhou, Y., S. Wang, Z. Yu, R.F. Hoyt, Jr., T. Hunt, B. Kindzelski, D. Shou, W. Xie, Y. Du, C. Liu, and K.A. Horvath, Induced pluripotent stem cell transplantation in the treatment of porcine chronic myocardial ischemia. Ann Thorac Surg, 2014. **98**(6): p. 2130-7.

435. Fu, W., S.J. Wang, G.D. Zhou, W. Liu, Y. Cao, and W.J. Zhang, Residual undifferentiated cells during differentiation of induced pluripotent stem cells in vitro and in vivo. Stem Cells Dev, 2012. **21**(4): p. 521-9.

436. Choi, H.W., J.S. Kim, S. Choi, Y.J. Hong, M.J. Kim, H.G. Seo, and J.T. Do, Neural stem cells differentiated from iPS cells spontaneously regain pluripotency. Stem Cells, 2014. **32**(10): p. 2596-604.

437.   Okita, K., T. Ichisaka, and S. Yamanaka, Generation of germline-competent induced pluripotent stem cells. Nature, 2007. **448**(7151): p. 313-7.

438.   Nakagawa, M., M. Koyanagi, K. Tanabe, K. Takahashi, T. Ichisaka, T. Aoi, K. Okita, Y. Mochiduki, N. Takizawa, and S. Yamanaka, Generation of induced pluripotent stem cells without Myc from mouse and human fibroblasts. Nat Biotechnol, 2008. **26**(1): p. 101-6.

439.   Fusaki, N., H. Ban, A. Nishiyama, K. Saeki, and M. Hasegawa, Efficient induction of transgene-free human pluripotent stem cells using a vector based on Sendai virus, an RNA virus that does not integrate into the host genome. Proc Jpn Acad Ser B Phys Biol Sci, 2009. **85**(8): p. 348-62.

440.   Hu, Q., A.M. Friedrich, L.V. Johnson, and D.O. Clegg, Memory in induced pluripotent stem cells: reprogrammed human retinal-pigmented epithelial cells show tendency for spontaneous redifferentiation. Stem Cells, 2010. **28**(11): p. 1981-91.

441.   Ghosh, Z., K.D. Wilson, Y. Wu, S. Hu, T. Quertermous, and J.C. Wu, Persistent donor cell gene expression among human induced pluripotent stem cells contributes to differences with human embryonic stem cells. PLoS One, 2010. **5**(2): p. e8975.

442.   Miura, K., Y. Okada, T. Aoi, A. Okada, K. Takahashi, K. Okita, M. Nakagawa, M. Koyanagi, K. Tanabe, M. Ohnuki, D. Ogawa, E. Ikeda, H. Okano, and S. Yamanaka, Variation in the safety of induced pluripotent stem cell lines. Nat Biotechnol, 2009. **27**(8): p. 743-5.

443. Ben-David, U. and N. Benvenisty, The tumorigenicity of human embryonic and induced pluripotent stem cells. Nat Rev Cancer, 2011. **11**(4): p. 268-77.

444. Wu, S., Y. Wu, X. Zhang, and M.R. Capecchi, Efficient germ-line transmission obtained with transgene-free induced pluripotent stem cells. Proc Natl Acad Sci U S A, 2014. **111**(29): p. 10678-83.

445. Leten, C., V.D. Roobrouck, T. Struys, T.C. Burns, T. Dresselaers, G. Vande Velde, J. Santermans, A. Lo Nigro, A. Ibrahimi, R. Gijsbers, K. Eggermont, I. Lambrichts, C.M. Verfaillie, and U. Himmelreich, Controlling and monitoring stem cell safety in vivo in an experimental rodent model. Stem Cells, 2014. **32**(11): p. 2833-44.

446. Schuldiner, M., J. Itskovitz-Eldor, and N. Benvenisty, Selective ablation of human embryonic stem cells expressing a "suicide" gene. Stem Cells, 2003. **21**(3): p. 257-65.

447. Kamiya, N., M. Ueda, H. Igarashi, Y. Nishiyama, S. Suda, T. Inaba, and Y. Katayama, Intra-arterial transplantation of bone marrow mononuclear cells immediately after reperfusion decreases brain injury after focal ischemia in rats. Life Sci, 2008. **83**(11-12): p. 433-7.

448. Yang, B., E. Migliati, K. Parsha, K. Schaar, X. Xi, J. Aronowski, and S.I. Savitz, Intra-arterial delivery is not superior to intravenous delivery of autologous bone marrow mononuclear cells in acute ischemic stroke. Stroke, 2013. **44**(12): p. 3463-72.

449. Brenneman, M., S. Sharma, M. Harting, R. Strong, C.S. Cox, Jr., J. Aronowski, J.C. Grotta, and S.I. Savitz, Autologous bone marrow mononuclear cells enhance recovery after acute ischemic stroke in

young and middle-aged rats. J Cereb Blood Flow Metab, 2010. **30**(1): p. 140-9.

450. Wagner, D.C., M. Bojko, M. Peters, M. Lorenz, C. Voigt, A. Kaminski, D. Hasenclever, M. Scholz, A. Kranz, G. Weise, and J. Boltze, Impact of age on the efficacy of bone marrow mononuclear cell transplantation in experimental stroke. Exp Transl Stroke Med, 2012. **4**(1): p. 17.

451. Phruksaniyom, C., P. Dharmasaroja, and S. Issaragrisil, Bone marrow non-mesenchymal mononuclear cells induce functional differentiation of neuroblastoma cells. Exp Hematol Oncol, 2013. **2**(1): p. 9.

452. Barone, F.C., D.J. Knudsen, A.H. Nelson, G.Z. Feuerstein, and R.N. Willette, Mouse strain differences in susceptibility to cerebral ischemia are related to cerebral vascular anatomy. J Cereb Blood Flow Metab, 1993. **13**(4): p. 683-92.

453. Sauter, A. and M. Rudin, Strain-dependent drug effects in rat middle cerebral artery occlusion model of stroke. J Pharmacol Exp Ther, 1995. **274**(2): p. 1008-13.

454. Braeuninger, S. and C. Kleinschnitz, Rodent models of focal cerebral ischemia: procedural pitfalls and translational problems. Exp Transl Stroke Med, 2009. **1**: p. 8.

455. Darsalia, V., S.J. Allison, C. Cusulin, E. Monni, D. Kuzdas, T. Kallur, O. Lindvall, and Z. Kokaia, Cell number and timing of transplantation determine survival of human neural stem cell grafts in stroke-damaged rat brain. J Cereb Blood Flow Metab, 2011. **31**(1): p. 235-42.

456. Popa-Wagner, A., A.M. Buga, T.R. Doeppner, and D.M. Hermann, Stem cell therapies in preclinical models of stroke associated with aging. Front Cell Neurosci, 2014. **8**: p. 347.

457.   Popa-Wagner, A., M. Filfan, A. Uzoni, P. Pourgolafshan, and A.M. Buga, Poststroke Cell Therapy of the Aged Brain. Neural Plast, 2015. **2015**: p. 839638.

458.   Scheller, A., D. Vivien, F. Kirchhoff, C. Orset, R.E. Sandu, and A. Popa-Wagner, Imaging neuroinflammation after brain injuries by ultrasensitive MRI and two-photon laser-scanning microscopy. Romanian Journal of Morphology and Embryology, 2014. **55**(3): p. 735-743.

459.   Popa-Wagner, A., S.T. Carmichael, Z. Kokaia, C. Kessler, and L.C. Walker, The response of the aged brain to stroke: too much, too soon? Curr Neurovasc Res, 2007. **4**(3): p. 216-27.

460.   Badan, I., B. Buchhold, A. Hamm, M. Gratz, L.C. Walker, D. Platt, C. Kessler, and A. Popa-Wagner, Accelerated glial reactivity to stroke in aged rats correlates with reduced functional recovery. J Cereb Blood Flow Metab, 2003. **23**(7): p. 845-54.

461.   Zechariah, A., A. ElAli, N. Hagemann, F. Jin, T.R. Doeppner, I. Helfrich, G. Mies, and D.M. Hermann, Hyperlipidemia attenuates vascular endothelial growth factor-induced angiogenesis, impairs cerebral blood flow, and disturbs stroke recovery via decreased pericyte coverage of brain endothelial cells. Arterioscler Thromb Vasc Biol, 2013. **33**(7): p. 1561-7.

462.   Ay, H., W.J. Koroshetz, M. Vangel, T. Benner, C. Melinosky, M. Zhu, N. Menezes, C.J. Lopez, and A.G. Sorensen, Conversion of ischemic brain tissue into infarction increases with age. Stroke, 2005. **36**(12): p. 2632-6.

463. Buga, A.M., C. Margaritescu, C.J. Scholz, E. Radu, C. Zelenak, and A. Popa-Wagner, Transcriptomics of post-stroke angiogenesis in the aged brain. Front Aging Neurosci, 2014. **6**: p. 44.

464. Wolfs, E., C.M. Verfaillie, K. Van Laere, and C.M. Deroose, Radiolabeling strategies for radionuclide imaging of stem cells. Stem Cell Rev, 2015. **11**(2): p. 254-74.

465. Arbab, A.S., L.A. Bashaw, B.R. Miller, E.K. Jordan, B.K. Lewis, H. Kalish, and J.A. Frank, Characterization of biophysical and metabolic properties of cells labeled with superparamagnetic iron oxide nanoparticles and transfection agent for cellular MR imaging. Radiology, 2003. **229**(3): p. 838-46.

466. Struys, T., A. Ketkar-Atre, P. Gervois, C. Leten, P. Hilkens, W. Martens, A. Bronckaers, T. Dresselaers, C. Politis, I. Lambrichts, and U. Himmelreich, Magnetic resonance imaging of human dental pulp stem cells in vitro and in vivo. Cell Transplant, 2013. **22**(10): p. 1813-29.

467. Hoehn, M., E. Kustermann, J. Blunk, D. Wiedermann, T. Trapp, S. Wecker, M. Focking, H. Arnold, J. Hescheler, B.K. Fleischmann, W. Schwindt, and C. Buhrle, Monitoring of implanted stem cell migration in vivo: a highly resolved in vivo magnetic resonance imaging investigation of experimental stroke in rat. Proc Natl Acad Sci U S A, 2002. **99**(25): p. 16267-72.

468. Gu, E., W.Y. Chen, J. Gu, P. Burridge, and J.C. Wu, Molecular imaging of stem cells: tracking survival, biodistribution, tumorigenicity, and immunogenicity. Theranostics, 2012. **2**(4): p. 335-45.

469.   Vandsburger, M.H., M. Radoul, B. Cohen, and M. Neeman, MRI reporter genes: applications for imaging of cell survival, proliferation, migration and differentiation. NMR Biomed, 2013. **26**(7): p. 872-84.

470.   Vandeputte, C., V. Reumers, S.A. Aelvoet, I. Thiry, S. De Swaef, C. Van den Haute, J. Pascual-Brazo, T.D. Farr, G. Vande Velde, M. Hoehn, U. Himmelreich, K. Van Laere, Z. Debyser, R. Gijsbers, and V. Baekelandt, Bioluminescence imaging of stroke-induced endogenous neural stem cell response. Neurobiol Dis, 2014. **69**: p. 144-55.

471.   Adamczak, J.M., G. Schneider, M. Nelles, I. Que, E. Suidgeest, L. van der Weerd, C. Lowik, and M. Hoehn, In vivo bioluminescence imaging of vascular remodeling after stroke. Front Cell Neurosci, 2014. **8**: p. 274.

472.   Quattromani, M.J., P. Cordeau, K. Ruscher, J. Kriz, and T. Wieloch, Enriched housing down-regulates the Toll-like receptor 2 response in the mouse brain after experimental stroke. Neurobiol Dis, 2014. **66**: p. 66-73.

473.   Wang, J., F. Chao, F. Han, G. Zhang, Q. Xi, J. Li, H. Jiang, J. Wang, G. Yu, M. Tian, and H. Zhang, PET demonstrates functional recovery after transplantation of induced pluripotent stem cells in a rat model of cerebral ischemic injury. J Nucl Med, 2013. **54**(5): p. 785-92.

474.   Vandeputte, C., C. Casteels, T. Struys, M. Koole, D. van Veghel, N. Evens, A. Gerits, T. Dresselaers, I. Lambrichts, U. Himmelreich, G. Bormans, and K. Van Laere, Small-animal PET imaging of the type 1 and type 2 cannabinoid receptors in a photothrombotic stroke model. Eur J Nucl Med Mol Imaging, 2012. **39**(11): p. 1796-806.

475.   Zinnhardt, B., T. Viel, L. Wachsmuth, A. Vrachimis, S. Wagner, H.J. Breyholz, A. Faust, S. Hermann, K. Kopka, C. Faber, F. Dolle, S.

Pappata, A.M. Planas, B. Tavitian, M. Schafers, L.M. Sorokin, M.T. Kuhlmann, and A.H. Jacobs, Multimodal imaging reveals temporal and spatial microglia and matrix metalloproteinase activity after experimental stroke. J Cereb Blood Flow Metab, 2015. **35**(11): p. 1711-21.

476.   Nair, D.G., About being BOLD. Brain Res Brain Res Rev, 2005. **50**(2): p. 229-43.

477.   Weber, R., P. Ramos-Cabrer, C. Justicia, D. Wiedermann, C. Strecker, C. Sprenger, and M. Hoehn, Early prediction of functional recovery after experimental stroke: functional magnetic resonance imaging, electrophysiology, and behavioral testing in rats. J Neurosci, 2008. **28**(5): p. 1022-9.

478.   Neumann-Haefelin, T., H.J. Wittsack, F. Wenserski, M. Siebler, R.J. Seitz, U. Modder, and H.J. Freund, Diffusion- and perfusion-weighted MRI. The DWI/PWI mismatch region in acute stroke. Stroke, 1999. **30**(8): p. 1591-7.

479.   Meng, X., M. Fisher, Q. Shen, C.H. Sotak, and T.Q. Duong, Characterizing the diffusion/perfusion mismatch in experimental focal cerebral ischemia. Ann Neurol, 2004. **55**(2): p. 207-12.

480.   Reid, E., D. Graham, M.R. Lopez-Gonzalez, W.M. Holmes, I.M. Macrae, and C. McCabe, Penumbra detection using PWI/DWI mismatch MRI in a rat stroke model with and without comorbidity: comparison of methods. J Cereb Blood Flow Metab, 2012. **32**(9): p. 1765-77.

481.   Assaf, Y. and O. Pasternak, Diffusion tensor imaging (DTI)-based white matter mapping in brain research: a review. J Mol Neurosci, 2008. **34**(1): p. 51-61.

482.   Liu, Y., H.E. D'Arceuil, S. Westmoreland, J. He, M. Duggan, R.G. Gonzalez, J. Pryor, and A.J. de Crespigny, Serial diffusion tensor MRI after transient and permanent cerebral ischemia in nonhuman primates. Stroke, 2007. **38**(1): p. 138-45.

483.   van der Zijden, J.P., O. Wu, A. van der Toorn, T.P. Roeling, R.L. Bleys, and R.M. Dijkhuizen, Changes in neuronal connectivity after stroke in rats as studied by serial manganese-enhanced MRI. Neuroimage, 2007. **34**(4): p. 1650-7.

484.   van Meer, M.P., K. van der Marel, W.M. Otte, J.W. Berkelbach van der Sprenkel, and R.M. Dijkhuizen, Correspondence between altered functional and structural connectivity in the contralesional sensorimotor cortex after unilateral stroke in rats: a combined resting-state functional MRI and manganese-enhanced MRI study. J Cereb Blood Flow Metab, 2010. **30**(10): p. 1707-11.

485.   Thomas, D.L., Arterial spin labeling in small animals: methods and applications to experimental cerebral ischemia. J Magn Reson Imaging, 2005. **22**(6): p. 741-4.

486.   Bratane, B.T., R.P. Walvick, C. Corot, E. Lancelot, and M. Fisher, Characterization of gadolinium-based dynamic susceptibility contrast perfusion measurements in permanent and transient MCAO models with volumetric based validation by CASL. J Cereb Blood Flow Metab, 2010. **30**(2): p. 336-42.

Curriculum Vitae

Biography

Pascal Gervois was born on September 8th, 1987 in Cologne, Germany. He finished his secondary education in 2005 (Math-Sciences) at Sint-Jan Berchmanscollege Diest. He continued his studies at Hasselt University (Diepenbeek, Belgium), were he graduated as a Bachelor (2005-2008) and Master (2008-2010) in Biomedical Sciences both magna cum laude. His master thesis was entitled 'Dental pulp stem cells: neurogenic differentiation potential and ferumoxide nanoparticle labelling' and was achieved at the Laboratory of Morphology of the Biomedical Research Institute of the Universiteit Hasselt under the supervision of Prof. Dr. Ivo Lambrichts. He also graduated cum laude as a Master in Management (2010-2011), for which he studied at the Katholieke Universiteit Leuven. His master thesis was entitled 'Dictator Games: experiments and results'. In September 2011 he was appointed as teaching assistant and PhD student in the Laboratory of Morphology of the Biomedical Research Institute of the Hasselt University under supervision of Prof. Dr. Ivo Lambrichts. The research that is described in this thesis was conducted between September 2011 and January 2017. During this period, the PhD-programme of The Doctoral School of Medicine and Life Sciences of the Hasselt University was successfully completed. As an assistant he was involved in the educational curricula of Medicine and Biomedical Sciences.

Publication list

First author publications

Gervois, P., E. Wolfs, Y. Dillen, P. Hilkens, J. Ratajczak, RB. Driesen, T. Vangansewinkel, A. Bronckaers, B. Brône, T. Struys, I. Lambrichts. Paracrine maturation and migration of SH-SY5Y cells by dental pulp stem cells. J. Dent. Res. Accepted January 4th, 2017.

Gervois, P., E. Wolfs, J. Ratajczak, Y. Dillen, T. Vangansewinkel, P. Hilkens, A. Bronckaers, I. Lambrichts, and T. Struys, Stem Cell-Based Therapies for Ischemic Stroke: Preclinical Results and the Potential of Imaging-Assisted Evaluation of Donor Cell Fate and Mechanisms of Brain Regeneration. Med Res Rev, 2016. 36(6): p. 1080-1126.

Gervois, P., T. Struys, P. Hilkens, A. Bronckaers, J. Ratajczak, C. Politis, B. Brone, I. Lambrichts, and W. Martens, Neurogenic maturation of human dental pulp stem cells following neurosphere generation induces morphological and electrophysiological characteristics of functional neurons. Stem Cells Dev, 2015. 24(3): p. 296-311.

Hilkens, P.*, **P. Gervois***, Y. Fanton, J. Vanormelingen, W. Martens, T. Struys, C. Politis, I. Lambrichts, and A. Bronckaers, Effect of isolation methodology on stem cell properties and multilineage differentiation potential of human dental pulp stem cells. Cell Tissue Res, 2013. 353(1): p. 65-78.

*= shared first author

Contributing Author

Peer-reviewed papers

Ratajczak, J., P. Hilkens, **P. Gervois**, E. Wolfs, R. Jacobs, I. Lambrichts, and A. Bronckaers. Angiogenic Capacity of Periodontal Ligament Stem Cells Pretreated with Deferoxamine and/or Fibroblast Growth Factor-2. PLoS One, 2016. 11(12): p. e0167807.

Ratajczak, J., A. Bronckaers, Y. Dillen, **P. Gervois**, T. Vangansewinkel, R.B. Driesen, E. Wolfs, I. Lambrichts, and P. Hilkens, The Neurovascular Properties of Dental Stem Cells and Their Importance in Dental Tissue Engineering. Stem Cells Int, 2016. 2016: p. 9762871.

Bronckaers A, Hilkens P, Martens W, **Gervois P**, Ratajczak J, Struys T, Lambrichts I. Mesenchymal stem/stromal cells as a pharmacological and therapeutic approach to accelerate angiogenesis. Pharmacol Ther 2014;143(2):181-196.

Hilkens P, Fanton Y, Martens W, **Gervois P**, Struys T, Politis C, Lambrichts I, Bronckaers A. Pro-angiogenic impact of dental stem cells *in vitro* and *in vivo*. Stem Cell Res 2014;12(3):778-790.

Bronckaers A, Hilkens P, Fanton Y, Struys T, **Gervois P**, Politis C, Martens W, Lambrichts I. Angiogenic properties of human dental pulp stem cells. PLoS One 2013;8(8):e71104.

Struys T, Ketkar-Atre A, **Gervois P**, Leten C, Hilkens P, Martens W, Bronckaers A, Dresselaers T, Politis C, Lambrichts I, Himmelreich U. Magnetic resonance imaging of human dental pulp stem cells *in vitro* and *in vivo*. Cell Transplant 2013;22(10):1813-1829.

Book chapters

Petra Hilkens, Ronald B. Driesen, Esther Wolfs, **Pascal Gervois**, Tim Vangansewinkel, Jessica Ratajczak, Yörg Dillen, Annelies Bronckaers, and Ivo Lambrichts. Cryopreservation and Banking of Dental Stem Cells. In book: Biobanking and Cryopreservation of Stem Cells, 2016, pp.199-235

Bronckaers A, Wolfs E, Ratajczak J, Hilkens P, **Gervois P**, Lambrichts I, Martens W, Struys T. Dental Stem Cells: Their Potential in Neurogenesis and Angiogenesis. In book: Dental Stem Cells,2016, pp.217-241

Conference proceedings

Pascal Gervois, Tom Struys, Petra Hilkens, Annelies Bronckaers, Constantinus Politis, Bert Brône, Ivo Lambrichts, Wendy Martens. "The human dental pulp as a source for stem cells with neurogenic differentiation potential". 2014 EACMFS Congress Proceedings pag.: 159 – 159

Faridi Narain,Koos Jaap Van Zwieten, Peter Lippens,Klaus Schmidt, **Pascal Gervois**, Paul Colla, Yvan Palmers, Marjan Vandersteen, Ann Reyskens, Inge Robeyns, S. A. Varzin,A. V. Zinkovsky, Irina ZOUBOVA, K. S. Lamur. "Foot inversion and eversion movements in stance and swing - some comparative-anatomical and functional-morphological aspects." Materials of Fourth All Russian Scientific-Practical Conference with International Participants "Health - the base of human potential: problems and ways to their solution" pag.: 428 – 430

Oral presentations

Gervois P, Martens W, Struys T, Hilkens P, Bronckaers A, Politis C, Brône B and Lambrichts I. Neurogenic maturation of human dental pulp stem cells following neurosphere generation induces morphological and electrophysiological characteristics of mature neurons: a hope for neurological disorders. *Belgian Society for Cell and Development Biology, Joint Meeting, November 7th, 2014, Antwerp, Belgium*

Gervois P, Martens W, Struys T, Hilkens P, Bronckaers A, Politis C, Brône B and Lambrichts I. Neuroregeneration with dental pulp stem cells. *European Association for Cranio-Maxillo-Facial Surgery congress, September 26th, 2014, Prague, Czech Republic*

Gervois P, Martens W, Struys T, Hilkens P, Bronckaers A, Politis C, Brône B and Lambrichts I. The human dental pulp as a source for stem cells with neurogenic differentiation potential. *European Association for Cranio-Maxillo-Facial Surgery congress, September 24th, 2014, Prague, Czech Republic*

Gervois P, Martens W, Struys T, Hilkens P, Bronckaers A, Politis C, Brône B and Lambrichts I. Neurogenic maturation of human dental pulp stem cells following neurosphere generation induces morphological and electrophysiological characteristics of mature neurons: a hope for neurological disorders. *World Conference on Regenerative Medicine, October 23rd, 2013, Leipzig, Germany*

Gervois P, Hilkens P, Martens W, Bronckaers A, Struys T, Politis C, Lambrichts I. Labelling of human dental pulp stem cells with iron oxide based nanoparticles. *14th Maastricht Medical Students Research Conference, April 28th, 2010; Maastricht, The Netherlands.*

Poster Presentations (presenting author only)

Gervois P, Wolfs E, Dillen Y, Hilkens P, Bronckaers A, Ratajczak J, Driesen RB, Vangansewinkel T, Struys T and Lambrichts I. Leukocyte- and Platelet-Rich Fibrin stimulates dental pulp stem cell-proliferation and enriches their secretome without enhancing their neuroregenerative effect

Enhanced Natural Healing in Dentistry, October 14-16, 2016, Leuven, Belgium

Gervois P, Wolfs E, Ratajczak J, Dillen Y, Vangansewinkel T, Driesen RB, Hilkens, P, Bronckaers A, Struys T and Lambrichts I. Paracrine effects of human dental pulp stem cells on neuronal differentiation, neuritogenesis and migration of SH-SY5Y cells.

3rd Annual Meeting of the Belgian Society for Stem Cell Research, September 16th, 2016, Hasselt, Belgium

9th International Symposium on Neuroprotection and Neurorepair, April 19-22, 2016, Leipzig, Germany

Gervois P, Martens W, Dillen Y, Hilkens P, Ratajczak J, Bronckaers A, Wolfs E, Struys T and Lambrichts I. The secretome of human dental pulp stem cells stimulates neurite outgrowth and neuronal differentiation of SH-SY5Y neuroblastoma cells

International Society for Stem Cell Research 2015 Annual Meeting, June 24-27, 2015, Stockholm, Sweden

Interuniversity Stem Cell Meeting, April 20th, 2015, Leuven, Belgium

The immune-brain axis: from molecules to behavior, March 12-13, 2015, Diepenbeek, Belgium

Gervois P, Struys T, Hilkens P, Bronckaers A, Politis C, Brône B, Lambrichts I and Martens W. Neurogenic maturation of human dental pulp stem cells following neurosphere generation induces morphological and electrophysiological characteristics of mature neurons

1st Belgian Society for Stem Cell Research meeting, September 12th, 2014, Ghent, Belgium

Recent Advances in Neuronal and Cardiac Tissue Engineering: From Lab to Clinic, June 13th, 2014, Diepenbeek, Belgium

World Conference on Regenerative Medicine, October 23-25, 2013, Leipzig, Germany

Gervois P, Martens W, Struys T, Bronckaers A, Hilkens P, Politis C and Lambrichts I. Neurosphere-derived dental pulp stem cells differentiate to neuron-like cells. *16th Euron PhD student meeting. September 27-28, 2012; Maastricht, The Netherlands*

Gervois P, Struys T, Bronckaers A, Martens W, Hilkens P, Politis C and Lambrichts I. Dental pulp stem cells: neurogenic differentiation potential and ferumoxide nanoparticle labelling. *Joint meeting of the BSCDB/BSM, Advanced microscopy meets cell and developmental biology, October 22nd, 2011; Antwerp, Belgium*

Awards

Best Poster Presentation, 1st Belgian Society for Stem Cell Research meeting, September 12th 2014, Ghent, Belgium. Poster title: *"Neurogenic maturation of human dental pulp stem cells following neurosphere generation induces morphological and electrophysiological characteristics of mature neurons".*

Dankwoord

Na al die jaren doet het deugd om eindelijk de laatste hand te kunnen leggen aan deze doctoraatsthesis. Tijdens een doctoraat kom je vele mensen tegen, die je op de één of andere manier wil bedanken voor hun tijd, motivatie en/of geduld maar ook anderen die je nog veel succes wil wensen in hun verdere loopbaan en bij het afronden van hun onderzoek.

Allereerst wil ik mijn supervisor, Prof. Dr. Ivo Lambrichts bedanken voor zijn eeuwig enthousiasme en optimisme. Zijn uitstraling bij het zien van zelfs de kleinste vooruitgang dan ook in het onderzoek, werkte enorm motiverend en heeft bijgedragen tot het uiteindelijke resultaat dat beschreven staat in deze thesis. Ik heb een ongelofelijke bewondering voor je kennis en je kijk op de verschillende problemen doorheen de jaren werkte zeer inspirerend. Verder wil ik je ook danken voor het vertrouwen dat in mij gesteld werd bij het uitoefenen van de vele onderwijsopdrachten die me werden toegewezen als assisterend academisch personeelslid.

Ook wil ik mijn co-supervisor, Dr. Esther Wolfs, hier bedanken voor de vele feedbackmomenten en praktische begeleiding. Ons wekelijks overleg op vrijdagnamiddag hoefde niet altijd even serieus te zijn en draaide steevast uit op wetenschappelijke suggesties die hebben bijgedragen tot de resultaten die in dit boekje beschreven staan. Bedankt voor je dagdagelijkse begeleiding en de soms broodnodige spreekwoordelijke trap onder het achterwerk.

Graag wil ik ook de overige leden van de jury bedanken voor hun tijd en de grondige analyse van deze thesis. De constructieve commentaren en kritische opmerkingen die ik mocht ontvangen hebben zeker bijgedragen tot het eindresultaat.

Alvorens de andere collega's van de onderzoeksgroep Morfologie te danken, wil ik graag Dr. Tom Struys en Dr. Wendy Martens bedanken voor hun co-supervisorschap gedurende de eerste jaren van mijn doctoraatsonderzoek. Bedankt voor jullie suggesties en begeleiding. Ik wens jullie alle succes in jullie nieuwe functie en verdere leven.

In de onderzoeksgroep Morfologie heerst steeds een goede sfeer, welke de productiviteit (niet altijd) ten goede komt. Een goede werkomgeving leidt tot een gemotiveerd onderzoeksteam, en de resultaten in dit boekje zijn dan ook tot stand gekomen door wederzijds samen te werken om tot een wetenschappelijk verantwoord werkstuk te komen. Allereerst wil ik mijn bureaugenoten en Baar Geraar sympathisanten over de jaren heen bedanken, en dat zijn er heel wat. Dr. Petra, bedankt om mijn agenda beter te kennen dan mezelf en om de rommel op en rond mijn bureau te verdragen, deze laatste functie werd alvast door Yörg succesvol overgenomen. Succes met je verdere onderzoek en met Pixel! Stefanie, Jessica, bedankt voor het mee doorstaan van de laatste fase van het doctoraatsonderzoek en veel succes met het afronden en verdedigen van jullie thesis, wat jullie zoizo uitstekend gaan doen. Tim en Yörg, bedankt voor de sportmomenten en om de Y-factor in onze groep mee te helpen verdedigen. Veel succes met jullie onderzoek. Even though both of you are pursuing new endeavours, Dr. Pia and Dr. Derv, thanks a lot for the wonderful times in and out of the office. My best wishes for the rest of your professional and personal life. Derv, I believe I still owe you a Bon Jovi song. Ook de andere onderzoeksleden van onze groep wil ik hierbij bedanken: Daniela, Selien, Céline, Greet en Melissa, veel success met jullie doctoraatsonderzoek en hou de moed erin! Ook wil ik Dr. Ronald graag bedanken voor de altijd kritische maar goede commentaar. Daarnaast ben ik alvast jaloers op je collectie Star Wars prul/memorabilia. Prof. Dr. Annelies Bronckaers, veel succes met het uitbouwen van je eigen onderzoeksgroep en bedankt voor je goede raad en (soms iets te veel) ideeën doorheen de jaren. Jeanine, bedankt voor je hulp bij het verwerken van de kilometers paraffinecoupes die je voor mij en anderen hebt aangeleverd. Prof. Dr. Vandersteen, Prof. Dr. em. Vanormelingen, Prof. Dr. em. Van Zwieten, Liliane, Kathleen, Katrien: bedankt voor jullie interesse, rechtstreekse en onrechtstreekse steun in de loop van dit project.

Toen ik begon als assistent aan de Universiteit Hasselt, werd me snel duidelijk dat ik maar beter kon leren Wiezen. Deze sport staat op de shortlist van het BOIC en de atleten doen alvast hun best om zich voor te bereiden op het wereldkampioenschap: Marc 'The Flash' Jans, bedankt voor de leuke babbels en de ondersteuning met de elektronenmicroscoop, zonder u blijft dit ding niet bollen. (Eu)Gene 'The Machine' Steegen, bedankt voor de altijd goedlachse

middagpauze, dat je nog veel saucissekes mag eten! Dennis en Davy, bedankt voor de altijd leuke momenten die we al delen sinds mijn stages in 2009-2011, zowel tijdens als na de werkuren. Verdere muzikaal ondersteunde, cultureel verantwoorde, thema-uitstapjes in tenue zullen zeker nog gemaakt worden.

Ook wil ik alle BIOMED collega's niet vergeten. Katrien, Igna, Leen, Kim, Christel, Rosette, Jo, Erik: bedankt voor jullie hulp met alle technische problemen. Hierbij wil ik ook Petra nog eens extra bedanken voor haar vele uren patch-clamp experimenten die in dit boekje beschreven staan. Aan alle overige onderzoekers: veel succes met het opstarten/afronden van jullie onderzoek. Joke, Paul, Yennick: bedankt om alles in het animalium steeds te laten draaien. Rani, Veronique bedankt voor al jullie administratieve ondersteuning en paraatheid wanneer ik weer maar eens aan jullie deur stond.

Graag wil ik Prof. Dr. Uwe Himmelreich, Dr. Willy Gsell, Ann Van Santfoort en Tine Buelens van het MoSAIC van de KULeuven danken voor hun hulp en ondersteuning bij het uitvoeren van de imaging experimenten.

De personen die misschien wel het meest morele steun bieden tijdens deze onderzoeksperiode, zijn de mensen in je naaste omgeving. Bedankt aan alle vrienden om naast een luisterend oor ook voor de nodige hoeveelheid afleiding te zorgen tijdens de voorbije jaren: festivals, uitjes, café avondjes, etc.

Ook wil ik mijn ouders graag bedanken om altijd onvoorwaardelijke steun te bieden tijdens de voorbije jaren en om me alle kansen te bieden die ik maar wou grijpen. Hopelijk wordt met dit boekje een beetje duidelijker wat ik bedoelde met 'ik moet mijn cellen gaan eten geven' wanneer ik op weekend- of vakantiedagen in het lab stond.

Als laatste wil ik de persoon bedanken die misschien wel het meest heeft afgezien met mij, zeker gedurende de laatste maanden. Alexis, mijn partner en beste vriendin, bedankt om lief en leed met mij te delen en voor de extra inspanningen om mij te kunnen laten doorwerken. Zonder uw steun en begrip was dit werk niet hetzelfde tot stand kunnen komen. Bedankt om te zijn wie je bent. Uw positieve, hartelijke, enthousiaste en altruïstische ingesteldheid zijn het mooiste dat in een persoon aanwezig kan zijn. Bedankt voor alles.